TUM School of Life Sciences

The Use of Intestinal Organoids to Study Colorectal Cancer in Pigs

Alessandro Grodziecki

Vollständiger Abdruck der von der TUM School of Life Sciences der Technischen Universität München zur Erlangung des akademischen Grades eines

Doktors der Naturwissenschaften

genehmigten Dissertation.

Vorsitzender: Prof. Dr. Martin Klingenspor

Prüfende der Dissertation:

1. Prof. Angelika E. Schnieke, Ph.D.

2. apl. Prof. Dr. Klaus-Peter Janssen

Die Dissertation wurde am 01.07.2021 bei der Technischen Universität München eingereicht und durch die TUM School of Life Sciences am 21.09.2021 angenommen.

Eidesstattliche Erklärung

Ich erkläre an Eides statt, dass ich die bei der promotionsführenden Einrichtung, TUM School of Life Sciences, zur Promotionsprüfung vorgelegte Arbeit mit dem Titel:

„The Use of Intestinal Organoids to Study Colorectal Cancer in Pigs”

am Lehrstuhl Biotechnologie der Nutztiere, TUM School of Life Sciences, unter der Anleitung und Betreuung durch Prof. Angelika E. Schnieke, Ph.D., ohne sonstige Hilfe erstellt und bei der Abfassung nur die gemäß § 6 Ab. 6 und 7 Satz 2 angebotenen Hilfsmittel benutzt habe.

Ich habe keine Organisation eingeschaltet, die gegen Entgelt Betreuerinnen und Betreuer für die Anfertigung von Dissertationen sucht, oder die mir obliegenden Pflichten hinsichtlich der Prüfungsleistungen für mich ganz oder teilweise erledigt.

Ich habe die Dissertation in dieser oder ähnlicher Form in keinem Prüfungsverfahren als Prüfungsleistung vorgelegt.

Ich habe den angestrebten Doktorgrad noch nicht erworben und bin nicht in einem früheren Promotionsverfahren für den angestrebten Doktorgrad endgültig gescheitert.

Hannover, 28.06.2021 _____

Alessandro Grodziecki

Table of Contents

Abstract

Colorectal cancer (CRC) is the second leading cause of cancer related deaths worldwide. Germline mutations in the *APC* gene, like the truncating mutation APC^{1309}, are responsible for familial adenomatous polyposis (FAP) – a genetic predisposition to CRC. Pigs that carry the truncating mutation APC^{1311}, which is orthologous to the human APC^{1309} mutation, model early stages of FAP. However, additional mutations are required to recapitulate advanced disease.

Here, the cultivation and genetic manipulation of porcine intestinal cells are described as versatile technique for preclinical cancer research. For this purpose, existing protocols for human and murine organoid culture had to be adapted for the pig. Crypts were isolated from intestinal biopsies and cultivated in a three-dimensional matrix with conditioned media to generate intestinal organoids, called enteroids. The presence of all major intestinal cell types was verified by expression of marker genes in enteroids. Furthermore, electropermeabilisation was established as efficient transfection method for porcine enteroids. In order to introduce additional mutations in polyp-derived epithelial cells, enteroids were generated from colonic polyps removed during endoscopy of APC^{1311} $KRAS^{LSL\text{-}G12D}$ pigs. Using CRISPR/Cas9-based multiplex gene editing and Cre recombinase, five CRC-associated tumour suppressor genes were inactivated and the silent oncogenic *KRAS-G12D* mutation was activated. Transformation of enteroids was verified by unrestricted *in vitro* proliferation independent from growth factors. In addition, invasiveness was verified in a transwell invasion assay and cell growth was visible in a chorioallantoic membrane assay. Using gene editing of *B2M* and a *LE29Y* expression vector, the destruction of transformed enteroids by the immune system should be avoided after transplantation. Transformed enteroids were injected under the skin of pigs to easily assess tumour growth. However, no tumour formation was observed *in vivo*. In future experiments, orthotopic autologous transplantation will be used to test if transformed enteroids are suitable to accelerate colorectal carcinogenesis in FAP pigs. Additionally, basic work was conducted on the generation of a *TNF*-edited pig line with a predisposition to intestinal inflammation. This line can be used to establish a colitis-associated CRC model.

Zusammenfassung

Darmkrebs ist weltweit die zweithäufigste Todesursache bei Krebserkrankungen. Erbliche Mutationen im *APC* Gene, wie die Truncating-Mutation APC^{1309}, sind verantwortlich für die familiäre adenomatöse Polyposis (FAP), einer genetischen Prädisposition für Darmkrebs. Als Model früher Stadien der FAP dienen Schweine, die die Truncating-Mutation APC^{1311} tragen, die ortholog zur menschlichen APC^{1309} Mutation ist. Allerdings sind weitere Mutationen nötig, um fortgeschrittene Krankheitsstadien zu modellieren.

In dieser Arbeit werden die Kultivierung und genetische Manipulation von Schweinedarmzellen als vielseitige Technik für die präklinische Krebsforschung beschrieben. Hierzu wurden Protokolle für die Kultivierung humaner und muriner Organoide für das Schwein angepasst. Krypten wurden von Darmbiopsien isoliert und in einer dreidimensionalen Matrix kultiviert, um Darmorganoide zu erhalten, die „Enteroide“ genannt werden. Alle grundlegenden Darmzelltypen wurden durch die Expression von Markergenen in Enteroiden nachgewiesen. Außerdem wurde Elektropermeabilisierung als effiziente Transfektionsmethode zum Genome-Engineering etabliert. Um weitere Mutationen in Epithelzellen von Polypen einzubringen, wurden Enteroide aus Darmpolypen erzeugt, die während der Endoskopie von APC^{1311} $KRAS^{LSL\text{-}G12D}$ Schweinen entnommen wurden. Mit Hilfe von CRISPR/Cas9-basiertem Multiplex-Gene-Editing und Cre Rekombinase wurden fünf darmkrebsassoziierte Tumorsuppressorgene inaktiviert und eine stille KRAS-G12D Mutation aktiviert. Die Transformation der Enteroide wurde durch die ungehemmte Zellteilung *in vitro* unabhängig von Wachstumsfaktoren nachgewiesen. Zusätzlich wurde ein invasiver Phänotyp im Transwell-Invasionsassay nachgewiesen und Tumorbildung im Chorioallantoismembran-Assay beobachtet. Die transformierten Enteroide wurden unter die Schweinehaut injiziert, um das Tumorwachstum besser beurteilen zu können. Allerdings wurde keine Tumorbildung *in vivo* beobachtet. In zukünftigen Experimenten, wird die orthotope autologe Transplantation verwendet werden, um zu testen, ob transformierte Enteroide geeignet sind, die Darmkrebsentwicklung in FAP-Schweinen zu beschleunigen. Darüber hinaus, wurden grundlegende Arbeiten zur Generierung einer TNF-editierten Schweinelinie mit einer Prädisposition für Darmentzündung durchgeführt. Diese Linie kann zur Etablierung eines Kolitis-assoziierten Darmkrebsmodell verwendet werden.

1. Introduction

1.1. Epidemiology of colorectal cancer

Colorectal cancer (CRC) has been the subject of intense research for decades. The WHO estimated 862 000 people died from CRC worldwide in 2018, which makes CRC the second leading cause of cancer related deaths. Notably, the mortality might rise because of the 'westernisation' of developing countries in terms of diet and lifestyle (Figure 1).

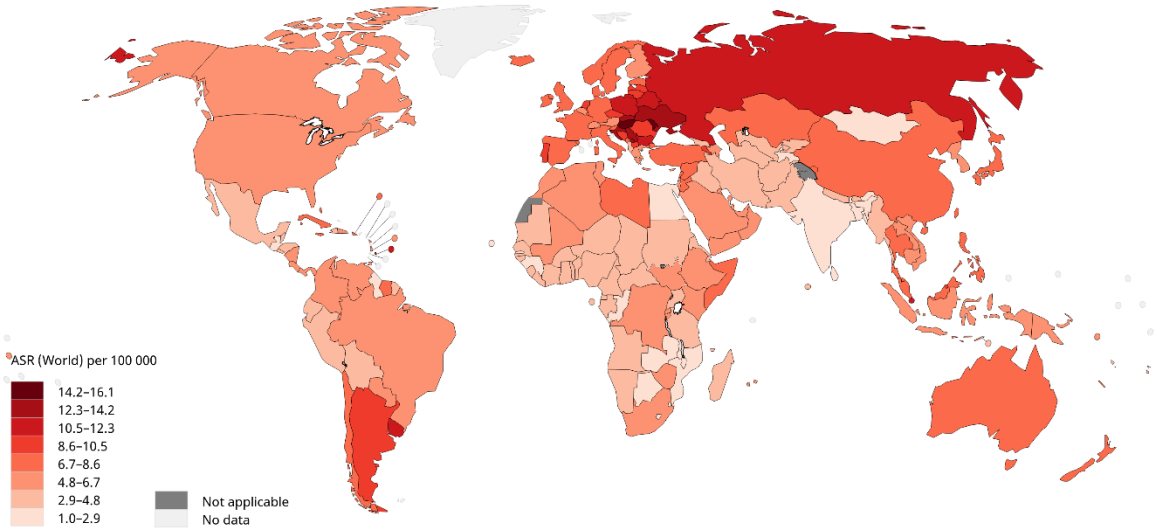

Figure 1: Estimated age-standardised mortality rates (ASR) in 2018 for CRC (both sexes, age 0-74, created from open source database https://gco.iarc.fr/[1])

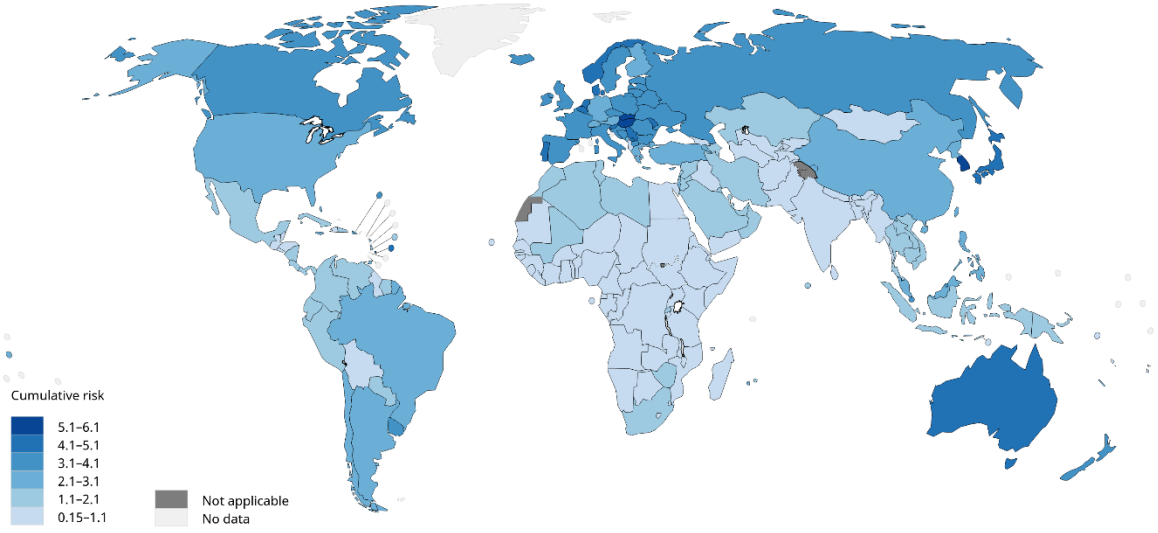

Figure 2: Estimated cumulative risk of colorectal cancer in 2018 (both sexes, age 0-74, created from open source database https://gco.iarc.fr/[1])

Although age is the major risk factor for CRC, epidemiologists warn of an alarming increase also in young patients[2]. Nowadays, the overall lifetime risk for developing CRC is 1.1-1.5% (Figure 2) with an overall survival of 3 years for advanced disease[3]. Survival is enhanced if the tumour is diagnosed early. Unfortunately, early stages of CRC are asymptomatic and patients usually present with advanced disease which requires intense radio- and chemotherapy at the time of diagnosis. Advances in the omics technologies have revealed the heterogeneous nature of CRC with great hopes for precision medicine. However, targeted therapy with antibodies or small molecule inhibitors is only suitable for certain molecular subtypes and the range of chemotherapeutics hardly increased since the 1960s[4].

Preclinical models of CRC are continuously refined to understand its complex pathology, to explore molecular targets with fewer adverse effects for therapy, and to develop predictive and prognostic tools.

1.2. Genetic predisposition and pathogenesis of CRC

According to the German Cancer Aid[5], the average age for CRC diagnosis is 72 for men and 76 for women. Physical activity reduces the individual risk for CRC by 20-30%. A diet rich in fibres and abstinence from alcohol and smoking are also beneficial. Besides age and lifestyle, hereditary factors account for 12-35% of CRC cases[6] and are best understood due to genetically engineered animal models[7]. Between 10 and 20% of patients have a history of cancer in their family[8]. Hereditary CRC can be classified into two phenotypes, the polyposis and non-polyposis syndrome, depending on the number of polyps at the time of diagnosis[9]. The polyposis syndrome is characterised by hundreds of abnormal mucosal lesions, so called ‘adenomas’ or ‘adenomatous polyps’, in the large intestine, whereas the non-polyposis syndrome (including Lynch syndrome) shows only few sporadic lesions that require molecular analysis for diagnosis. It is the accumulation of genome alterations, like gene mutations or chromosomal instability, that causes malignant tumours.

In the past, two molecular distinct pathways of CRC were distinguished, the ‘adenoma-carcinoma pathway’ and the ‘serrated neoplasia pathway’[10]. Since Fearon and Vogelstein proposed the first model of a sequential accumulation of genetic and epigenetic factors along CRC progression[11] additional pathways have been identified.

About 80% of CRC carry sporadic or germline mutations in the *adenomatous polyposis coli* tumour suppressor gene (*APC*)[12,13]. Over time mutations in proto-oncogenes, like *KRAS*[A] and *BRAF*[B], occur followed by mutations in the tumour suppressors *SMAD4*[C] and *TP53*[D] [14]. This progression of mutations is characteristic for the adenoma-carcinoma pathway[14] and some of these mutations are explained in more detail later. In the adenoma-carcinoma model, benign tumours arise from healthy colon epithelium, (adenomas) and gain an invasive, metastatic phenotype, called carcinoma, within 10-20 years. In the serrated neoplasia pathway, oncogenic alterations are the initial events[10]. Serrated tumours show a characteristic 'saw-toothed' infolded crypt epithelium.

Holistic approaches, like gene expression and DNA methylation signatures, have sharpened CRC classification accounting for the epigenetic, microsatellite and chromosomal instability seen in tumours. As a result, four consensus molecular subtypes (CMS, Table 1) were identified that partially recapitulate the pathways mentioned earlier and cover 87% of CRC cases[15].

	CMS1	**CMS2**	**CMS3**	**CMS4**
Frequency [%]	14	37	13	23
Tumour location	proximal	distal	proximal or distal	distal
Precursor polyp	sessile serrated	adenomatous	serrated or adenomatous	adenomatous
DNA sequence stability	MSI	MSS	MSS or MSI	MSS
DNA methylation	CIMP-H	no CIMP	CIMP-L	no CIMP
Chromosome number	stable	CIN	stable or CIN	CIN
Mutated genes	*BRAF*	*APC, TP53*	*KRAS*	EMT associated genes
Pathway signature	immune activation	WNT and MYC	metabolic deregulation	TGF-β, mesenchymal

Table 1: Comparison of the four consensus molecular subtypes (CMS) of colorectal tumours defined by gene expression-based clustering. CIMP CpG island methylator phenotype, -H high, -L low, MSI microsatellite instability, MSS microsatellite stability, CIN chromosomal instability, EMT epithelial to mesenchymal transition (adapted from P. Jordan, Targeted Therapy of Colorectal Cancer Subtypes, Advances in Experimental Medicine and Biology, 2018)

[A] *Kirsten rat sarcoma viral oncogene homolog*
[B] *B-Raf proto-oncogene serine/threonine-protein kinase*
[C] *SMAD, mothers against decapentaplegic homolog 4*
[D] *tumour suppressor p53*

Microsatellite instability is the result of defective DNA repair by mutation or epigenetic silencing of mismatch repair (MMR) genes. Germline mutations in MMR genes are known in Lynch syndrome, a hereditary predisposition to a variety of tumours[16]. In addition to pathological and genetic features, the regulation of metabolism and cell signalling pathways were considered. The next chapters discuss the genes and pathways involved in these subtypes.

1.2.1. Adenomatous polyposis coli tumour suppressor gene (*APC*)

The subtype with the highest incidence rate is CMS2 with 37% of CRC cases. It originates in the distal colon and rectum and is characterised by activation of Wnt and EGFR signalling. Interestingly, elevated Wnt signalling correlates with reduced T cell expression signatures[17] which could explain the low immunogenicity of this subtype. The canonical Wnt signalling pathway, also known as 'β-catenin pathway', is activated when Wnt ligands bind to a complex formed by the Frizzled receptor and LRP5/6 co-receptor on the plasma membrane (Figure 3).

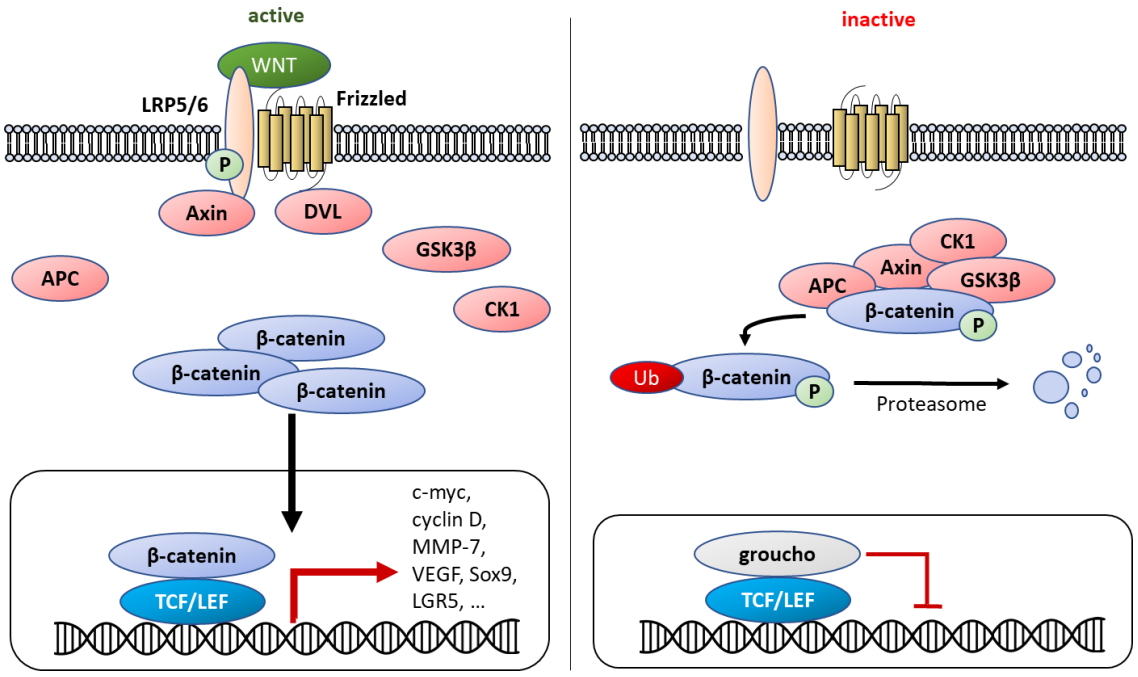

Figure 3: Canonical Wnt signalling pathway. Wnt ligands activate the canonical Wnt signalling pathway, also known as 'β-catenin pathway', by binding to a complex formed by LRP5/6 (low-density lipoprotein-related protein 5/6) and Frizzled. LRP5/6 is phosphorylated and recruits Axin and DVL to the plasma membrane, thereby, inhibiting the formation of the β-catenin destabilisation complex. Now, β-catenin accumulates and is translocated into the nucleus where it activates the expression of Wnt target genes (left). Without Wnt ligands, the destabilisation complex composed of Axin-1/2, CK1, GSK3β proteins, and APC forms and phosphorylates β-catenin which leads to its ubiquitination and proteasomal degradation. As a result, the transcription of Wnt target genes is restrained (right).

LRP5/6 is phosphorylated and recruits Dishevelled (DVL) and Axin. This prevents the assembly of the β-catenin destruction complex. Unmodified β-catenin accumulates in

the cytoplasm and is translocated into the nucleus. In complex with TCF/LEF (T cell factor/lymphoid enhancer factor family) transcription factors β-catenin drives expression of genes that promote stem cell renewal and inhibit differentiation.

In absence of Wnt ligands or equivalent signals from other signalling cascades, the destruction complex is formed by APC, Axin-1/2, CK1 (casein kinase 1) and GSK3β proteins. Within this complex β-catenin is phosphorylated and directed to proteasomal degradation. This pathway is highly conserved in animals and essential for cell proliferation, apoptosis and stemness in the intestine.

Fifteen transcripts of the human *APC* gene are reported[18] and the most abundant encodes for a protein of 2843 amino acids[19]. It plays a critical role in various cellular processes like migration, adhesion and apoptosis and is best studied as negative regulator of β-catenin. Germline mutations in *APC*, E1309* for instance, are the cause for familial adenomatous polyposis (FAP), a hereditary form of colorectal adenocarcinoma[20]. Somatic mutations usually accumulate in the early β-catenin regulatory region, also called *mutation cluster region* that is crucial for cytoplasmatic degradation of β-catenin (Figure 4).

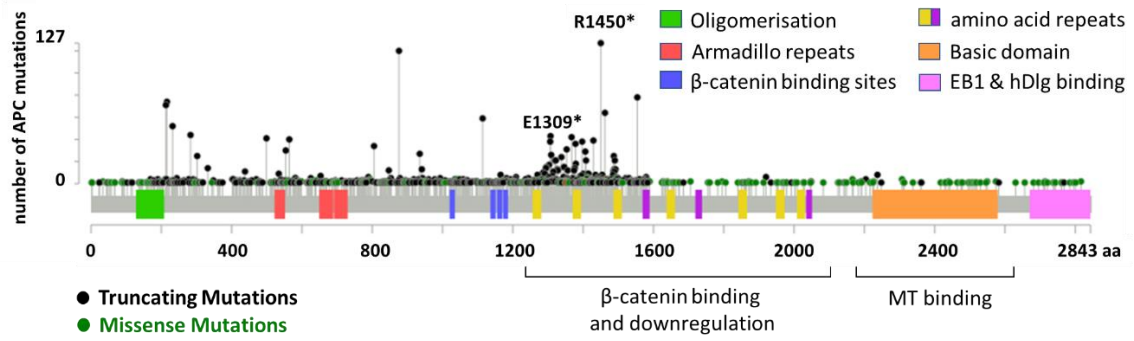

Figure 4: Scheme of the APC protein domains and regions of mutation found in CRC patients. Armadillo repeats are repeats of unknown function with similarity to Drosophila's armadillo protein; MT domain facilitates complexing with microtubules; sequences near the carboxy terminus interact with EB1 (end binding 1 protein) and human homolog of Drosophila's disc large (hDlg) protein. Mutations affect half of the sequence directed to the amino terminus including the truncating mutations at position 1309 and 1450 or cumulate within the 'mutation cluster region' affecting β-catenin binding and downregulation. Truncating mutations contain nonsense, nonstop, frameshift deletion, frameshift insertion and splice site mutations (data adapted from 10 studies including 3806 CRC patients are provided at the open source database http://www.cbioportal.org, 2020).

Although hyperactivation of β-catenin is a hallmark of colorectal tumorigenesis, there is evidence from patient-derived xenografts that Wnt signalling is attenuated towards metastatic stage[21].

Most CMS2 tumours are diagnosed at advanced disease (stage II/III) and chemotherapy is applied with high response[22]. The 5-year survival rate is 77% and the highest among all CRC subtypes[23]. If *KRAS*, a potent proto-oncogene, is mutated survival further decreases to less than 60%[24].

1.2.2. Kirsten rat sarcoma viral oncogene (*KRAS*)

Prognosis in the CMS2 subtype is worse if the human homologue of the *Kirsten rat sarcoma viral oncogene* (*KRAS*) is mutated. Furthermore, alterations in *KRAS* are characteristic for the CMS3 subtype. Those tumours are genetically stable and metabolically active[15]. This observation is described as Warburg Effect[25], a hallmark of cancer, in which the degrees of glycolysis and lactate metabolism remain constitutively high – even with sufficient oxygen supply for oxidative phosphorylation. The urgent need of glycose for this metabolically exhausting plasticity is met by *KRAS* mutations that also boost glucose uptake into the cell[26]. Sixty-eight percent of CMS3 tumours carry a *KRAS* mutation[27] which confers resistance against cetuximab and panitumumab, two monoclonal antibodies that target the EGF receptor[28]. In order to circumvent the intrinsic resistance, new engineered monoclonal antibodies and small molecule inhibitors are explored for metabolic targets, like the GLUT-1 transporter[29] or pyruvate kinase PKM2[30].

Coding mutations of the *KRAS* proto-oncogene are dominant in CRC as shown in Figure 5. Furthermore, the amino acid substitutions at positions 12 and 13 are the most prominent.

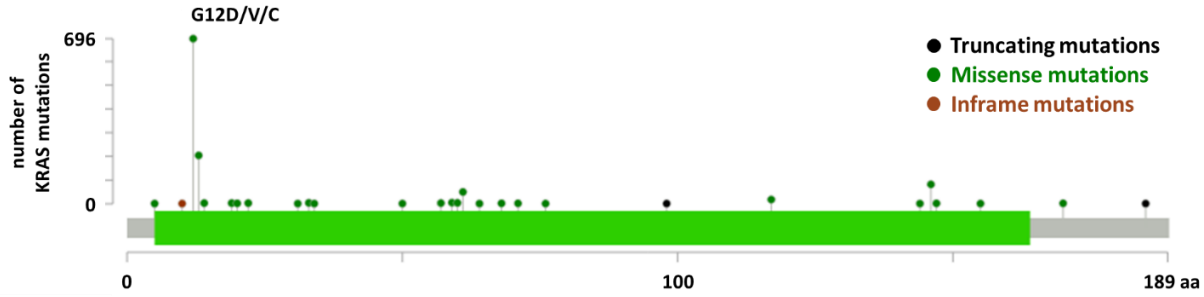

Figure 5: Scheme of the KRAS protein and regions of mutation found in CRC patients. The longest isoform is displayed. KRAS contains the Ras domain and is a member of the small GTPase superfamily (data reproduced from 10 studies including 3806 CRC patients are provided at http://www.cbioportal.org, 2020).

Under physiological conditions Kras is activated after dimerization of receptor tyrosine kinases that bind growth factors, like the epithelial, fibroblast or hepatocyte growth factor (Figure 6). The phosphorylated receptor can bind to cytoplasmatic Grb2 which recruits Sos, the nucleotide exchange factor that releases GDP from Kras

(inactive state). Kras binds GTP and remains active until the nucleotide is converted to GDP. GTP is hydrolysed by Kras-intrinsic kinase activity and GAP (GTPase-activating protein) serves as catalyst. In its active conformation Kras stimulates the MAP kinase pathway by activating Raf which ultimately leads to proliferation and angiogenesis. In addition, Kras-GTP activates PI3K that phosphorylates phosphatidylinositol diphosphate (PIP_2) which in turn inhibits apoptosis through the PI3K/Akt pathway. The tumour suppressor PTEN (phosphatase and tensin homolog) inhibits PI3K-Akt pathway by dephosphorylation of PIP_3.

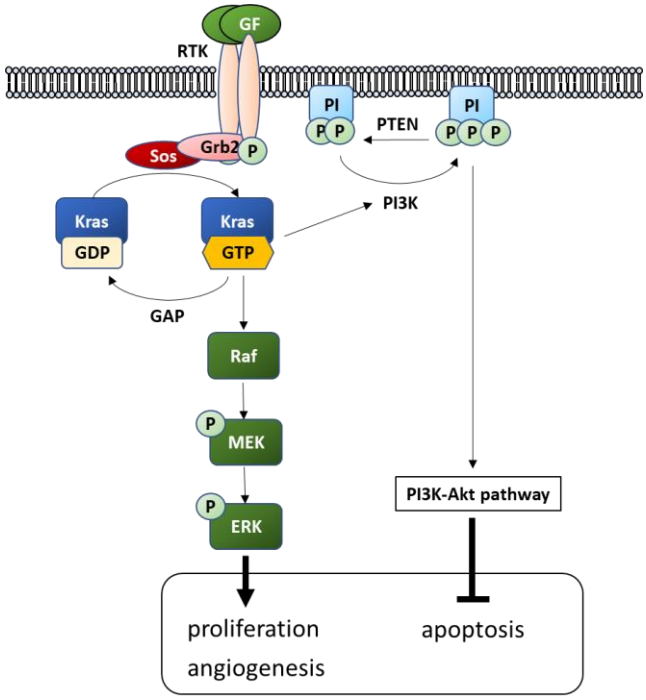

Figure 6: Effects of physiological KRAS activation including receptor-tyrosine kinase and PI3K-Akt signalling. Binding of growth factors (GF), like EGF or IGF, to their receptors (receptor-tyrosine kinase, RTK) induces their phosphorylation which attracts Grb2 (growth factor receptor-binding protein 2). Grb2 is associated with Sos (son of sevenless) that serves as guanine nucleotide exchange factor and activates Kras (Kras-GTP). The amount of active Kras is balanced by GTPase-activating protein (GAP) which catalyses Kras dephosphorylation (Kras-GDP). Kras is involved in Ras-MAPK signalling and the PI3K-Akt signalling pathway.

Taken together, *KRAS* is a potent ubiquitously expressed proto-oncogene. Substitution mutations, like the G12D mutation, affect its GTPase activity and arrest the protein in a constitutively active GTP-bound conformation, thereby promoting growth factor independent cell growth and survival. A Cre-inducible G12D mutation had been introduced in a porcine *KRAS* allele[31] and was used in my work to replicate oncogene activation in the porcine model for CRC.

1.2.3. *TP53* tumour suppressor gene

CMS2 tumours show the highest copy numbers of oncogenes and the most dramatic loss of tumour suppressor genes (TSGs), including *TP53*[27]. Intense research since

the 1970s has proven the indispensable value of *TP53* for genome integrity. It induces cell cycle arrest, DNA repair, senescence and apoptosis upon DNA damage[32]. Therefore, *TP53* is known as 'guardian of the genome' and is frequently mutated in human cancers[33]. Germline mutations in *TP53* cause Li Fraumeni syndrome which is characterised by early onset of a variety of cancers in childhood[34]. Most of the mutations are reported in the DNA binding domain.

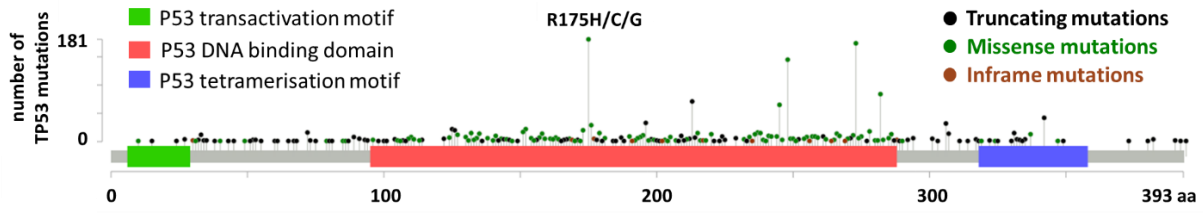

Figure 7: Scheme of the TP53 protein domains and regions of mutation found in CRC patients. The longest isoform is displayed. In total 29 transcripts (ENSG00000141510) and multiple isoforms exist due to alternative splicing, alternative promoters, and alternative start codons. P53 transactivation motif regulates *TP53* transcription. The DNA binding domain is the primary site for single nucleotide missense mutations. The tetramerization motif is required for its proper function as transcription factor. Consequently, heterotetramers of wildtype and missense P53 proteins cause a (oncogenic) dominant negative phenotype (data reproduced from 10 studies including 3806 CRC patients are provided at http://www.cbioportal.org, 2020).

In addition to numerous truncating mutations that impair its tumour suppressor function, some alterations lead to an oncogenic gain-of-function[35]. The most abundant mutation is the missense mutation R175H that exhibits an oncogenic phenotype independent of wildtype p53 (Figure 7). Although *TP53* has a pivotal role in replicative senescence, its inactivation is not sufficient to overcome growth arrest.

In contrast to mice, human cancer cells additionally require loss of the tumour suppressor protein p16, encoded by *CDKN2A*, to overcome senescence due to telomere erosion[36]. Figure 8 shows that both, p16 and p53, inhibit the phosphorylation of retinoblastoma protein Rb via independent pathways. Before passing the G1/S checkpoint, the cell must ensure that DNA damage, oxidative stress, and the activation of oncogenes do not interfere with the completion of the cell cycle. Otherwise, the cell risks apoptosis. Therefore, p16 and p53 are induced by stress stimuli and inhibit cyclin-dependent kinases CDK4/6 and CDK2 which inactivate Rb by phosphorylation. Unphosphorylated Rb binds E2F protein, the factor that promotes transition from G1 to S phase. Consequently, stress-induced activation of p16 and p53 arrest the cell cycle at G1 phase. Moreover, high expression of p16 is a marker for cellular senescence which irreversibly stops cell growth[37].

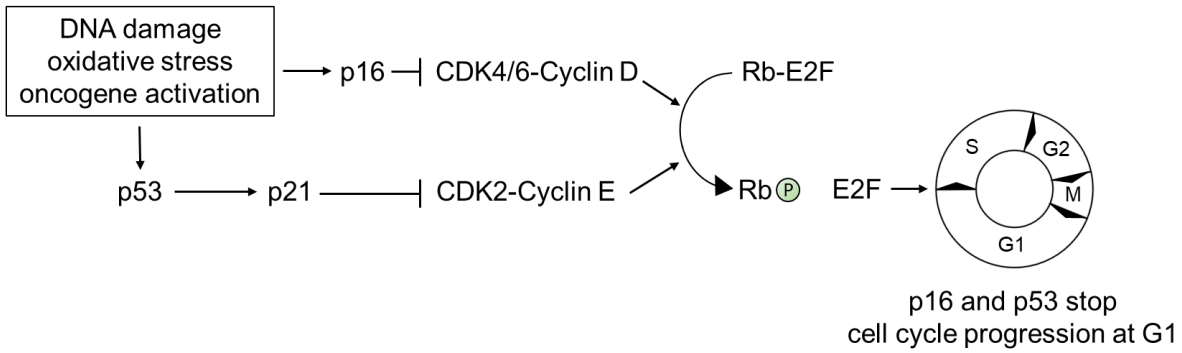

Figure 8: The tumour suppressors p16 and p53 inhibit Rb through independent pathways to control cell cycle progression. In the cell, different stress stimuli activate expression of p16 and p53. p53 transactivates the CDK2/cyclin E inhibitor, p21, which consequently inhibits phosphorylation of Rb. Similarly, the CDK inhibitor, p16 acts suppresses Rb phosphorylation by the CDK4-6/cyclin D complex. Unphosphorylated Rb binds E2F, the G1/S phase-promoting factor, which results in cell cycle arrest in G1 phase.

1.3. Inflammation and CRC

The role of inflammation in tumour progression is ambivalent. The immune system recognises neoantigens – novel peptides that are expressed due to genetic instability, e.g. in MSI tumours, and presented by the major histocompatibility complex class I molecules[38]. In response to the appearance of cancer cells and the invasion of the stroma, inflammation is triggered leading to the recruitment of leukocytes and plasma proteins. Tumours of the CMS1 are associated with a high degree of infiltration by leukocytes, primarily CD8+ cytotoxic T cells[39]. Prognosis and survival are better in this subgroup compared to others. However, cancer cells developed strategies to evade the immune response.

Increased expression of PD-L1 (inhibitory programmed cell death 1 ligand 1) is found in malignant tumours. Binding of PD-L1 to its receptor on T cells suppresses the cytotoxic activity. Consequently, patients with BRAF/MSI tumours benefit from PD-L1 inhibitors, like pembrolizumab, that reactivate T lymphocytes to attack cancer cells[40].

Another immune checkpoint blocker, ipilimumab, targets CTLA-4 which is expressed on cytotoxic and regulatory T cells and conveys immunosuppressive signals. This human monoclonal antibody increases proliferation of T cells and depletes inhibitory regulatory T cells. The combination of ipilimumab (anti-CTLA-4) and nivolumab (anti-PD-1) is indicated for metastatic colorectal cancer with MSI[41].

These examples illustrate how inducing inflammation is used to activate the anti-cancer immune response. However, an inflammatory environment fuelled by cytokines, like TNFα and IL-6, was shown to stimulate tumorigenic pathways. Interleukin-6, for example, downregulates E-cadherin and upregulates vimentin.

Thereby, it triggers the transition from an epithelial to mesenchymal phenotype which initiates invasiveness of cancer cells[42].

Indeed, polyps regressed in FAP patients after administration of sulindac, an anti-inflammatory drug that inhibits cyclooxygenase (COX)[43]. Interestingly, daily administration of aspirin was shown to reduce the incidence of colorectal cancer in patients with Lynch syndrome[16]. In 2016, the United States Preventive Services Taskforce, a federal advisory panel on disease prevention, supported the use of aspirin to reduce the risk of cardiovascular disease and colorectal cancer.

Colitis-associated colorectal cancer accounts for 15% of deaths in patients with inflammatory bowel disease (IBD)[44]. IBD is a multifactorial disease characterised by chronic or repeated inflammation of the gut. Approximately one hundred risk loci are identified but the development of disease is strongly influenced by environmental factors[45,46]. TNFα biosynthesis is chronically elevated in *TNF*$^{\Delta ARE}$ mice which stimulates NF-κB – a key transcription factor that regulates various inflammatory responses[47]. Chronic activation of NF-κB was shown to support the transition from inflamed tissue to mucosal dysplasia in mice and a more severe phenotype was observed if one *APC* allele was deleted[48] – suggesting that TNFα-induced colitis should accelerate CRC progression in *APC*$^{1311/WT}$ pigs. Interestingly, NF-κB was found to enhance Wnt signalling which finally leads to dedifferentiation of murine epithelial cells – an observation also made in patients with ulcerative colitis[49].

1.4. Rodent and in vitro models

Genes relevant for human cancers were identified and characterised in animal models. In 1911, the first oncogene was identified in the Rous sarcoma virus as the cause of transmissible cancer in chicken. Sixty-five years later a homologue of this viral oncogene was found in the chicken genome. The first proof of tumorigenic chemicals was demonstrated in 1915 on rabbits that were exposed to coal tar and in 1984, the oncogene ‘neu’ (human homologue: HER2) was identified in rat cells[50]. Today, CRC models are dominated by genetically engineered mouse models (GEMM) and human cell lines. Within the last decade three-dimensional cell culture emerged as another promising system to model cancer in a dish. Here, I outline the benefits and limitations of these systems and build the bridge to large animal models of CRC.

In 1990, a mouse line with predisposition to multiple intestinal neoplasia (Min) was generated by chemical mutagenesis[51]. The reason is a truncating mutation at codon 850 of the APC gene and the loss of the remaining full length wildtype allele (loss of heterozygosity, LOH) eventually leads to adenoma formation in the small intestine. In contrast, 98% of adenomas are found in the distal colon of CRC patients[52]. Although the *APC*$^{Min/+}$ mouse does not replicate the localisation of human polyps in CRC, the line was intensively used to study FAP[53]. Colon adenomas and adenocarcinomas are reported in some old *APC*$^{Min/+}$ mice (120-150 days). In order to improve the life span and the localisation of polyp formation in mice models, *APC* is deleted specifically in the colon. For this purpose, Cre recombinase is used to inactivate floxed *APC* in *APC*$^{flox/flox}$ mice. Cre can be delivered as adenoviral vector to the colon or by breeding with GEMM that express Cre specifically in the colon, such as *CDX2P-NLS Cre* mice[54].

Preclinical models should enable the study of cancer pathogenesis based on defined molecular aberrations and help to evaluate the response to treatment. They are crucial throughout the process of drug discovery, including biomarker identification, target selection and validation[52,55–57]. Two-dimensional human cell culture is the starting point for high-throughput screening of anticancer drugs in the pipeline of drug discovery[58]. These cultures are easy to modify genetically and many isogenic cell lines are available. Furthermore, it has been shown that 70 human CRC cell lines display the most prevalent exome mutations and DNA copy number variations which are found in primary tumours and collected in The Cancer Genome Atlas[59].

Since these systems are devoid of the extracellular environment, cell lines are transplanted into immunocompromised mice as xenograft. Xenograft models represent translational tools that extend the use of genetically engineered mouse models[60,61]. Vascularized tumours usually form within weeks and drugs can be evaluated for pharmacological characteristics. Although, the predictive value of this system – the quality of the estimated response to a therapy – seems low (except for lung cancer)[57] and the molecular diversity is lost due to repeated passaging of cell lines[62].

Xenografts with primary tumour specimen taken from a patient's biopsy could model individual tumours with great hopes for precision medicine. However, patient-derived xenografts (PDX) require six to eight months of continuous propagation. Regarding

the limited time for therapy and low engraftment rates of only 60% for CRC samples[60], this system is suitable for a minor patient subgroup. Nevertheless, the search of cancer treatments with tumour grafts could identify non-conventional drug combinations for patients in relapse[61]. This model resembles the primary tumour better than cell line xenografts with respect to gene expression, chromosomal stability and histology. However, increasing evidence suggests that strong clonal dynamics in the murine recipient result in divergent tumour evolution from the patient[62].

Economically, cancer models need improvement because only 6.7% of candidate drugs evaluated in clinical phase I achieve FDA approval[63]. The selection of anti-cancer substances could be improved with advanced *in vitro* systems. In the last seven years, three dimensional systems have evolved rapidly providing researchers with *in vitro* cultures of increased cellular diversity, termed organoids.

Organoid cultures rely on the ability of adult or induced pluripotent stem cells to self-renew and differentiate in a three-dimensional scaffold[64]. Here, I want to highlight their application as preclinical cancer model and more information will be provided later. Successful establishment of human tumour organoids is reported for a variety of organs, such as breast, colon, pancreas and prostate[65]. Compared to previous models, the success rate for *in vitro* cultivation of tumours is best in organoid culture. Engraftment rates are similar to current PDX rates with reduced costs and labour[65]. Furthermore, organoid cultures were found to preserve genetic and phenotypic stability after transplantation better than 2D cell lines[66]. Therefore, mouse and human organoids are now extensively used in CRC research.

By knockout of *APC* and activation of oncogenic *TP53* and *KRAS* mutations, murine colon organoids induced tumours after orthotopic transplantation in immunocompetent mice[67]. The tumours were restricted to the colon and transformation from adenoma to metastatic carcinoma was reported. In another study, human organoids were generated from normal mucosa. The TSGs *APC, TP53, SMAD4* were inactivated using CRISPR/Cas and oncogenic *KRAS* and *PIK3CA* were activated[68]. Xenografts from these engineered organoids and adenomas were compared for their metastatic potential and only adenomas metastasized to the liver indicating that further alterations are crucial for invasiveness.

Taken together, organoids and especially patient-derived tumour organoids have evolved as a novel powerful culture system that holds great promises for both basic and translational research. So far, research has focused on mouse and human organoids but little is known about the requirements for long-term organoid cultivation from other species. Although frequently used as laboratory animals, the mouse has critical limitations for preclinical research. Besides the most obvious drawbacks – size, lifespan and organ anatomy – murine cells transform faster in cell culture than human cells[69]. Furthermore, differences in immunology and drug metabolism can hamper the translation of pharmacological studies to the clinic[70,71]. As there is no ideal animal model for a particular disease, comparative studies including various models are necessary.

1.5. The need for large animal CRC models

Pigs are well suited to complement the already existing colorectal cancer models due to their similar size and lifespan to humans. Compared to other large animal models – like dogs, cats or primates – ethical restrictions are of minor concern[55]. Longitudinal studies could be performed over a period of 12-15 years[72] which is mandatory to detect rare oncogenic events similar to humans[73]. Human scale equipment makes the pig a valuable tool for medical training and its pharmacokinetic response replicates the human condition more closely than traditional preclinical models[74].

1.5.1. A porcine model of familial adenomatous polyposis

In order to meet the need for a large animal model for colorectal adenocarcinoma, a recombinant pig line was generated. An early stop codon was introduced in one *APC* allele at codon 1311, homologous to the nonsense substitution *APC*^{1309} found in some FAP patients[75]. Pigs carrying the targeted allele develop polyps throughout the colon and rectum within the first year of age. The line develops polyps which are similar to human neoplastic lesions in localisation, anatomy, morphology and histology. Like in humans, the severity of polyposis differs between pigs. Molecular analysis revealed that *TP53* mRNA expression is elevated in high-grade polyps compared to low grade samples[76]. Additionally, differential promoter methylation was detected in CpG islands of *TAP1*, a gene coding for an ATP-dependent transporter[77]. The downregulation of *TAP1* is associated with poor prognosis in CRC.

Although the *APC*$^{1311/WT}$ pig closely resembles early stage FAP, it currently fails to progress to advanced, metastatic disease. Therefore, two strategies were envisioned to accelerate tumour progression in the colon.

First, additional tumorigenic mutations should be introduced into epithelial cells of the colon to trigger invasion and metastasis *in vivo*. To this end, the TSGs *APC*, *p16INK4a*, *PTEN, SMAD4*, and *TP53*, will be inactivated by CRISPR/Cas and Cre-inducible KRAS-G12D will be activated. *SMAD4* is of particular interest because it is involved in growth inhibition via TGFβ signalling[78] and its inactivation is associated with invasiveness and poor prognosis in early and late stages of CRC[79].

Secondly, inflammation in the intestine induced by chronically high TNFα levels should stimulate tumour progression. For this purpose, pigs with a *TNF*$^{\Delta ARE}$ genotype similar to *TNF*$^{\Delta ARE}$ mice will be generated. Deleting elements, like the AU-rich element (ARE), in the 3' UTR of *TNF* disrupts the posttranscriptional regulation of TNFα transcript. Consequently, TNFα levels rise and have been shown to induce chronic inflammation of the gastrointestinal tract in *TNF*$^{\Delta ARE}$ mice[80]. Inflammation of the colon is associated with colorectal cancer and should enhance tumour progression in the *APC*$^{1311/WT}$ pig, as described in section 1.3.

1.5.2. Intestinal organoids from pig

The culture of epithelial cells is a valuable tool to understand the function of the intestine. However, primary cultures of human epithelial cells from the intestine were not available as long-term culture unless modified by introducing the human telomerase reverse transcriptase (hTERT) gene, for example[81]. Likewise, no efficient protocols existed for the cultivation of porcine intestinal epithelial cells.

In 2011, Clevers and Sato described the long-term culture of intestinal human biopsies from healthy tissue and tumours for the first time. The culture of intestinal cells demands factors that support stem cell renewal and differentiation. As a result, primary cells isolated from the intestine are propagated indefinitely[64]. Moreover, cells grow in a three-dimensional matrix, thus, the culture closely resembles the original tissue in cellular composition and architecture. Many studies have explored the potential of such *in vitro* systems, termed organoids, to model organ developmental and disease[82]. Intestinal organoids derived from biopsies, termed enteroids, preserve their native cellular diversity. The expression of markers indicative for stem cells and

differentiated cells was confirmed by single-cell RNA sequencing and immunofluorescence[83].

Organoids can be generated from several sources. In addition to intestinal biopsies, human enteroids were generated by direct reprogramming of foetal somatic cells[84] and differentiation of induced pluripotent stem cells (iPSCs)[85]. The protocol based on foetal somatic cells requires transient overexpression of transcription factors by retroviruses. In contrast, human enteroids can be generated more efficiently from iPSCs in media that direct differentiation to epithelial and mesenchymal lineages. Co-cultures of enteroids and mesenchymal cells, like myofibroblasts and smooth muscle cells, have the advantage of being more complex and thus more physiologically relevant.

Since embryonic stem cells and induced pluripotent stem cells are not available from the pig, the only source of porcine enteroids are crypts isolated from the intestine.

Table 2 summarizes the use of porcine enteroids from different parts of the intestine and shows that the age of pigs, the culture medium and the viability greatly differ between research groups.

Purpose of the study	Organ	Age	Medium	Viability	Ref.
Establishment of porcine cultures: 3D, 2D, suspension	colon	< 26 days	purified rec. factors	15 pa.	[86]
Improvement of viability	ileum	no data	L-WRN cond. medium	49 pa./ 174 days	[87]
Activation of an inducible oncogenic cassette (proof of concept)	colon	no data	IntestiCult™	no data	[88]
Improvement of 2D epithelial cultures	ileum	5 months	separate Wnt, noggin, and R-spondin cond. media	2D: 2 weeks	[89]
Bacterial infection	jejunum	20-30 months	IntestiCult™	13 pa./ 3 months	[90]
Role of glutamate for the health of the intestinal epithelium	jejunum	7 days	L-WRN cond. medium	12 pa.	[91,92]
Transmembrane 2D model for pathogen infection	ileum	20 weeks	IntestiCult™	no data	[93]
Rotavirus infection	ileum	3 weeks	IntestiCult™	≥ 54 pa.	[94]

Table 2: Use of porcine intestinal organoids in literature from 2015 – 03/2021. The use of intestinal organoids from pig is summarised with parameters critical for the viability of organoids. No correlation between viability and the other parameters can be deduced. Age of pigs varied from 7 days to 5 months. Purified recombinant factors, conditioned medium from different cell lines or commercial medium (IntestiCult™) were used in culture medium. The viability of organoids varied between 3 and 6 months and organoids were passaged (pa.) differently (every 3-10 days). Standardisation of porcine organoid culture is urgently needed to obtain consistent results.

Most research is conducted with enteroids from the small intestine (jejunum, ileum) and cultures from these parts are known to be more robust and viable than from colon which might be due to differences in the stem cell response towards differentiation stimuli *in vitro*[95]. Notably, considerable differences exist in culture media. Some groups rely on commercial formulations (IntestiCult™) which is optimised for human organoid culture and problems with the viability and differentiation of porcine enteroids are reported[94]. Conditioned media are an economic resource of growth factors but many cell lines are in use. All three essential factors, namely Wnt, noggin, and R-spondin 1, are currently produced by a single cell line or separate cell lines from different vendors and research groups. The comparison of cultures is complicated because the concentration of active protein in conditioned medium is not reported. Additionally, statements about the passage numbers must be considered carefully since cultures are splitted every third, seventh

or tenth day. Consequently, there are no reliable protocols for the cultivation and differentiation of porcine enteroids. Viability of 3D cultures usually does not exceed 3 months and the degree of differentiation might vary due to the poorly documented media composition.

1.6. The CRISPR/Cas9 system

In 2020, Emmanuelle M. Charpentier and Jennifer A. Doudna were awarded the Nobel prize in Chemistry for developing the CRISPR/Cas9 system which became a time- and cost-efficient tool widely used for precise genome editing of various species. Compared to previous site-specific nucleases (Zink Finger, Transcription Activator-like Effector Nucleases), this revolutionary system combines a single endonuclease, that introduces DNA double strand breaks, with short non-coding RNAs to specifically direct the nuclease to the target site[96]. These components were originally described in bacteria and archaea where they confer adaptive protection against foreign plasmid or viral DNA[97].

The system used in this work consist of two components derived from the Streptococcus pyogenes CRISPR system type II (Figure 9) which are Cas9 endonuclease and guide RNA. The guide RNA is an artificial fusion product of CRISPR-RNA (crRNA) linked to the trans-activating crRNA (tracrRNA). The crRNA is homologous to the 18-20 bp DNA target sequence that must be followed by the Cas9-specific protospacer adjacent motif (PAM) ‘NGG’. The tracrRNA mediates binding of crRNA and Cas9 to form the functional complex. Usually, the CRISPR/Cas9 complex introduces DNA double strand breaks 1-3 bp upstream of the PAM.

Strategies have been developed to edit several target sites simultaneously, called guide RNA multiplexing.

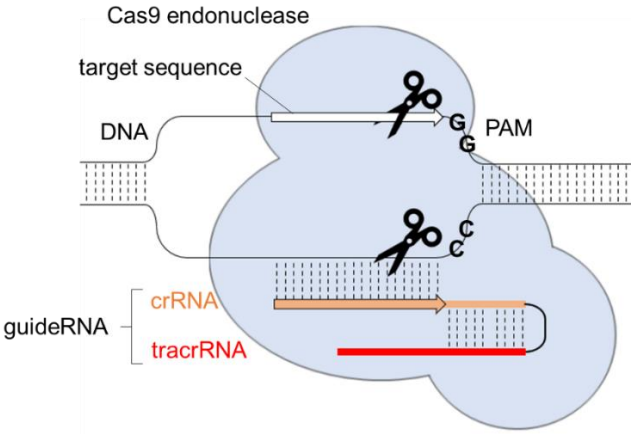

Figure 9: CRISPR/Cas9 complex induces site-specific DNA double strands. The CRISPR/Cas9 system consists of the Cas9 endonuclease and the artificial guide RNA which is a combination of the sequence of the crRNA and the trans-activating crRNA connected by an RNA linker. The crRNA contains 18-20 bp homology to the target sequence immediately upstream of the Cas9-specific PAM sequence (protospacer adjacent motif) NGG. The tracrRNA binds Cas9 to ensure complex formation of guide RNA and endonuclease to introduce a double strand break, typically 1-3 bp upstream of the PAM.

The CRISPR/Cas system is used to inactivate genes due to the error prone DNA double strand repair mechanism, called non-homologous end joining (NHEJ). Compared to homology directed repair, which uses a repair template with sufficient homology to the damaged region – usually the sister chromatid – NHEJ ligates DNA strands without template[98]. Typically, this mechanism results in the insertion or deletion of nucleotides which can result in frame shift of the coding sequence. Consequently, the mutation destroys the function of the gene – either by altering the protein coding sequence downstream of the mutation or by introducing a premature stop codon.

1.7. Objectives

The objective of this work was to optimise porcine enteroid culture to generate genetically modified intestinal enteroids which are supposed to accelerate colorectal cancer formation in pigs. To this end, crypts had to be isolated from porcine colon biopsies and cultivated in a three-dimensional matrix. Enteroids should grow in medium supplemented with conditioned media. Cell lines secreting Wnt or R-spondin were available but a new cell line had to be generated to produce porcine noggin conditioned medium. Another aim was to evaluate the cellular diversity of enteroids by qPCR and fluorescent microscopy.

Inactivation of TSGs was supposed to transform colon enteroids of FAP pigs which should initiate growth to invasive tumours after transplantation *in vivo.* In order to assess the ability of enteroids to be transformed, tools had to be developed. Efficient means of DNA delivery had to be tested to transfect enteroids with CRISPR/Cas9 constructs. Since five porcine TSGs (*APC, p16INK4a, PTEN, SMAD4, TP53*) had to be inactivated using CRISPR/Cas9, a guide RNA multiplexing strategy had to be developed. This strategy was based on the protocol described by Xie et al. and exploits the cellular tRNA-processing system to produce multiple guide RNAs from a single polycistronic gene[99]. A detailed description of the cloning strategy is provided in section 2.2.4. Besides inactivation of TSGs, the transforming potential of the KRAS-G12D oncogene had to be tested. Using in vitro assays, the tumorigenic phenotype of successfully transformed enteroids had to be characterised before autologous transplantation was performed.

As shown in mice[100], colonoscopy-based transplantation of CRISPR/Cas-edited colon organoids was assumed to initiate tumour formation in pigs. Modified cells that are transplanted under the colonic mucosa of the donor animal should avoid rejection of the transplant (autologous transplantation). However, the presentation of neoantigens was expected to cause depletion of transplanted enteroids by the immune system. Therefore, *B2M,* a gene relevant for antigen presentation on MHC class I molecules, had to be inactivated. In addition, *LEA29Y* expression of enteroids should inhibit T cell activity and improve dissemination of transformed enteroids.

Additionally, I worked on the generation of a pig edited in the *TNF* 3'UTR to induce inflammation in the porcine colon which should promote tumour formation after breeding with $APC^{1311/WT}$ pigs.

2. Materials and Methods

2.1. Material

2.1.1. Antibodies

Target	Origin	Company	Cat#	Dilution	Use
Primary Antibodies					
Human APC C-Terminus	goat IgG	R&D Systems	AF3695	1:1000	WB
human β2-microglobulin (2M2), biotinylated	mouse IgG1κ	BioLegend	316308	1:50	FACS
human CA II (G-2)	mouse IgG2a	Santa Cruz	sc-48351	1:200	IF
human Chromogranin A	mouse IgG1κ	Thermo Sc.	MA5-13096	1:200	IF
human HOP (E-1)	mouse IgG1	Santa Cruz	sc-398703	1:200	IF
human Ki-67 (SP6)	rabbit IgG	DCS Innovative Diagnostics	KI681C002	1:200	IF
human Lysozyme	rabbit IgG	abcam	ab74666	1:200	IF
human Mucin 2 (F-2)	mouse IgG1κ	Santa Cruz	sc-515032	1:200	IF
human Noggin	rabbit IgG	ThermoFisher	PA5-34595	1:1000	ELISA
human p16INK4A	rabbit IgG	Cell Signaling	4824	1:1000	WB
human p16INK4a (1D7D2)	mouse IgG1	Invitrogen	MA5-17054	1:1000	WB
human p53 (DO-1)	mouse IgG2a	Invitrogen	MA5-12571	1:1000	WB
human PTEN (1B8)	mouse IgG1	Invitrogen	MA5-15560	1:1000	WB
human SMAD4 (4G1C6)	mouse IgG1	Invitrogen	MA5-15682	1:1000	WB
human Sox9	rabbit IgG	MerckMillipore	AB5535	1:200	IF
human Villin (B-12)	mouse IgG2bκ	Santa Cruz	sc-373997	1:200	IF
Secondary Antibodies/Second-Step Reagent					
rabbit IgG-FITC	goat	Santa Cruz	sc-2012	1:400	IF
rabbit IgG (H+L)-Alexa Fluor 594	goat	invitrogen	A11012	1:400	IF
m-IgGκ BP-HRP	mouse	SantaCruz	sc-516102	1:1000	WB
mouse IgG-Alexa Fluor 594	donkey	Jackson	715-545-150	1:400	IF
mouse IgG-FITC	rat	BioLegend	406001	1:400	IF
rabbit IgG -HRP	donkey	Rockland	discontinued	1:1000	ELISA
streptavidin-PE		BD Biosciences	554061	1:200	FACS

2.1.2. Eukaryotic cells

2.1.2.1. Enteroids

Pig#	Genotype	Tissue
910	*APC*$^{1311/WT}$	colon: polyp
1336	*APC*$^{1311/WT}$	colon: polyp
1508	*APC*$^{1311/WT}$	colon: polyp
1563	*APC*$^{1311/WT}$	colon: polyp
1566	*APC*$^{1311/WT}$	colon: polyp
1665	*APC*$^{1311/WT}$	colon, duodenum: normal mucosa, polyp
305	*APC*$^{1311/WT}$ *KRAS*$^{LSL\text{-}G12D/WT}$	colon: normal mucosa
1636	*APC*$^{1311/WT}$ *KRAS*$^{LSL\text{-}G12D/WT}$	colon: polyp
1658	*APC*$^{1311/WT}$ *KRAS*$^{LSL\text{-}G12D/WT}$	colon: polyp
1664	*APC*$^{1311/WT}$ *KRAS*$^{LSL\text{-}G12D/WT}$	colon: polyp
1776	*Cas9*	colon: normal mucosa
1955	*Cas9 TP53*$^{R167H/WT}$	colon, duodenum: normal mucosa
1800	*Cas9 APC*$^{1311/WT}$	colon: normal mucosa
1882	*Cas9 APC*$^{1311/WT}$ (severe polyposis)	colon, duodenum: normal mucosa
1885	*Cas9 APC*$^{1311/WT}$ (mild polyposis)	colon, duodenum: normal mucosa
395	*Cas9 KRAS*$^{LSL\text{-}G12D/WT}$	colon: normal mucosa
393	*KRAS*$^{LSL\text{-}G12D/WT}$	colon: normal mucosa
939	*KRAS*$^{LSL\text{-}G12D/WT}$	colon, duodenum: normal mucosa
1908	*TGROSA KRAS*$^{LSL\text{-}G12D/WT}$	colon, normal mucosa
1689	*TNF*$^{\Delta(ARE\ CDE1)/\Delta(ARE\ CDE1)}$	ileum: normal mucosa
1692	*TNF*$^{\Delta(ARE,\ CDE1)/\Delta(ARE,\ CDE1)}$	ileum: normal mucosa
1729	*TP53*$^{R167H/WT}$	colon, duodenum: normal mucosa
1027	*TP53*$^{R167H/R167H}$	colon: normal mucosa
1260	*TP53*$^{R167H/R167H}$	colon: normal mucosa
1619	*TP53*$^{R167H/R167H}$	colon: normal mucosa
1528	*WT*	colon: normal mucosa
1694	*WT*	colon, duodenum: normal mucosa
1777	*WT*	colon, duodenum: normal mucosa

2.1.2.2. Mammalian 2D cell culture

Name	**Source**
CHO cell line	Chair of Livestock Biotechnology, TUM, Freising, GER
HEK293 cell line	Chair of Livestock Biotechnology, TUM, Freising, GER
HEK293T cell line	Chair of Livestock Biotechnology, TUM, Freising, GER
primary kidney-derived cells	Chair of Livestock Biotechnology, TUM, Freising, GER (several preparations)
primary kidney-derived cells, isolate #202111	Dr. Daniela Huber, Chair of Livestock Biotechnology, TUM, Freising, GER

2.1.3. Prokaryotic cells

Name: *E. coli* ElectroMAX DH10B

Genotype: F⁻*mcr*A Δ(*mrr-hsd*RMS-*mcr*BC) Φ80*lac*ZΔM15 Δ*lac*X74 *rec*A1 *end*A1 *ara*D139Δ(*ara, leu*)7697 *gal*U *gal*K λ⁻*rps*L *nup*G

Source: Thermo Fisher Scientific, Waltham, MA, USA

2.1.4. Buffers and solutions

Type	**Component**	**Quantity**
APS 10%	$(NH_4)S_2O_8$	0.1 g/mL (aq)
Blocking buffer for western blot	Milk powder	5% (m/v) (1x TBST)
DNA miniprep solution I	Sucrose EDTA Tris water	1.7 g 2.9 g 3.0 g Add to 1 L
DNA miniprep solution II	NaOH SDS water	8.0 g 10.0 g add to 1 L
DNA miniprep solution III	sodium acetate water	246.1 g Add to 1 L
Electropermeabilisation buffer pH = 7.2	KCl $MgCl_2$ Na_2HPO_4 NaH_2PO_4	5 mM (aq) 10 mM (aq) 70 mM (aq) 70 mM (aq) filtrated 0.22 µm
Electrophoresis running buffer 10x	Tris glycine SDS water	30 g 144 g 10 g add to 1 L
ELISA antibody dilution	BSA	1% (m/v) (PBS),

buffer		filtrated 0.45 µm
ELISA blocking buffer	BSA	2% (m/v) (PBS)
ELISA stop solution 0.5 M sulfuric acid	96% sulfuric acid water	2.7 mL add to 100 mL
ELISA wash buffer	Tween 20	0.05% (v/v) (PBS)
FACS wash buffer	BSA NaN_3 PBS	500 mg 100 mg add to 100 mL
Immunofluorescence staining buffer	BSA	4% (m/v) (1x TBST)
Lämmli buffer 4x	0.5 M Tris-HCl, pH 6.8 10% SDS Sucrose DTT 1 M Saturated bromophenol blue water	5 mL 4 mL 4 g 260 µL 110 µL Add to 10 mL
SDS 10%	SDS	10% (m/v) (aq)
Semi-dry blotting buffer	Tris glycine methanol SDS H2O	3.0 g 14.4 g 200 mL 1.0 g add to 1 L
TAE, 50x	Tris 0.5M EDTA acetic acid water	242 g 100 mL 57.1 mL add to 1 L
TBE, 10x	Tris boric acid EDTA water	545 g 275 g 39.2 g add to 5 L
TBS, 10x	Tris NaCl water	24.2 g 80 g add to 1 L
TBST, 1x	10x TBS Tween 20 water	100 mL 1 mL add to 1 L
Tris-HCl 0.5 M, pH 6.8	Tris water	15.1 g add to 250 mL
Tris-HCl 1 M, pH 8.8	Tris water	30.3 g add to 250 mL
Western Blot running buffer, 10x, pH = 8.3	Tris glycine SDS water	30 g 144 g 10 g add to 1 L

2.1.5. Chemicals and Reagents

Name	**Source**
Acetic acid ($C_2H_4O_2$)	AppliChem, Darmstadt, GER
Acrylamide, Rotiphorese Gel 29:1	Carl Roth, Karlsruhe, GER
Advanced protein assay reagent	Cytoskeleton, Denver, USA
Agarose	Sigma-Aldrich, Steinheim, GER
Ammonium chloride (NH_4Cl)	Sigma-Aldrich, Steinheim, GER
Ammonium persulphate ($(NH_4)_2S_2O_8$)	Carl Roth, Karlsruhe, GER
B27 Supplement (50X)	Thermo Fisher Scientific, Waltham, USA
Bromophenol blue	Sigma-Aldrich, Steinheim, GER
BSA (fraction V)	Biomol, Hamburg, GER
Calcium chloride dihydrate ($CaCl_2$ x 2 H_2O)	Sigma-Aldrich, Steinheim, GER
CHIR-99021 HCl (CT99021)	Selleck Chemicals, Houston, USA
Deoxynucleotide (dNTP) solution mix	New England Biolabs, Frankfurt, GER
DTT ($C_4H_{10}O_2S_2$)	Omnilab-Laborzentrum, Bremen, GER
EDTA	AppliChem, Darmstadt, GER
eFluor780 viability dye	Thermo Fisher Scientific, Waltham, USA
Epidermal Growth Factor, human, recombinant	Invitrogen, Karslruhe, GER
ELISA substrate solution 1x TMB	Sigma-Aldrich, Steinheim, GER
Ethanol (EtOH) absolute	Fisher Scientific, Loughborough, GBR
Fluorescein diacetate	Sigma-Aldrich, Steinheim, GER
Formaldehyde solution 37% (CH2O)	AppliChem, Darmstadt, GER
Galunisertib (LY2157299)	Selleck Chemicals, Houston, USA
Gastrin I, human (L-Gastrin)	Sigma-Aldrich, Steinheim, GER
Gel loading dye purple (6x)	New England Biolabs, Frankfurt, GER
Glycerol anhydrous (C3H8O3)	AppliChem, Darmstadt, GER
Glycine ($C_2H_5NO_2$)	Carl Roth, Karlsruhe, GER
HEPES	Sigma-Aldrich, Steinheim, GER
IPTG	Bioline, Luckenwalde, GER
IWR1-endo	Selleck Chemicals, Houston, USA
Matrigel, growth factor reduced	Corning B.V. Live Sciences, Amsterdam, NL
Magnesium chloride hexahydrate ($MgCl_2$ x 6 H_20)	Carl Roth, Karlsruhe, GER
Methanol (CH_3OH)	Sigma-Aldrich, Steinheim, GER
Milk powder, blocking grade	Carl Roth, Karlsruhe, GER
N-Acetyl-L-cystein	Sigma-Aldrich, Steinheim, GER

N2 Supplement (100x)	Thermo Fisher Scientific, Waltham, USA
Nicotinamide	Sigma-Aldrich, Steinheim, GER
Noggin, human, recombinant	Peprotech, Hamburg, GER
NP40 Cell Lysis Buffer	Invitrogen, Carlsbad, USA
peqGREEN dye	VWR International, Ismaning, GER
Pierce ECL Plus western blotting substrate	Thermo Fisher Scientific, Waltham, USA
Potassium bicarbonate ($KHCO_3$)	Sigma-Aldrich, Steinheim, GER
Potassium chloride (KCl)	Carl Roth, Karlsruhe, GER
Propan-2-ol (C_3H_8O)	Fisher Scientific, Loughborough, GBR
Propidium Iodide	Sigma-Aldrich, Steinheim, GER
Proteinase inhibitor cocktail (PIC) tablets, Mini EASY pack	Roche Diagnostics, Mannheim, GER
R-spondin 1, human, recombinant	Peprotech, Hamburg, GER
SB202190	Sigma-Aldrich, Steinheim, GER
SDS	Omnilab-Laborzentrum, Bremen, GER
Sodium acetate ($C_2H_3NaO_2$)	AppliChem, Darmstadt, GER
Sodium bicarbonate ($NaHCO_3$)	Sigma-Aldrich, Steinheim, GER
Sodium chloride (NaCl)	AppliChem, Darmstadt, GER
Sodium dihydrogen phosphate monohydrate	Merck, Darmstadt, GER
TEMED ($C_6H_{16}N_2$)	Carl Roth, Karlsruhe, GER
Thiazovivin	Sigma-Aldrich, Steinheim, GER
TransDux Virus Transduction Reagent (200x)	BioCat GmbH, Heidelberg, GER
Tris, ultrapure ($C_4H_{11}NO_3$)	AppliChem, Darmstadt, GER
Tris-HCl ($C_4H_{11}NO_3$ x HCl)	Sigma-Aldrich, Steinheim, GER
Tri-sodium citrate dihydrate ($C_6H_5NaO_7$ x 2 H_2O)	AppliChem, Darmstadt, GER
Triton-X100	Omnilab-Laborzentrum, Bremen, GER
Trypan blue solution	Sigma-Aldrich, Steinheim, GER
Tween 20	Sigma-Aldrich, Steinheim, GER
Vectashield Antifade Mounting Medium with DAPI (H-1200-10)	Vector Laboratories, Burlingame, USA
Wnt3a, murine, recombinant	PromoCell GmbH, Heidelberg, GER
X-Gal	Bioline, Luckenwalde, GER
X-ray developer T32	Calbe Chemie GmbH, Calbe, GER
X-ray fixing solution Superfix 25	Tetenal Europe, Norderstedt, GER

2.1.6. Consumables

Name	**Source**

Cellstar tubes (15 ml and 50 ml)	Greiner Bio-One, Frickenhausen, GER
Cloning rings	Brand, Wertheim, GER
Cover slips (24x 60 mm)	Menzel, Braunschweig, GER
Cryo vials	Corning Incorporated, Corning, USA
DG8 cartridge for QX200 droplet generator	Bio-Rad Laboratories, Hercules, USA
DG8 gasket	Bio-Rad Laboratories, Hercules, USA
Electroporation cuvette (2 mm)	Peqlab Biotechnologie, Erlangen, GER
Electroporation cuvette (4 mm)	Bio-Rad Laboratories, Hercules, USA
ELISA plate “Costar EIA/RIA plate 96 well”	Corning Incorporated, Corning, USA
Filter paper (extra thick blot paper)	Biorad Laboratories, Munich, GER
Filter pipette tips „Fisherbrand Sure One“	Fisher Scientific, Hampton, USA
Glass pasteur pipettes	Brand, Wertheim, GER
MicroAmp fast optical 96-Well reaction plates	Life Technologies, Carlsbad, USA
Microscope slide “Menzel Gläser Superfrost Plus”	Thermo Fisher Scientific, Waltham, USA
Needles, blunt, 18G	BBraun, Melsungen, GER
Nunc MaxiSorp 96 well plate	Thermo Fisher Scientific, Waltham, USA
PCR tubes 0.2 ml 8-Strip PCR tubes	Starlab, Hamburg, GER
Petri dishes	Greiner Bio-One, Frickenhausen, GER
Phase lock gel pierceable foil heat seal	Bio-Rad Laboratories, Hercules, USA
Pipette tips	Brand, Wertheim, GER
Plastic pipettes “Costar Stipette” (1-50 ml)	Corining Incorporated, Corning, USA
PVDF membrane “Roti-PVDF; 0.45 µm)	Carl Roth, Karlsruhe, GER
Reaction tubes (1.5 ml and 2 ml)	Zefa Laborservice, Harthausen, GER
Reaction tubes (5 ml)	Starlab, Hamburg, GER
Scalpel	Braun, Melsungen, GER
Sterile filters 0.22 µm, 0.45 µm	Berrytec, Grünwald, GER
Syringes BD	Bioscience, Le Pont De Claix, FRA
Tissue culture flasks (T25, T75, T150)	Corning Incorporated, Corning, USA
Tissue culture plates (10 cm, 15 cm, 6well, 12well, 24well, 48well)	Corning Incorporated, Corning, USA
Tubes (14 ml)	Corning Incorporated, Corning, USA
X-Ray film “Cronex 5”	Agfa Healthcare, Mortsel, BEL

2.1.7. Enzymes and their buffers

Name	**Source**
Calf intestinal phosphatase	New England Biolabs, Frankfurt, GER
ddPCR supermix for probes (no	Bio-Rad Laboratories, Hercules, USA

dUTP) 2x	
DNA polymerase I large (Klenow) fragment	New England Biolabs, Frankfurt, GER
GoTaq G2 DNA polymerase	Promega, Mannheim, GER
5x Green GoTaq reaction buffer	Promega, Mannheim, GER
Proteinase K (20 mg/ml)	Sigma-Aldrich, Steinheim, GER
Q5 high-fidelity DNA polymerase	New England Biolabs, Frankfurt, GER
5x Q5 reaction buffer	New England Biolabs, Frankfurt, GER
5x Q5 high GC enhancer	New England Biolabs, Frankfurt, GER
Restriction endonucleases	New England Biolabs, Frankfurt, GER
Restriction buffers 1.1, 2.1, 3.1, CutSmart	New England Biolabs, Frankfurt, GER
RNAse A	Sigma-Aldrich, Steinheim, GER
T4 DNA ligase	New England Biolabs, Frankfurt, GER
T4 DNA ligase buffer (10x)	New England Biolabs, Frankfurt, GER
TaqMan Fast Universal PCR master mix	Life Technologies, Carlsbad, USA
AccuStart Taq DNA polymerase HiFi	NIPPON Genetics Europe, Düren, GER
10x HiFi PCR buffer	QuantaBio, Beverly, USA
2x FastGene Optima HotStart ready mix	NIPPON Genetics Europe, Düren, GER

2.1.8. Equipment

Name	**Source**
Attune NxT flow cytometer	Thermo Fisher Scientific, Waltham, USA
Automated cell counter 'Countess'	Invitrogen, Carlsbad, USA
Blue light table	Serva, Heidelberg, GER
Centrifuges 'Sigma 3-16', 'Sigma 1-15K', 'Sigma 1-15', 'Sigma 4K15'	Sigma, Osterode, GER
CO_2 incubator 'Forma Steri-Cycle 371'	Thermo Fisher Scientific, Waltham, USA
Cryo 1°C freezing container 'Mr. Frosty'	Thermo Fisher Scientific, Waltham, USA
Droplet generator 'QX200'	Bio-Rad Laboratories, Hercules, USA
Droplet reader 'QX200'	Bio-Rad Laboratories, Hercules, USA
ECM 830 Square Wave Electroporation System	BTX, Holliston, USA
Electrophoresis system (buffer chamber, gel trays, combs)	Peqlab Biotechnologie, Erlangen, GER
Electroporator 'Multiporator'	Eppendorf, Hamburg, GER
ELISA reader 'Multiscan Ex'	Thermo Fisher Scientific, Waltham, USA
Freezer -20°C 'GS 2481'	Liebherr, Bulle, SUI
Freezer -80°C 'Forma 900 Series'	Thermo Fisher Scientific, Waltham, USA
Fridge 'TSE1283'	Beko, Neu-Isenburg, GER

Gel documentation imaging system 'Quantum ST5'	Vilber Lourmat, Eberhardzell, GER
Glasware	Marienfeld GmbH, Landa, GER
iBind™ Western Device	Thermo Fisher Scientific, Waltham, USA
Ice maker	Manitowoc Ice, Manitowoc, USA
Incubator 'BD115'	Binder, Tuttlingen, GER
LUMIstar Omega Microplate Luminometer	BMG Labtech, Ortenberg, GER
Magnet 'Dynamag-15'	Life Technologies, Carlsbad, USA
Magnetic stirrer 'AREC X'	VELP Scientific, Usmate, ITA
Microscope 'Axiovert 40CLF', 'Axiovert 200M', 'Primo Star'	Carl Zeiss, Jena, GER
Microwave 'MW17M70G-AU'	MDA Haushaltswaren, Barsbüttel, GER
Mini centrifuge 'perfect spin mini'	Peqlab Biotechnologie, Erlangen, GER
NanoDrop Lite Spectrophotometer	Thermo Fisher Scientific, Waltham, USA
Orbital shaker	Thermo Fisher Scientific, Waltham, USA
PCR cycler 'peqStar 2x'	Peqlab Biotechnologie, Erlangen, GER
PCR cyler 'DNA Engine DYAD PTC-220'	BioRad Laboratories, Munich, GER
PCR plate sealer 'PX1'	Bio-Rad Laboratories, Hercules, USA
Pipettes “Pipetman” (0.2-2 µl; 2-20 µl; 20-200 µl; 200-1000 µl)	Gilson, Middleton, USA
Plate centrifuge 'MPS 100'	Labnet International, Edison, USA
Radiographic cassette 24x30cm	Rego X-Ray GmbH, Augsburg, GER
Real-time PCR cycler 7500 Fast	Thermo Fisher Scientific, Waltham, USA
Rocker shaker 'Unitwist 3-D'	Uniequip, Munich, GER
Safety cabinet 'HERAsafe HS 12'	Kendro Laboratory Products, Hanau, GER
Thermal printer 'P95'	Mitsubishi Electric, Kyoto, JPN
Vortex mixer 'Vortex Genie 2'	VELP Scientifica, Usmate, ITA
Water bath 'WNB22'	Memmert, Schwabach, GER
Western blot 'Mini PROTEAN tetra handcast system'	Biorad Laboratories, Munich, GER

2.1.9. Kits

Name	**Source**
AllPrep DNA/RNA Micro, Macro kit	Qiagen, Hilden, Austria
CloneJET PCR Cloning Kit	Thermo Fisher Scientific, Waltham, USA
CytoBuster protein extraction reagent Merck KGaA	Merck, Darmstadt, GER
Firefly & Renilla Luciferase Single Tube	Biotium, Fremont, USA

Assay Kit	
GenElute mammalian genomic DNA miniprep kit	Sigma-Aldrich, Steinheim, GER
iBind™ Solution Kit	Thermo Fisher Scientific, Waltham, USA
Mix2Seq kit	Eurofins, Ebersberg, GER
NucleoBond Xtra Maxi kit	Macherey-Nagel, Düren, GER
NucleoBond Xtra Midi kit	Macherey-Nagel, Düren, GER
Ras Activation Assay Kit	Merck, Darmstadt, GER
SuperScript III/IV reverse transcriptase kits	Invitrogen, Karslruhe, GER
Wizard SV gel and PCR clean-up system	Promega, Mannheim, GER

2.1.10. Ladders

Name	**Source**
1 kb DNA ladder	New England Biolabs, Frankfurt, GER
2-log DNA ladder (0.1-10.0 kb)	New England Biolabs, Frankfurt, GER
Colour prestained protein standard broad range (11-245 kDa)	New England Biolabs, Frankfurt, GER
Ribo Ruler high range RNA ladder	Thermo Scientific, Waltham, USA
2x RNA loading dye	Thermo Scientific, Waltham, USA

2.1.11. Media, supplements and reagents

Name	**Source**
Accutase	Sigma-Aldrich, St. Louis, USA
Advanced DMEM/F12	Sigma-Aldrich, St. Louis, USA
Ala-Gln 200 mM	Sigma-Aldrich, St. Louis, USA
Ammonium persulfate	Carl Roth, Karlsruhe, GER
Amphotericin B	Sigma-Aldrich, St. Louis, USA
Ampicillin ($C_{16}H_{19}N_3O_4S$)	Carl Roth, Karlsruhe, GER
Cell culture water	Sigma-Aldrich, St. Louis, USA
Chloramphenicol ($C_{11}H_{12}Cl_2N_2O_5$)	Sigma-Aldrich, Steinheim, GER
Collagenase type IA (C2674)	Sigma-Aldrich, St. Louis, USA
DMEM-high glucose	Sigma-Aldrich, St. Louis, USA
DMSO	Sigma-Aldrich, St. Louis, USA
FBS Superior	Biochrom GmbH, Berlin, GER
G418 sulphate	Genaxxon Bioscience, Ulm, GER
LB agar, Miller (Luria-Bertani)	Difco BD, Sparks, MD, USA
Lipofectamine 2000	Thermo Fisher Scientific, Waltham, USA
Luria Broth, Base, Miller	Difco BD, Sparks, MD, USA
MEM non-essential amino acid solution 100x	Sigma-Aldrich, St. Louis, USA

Penicillin/Streptomycin (in PBS)	Sigma-Aldrich, St. Louis, USA
Primocin	Invivogen, San Diego, USA
Puromycin	InvivoGen, San Diego, USA
Sodium pyruvate solution 100 mM	Sigma-Aldrich, St. Louis, USA
Trypan blue	Life Technologies, Paisley, GBR
TrypLE Express	Thermo Fisher Scientific, Waltham, USA

2.1.12. Vectors

Name	**Source**
pX330-U6-Chimeric_BB-CBh-hSpCas9-T2A-puro_MCS	Dr. Oskar Ortiz Sanchez, Helmholtz Zentrum München, Oberschleißheim, GER
pCAG-Cas9-bpA	Dr. Oskar Ortiz Sanchez, Helmholtz Zentrum München, Oberschleißheim, GER
pcDNA3.1-hygro-mutCIITA	Dr. Konrad Fischer, TUM, Freising, GER
pPGK-Cre-bpA	Dr. Tatiana Flisikowska, TUM, Freising, GER
pcDNA3.1-EGFP	Dr. Tatiana Flisikowska, TUM, Freising, GER
pGL4-PGK-Firefly	Dr. Benjamin Schusser, TUM, Freising, GER
pcDNA-Wnt3a	Addgene Cat#35908, Watertown, USA

2.1.13. Webtools and Software

Name	**Source**
Cellpose algorithm for cellular segmentation (https://www.cellpose.org/)	HHMI Janelia Farm Research Campus, Ashburn, USA
Chromatogram viewer software 'Finch TV'	Geospiza Inc., Seattle, USA
Crispr design tool (http://crispr.mit.edu/)	Zhang Lab, MIT, Cambridge, USA
ddPCR software 'QuantaSoft Software'	Bio-Rad Laboratories, Hercules, USA
Flow cytometry software 'FlowJo'	FlowJo LLC, Ashland, USA
Gel documentation software 'Quantum ST5 v16.15'	Vilber Lourmat, Eberhandzell, GER
Genome database 'Ensembl' (https://www.ensembl.org/index.html)	EMBL-EBI, Hinxton, GBR
ICE Analysis tool Synthego (https://ice.synthego.com)	Synthego, Redwood City, USA
ImageJ/Fiji (https://imagej.net/Fiji)	University of Wisconsin, Madison, USA
Microscope software 'Axio Vision'	Carl Zeiss, Göttingen, GER
Multi-user Reader Control and MARS Data Analysis Software	BMG Labtech, Ortenberg, GER
Primer design tool 'Primer3' (http://primer3.ut.ee/)	Whitehead Institute for Biomedical Research, Cambridge, USA
qPCR software '7500 fast real time PCR	Applied Biosystems, Carlsbad, USA

system'	
Rstudio (https://www.rstudio.com/)	Boston, USA
Sequence alignment tool 'Clustal Omega' (https://www.ebi.ac.uk/Tools/msa/clustalo/)	EMBL-EBI, Hinxton, GBR
TIDE: Tracking of Indels by DEcomposition (https://tide.deskgen.com/)	Desktop Genetics, London, GBR
Vector design software 'benchling' (https://www.benchling.com/)	San Francisco, USA

2.2. Methods

2.2.1. Microbiological methods

2.2.1.1. Culture of bacterial cells

DH10B electrocompetent cells were used for amplification of plasmids (for molecular cloning) and vectors (for mammalian cell culture). Transformed cells were selected on LB-agar plates supplemented with 100 µg/mL ampicillin overnight at 37°C. Single cell clones carrying the correct construct were identified by Colony PCR (section 2.2.2.7). Single colonies were used to inoculate 5 or 100 mL LB-medium (Mini- or Midiprep) and grown under constant shaking (210 rpm) at 37°C overnight.

2.2.1.2. Cryoconservation of bacterial cells

Bacteria were cryoconserved by mixing an aliquot of 0.5 mL of the overnight culture with the same volume of 99% glycerol. The suspension was stored at -80°C.

2.2.1.3. Electropermeabilisation of bacterial cells

Electropermeabilisation was used to deliver plasmid DNA into DH10B cells. Existing Midipreps were diluted 1:10 000 in water and 2 µL of the dilution was mixed with 50 µL of freshly thawed DH10B preparations. Transformation with ligation products was conducted with 4 µL of the ligation reaction in 50 µL of DH10B suspension. Electropermeabilisation was performed with a single pulse of 2.5 kV for 5 ms using the Eppendorf Multiporator. Cells were plated on ampicillin-supplemented LB-agar to select for successfully transformed cells.

2.2.1.4. Isolation of plasmid DNA from bacteria

Depending on the required amount and purity of plasmids amplified in DH10B cells, bacterial overnight cultures were either processed according to the inhouse Miniprep DNA precipitation protocol or the commercial column-based Midiprep kit. Purified DNA was stored at -20 °C.

2.2.1.5. Miniprep

The inhouse Miniprep protocol was applied to bacterial overnight cultures of 5 mL to verify the correct assembly of DNA in plasmids by restriction digest, for example. The method includes an alkaline lysis step followed by ethanol precipitation of total DNA.

Overnight cultures were harvested by centrifuging 2 mL of the bacterial suspension and resuspending the pellet in 100 µL equilibration solution I. The suspension was mixed with 200 µL of lysis solution II and incubated for 3 min at RT. Lysis was stopped by adding 150 µL of neutralisation solution III. The sample was shaken and incubated for 30 min on ice. The mixture was centrifuged for 5 min at 13227xg and the precipitate was washed with 95 %, 80%, and 95% ethanol. The pellet was air-dried and dissolved in 50 µL of nuclease-free water.

2.2.1.6. Midiprep

In order to purify large amount of vectors with high purity and low endotoxin concentrations for transfection in mammalian cell culture, bacterial overnight cultures of 100 mL were processed with the NucleoBond® Xtra Midi Kit according to the manufacturer's instructions. The purified DNA was solved in 100 µL of nuclease-free water.

2.2.2. Molecular biological methods

2.2.2.1. Isolation of genomic DNA and RNA from mammalian cell culture

Total RNA and genomic DNA was purified with the AllPrep DNA/RNA Micro Kit for sequencing of PCR products and qPCR. Cells were harvested and pelleted at 300xg for 5 min. The cell pellet was either stored at -80°C or immediately processed according to the manufacturer's instructions. DNA was isolated in 50 µL of nuclease-free water, RNA in 14 µL, respectively. Purified DNA was stored at -20 °C, RNA was stored at -80°C.

2.2.2.2. Quick extract

DNA was isolated from dissociated cells using QuickExtract to perform Screening PCR of genetically modified porcine single cell clones. Cells were pelleted and resuspended in 30-50 µL QuickExtract™ DNA extraction solution. The sample was lysed by incubation at 65°C for 15 min followed by heat inactivation at 95°C for 8 min.

2.2.2.3. Purification and quality control of RNA

Residual genomic DNA was removed from RNA isolates using the TURBO DNA-free™ kit according to the manufacturer's instructions. The amount of DNA contamination and the degree of RNA degradation was evaluated on a 0.8% agarose-TBE gel containing 0.3% formaldehyde. An aliquot of 4 µL was mixed with loading dye, denatured for 10 min at 70°C and chilled on ice for 5 min. Intact RNA samples show two distinct bands for 18S and 28S ribosomal RNA after gel electrophoresis.

2.2.2.4. Concentration measurement of DNA and RNA

The concentration of nucleic acids was measured with the NanoDrop® Lite according to the manufacturer's instructions.

2.2.2.5. Synthesis of cDNA

RNA was reverse transcribed into cDNA with the SuperScript® III or IV Reverse Transcriptase kit and RNase inhibitor. Random hexamers and 200-500 ng total RNA were used for cDNA synthesis.

2.2.2.6. Polymerase chain reaction (PCR)

DNA was amplified using different polymerases. For the final detection of genotypes by gel electrophoresis GoTaq® G2 Polymerase was used. Q5® High-fidelity Polymerase was applied for templates longer than 2 kb and for generating blunt end amplicons that were required for molecular cloning with the CloneJet PCR Cloning kit. In Table 3 the polymerases are listed with their specifications.

GoTaq® G2 Polymerase: generates A-overhang on PCR products

PCR mix		**Thermocycler settings**			
Component	**Final conc.**	**Cycling step**	**T [°C]**	**Time**	**Number of cycles**
DNA or cDNA	50-100 ng or 2 µL	Initial Denaturation	95	2 min	1
5x GoTaq® Buffer	1x	Denaturation	95	30 sec	35-40
dNTPs	4x 200 µM	Annealing	58-65	30 sec	
Forward primer	0.2 µM	Extension	72	1 min/kb	
Reverse primer	0.2 µM	Final Extension	72	5 min	1
GoTaq® G2	1.25 units	Storage	8	infinite	

DNA Polymerase					
Nuclease-free water	add to 50 µL				

Q5® High Fidelity DNA Polymerase: generates blunt end products

PCR mix		**Thermocycler settings**			
Component	**Final conc.**	**Cycling step**	**T [°C]**	**Time**	**Number of cycles**
DNA or cDNA	50-100 ng or 2 µL	Initial Denaturation	98	30 sec	1
5x Q5® Reaction Buffer	1x	Denaturation	98	30 sec	35
dNTPs	4x 200 µM	Annealing	58-65	30 sec	
Forward primer	0.5 µM	Extension	72	30 sec/kb	
Reverse primer	0.5 µM	Final Extension	72	2 min	1
Q5® High Fidelity DNA Polymerase	0.01 units	Storage	8	infinite	
Nuclease-free water	add to 50 µL				

Table 3: Polymerase specific PCR mixtures and thermocycler settings

2.2.2.7. Colony PCR

The correct assembly of DNA fragments into plasmids and vectors was tested by PCR with single bacterial colonies resuspended in GoTaq® PCR mix. Primers were used that bind in each of the ligated fragments. Bacterial colonies carrying the correct plasmid were plated on a fresh LB-agar with antibiotic for postponed Midiprep.

2.2.2.8. Agarose gel electrophoresis

DNA fragments and PCR products were separated in agarose gels by electrophoresis. In order to visualise the presence of DNA fragments with a specific length, gels were prepared with TBE buffer. If the fragments were used for molecular cloning or sequencing TAE buffer was chosen. The concentration of agarose varied between 0.8 and 2% (m/v) depending on the density of agarose necessary to separate single fragments. Using 4 µL of peqGREEN® per 100 mL of gel, DNA was visualised by fluorescence under UV light. Samples were loaded with loading dye at a ratio of 4:1. Gels were run for 1-3 h at 80-120 V and images were taken using the

Bio Imaging System Quantum ST5. DNA fragments were excised with a scalpel under black light for DNA extraction and molecular cloning.

2.2.2.9. DNA extraction and purification

DNA from PCR, T4 ligation, blunting reactions and TAE gels was extracted and purified with the Wizard® SV Gel and PCR Clean-Up System according to the manufacturer`s instructions.

2.2.2.10. Ligation

DNA fragments were ligated using T4 DNA ligase. The reaction was performed according to the manufacturer's instructions. The mix was either incubated for 2 h at RT or at 16°C overnight. Blunt-end PCR products were ligated with the pJet backbone according to the CloneJET PCR Cloning Kit protocol.

2.2.2.11. Restriction digest

Analytical digests were performed to verify the size and elements of plasmids, whereas preparative digests were used to excise fragments for further cloning or transfection of mammalian cells. The enzymes and corresponding buffers were purchased from NEB. Table 4 summarizes the two reaction protocols.

	Final concentration	
Digest mix	**Analytical digest**	**Preparative digest**
DNA	10 ng/µL	100-200 ng/µL
NEB Buffer	1x	1x
Enzyme	0.1-0.2 U/µL	1-2 U/µg DNA
ddH_2O	add to 30 µL	add to 50 µL
Incubation time	15-30 min	2 h

Table 4: Conditions for analytical and preparative digests. The optimal temperature and buffer were chosen according to the manufacturer's instructions.

2.2.2.12. Blunting of DNA fragments

If no compatible overhangs could be generated on DNA fragments for ligation, the overhangs were removed (blunted) using the DNA polymerase I Large (Klenow) Fragment. Although blunt-end fragments can be ligated by T4 DNA ligase, the efficiency is dramatically reduced. Table 5 shows the blunting reaction mix.

Blunting mix	**Final concentration**
Digest mix	50 µL
dNTPs	4x 33 µM
DNA polymerase I Large (Klenow) Fragment	1 U/µg DNA

Table 5: Conditions for blunting of DNA with DNA Polymerase I Large (Klenow) Fragment

The mix was incubated for 15 min at 25°C and inactivated by adding EDTA to a final concentration of 10 mM. DNA purification was performed with the Wizard® SV Gel and PCR Clean-Up System as described in section 2.2.2.9.

2.2.2.13. Dephosphorylation of DNA fragments

Dephosphorylation of restriction ends reduces the chance of backbone religation and increases the efficiency of incorporating the desired DNA insert. In order to remove phosphate residues from 5' ends, 10 U of Calf Intestinal Alkaline Phosphatase (CIP) were added to the heat inactivated digest mix (or purified blunting reaction) and incubated for 30-60 min at 37°C. The desired DNA fragment was purified as described in 2.2.2.9.

2.2.2.14. Phenol-Chloroform extraction

DNA fragments used for stable integration of transgenes into mammalian cells were purified by adding an equal volume of phenol-chloroform-isoamyl alcohol (25:24:1) to DNA that was linearized with restriction enzymes. The extraction was conducted under a chemical hood. The emulsion was shaken and incubated at RT for 10 min and centrifuged at 13227xg for 10 min. The upper aqueous phase was collected and 10% (v:v) 5 M sodium acetate and 200% (v:v) of pure ethanol were added. The mix was gently shaken and incubated at -20°C or -80°C overnight or 1 h, respectively. DNA was pelleted by centrifugation at 13227xg for 15 min at 4°C, air-dried and dissolved in cell culture grade water.

2.2.2.15. Quantitative real-time PCR (qPCR)

Gene expression levels of intestinal tissue and cells were measured by quantitative real time PCR (qPCR) using SYBR® Green PCR Master Mix. Suitable primers were tested by GoTaq RT-PCR and their specificity was evaluated on amplification plots and melting curves during qPCR runs. RNA was reversely transcribed as described in section 2.2.2.5 and cDNA was diluted 1:5 or 1:25. In order to perform expression analysis, samples were measured in triplicate with the 7500 Fast Real-Time PCR Cycler with the parameters given in Table 6. The signal from *RPS28* (gene coding for ribosomal protein S28) was used for normalisation to calculate the expression fold change of a gene of interest with the ΔΔCt method.

Reaction mix		Thermal cycling conditions			
Component	**Final conc.**	**Cycling step**	**T [°C]**	**Time**	**Number of cycles**
cDNA	1 µL	Activation	95	20 sec	1
2x SYBR® Green Master Mix	5 µL	Denaturation	95	3 sec	40
Forward primer	0.2 µM	Annealing/ Extension	60-95	30 sec	
Reverse primer	0.2 µM				
Nuclease-free water	add to 10 µL				

Table 6: Parameters for q-PCR with SYBR® Green PCR Master Mix

2.2.2.16. Sequencing

Using the Mix2Seq kit, DNA was sent for Sanger sequencing to Eurofins. The concentration of primer and DNA was adjusted according to the company's instructions.

2.2.3. Generation of single guide RNA CRISPR/Cas9 vectors

2.2.3.1. Hybridisation of oligonucleotides

Lyophilised ssDNA oligonucleotides were purchased from Eurofins Genomics (Ebersberg, GER) and solved in nuclease-free water. Two complementary ssDNA oligos were mixed in water at a final concentration of 10 ng/µL each. In order to generate the crRNA template, the complementary ssDNA was hybridised to create a double stranded oligo with overhangs for molecular cloning. Hybridisation was performed by heating the solution to 100°C and passive cooling to RT.

2.2.3.2. Ligation of hybridised oligonucleotides into vector backbones

Hybridised oligonucleotides (dsOligo) comprise the crRNA sequence and compatible overhangs for the ligation into the plasmid pX330-U6-Chimeric_BB-CBh-hSpCas9, named pX330. Plasmid pX330 was linearized by restriction digest with *BbsI* and purified after gel electrophoresis as described in section 2.2.2.9. Ligation was performed as described in section 2.2.2.10 using 1.5 µL dsOligo and 100 ng linearized plasmid in a final volume of 20 µL.

2.2.3.3. InDel detection

Single nucleotide mutations, that were introduced in mammalian DNA upon CRISPR/Cas9-mediated DNA double strand break, were detected by sequencing. For this purpose, the CRISPR/Cas9 target site was amplified by Q5 PCR and

sequenced with the PCR primer that binds upstream of the target site. The primer sequences used to analyse InDels in the seven genes edited in this work are listed in Table 4.

porcine gene, CRISPR/Cas9 target	targeted exon	forward primer	reverse primer
APC	3	AAGTGCTCATGATTATCCACCA	GTCCTCTGTTTTGCTGCTCA
CDKN2A/p16INK4A	2	TGTCCTCCGACGGATTTCTG	CTCCGGGTGGAAAGATACCG
PTEN	1	GTCGCTGCAACCATCCAG	AGATGAACACACCCTAGGCT
SMAD4	3	GACTAACCTGAAGCCTCCCA	AGCAATTTCATCTTTTCCCAAGT
TP53	5	GCCCACTCACCATCGCTATA	ACCCTGGTCCCAAAGTTGAA
B2M	1	CCACCCAGTCCAACCTTTGCC	ACTCCGGGCGCTAACTCTGG
TNFα	4	GGGTTTGGATTCCTGGATGC	GCGGTTACAGACACAACTCC

Table 7: Primers used for InDel detection after CRISPR/Cas9-mediated double strand break.

Amplicons were sequenced (Eurofins Genomics, Germany) with the respective forward primer and analysed for insertions and deletions with the 'TIDE' or the 'ICE CRISPR Analysis' tool (2.1.13).

2.2.4. Guide RNA multiplexing

Guide RNA multiplexing is the simultaneous expression of multiple guide RNAs (gRNAs) from a single polycistronic gene. This protocol is based on the strategy described by Xie et al.[99] and exploits the cellular tRNA-processing system to cleave the single transcript into multiple guide RNAs. The synthesis of such a polycistronic reading frame is hampered by the presence of several repetitive elements, namely pre-tRNA and tracrRNA sequences, that flank each crRNA. The strategy developed in this work uses standard PCRs and overlap extension PCRs in which tRNA and tracrRNA sequences are added to each of the crRNAs of interest. Hence, two primers are designed per crRNA carrying short homologous sequences to either the tRNA or the gRNA (tracrRNA with RNA linker) sequence. The sequences are added to the crRNAs by PCR using a scaffold plasmid as template that carries the sequences of tRNA and gRNA.

#primer	element	direction of crRNA seq.	homologies added to crRNA primer		cut sites	homology
			5' end	3' end		
1	universal_Fw				FokI	tRNA
6	universal_Rev				FokI, 2x BbsI	gRNA
2	crRNA1	RC		AGGTCCCACCGAGAT		tRNA
3	crRNA1	FW		GTTTTAGAGCTAGAAA		gRNA
4	crRNA2	RC		AGGTCCCACCGAGAT		tRNA
5	crRNA2	FW		GTTTTAGAGCTAGAAA		gRNA
7	crRNA3	RC		AGGTCCCACCGAGAT		tRNA
8	crRNA3	FW		GTTTTAGAGCTAGAAA		gRNA
9	crRNA4	RC		AGGTCCCACCGAGAT		tRNA
10	crRNA4	FW		GTTTTAGAGCTAGAAA		gRNA
11	crRNA5	RC	GAAGACTCAAAC	AGGTCCCACCGAGAT	BbsI	tRNA

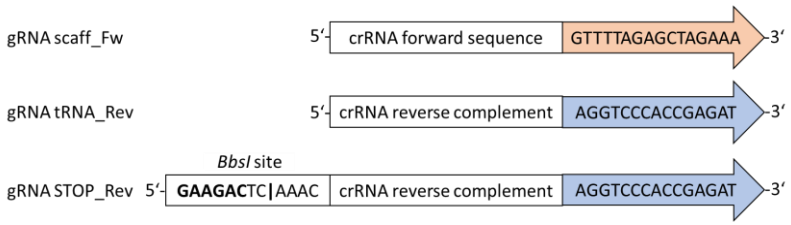

Table 8: Scheme for the design of primers for any pentaplex (multiplex of four gRNA). The short 5' and 3' homologies added to the primers are used to extend the crRNA with tRNA and tracrRNA sequences by PCR. These single elongated sequences are combined to a multiplex of guide RNAs by overlap extension PCR. The multiplex is finally cloned into the original CRISPR/Cas9 vector by restriction digest and T4 ligation. As example, one pair of primers is shown with the homologies added to 5' and 3' ends. Except for the last crRNA in the multiplex, every crRNA is cloned using two primers. The first primer carries the crRNA in forward direction with homology to the gRNA sequence and the second is the reverse complement cRNA with homology to the tRNA sequence. The last crRNA in the multiplex is added to the multiplex with a single reverse complement primer carrying the homologous sequence for the tRNA. RC: reverse complement of crRNA target site; FW: forward direction of crRNA target site; tRNA: part of the human tRNA sequence that is recognised for intracellular splicing; gRNA: tracrRNA with RNA linker sequence; tRNA and gRNA are present on the tRNA-gRNA scaffold plasmid for amplification by PCR. The universal cloning strategy for a multiplex is depicted in Figure 10.

The protocol presented here can be used to generate any multiplex of interest. An overview of the primer elements and their combination is shown in Table 8 for a vector encoding for five *guide RNAs* (pentaplex). The crRNA sequences used for the pentaplex cloned in this work are listed in Table 10.

There are two universal primers that are used independent from the crRNA sequences:

- #1 universal_Fw 5'-GGATGGGCAGTCTGCACCGCAGCAGGTCCCAT-3' (binds to the tRNA sequence on the scaffold plasmid)
- #6 universal_Rev 5'-GGCAGGATGAGCGACAGCAAACTCGTCTTCTCGAA-GACTCGCACCGACTCG-3' (binds to the gRNA sequence on the scaffold plasmid)

Using the primers designed in Table 8, PCRs and overlap extension PCRs were performed to generate the *guide RNA* multiplex. A summary of the intermediate PCR products is shown in Table 9.

pair of primers	PCR product	length [bp]	overlap extension PCR	
#1, #2	product 1	116	fragment A (290 bp)	fragment B (406 bp)
#3, #4	product 2	194		
#5, #6	product 3	136		
#1, #8	product 4	116	fragment C (290 bp)	fragment D (406 bp)
#9, #10	product 5	194		
#11, #6	product 6	136		
#1, #11	product 7	128		

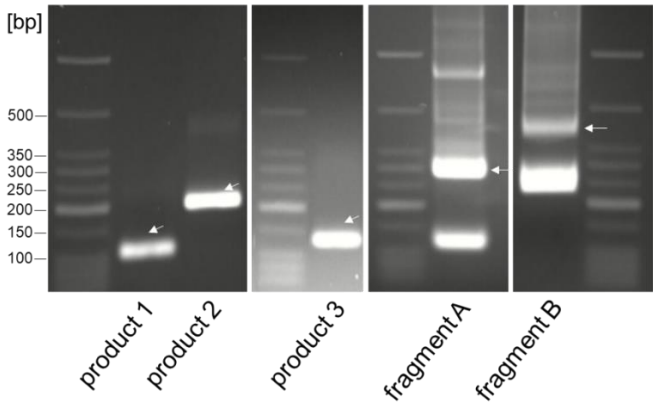

Table 9: Overview of PCRs and overlap extension PCRs for gRNA multiplexing. The PCR products and their length is listed for a multiplex of five guideRNAs. Representative results from gel electrophoresis are shown for the PCRs and overlap extension PCRs that are used to clone the first amplification vector carrying crRNAs 1 and 2 (see also Figure 10). Note that the complementary crRNA sequences of forward and reverse complement primers provide the homology required for overlap extension PCR. Consequently, the product length is shorter than the sum of the single PCR products after overlap extension PCR.

Q5® High-fidelity polymerase was used to generate blunt end PCR products. The PCRs for products 1-7 were performed with an individual primer concentration of 10 µM, 10 ng of the scaffold plasmid and the thermal cycling conditions: 98°C, 30 sec followed by 35 cycles at 98°C for 10 sec; 50°C for 30 sec; 72°C for 20 sec, and a final extension at 72°C for 2 min (Figure 10 A). PCR products were purified (section 2.2.2.9), eluted in 25 µL nuclease-free water and used as templates for overlap extension PCR. Overlap extension PCR was performed with 2 µL of two overlapping PCR products (products 1 and 2, e.g., Table 9), the Fw-primer of the first, and the Rev-primer of the second PCR product (Figure 10 B). The cycling was splitted into one low annealing and one moderate annealing step as follows: 98°C, 30 sec followed by 5 cycles at 98°C for 5 sec; 48°C for 15 sec; 72°C for 15 sec, followed by 30 cycles at 98°C for 5 sec; 58°C for 15 sec; 72°C for 15 sec and final extension at

72°C for 2 minutes. The products of overlap extension PCRs were separated by gel electrophoresis, excised, purified, and the DNA concentration was measured. In order to obtain fragments B and D overlap extension PCR was performed by combining the purified fragment A with product 3, and fragment C with product 6, respectively.

Fragments B, D and PCR product 7 were subcloned into the pJet vector (amplification vectors 1, 2 and 3) from the CloneJET PCR Cloning Kit for amplification in DH10B cells. Using *FokI* and *BbsI* restriction digest and T4 ligation, fragment B was cloned into the CRISPR/Cas9 cloning vector (pX330-U6-Chimeric_BB-CBh-hSpCas9, Figure 10 C). For this purpose, pJet-fragment B was cut with *FokI* and inserted by T4 ligation into the *BbsI*-digested CRISPR/Cas9 cloning vector, named 'intermediate CRISPR/Cas9 vector'.

The pJet-fragment D and pJet-product7 were combined by insertion of *FokI*- and *BbsI*- digested pJet-product7 into the *BbsI*-digested pJet-fragment D to generate an intermediate triplex plasmid (Figure 10 D). Finally, the intermediate triplex was digested with *FokI* and inserted into the *BbsI*-digested intermediate CRISPR/Cas9 vector (Figure 10 E). As a result, five guide RNAs are transcribed as single transcript (pentaplex) by the *U6 promoter*. This transcript is spliced into the single guide RNAs by the cellular tRNA splicing machinery. The pentaplex including the U6 promoter and U6 termination site comprises 1.1 kb and the complete CRISPR/Cas9 pentaplex vector is 10.0 kb long. All crRNA sequences for the pentaplex generated in this work are listed in Table 10. Additionally, the crRNA targeting porcine *B2M* is included but was transfected on a separate CRISPR/Cas9 vector as described in section 3.9.

Porcine gene	Targeted exon	crRNA sequence	reference
APC	3	GACCGTAGTTTCACTCCA	
CDKN2A/p16INK4A	2	GAGGCTAGCCAGTCGGCCGA	Daniela Kalla
PTEN	1	AGATCGTTAGCAGAAACAAA	Dr. Caroline Perleberg
SMAD4	3	ACTATGTACAATGCTCAGAC	Daniela Kalla
TP53	5	GGCAAAACAGCTTATTGA	Dr. Caroline Perleberg
B2M	1	TAGCGATGGCTCCCCTCG	Dr. Beate Rieblinger
TNFα (crRNA1)	4 (3'UTR)	TAAGAGGGAGCTGGCCCTGT	
TNFα (crRNA2)	4 (3'UTR)	GTATTTATTCAGGAGGGCG	
TNFα (crRNA3)	4 (3'UTR)	AACCAAGGCAGCCCTTATGC	

Table 10: Sequences of the crRNAs against TSGs used in this study. For the design of crRNAs, the NCBI and Ensemble database was searched for isoforms of the desired genes. If the gene had to be inactivated, the coding sequences were aligned to find the earliest shared exon. Suitable crRNA sequences were computed using CRISPOR (http://crispor.tefor.net/) and tested in porcine primary kidney-derived cells. Five of the crRNA

sequences had been tested and validated in pKDCs by colleagues at the Chair of Livestock Biotechnology (indicated as reference).

A

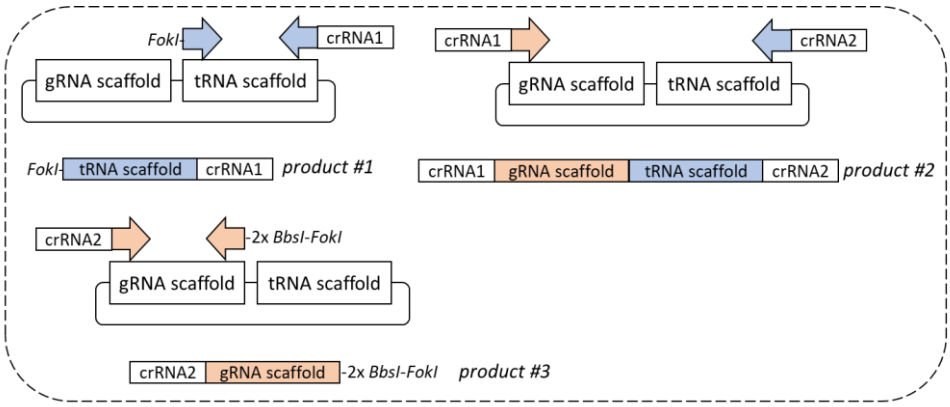

→ Likewise, primers for crRNA 3 and 4 are combined to generate products 4, 5, and 6.

B

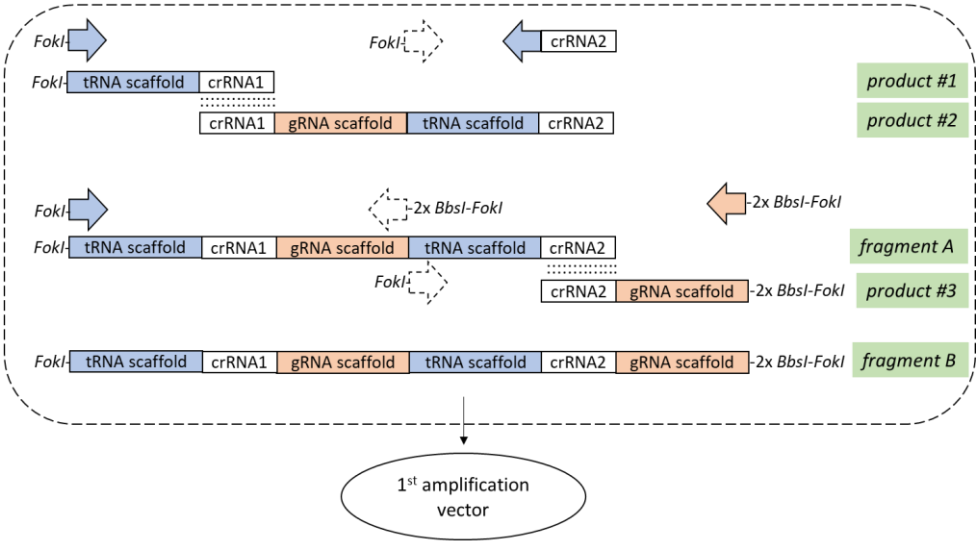

→ Likewise, products 4, 5, and 6 are combined to generate the 2nd amplification vector with crRNAs 3 and 4.

C

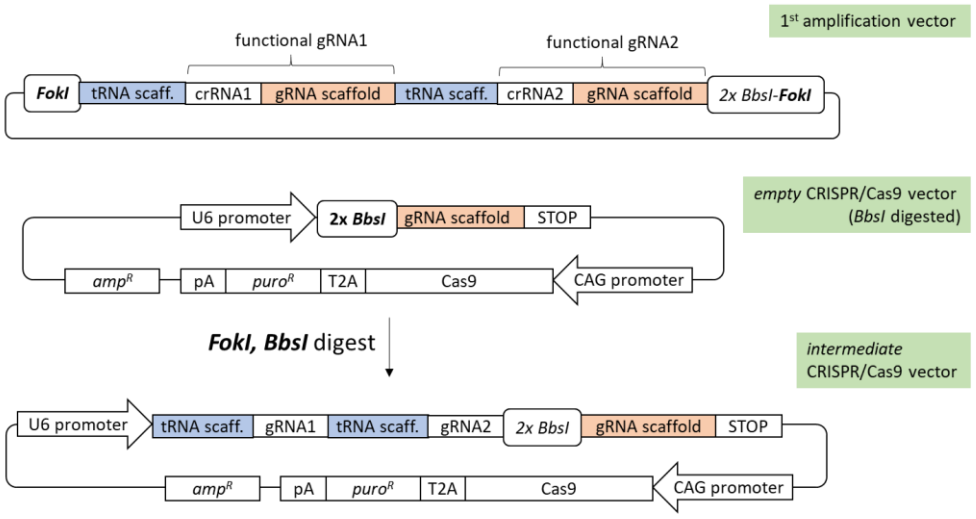
1st amplification vector
functional gRNA1
functional gRNA2
FokI
tRNA scaff.
crRNA1
gRNA scaffold
tRNA scaff.
crRNA2
gRNA scaffold
2x BbsI-FokI
empty CRISPR/Cas9 vector (BbsI digested)
U6 promoter
2x BbsI
gRNA scaffold
STOP
ampR
pA
puroR
T2A
Cas9
CAG promoter
FokI, BbsI digest
intermediate CRISPR/Cas9 vector
U6 promoter
tRNA scaff.
gRNA1
tRNA scaff.
gRNA2
2x BbsI
gRNA scaffold
STOP
ampR
pA
puroR
T2A
Cas9
CAG promoter

D

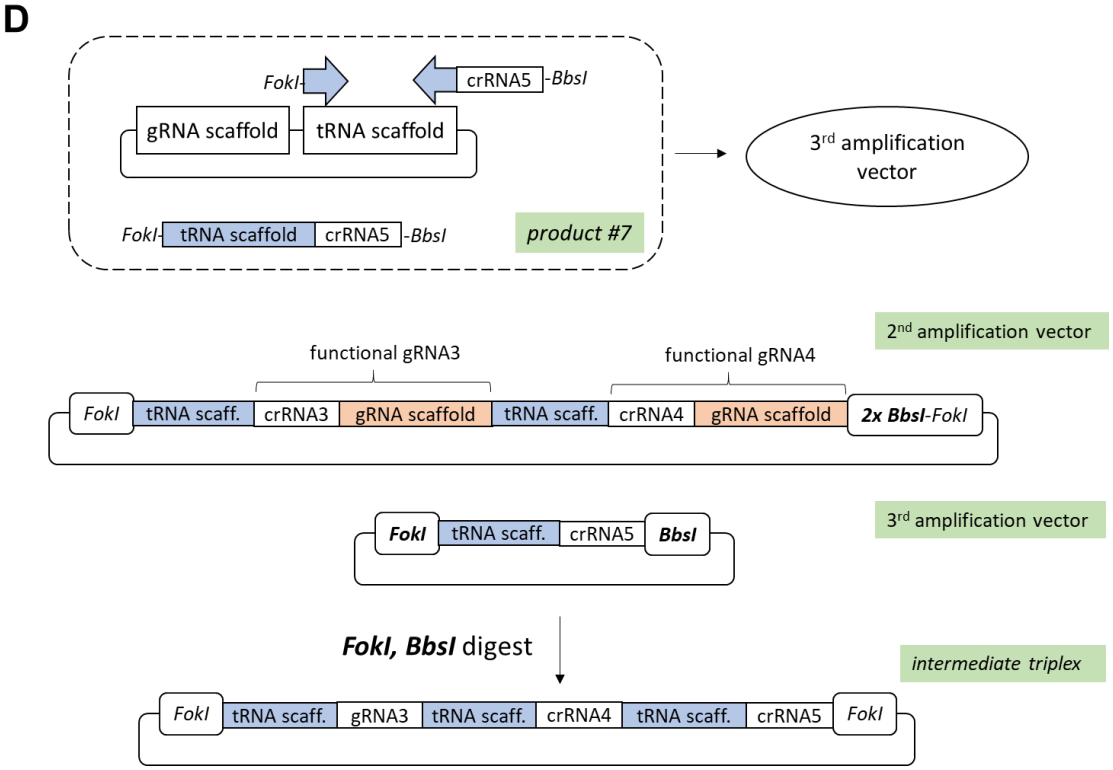
FokI-
crRNA5
-BbsI
gRNA scaffold
tRNA scaffold
FokI-
tRNA scaffold
crRNA5
-BbsI
product #7
3rd amplification vector
2nd amplification vector
functional gRNA3
functional gRNA4
FokI
tRNA scaff.
crRNA3
gRNA scaffold
tRNA scaff.
crRNA4
gRNA scaffold
2x BbsI-FokI
3rd amplification vector
FokI
tRNA scaff.
crRNA5
BbsI
FokI, BbsI digest
intermediate triplex
FokI
tRNA scaff.
gRNA3
tRNA scaff.
crRNA4
tRNA scaff.
crRNA5
FokI

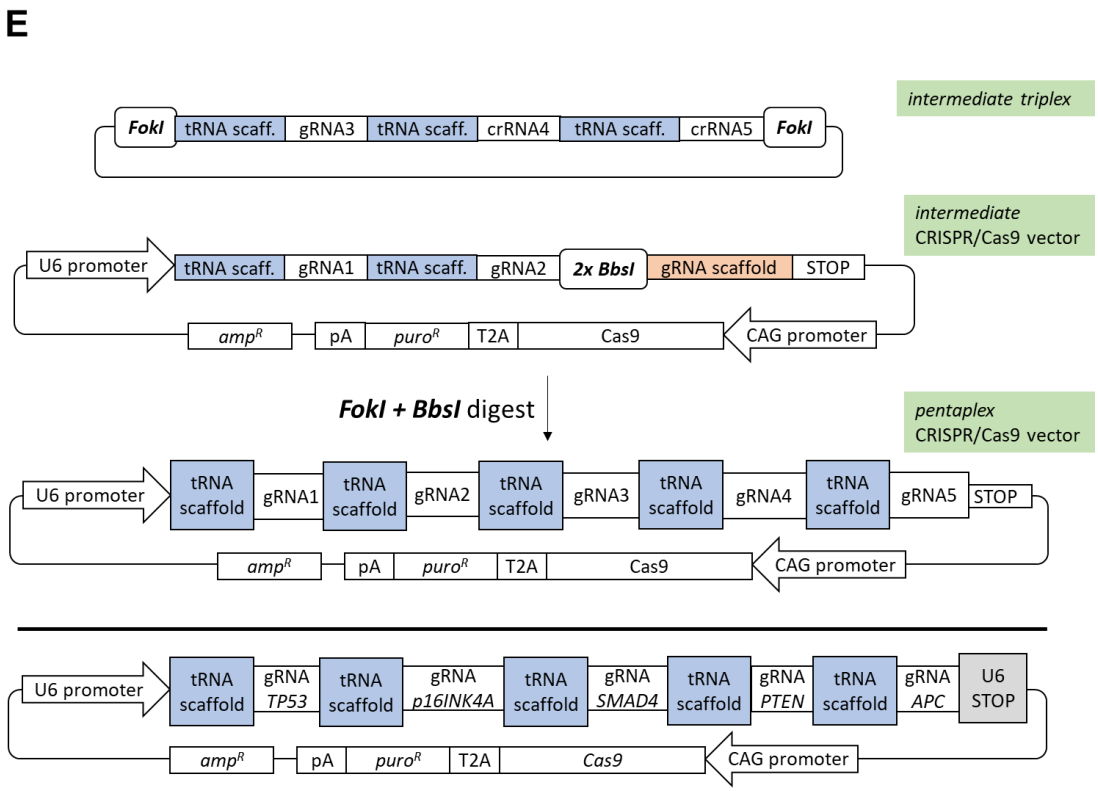

Figure 10: Cloning strategy for a CRISPR/Cas9 pentaplex. The cloning strategy including PCRs, overlap extension PCRs and cloning steps is depicted. PCRs and overlap extension PCRs are framed in dashed lines to separate them from ligation of restriction fragments. The restriction enzymes used to digest a plasmid/vector are highlighted in bold type. The strategy is described for any set of five crRNAs (crRNAs 1-5) and the crRNA sequences used in this work are listed in **Table 10**. The final structure of the pentaplex cloned in this work is shown at the bottom.

2.2.3.4. Protein isolation from mammalian cell culture

Total protein was isolated from pellets obtained by centrifugation of at least 3x 10^6 cells from mammalian cell culture at 300xg for 5 min at RT. The pellet was stored on ice throughout protein isolation. Cells were lysed in 200 µL NP40 cell lysis buffer by vortexing for until floating cell debris became visible (3-5 min). Of note, NP40 cell lysis buffer was supplemented freshly with proteinase inhibitor according to the manufacturer's instructions. The suspension was centrifuged for 10 min at 1000xg, 4°C and the supernatant containing protein was collected. Using Bradford Assay and serial dilutions of BSA protein in PBS as standard, the absorbance at 595 nm was used to determine the concentration of total protein in the lysate. Aliquots of 30 µL were prepared from the cell protein solution and stored for postponed Western Blot at -80°C.

2.2.3.5. Western Blot

Western Blot was performed to detect expression of recombinant noggin and tumour suppressor genes in HEK293T cells and porcine enteroids. In order to separate

proteins by length, denaturing SDS-PAGE was performed with discontinuous polyacrylamide gels comprised of 5% stacking and 12% separation SDS gels (Table 11). Preparation of gels and SDS-PAGE were conducted with the 'Western blot Mini PROTEAN tetra handcast system'. Protein samples and protein ladder were thawed on ice and denatured by mixing with 4x Lämmli buffer and incubated for 5 min at 95°C. The gel was loaded with 10-20 µg of protein/well and electrophoresis was performed in running buffer for 30 min at 80 V followed by 140 V for 1 h.

	separation gel	**stacking gel**
polyacrylamide [%]	12%	5%
40% polyacrylamide	2.31 mL	0.55 mL
1 M Tris-Cl pH 8.8	2.9 mL	
0.5 M Tris-Cl pH 6.8		1.1 mL
10% SDS	77 µL	44 µL
ddH2O	2.35 mL	2.65 mL
10% APS	77 µL	44 µL
TEMED	3.1 µL	4.4 µL
sum	7.7 mL	4.4 mL

Table 11: Composition of separation and stacking gel for SDS-PAGE

Semi-dry Blotting was performed with a PVDF membrane activated by incubation for 1 min in methanol prior to blotting. The activated membrane, filter papers, SDS gel, and sponges were equilibrated in semi-dry blotting buffer and set up according to Figure 11. After removal of air bubbles, blotting was performed at 80 V, 220 mA for 1 min/kDa in ice. The membrane was washed in TBST buffer and blocked in 5% (m/v) milk powder solution (in TBST) for 1 h at RT.

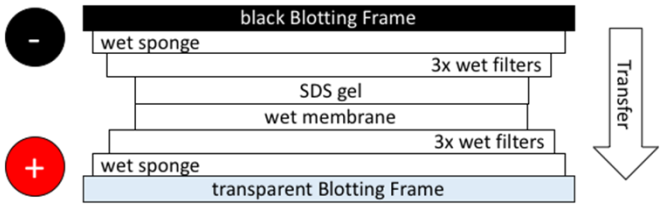

Figure 11: Setup for semi-dry Western Blot

Incubation of the membrane with antibodies and washing was performed with the 'iBind Western Device'. The membrane and iBind filter were equilibrated in iBind solution according to the manufacturer's instructions. The chambers of the device were filled with dilutions of primary binding antibody, secondary HRP-conjugated detection antibody, and iBind solution for washing. After 3.5 h, the membrane was

removed from the device, washed with TBST buffer and HRP luminescence reagent was added dropwise onto the membrane. In the dark, chemiluminescence was detected on an X-ray film that was exposed to the membrane for 10 s to 30 min. The film was developed in X-ray developer T32 and fixed in X-ray fixing solution Superfix 25. Recombinant human GAPDH protein and HEK293 protein lysate were used as positive controls.

2.2.3.6. Ras Activation Assay

Activation of Ras protein was measured by comparing the amount of active GTP-bound Ras with total Ras protein. For this pupose, Ras Activation Assay was performed according to the manufacturer's instructions. Briefly, cells grown on two 150 cm^2 flask were washed, lysed using Lysis buffer (with 10 µg/mL aprotinin, 10 µg/mL leupeptin) and equivalently separated in two aliquots. One aliquot was mixed with 10 µL Ras Assay Reagent (Raf-1 RBD, agarose) and incubated for 1 h at 4°C to bind GTP-Ras to agarose beads. The second aliqout was mixed with 10 µL of 0.5 M EDTA and 5 uL of 100x GTPγS to load whole Ras protein. After incubation with Ras Assay Reagent for 30 min at 30°C loading with GTPγS was stopped by addition of 32.5 uL of 1 M $MgCl_2$. The beads were washed three times with 500 uL of 1x MLB buffer (with 10 µg/mL aprotinin, 10 µg/mL leupeptin) and centrifugation at 12000 x g for 30 sec at 4°C. The pellet was resuspended and boiled for 5 min in 40 uL of 2x Laemmli Buffer and 2 µL of 1 M DTT to release GTP-Ras from agarose beads. Beads and supernatant were resuspended and 20 µL were used for Western Blot as described in section 2.2.3.5.

GTP- and GTPγS-bound Ras was detected with anti-Ras antibody clone RAS10 and m-IgGκ BP-HRP.

2.2.5. 2D cell culture

Mammalian cell culture experiments were performed in class II laminar flow hoods with sterilised material. Cells were cultivated in an incubator set to 37°C, 5% CO_2 and 95% humidity. Standard 2D cell culture medium was DMEM supplemented with 1x non-essential amino acids, 1 mM sodium pyruvate, 2 mM Ala-Gln and 10% foetal calf serum. Medium was changed every 2-3 days. Media were only supplemented with

antibiotics if cells were isolated from tissue samples or after transfection with an antibiotic resistance marker for selection.

Cells were passaged at a confluency of 80-90%. In order to passage adherent monolayers, medium was aspirated and the culture was washed once with PBS. The cells were then incubated for 5-15 min in pre-warmed Accutase in the incubator and dissociated by pipetting. The single cell suspension was splitted 1:5-1:10 in fresh medium.

2.2.5.1. Isolation of porcine primary kidney-derived cells (pKDCs)

Primary kidney cells were isolated from kidneys provided from the TUM livestock facility in Thalhausen. The tissue was cut in 2x2x2 cm^3 pieces and decontaminated with 80% ethanol. The epithelium and endothelium was removed and the connective tissue was washed in PBS, 80% ethanol and PBS again. Connective tissue was further dissected with a scissor and washed with PBS until most of the cell debris was removed. The tissue pieces were collected in 10 mL of Collagenase type IA diluted in PBS and stirred for 30 min at 30-40°C. Enzymatic dissociation of the tissue was stopped by adding 40 mL of 2D cell culture medium. Cells were pelleted by centrifugation at 300xg for 10 min, resuspended in medium supplemented with 100 U/mL penicillin and 100 µg/mL streptavidin, and distributed onto 4-12 T150 cell culture flasks. Primary cultures were daily monitored for contamination under the microscope and the supernatant was tested for mycoplasma contamination by PCR.

2.2.5.2. Cryoconservation and thawing of cells

Mammalian cells were dissociated and resuspended in 1 mL of cryomedium that contained 80% (v:v) FCS, 10% DMSO and 10% 2D cell culture medium. The sample was transferred to cryovials and cooled down in a freezing container (Mr. Frosty®) at -80°C. Samples were moved to liquid nitrogen for long-term storage.

Samples were resuscitated by thawing the cryovial in a 37°C water bath. Culture medium was added to dilute the DMSO-containing cryomedium, which was aspirated after centrifugation. Cells were finally resuspended and cultivated on cell culture flasks.

2.2.5.3. Counting of cells

The concentration of dissociated cells was either determined automatically using the Countess™ automated cell counter or calculated by counting cells manually with a Neubauer's Chamber. Trypan blue was used to distinguish live and dead cells.

2.2.5.4. Electropermeabilisation for 2D mammalian cell culture

Electropermeabilisation was used to transfect mammalian cells, including CHO cells, HEK cells and pKDCs. After dissociation, cells were counted and $1x10^6$ were resuspended in 100 µL of electroporation buffer with 1-4 µg of DNA. The suspension was transferred into a 2 mm electroporation cuvette and immediately electroporated with the ECM 830 Square Wave Electroporation System (BTX). The settings for pKDCs were one single pulse of 300 V and 1 ms/pulse. Infinite cell lines were transfected with two pulses of 180V and 5 ms/pulse. The sample was cultivated in a T25 cell culture flask with 5 mL of equilibrated cell culture medium and the cuvette was washed once with medium to collect most of the cells.

2.2.5.5. Lipofection

Lipofection was performed to transfect immortalised cell lines, such as CHO and HEK cells. Cells were seeded on a 24 well plate before transfection at a density of $5x10^4$ cells/well to reach 70-80% confluency the next day. The culture was washed once with PBS to remove FCS and overlaid with 250 µL of DMEM. The lipofection reaction mix consisted of DNA solution (30-100 ng DNA in 25 µL of DMEM) and Lipofectamine 2000 solution (0.2 µL in 25 µL of DMEM). The lipofectamine solution was incubated for 5 min at RT and added dropwise to the DNA solution. The reaction mix (50 µL/reaction) was inverted several times, incubated for 25 min and added dropwise to the well. Cells were incubated for 4 h in the incubator. Afterwards, the reaction mix was replaced by 0.5 mL of cell culture medium.

2.2.5.6. Generation of single cell clones

The generation of genetically identical cell clones was required for somatic cell nuclear transfer (SCNT). Successfully transfected pKDCs were selected with antibiotics (see section 2.2.5.7), dissociated, and seeded on culture dishes at a density of 500 cells per 145 cm^2. The cultures were grown until cell clones of appr. 100-200 cells had formed. Single cell cloning was performed with sterilised cloning rings as follows. The cloning rings were immersed in silicone grease. The culture was washed once with PBS to remove FCS and cloning rings were placed around the

single cell clones. Clones were detached with Accutase and cultivated on 24 well plates. The clones were propagated, the correct genotype was tested by Screening PCR (see section 2.2.5.8) and clones from 6 well plates were cryoconserved for SCNT.

2.2.5.7. Selection of transfected cells

Cells transfected with CRISPR/Cas9 plasmids were selected for transient expression of the construct with 1.5 µg/mL puromycin for 48 h. For stable integration of transgenes the cultures were selected with 200-700 µg/mL geneticin (G418) for 7-10 days.

2.2.5.8. Screening PCR

Porcine cells were analysed by PCR for the stable integration of transgenes and deletions introduced by the CRISPR/Cas9 system. For this purpose, primers were used to amplify the transgene or the genetic sequence flanking the deletion site. Genomic DNA was isolated (see section 2.2.2.2) and 2 µL of the quick extract was used for PCR with GoTaq or Q5 polymerase (see section 2.2.2.6).

2.2.6. 3D cell culture

2.2.6.1. Isolation of intestinal crypts

Crypts were either isolated from tissue of killed pigs or from biopsies taken from the distal rectum during endoscopy. The samples were stored in ice-cold PBS and the isolation of crypts was performed on ice. All solutions were ice-cold and the tubes were pre-coated with 1% BSA solution (in PBS). Luminal content was removed by scraping the sample with tweezers and washing in 80% EtOH and PBS. The mucosa was released from muscle and fatty tissue and incubated for 20-25 minutes under constant shaking in dissociation buffer that contained 30 mM EDTA, 10 mM DTT (in PBS). The sample was washed once with PBS and transferred to basic medium supplemented with 10 µM thiazovivin and 100 µg/mL primocin. Crypts were mechanically dissociated with syringe needles under a stereo microscope and their concentration estimated by counting the number of intact crypts in a 20 µL aliquot. Crypts were embedded at a density of 350-500 crypts per 50 µL Matrigel. The desired volume of crypt suspension was centrifuged at 90xg for 5 min at 4°C. Centrifugation at 300xg was performed to pellet single cells that resulted from prolonged dissociation of crypts. The supernatant was aspirated and the pellet was resuspended in Matrigel. The suspension was aliquoted in a 24 well plate and

incubated for 15 minutes at 37°C, 5% CO2. After drops became solid the culture was overlaid with 250 µL of freshly prepared growth medium additionally supplemented with 10 µM thiazovivin and 100 µg/mL primocin. Thiazovivin was removed two days after isolation. Antibiotics were removed three days after the first passage.

Growth medium is Advanced DMEM/F12 with 1x Glutamax, 10 mM HEPES, 1 mM N-Acetyl-L-cystein, 100 ng/mL murine Wnt3a (or 50% mWnt3a-conditioned medium), 100 ng/mL hR-spondin 1 (equivalent to 4.2% hR-spondin 1-conditioned medium), 100 ng/mL hNoggin (equivalent to 1.3% porNoggin-conditioned medium), 1x B27, 1x N2, 100 ng/mL hEGF, 10 mM nicotinamide, 10 µM SB202190, 500 nM LY2157299, 2.5 µM CHIR99021, 10 nM L-Gastrin.

2.2.6.2. Conditioned media

Conditioned media were essential for the cultivation of enteroids because they show higher biological activity than recombinant proteins. Therefore, conditioned media were produced for murine Wnt3a, human R-spondin 1 and porcine noggin. Wnt3a and R-spondin were harvested from the supernatant of transgenic cell lines kindly provided by the Clever's Lab. The concentration of the cytokines in the supernatant was measured by TOPFlash Assay using HEK293 cells. The cell line was transfected by lipofection with a Wnt3a-responsive Firefly Luciferase construct and a Renilla Luciferase control plasmid., Recombinant murine Wnt3a and recombinant human R-spondin 1 were used as standards for TOPFlash Assay. The cell line secreting porcine noggin was established by lipofection of HEK293 cells with a linearized expression vector cloned in this work. In this construct the 696 bp long porcine *Noggin* coding sequence was cloned between the *CAG* promoter-*Kozak* sequence *GCCGCCACC* and the bovine *polyA*. Successfully transfected cells were selected with G418 via a *PGK-neo^R-bpA* cassette present on the vector. The concentration of noggin in conditioned medium was determined by ELISA using a polyclonal anti-human noggin antibody and recombinant human noggin as standard (see section 2.2.6.3).

2.2.6.3. Quantification of porcine Noggin in conditioned medium by ELISA

Noggin is a potent BMP pathway inhibitor and an essential supplement for enteroid culture medium. Porcine Noggin was produced as conditioned medium by HEK293 cells transfected with a vector coding for the porcine *Noggin* coding sequence. The

concentration of the protein was measured by indirect ELISA. The pH of all buffers was set to 7.4.

Serial dilutions were prepared of the conditioned medium (1:2 dilutions) and recombinant human noggin as standard (12.5-200 ng/mL in 1:2 dilutions) using 1x PBS for coating. Nunc MaxiSorp 96 well plates were coated with 400 µL dilutions of conditioned medium and recombinant protein in triplicate overnight at 8°C. Supernatant from untransfected HEK293 cells was used as negative control. PBS was used as blank. The wells were blocked for 1h at RT with 200 µL of blocking buffer, that contained 2% (m/v) BSA in PBS. The plates were washed twice with 200 µL of wash Buffer that contained 0.05% (v/v) Tween20 in PBS. Polyclonal rabbit IgG anti-hNoggin was used as primary antibody at a dilution of 1:1000 and 100 µL were added to the wells. After incubation at RT for 2 h the plates were washed four times. HRP-linked donkey anti-rabbit IgG was used as detection antibody. It was diluted 1:1000 and 100 µL were added to each well. After incubation at RT for 2 h the plates were washed four times and 50 µL of ELISA Substrate Solution was added per well. The reaction was incubated for 30 min at RT in the dark and stopped by adding 25 µL of 0.5 M sulfuric acid (aq). Absorption was measured at 450 nm.

2.2.6.4. TOPFlash Assay to determine the concentration of conditioned medium

The concentration of Wnt and R-spondin in conditioned media can be determined by a dual luciferase reporter system (TOPFlash Assay). The assay measures the activity of β-catenin, a Wnt-responsive transcription factor, by expression of *Firefly luciferase*. In HEK293 cells, that are transfected with the Firefly vector, β-catenin is translocated into the nucleus and drives expression of *Firefly luciferase* by binding to eight *TCF-LEF promoter* elements (CCTTTGATC) upstream of the *Firefly* coding sequence. *Renilla luciferase* is constitutively expressed by the *SV40 promoter* on the second, co-transfected vector and used for normalisation of the signal.

HEK293 cells were transfected by lipofection with 330 ng of Firefly vector and 10 ng of Renilla vector per well which at a molecular ratio of 24:1 Firefly per Renilla copies. One day after transfection, cells were washed with PBS and incubated with 1 mL of serial dilutions of conditioned medium or recombinant protein for 48 h. The cells were washed and collected in 100 µL of 1x Passive Lysis buffer per well. Lysis was performed under shaking at RT for 30 min. Debris was removed by centrifugation and

a 1:10 working dilution of the lysate was prepared for luciferase measurement. The assay was performed according to the manufacturer's (Firefly & Renilla Luciferase Single Tube Assay Kit, Biotium) instructions on the LUMIstar Omega luminometer. As standards recombinant murine Wnt3a was used in 1:2 dilutions (12.5-100 ng/mL), whereas recombinant human R-spondin 1 was diluted 1:10 (1-1000 ng/mL).

2.2.6.5. Cryoconservation and thawing of enteroids

Both freshly isolated crypts and dissociated enteroids were cryoconserved in cryomedium that contains 80% (v:v) FCS, 5% DMSO, 15% basic medium and 10 µM thiazovivin. Samples were transferred to cryovials and cooled down in a freezing container (Mr. Frosty®) at -80°C. Resuscitation of crypts and enteroids was performed as described for 2D culture but cells were finally resuspended and cultivated in Matrigel.

2.2.6.6. Dissociation of enteroids

Enteroids were enzymatically and mechanically dissociated. Two days before passaging the growth medium was supplemented with 10 µM thiazovivin. For electropermeabilisation the growth medium was supplemented with 10 µM thiazovivin and 1.25% DMSO (v:v). Enteroids were dissociated using ice-cold solutions supplemented with 10 µM thiazovivin and plated within 45 min. Bubble formation should was avoided. The enteroids were harvested by removing the medium and resuspended in PBS with a 1000 µL pipette. Enteroids were collected in 1 mL of basic medium per 50 µL Matrigel drop. Matrigel was removed by centrifugation at 300xg for 5 minutes at 4°C and the pellet was resuspended in TrypLE Express solution by flicking the tube. The cells were enzymatically dissociated for 5-10 minutes in a 37°C water bath followed by mechanical dissociation. The suspension was pipetted up and down for 10-20 times through a BSA-precoated blunt-end needle and the treatment was stopped by adding the same volume of basic medium supplemented with 5% FCS. The procedure results in small cell clusters of less than 10 cells. The concentration of cells was determined with a Neubauer chamber. Enteroids were passaged weekly and 10^4 cells were aliquoted per 50 µL drop in a 24 well plate. The desired volume of the suspension was centrifuged at 300xg for 5 minutes at 4°C. The pellet was resuspended in Matrigel and cultivated in growth medium which was supplemented with 10 µM thiazovivin the first two days after passaging.

2.2.6.7. Electropermeabilisation of enteroids

Dissociated enteroids were transfected by electropermeabilisation with the BTX device. Electropermeabilisation was performed with 1-5 x 10^5 cells in 100 µL electropermeabilisation buffer that contained 1-4 µg of DNA per 100 µL. The amount of DNA solution added to the buffer was less than 10%. The suspension was transferred to a 2 mm electroporation cuvette and electropermeabilisation was immediately performed with two pulses of 180V, 5 ms/pulse and 100 µsec interval. Ice-cold basic medium was added to the suspension and cells were incubated for 5 minutes on ice for recovery. The cells were then pelleted by centrifugation at 300xg for 5 minutes at 4°C and splitted to 5-10 Matrigel drops as described earlier. The growth medium was supplemented with 10 µM thiazovivin the first two days after transfection. Depending on the survival rate enteroids had to be splitted 5-10 days after transfection.

2.2.6.8. Cre delivery by lentiviral transduction

Cre recombinase was delivered to activate silent oncogenic mutations in tumour models carrying conditionally activated *KRAS*^{G12D} and *TP53*^{R173H}. Cre was delivered via a non-integrating lentiviral vector carrying the *SFFVp-Cre-WPRE* cassette (spleen focus-forming viral promoter), kindly provided by Dr. Marcel Rommel with a viral titer of 2.3x 10^4 TU/µL. Transduction experiments were performed under S2 conditions. Dissociated enteroids were resuspended in growth medium with 10 µM thiazovivin but without Wnt conditioned medium to avoid inhibition of transduction by residual FCS in the conditioned medium. TransDux Virus Transduction Reagent was added 1:200 according to the manufacturer's instructions. Virus was added to the cells at specific virus to single cell ratios. The suspension was mixed by pipetting, transferred to one BSA precoated well of a 24 well plate, sealed with parafilm and centrifuged for 1 h at 600x g, 32°C (spinoculation). After spinoculation the plate was incubated for 2 h in the incubator. The cells were harvested by centrifugation and cultivated in Matrigel.

2.2.6.9. Live/dead staining

Live/dead staining was performed using a solution of 8 ng/mL fluorescein diacetate and 20 ng/mL propidium iodide in PBS (stock solutions were stored for a maximum of two weeks). The medium was aspirated and 250 µL of the solution was added to enteroids in Matrigel. After incubation for 5 minutes at RT in the dark, the solution

was removed and the well was washed with PBS. The Matrigel drop was covered with PBS and observed under UV light.

2.2.6.10. Immunofluorescent staining

Immunofluorescent staining was conducted with enteroids seeded in Matrigel on 12well removable chamber glass slides. Matrigel drops were washed with PBS and fixed in 4% PFA (in PBS) for 30-60 minutes. The fixative was removed, enteroids were washed once with PBS and incubated for 5 minutes in PBS. This washing step was repeated once. To quench autofluorescence the sample was incubated in 50 mM NH_4Cl (aq) for 30 minutes at RT. Washing was performed as before. The sample was permeabilized by incubation in 0.4% (v/v) TritonX-100 (in PBS) for 30 minutes and washed. Then, 5% (m/v) BSA (in PBS) was added and incubated for 30 minutes at RT to prevent unspecific binding of the primary antibody. After washing the sample was incubated with 150 µL of the primary antibody overnight at 4°C. In order to remove the primary antibody the sample was washed five times. The secondary fluorescent-labelled antibody was incubated for 3 h at RT in the dark. Lastly, the sample was washed and the chamber removed to conserve the staining in mounting solution with DAPI. After incubation for 20 minutes at RT, fluorescent images were taken.

2.2.6.11. Flow Cytometry

Flow cytometry was performed to measure the efficiency of electropermeabilisation and to verify the knockout of β2-microglobulin in enteroids.

Electropermeabilisation was performed with pcDNA-GFP expression plasmid. GFP-expressing enteroids were dissociated as described before and $5x10^5$ cells were incubated with 50 µL of viability dye ZOMBI (1:400 in PBS). After incubation for 20 min in the dark, cells were washed twice with 300 µL PBS. The cells were resuspended in 300 µL of PBS and analysed using an Attune flow cytometer.

In order to verify the knockout of *B2M*, enteroids, that were electropermeabilized with the *B2M*-CRISPR/Cas9 construct, were dissociated. Staining was performed with $5x10^5$ cells and 100 µL of biotinylated anti-human β2-microglobulin primary antibody (1:50 in PBS) for 30 min. Afterwards, cells were washed and incubated with 100 µL of PE-conjugated streptavidin (1:200 in PBS) for 30 min. After washing, cells were incubated with 300 µL viability dye eFluor780 (1:1000 in PBS) for 15 min. Finally,

cells were washed three times with PBS and resuspended in 300 µL PBS and analysed by flow cytometry using the following settings: FSC 100V, SSC 280V, VL1 (laser for PE) 220V. A minimum of 10 000 events was collected for FlowJo analysis.

All incubation steps were performed on ice and centrifugation was conducted at 300xg, 4°C. The following controls were included using non-fluorescent enteroid-derived single cells: unstained Ctrl, viability dye only Ctrl, streptavidin-PE only Ctrl.

2.2.6.12. Imaging and image processing

ImageJ/Fiji (version 1.52p) was used to determine the number and area covered by the enteroids. The script was generated by recording the commands (macro recorder).

```
# 1. downsize bright field image for upload to Cellpose #
run("Size...", "width=512 height=382 depth=1 constrain average interpolation=Bilinear");
saveAs("Tiff","direction:/bright_field_image.tiff");
# 2. upload image into Cellpose that runs with Python #
# 3. run segmentation of Cellpose software with the basic settings and generate masks to create watershed line image in ImageJ/Fiji #
run("Morphological Segmentation");
selectWindow("Morphological Segmentation");
//setTool("multipoint");
call("inra.ijpb.plugins.MorphologicalSegmentation.setInputImageType", "object");
call("inra.ijpb.plugins.MorphologicalSegmentation.setGradientRadius", "1");
call("inra.ijpb.plugins.MorphologicalSegmentation.setGradientType", "Morphological");
call("inra.ijpb.plugins.MorphologicalSegmentation.segment", "tolerance=1.0", "calculateDams=true", "connectivity=4");
call("inra.ijpb.plugins.MorphologicalSegmentation.setDisplayFormat", "Watershed lines");
# 4. invert watershed lines for counting and measuring the area of segmented enteroids #
run("Outline");
run("Dilate");
w = getWidth();
h = getHeight();
makeRectangle(3, 3, w-6, h-6);
run("Make Inverse");
run("Cut");
w = getWidth();
h = getHeight();
makeRectangle(0, 0, w, h);
run("Invert");
```

```
run("Set Scale...", "distance=382 known=1035 pixel=0.999 unit=micron");
run("Analyze Particles...", "size=300-100000000 display exclude clear add in_situ");
# using a size exclusion > 300 avoids counting of debris of dead enteroids #
run("Clear Results");
# 5. Save counts and size of single enteroids in table for upload into R to perform descriptive statistics and analysis #
roiManager("Measure");
saveAs("Results","direcory/Results_enteroid_count_size.csv");
```

Table 12: ImageJ/Fiji script for measuring the area covered by enteroids in bright field images

The scale was initially set using one image for all images of the same magnification.

2.2.6.13. Statistical analysis

RStudio (version 1.2.5033) was used for plotting and statistical analysis. The means of the enteroids' area distribution was compared by Welch two-sided unpaired t-test. P-values < 0.05 were considered significant.

3. Results

Large animal models like the pig have great potential for translational research[55,101]. In this work, I describe the 3D culture of porcine intestinal cells, termed enteroids, as means to accelerate colorectal cancer.

Human and mice organoids are well described in literature but efficient protocols for the generation and manipulation of porcine enteroids are missing. In the following sections, I explain the adjustments of enteroid protocols for the pig. I show how porcine enteroids can be generated from intestinal biopsies and characterised on molecular and cellular level. I established electropermeabilisation for efficient non-viral transfection and present a versatile CRISPR/Cas9 tool to effectively edit multiple tumour suppressor genes (TSGs) in enteroids. I tested the effect of tumorigenic mutations on enteroid growth which indicates that genome engineered enteroids exhibit properties of cancer cells[102]. Afterwards, the ability of these enteroids to induce tumour formation *in vivo* was tested. Finally, I conducted basic work on the generation of a pig predisposed to intestinal inflammation which should promote colorectal cancer in the FAP model.

3.1. Generation of enteroids from the small and large intestine

Murine organoids were generated from embryonic, induced pluripotent and adult stem cells[103]. Fully functional embryonic and pluripotent stem cells from the pig are not available[104]. This section shows that porcine enteroids can be generated from biopsies taken from the small and large intestine. A variety of intestinal cell types was detected by quantitative real time PCR (Q-PCR) and fluorescent microscopy.

The isolation of crypts from intestinal mucosa and biopsies was achieved by mechanical separation of the epithelium from the lamina propria and chemical dissociation of the epithelium into small clusters of crypts. Luminal content and fatty tissue was removed from the tissue followed by incubation in dissociation buffer (EDTA and DTT in PBS). Biopsy specimen were directly incubated in dissociation buffer; large tissue samples isolated from killed animals were cut into smaller pieces. After chemical dissociation, the epithelium was washed with medium and dissected with needles under the stereomicroscope to obtain clusters of crypts. The concentration of EDTA and the incubation time in dissociation buffer was optimized for duodenum and colon samples.

In order to obtain colonic crypts, chemical dissociation was performed for 20-30 min in dissociation buffer containing 30 mM EDTA. Small clusters of 3-10 crypts showed fast organoid formation rates indicated by the closing of viable crypts during isolation. The longer the incubation in dissociation buffer the more single, fragmented crypts and single cells were harvested. A representative example is shown with wildtype colon crypts in Matrigel that were dissociated for 20 min or 30 min (Figure 12). Two days after isolation, spheric clusters developed from single cells after 30 min dissociation time. Nine days after isolation, few large enteroids formed using the short dissociation protocol and numerous large and small enteroids were obtained by longer dissociation. Crypts from duodenum dissociated rapidly after 15 min incubation in 10 mM EDTA (Figure 13). Consequently, enteroid formation capacity is increased by rigorous dissociation.

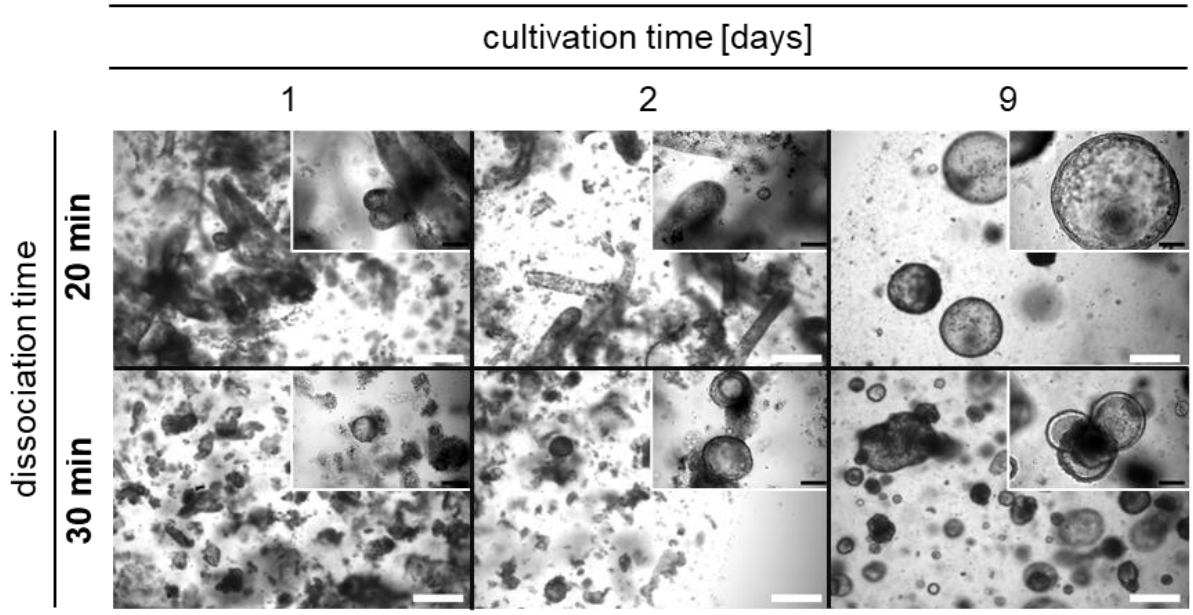

Figure 12 Cultivation of crypts isolated from colonic mucosa of *WT* pigs. Crypts were harvested by chemical and mechanical dissociation and cultivated in Matrigel for 9 days. Isolates incubated for 20 min in dissociation buffer showed numerous intact clusters of 5-10 crypts. Samples incubated for 30 min were dissociated into single (or fragmented) crypts and showed improved colony forming capacity. Representative bright field images are shown for three time points. Scale bars: 400 µm (white) 100 µm (black).

Organoids recapitulate key aspects of the organ's architecture and function. In order to compare the morphology of enteroids from the small and large intestine, I cultivated duodenum and colon enteroids for two weeks (Figure 13). Enteroids from both organs developed a highly budded (villus-like) morphology during crypt cultivation (passage 0). Duodenum enteroids recreated this structure after passaging. In contrast, colon enteroids changed to a round, plainer (crypt-like) morphology after the first passage.

Intriguingly, the morphological difference observed *in vitro* seems to mimic the mucosal structure of the organ[105]. The small intestine forms villi that protrude into the lumen and enlarge the surface area of the organ for maximal absorption of nutrients. The colon, however, has a flat mucosa with deep crypts for absorption of water and electrolytes. According to the morphological differences *in vivo*, the villus-like structure was preserved in duodenum cultures, whereas colon enteroids changed to a crypt-like morphology.

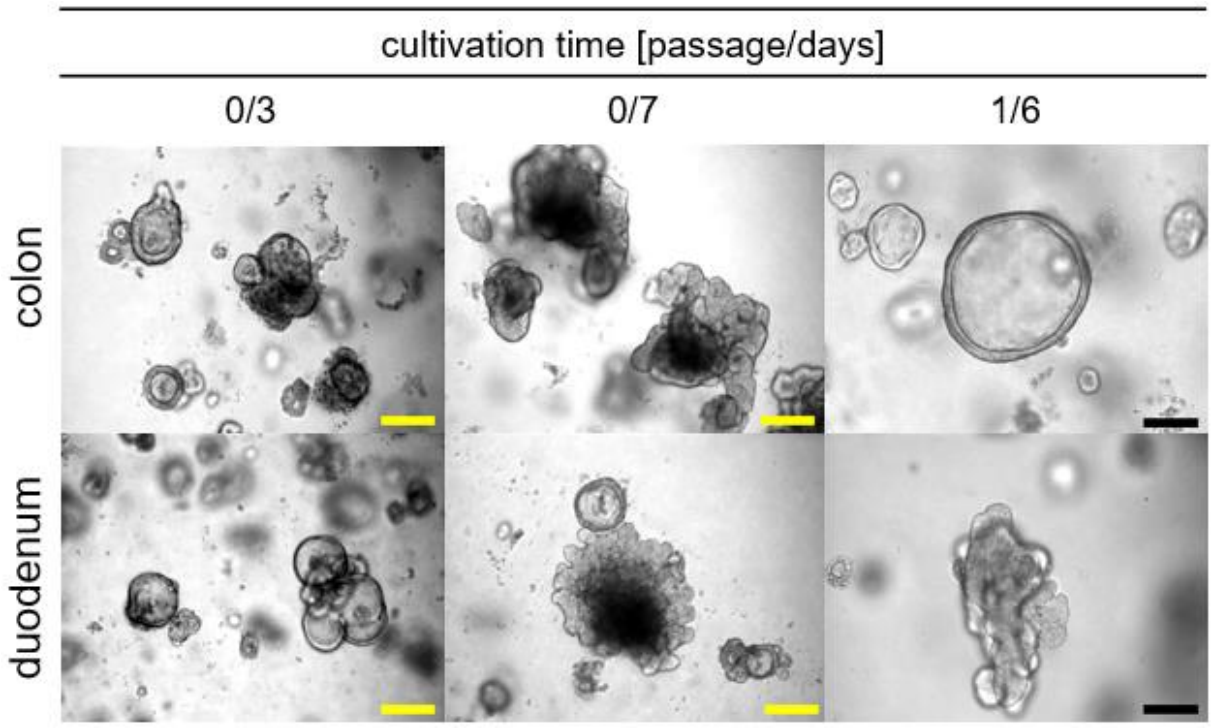

Figure 13 Morphological difference of enteroids derived from colon and duodenum of *WT* pigs. Crypts were harvested from either colon or duodenum of *WT* pigs and cultivated in Matrigel for 7 days. Afterwards the culture was split and cultivated for additional 6 days. Cultures from both samples showed a round, smooth (crypt-like) phenotype the first days of cultivation and grew into budded (villus-like) structures within one week. After passaging enteroids derived from duodenum showed villus-like structures, whereas colon enteroids maintained a cystic morphology. Representative bright field images are shown for three time points. Scale bars: 200 µm (yellow) 100 µm (black).

Porcine enteroid cultures have been used to study the role of nutrients for mucosal health[91] and susceptibility to enteric pathogens[93]. Similar to the organ, the functioning of an organoid depends on the composition of various cell types. The presence of several intestinal cell types in porcine enteroids was confirmed by the expression of specific markers (Figure 14 A). The most important cell type for enteroid cultivation is the fast-cycling LGR5-positive intestinal epithelial stem cell (IESC) because it generates the entire enteroid[106]. In contrast, reserve IESCs express HOPX and BMI1[107] and are activated after extensive tissue damage. In the intestine, Lyz-positive Paneth cells are located at the crypt base and support the stem cell niche

with growth factors[108] (Wnt, EGF, e. g.). The region between the crypt base and the surface epithelium contains highly proliferative pluripotent cells (transit amplifying cells) that are identified by expression of Ki67 and SOX9[109] and differentiate into a variety of secretory[90] (enteroendocrine, goblet cells) and absorptive cells[110] (enterocytes). The luminal site of the crypt is marked by VIL1-positive epithelial cells. Noteworthy, the inside-out polarity of the crypt is preserved in enteroids. The stem cell compartment is located at the periphery of enteroids and differentiated cells surround the lumen (inner cavity of the enteroid) where dead cells shed and accumulate.

The existence of the above-mentioned cell types was verified in porcine colon enteroids by RT-PCR (Figure 14 B) and a subset was visualised by immunofluorescence staining (Figure 15).

Enteroid-derived monolayers might be useful for future experiments including infection studies and co-cultures of lymphocytes and enteroids. In order to assess if the different cell types can be maintained in both culture environments, several antibodies and fixatives were tested on 3D enteroids (passage 1-2) and enteroid-derived 2D monolayers (passage 2).

Monolayers were generated by cultivating dissociated enteroids (passage 1) on adherent, uncoated cell culture plates in enteroid growth medium. Since fibroblasts are abundant in primary porcine kidney-derived cultures (pKDCs), pKDCs grown as 2D monolayers were used as negative control. The strongest signal for all antibodies was obtained with methanol for fixation of 2D cultures. Formaldehyde (4% PFA) was necessary to preserve the three-dimensional structure of enteroids but reduced the signal for most antibodies compared to 2D staining. Fully differentiated epithelial cells (VIL1+) were only visualised in enteroid-derived monolayers. Low numbers of ChgA-positive enteroendocrine cells and mucin-secreting goblet cells were present in enteroids and monolayers. HOPX-positive IESCs and transit amplifying cells (Ki67+, SOX9+) were the major cell types in 3D enteroids and monolayers. Noteworthy, the anti-HOPX antibody also stained a minor subpopulation of pKDCs. HOPX regulates proliferation and differentiation and is widely expressed, in heart, T helper cells, and follicular stem cells, for instance[111]. Although fibroblasts are dominant in pKDC culture, primary cultures, such as pKDCs, might include other cell types with stem cell-like properties which explains the HOPX-positive pKDC subpopulation. No *CAII*-

positive absorptive enterocytes nor fast cycling LGR5-positive IESCs were detected in porcine enteroids using anti-mouse and anti-human antibodies but expression of both marker genes was confirmed by RT-PCR. More antibodies need to be tested to find cross-reactive antibodies for these markers.

A

	marker	celltype
VIL1	Villin	epithelial cells
ChgA	chromogranin A	enteroendocrine cells
CAII	carbonic anhydrase II	absorptive enterocytes
MUC2	mucin	goblet cells
LYZ	lysozyme	Paneth cells
Sox9	SRY-box transcription factor 9	transit amplifying cells
BMI1	proto-oncogene, polycomb ring finger	reserve stem cells
LGR5	L-rich repeat containing Gpr 5	fast cycling stem cells
HOPX	HOP homeobox	reserve LGR4+ stem cells

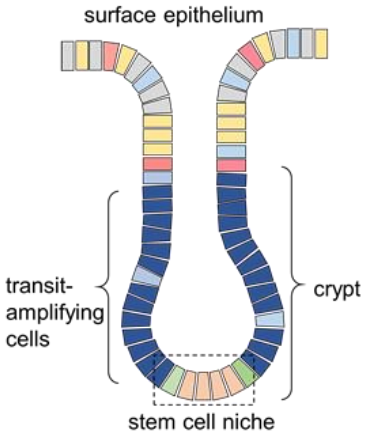

B

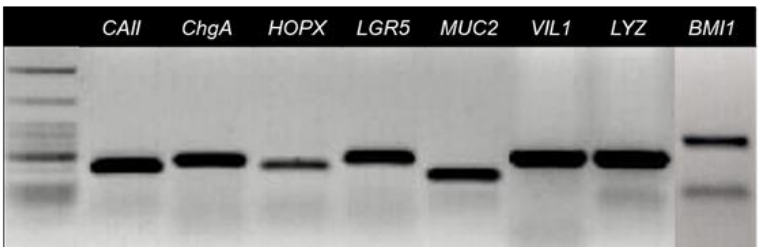

Figure 14 RT-PCR for identification of specific cell types of the intestine. The small and large intestine is composed of various cell types. The degree of differentiation increases towards the epithelial surface. Enteroids were analysed for the presence of cell types present in crypts and villi by expression of genetic markers. A table summarising cell type and marker genes in colonic crypts is shown (A). Colon enteroids were cultivated and RNA was isolated for RT-PCR. Intestine specific cell lineages were verified via cell type specific gene expression in colon enteroids (B).

Lysozyme-secreting Paneth cells were detected in monolayers as minor subpopulation but could not be precisely localised in enteroids. Instead, the lumen was stained in 3D cultures indicating the accumulation of lysozyme in the inner cavity. In order to quench autofluorescence of dead cells that shed into the lumen, fixed enteroids are treated with ammonium chloride after fixation. Consequently, no autofluorescence was detectable (secondary antibody control).

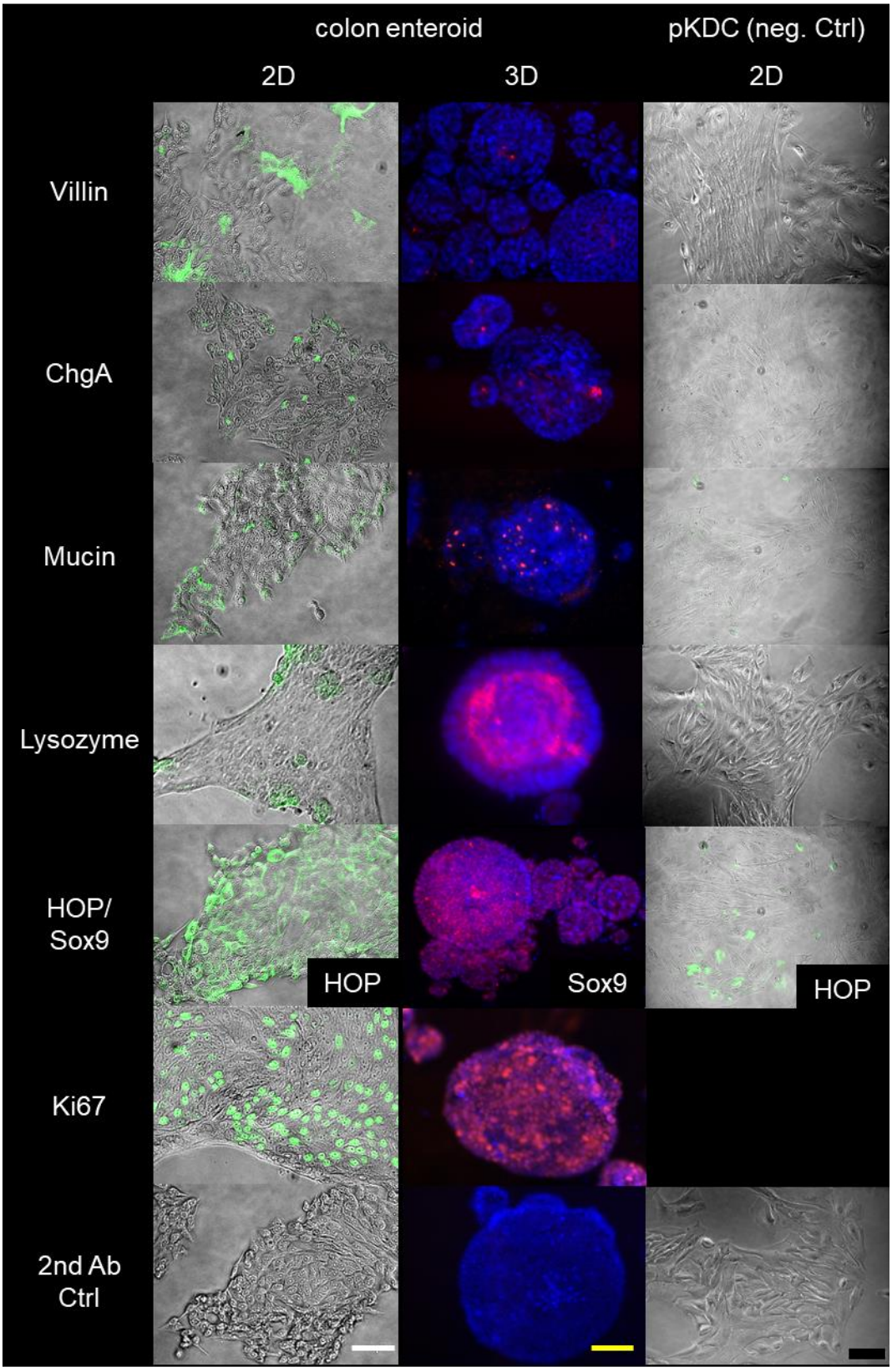

Figure 15 Staining of enteroid specific cell types. Colon enteroids were cultivated as 2D and 3D culture and stained for enteroid specific cell types. Cells gown in 2D were fixed in methanol and FITC-conjugated secondary Ab was used for fluorescent imaging. For 3D cultures PFA and Alexa594-conjugated Ab was used. Fluorescent images are shown for enteroid cultures and porcine kidney-derived primary cells (pKDC) as negative control. The secondary antibody control was performed to verify specificity of the detection antibody and exclude false-positive signal due to autofluorescence of cell debris. Scale bars: 400 µm (white), 200 µm (yellow), 100 µm (black).

Cultures from duodenum and colon could be expanded for 3-4 passages. Afterwards, enteroid formation stopped rapidly. Staining for Ki67 and Sox9 revealed that proliferation (Ki67) decreased over time but the proportion of transit amplifying cells (Sox9) remained high (Figure 16).

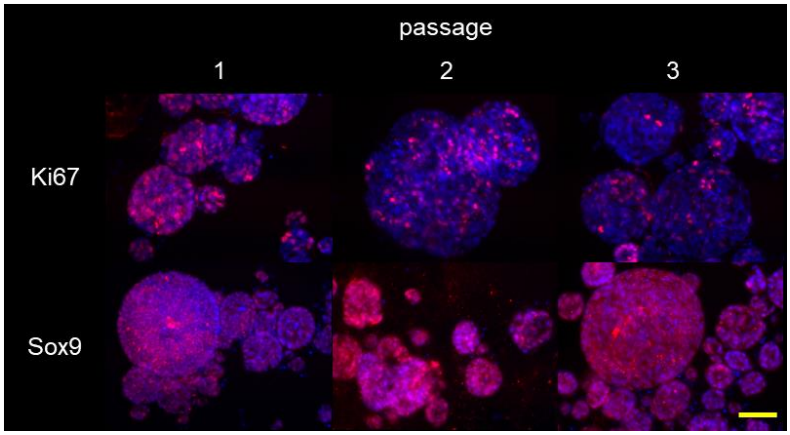

Figure 16 Staining of transit amplifying cells in enteroids. Colon enteroids were cultivated as 3D culture for 3 passages and stained for Ki67 and Sox9 (transit amplifying cell markers). PFA fixation and Alexa488-conjugated antibody were used. Enteroids were preserved in mounting medium with DAPI. The signal for Ki67 (proliferation marker) decreased during passaging, whereas Sox9 expression remained high. Scale bar: 200 µm.

To conclude, enteroids were successfully generated from the small and large intestine, including biopsies, and express all major intestinal cell lineage markers. However, the longevity of the culture had to be improved. It appears that, although stemness is preserved, the culture needs stronger proliferative signalling to expand. In the following sections, I will summarise attempts to improve the longevity of porcine enteroids.

3.2. Production of conditioned media for porcine enteroids

The medium used in this work is based on the supplement composition proposed by Clevers and Sato[64] which was optimised for murine and human intestinal organoids. The medium was shown to stimulate self-renewal of IESCs and differentiation of *LGR5*-positive cells. These cells were shown to form differentiated enteroids and could be expanded indefinitely. Essential components for the culture medium are Wnt and R-spondin, which induce stem cell renewal via stimulation of the Wnt pathway, and Noggin which controls differentiation via inhibition of the BMP pathway. Instead of using purified recombinant proteins, these supplements were produced as conditioned media to ensure better stability and biological activity[112].

3.2.1. Production of Wnt conditioned medium

The cell line for Wnt production is derived from murine subcutaneous connective tissue (L-cells) and was provided by the Clevers Lab. A dual luciferase assay (TOPFlash Assay, Figure 17) was used to determine Wnt concentration in conditioned medium. The TOPFlash Assay uses two luciferase cassettes that are transiently transfected into CHO (Chinese Hamster Ovary) cells.

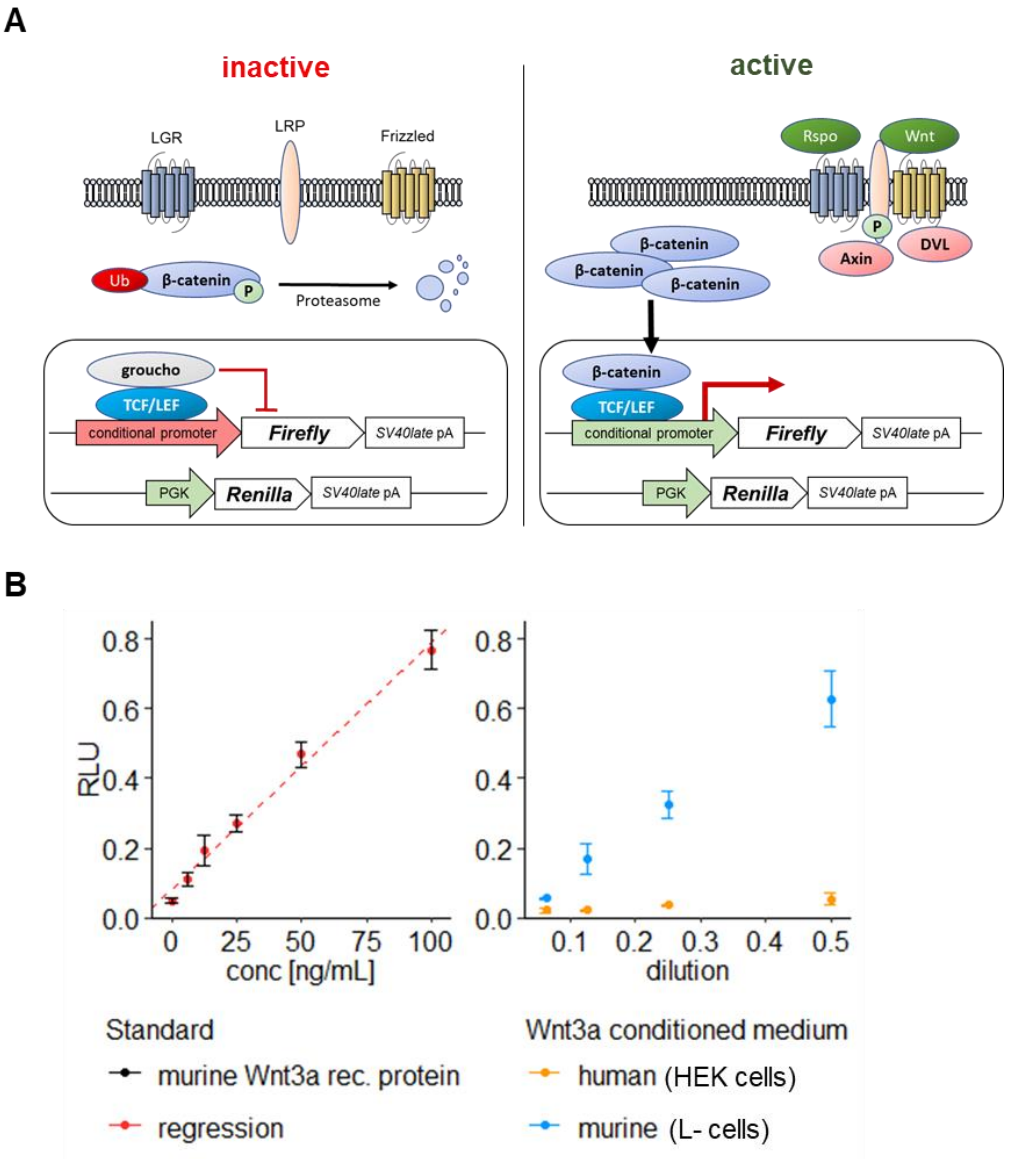

Figure 17 TOPFlash Assay of Wnt3a conditioned media. The concentration of Wnt in conditioned media (CM) was determined by TOPFlash Assay. (A) HEK cells were transfected with a dual luciferase construct that expresses *Firefly luciferase* under β-catenin responsive TCF-LEF promoter elements (Supplementary Figure 1). *Renilla luciferase* is expressed constitutively under the PGK promoter (Supplementary Figure 2). In presence of Wnt the proteasomal degradation of beta-catenin is inhibited. Beta-catenin can enter the nucleus, binds to TCF-LEF elements and activates the expression of Firefly. (B) Murine recombinant Wnt3a protein (mWnt3a) was used as standard to perform linear regression (red) of relative luciferase units (RLU, ratio of chemiluminescence signals Firefly:Renilla) and the protein concentration. CM were harvested from mWnt3a-producing L-cells and from HEK cells transfected with an expression vector for human Wnt3a (hWnt3a). Serial dilutions of each CM were tested to calculate the protein concentration of the batch. L-cells produce mWnt3a at concentrations of approximately 110 ng/mL, whereas no hWnt3a was detectable in CM from HEK cells.

Firefly luciferase is driven by repeats of TCF/LEF recognition elements which are bound by the transcription activator β-catenin during Wnt signalling (Supplementary Figure 1). Canonical Wnt signalling is activated by Wnt ligands and enhanced by R-spondin. Beta-catenin is translocated into the nucleus where it triggers expression of Firefly. Renilla luciferase is constitutively expressed by the PGK promoter (Supplementary Figure 2) and serves as reference signal (Figure 17 A). In this endpoint assay, the signal for both luciferases is measured separately and the relative signal intensity (RLU = Firefly:Renilla) is plotted against a linear dilution of the stimulus. The concentration of the stimulus in conditioned medium is calculated by comparing the signal of known concentrations (standard) to the signal from conditioned medium (Figure 17 B).

First attempts to produce Wnt conditioned medium resulted in a murine Wnt concentration of 110 ng/mL. According to the literature the optimal concentration of mWnt3a in enteroid culture medium is 100 ng/mL. Given the need to add several supplements the optimal concentration could not be attained.

In order to increase the concentration of mWnt3a, I modified the production of conditioned medium. I tested different batches of FCS (fetal calf serum), reduced the amount of medium that covers the cells to a minimum and doubled the incubation time to prolong the secretion of mWnt3a into the medium. However, the concentration could not be increased. I reasoned that the productivity of the cell line could be improved by transfecting the mWnt3a-producing cell line with an additional *Wnt3a* expression cassette. I decided to use a plasmid encoding for *human Wnt3a* (*hWnt3a*), whose protein sequence similarity to the porcine Wnt3a is 98% (compared to 97% for the murine protein). The plasmid was purchased from Addgene (Cat# 35908) and expresses the *hWnt3a* coding sequence under control of the *CAG promoter*. Stable expression of the transgene was ensured by selection via a *neo resistance* cassette cloned downstream of the *hWnt3a* coding sequence (Supplementary Figure 3).

First, I tested hWnt3a production in HEK293T cells. The linearized vector was transfected by electropermeabilisation and the culture was selected with G418. Successful selection was evident by the death of untransfected HEK293T cells after 7 days. Transfected cells were grown to confluency in G418 supplemented medium and hWnt3a conditioned medium was produced as described for mWnt3a.

Performing TOPFlash assay, I compared the productivity of the hWnt3a-producing HEK293T cells (HEK293T-hWnt3a) with the mWnt3a-secreting L-cell line (L-mWnt3a, Figure 17 B).

No hWnt3a was detectable in the supernatant of HEK293T-hWnt3a cells.

Among other post translational modifications, palmitoylation, which is the addition of monounsaturated palmitoleic acid to Ser-residues, is crucial for secretion and activity of Wnt proteins[113]. I assumed that posttranslational modification of recombinant Wnt by L-cells could be more efficient than in HEK cells. Thus, I repeated the transfection of the hWnt3a expression construct with L-mWnt3a cells (L-m+hWnt3a). In addition, I tested if Wnt is retained by the filter membranes during sterile filtration of conditioned medium. To test this hypothesis, I compared the Wnt concentrations of unfiltered conditioned medium from L-mWnt3a cells before and after sterile filtration with a PES filter (protein retentive, hydrophilic polyether sulfone) or CA filter (low binding cellulose acetate, Figure 18).

Regarding the standard error of the concentration of unfiltered conditioned medium, the concentration of mWnt3a was not increased by transfecting L-mWnt3a cells with the human expression construct and was not affected by sterile filtration. Of note, the concentration of Wnt in one batch is the arithmetic mean of the concentrations calculated from each serial dilution. Consequently, the standard error – displayed for transfected and untransfected conditioned medium – refers to the deviation from the mean of four serial dilutions as shown in Figure 17 B.

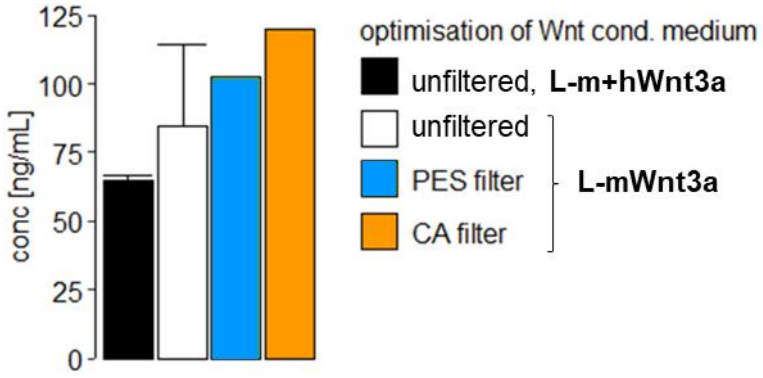

Figure 18 Optimisation of Wnt conditioned medium production. The concentration of murine Wnt3a conditioned medium was limited to 90-110 ng/mL. The concentration should be doubled to achieve 100 ng/mL in the culture medium as stated in the literature. In order to increase the production of Wnt protein, murine Wnt producing cells (L-mWnt3a, white) were selected for expression of a human Wnt3a expression vector (Supplementary Figure 3) (L-m+hWnt3a, black). One batch of conditioned medium harvested from the original L-mWnt3a cells (untransfected) was tested before and after filtration through a CA (Cellulose Acetate) or PES (Polyethersulfone) filter. Error bars indicate the deviation from the mean calculated from 4 serial dilutions. The concentration of Wnt was not improved.

L-cells had to be expanded in growth medium supplemented with Zeocin and G418 to ensure expression of both, murine and human Wnt. Due to this increased antibiotic stress, the productivity might be reduced compared to the original L-mWnt3a line.

Unable to improve the production of Wnt conditioned medium, I assumed that the shortage of Wnt could be compensated by supplementing culture medium with recombinant Wnt protein or increasing the concentration of R-spondin, which enhances Wnt-dependent signalling.

3.2.2. Production of R-spondin conditioned medium

Human R-spondin conditioned medium was produced with a 293T cell line expressing the coding sequence of *human R-spondin 1* (hR-spondin) fused to a C-terminal murine IgG2a Fc fragment. The cell line was provided by the Clevers' Lab and the production of human R-spondin conditioned medium is similar to Wnt conditioned medium. However, the TOPFlash Assay requires Wnt in the diluent (for activation of Wnt signalling) and serial ten-fold dilutions of hR-spondin conditioned medium are used to determine the concentration.

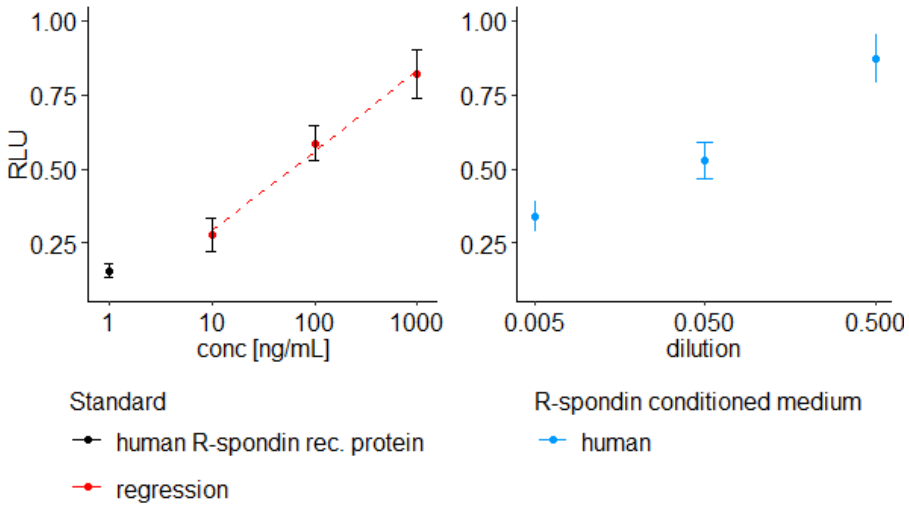

Figure 19 TOPFlash Assay of R-spondin conditioned medium. The concentration of human R-spondin-1 (hR-spondin) in conditioned medium (CM) was measured by TOPFlash Assay. Human recombinant protein was used as standard to perform linear regression (red) of relative luciferase units (RLU) and the protein concentration. Human R-spondin CM was harvested as cell culture supernatant. Serial 10-fold dilutions were prepared in 50% mWnt3a CM for TOPFlash Assay. The concentration of hR-spondin was 2.4 µg/mL.

R-spondin was produced at high concentrations equivalent to 24x the final concentration (100 ng/mL) needed for culture medium (Figure 19).

3.2.3. Production of Noggin conditioned medium

The *porcine NOG* gene contains only one coding exon which was amplified by PCR and cloned downstream of the *CAG promoter*. I added the coding sequence for four Gly-Gly-Ser repeats (GGS spacer) and a His_6-tag upstream of the *STOP* codon to facilitate the purification of the protein if needed (Figure 20 A, Supplementary Figure 4). Noggin forms a homodimer and its secondary structure is stabilised by five internal Cys-Cys disulfide bonds (Figure 20 B). The GGS spacer should reduce steric hindrance of the tag for dimerization. HEK293T cells express the simian virus 40 (SV40) large T antigen which induces replication of plasmids that carry the SV40 origin of replication (*SV40ori*). The presence of the *SV40ori* in the noggin expression vector ensured high copy numbers of the vector after transfection in HEK293T cells (HEK293T-pNoggin) and should improve protein expression[114].

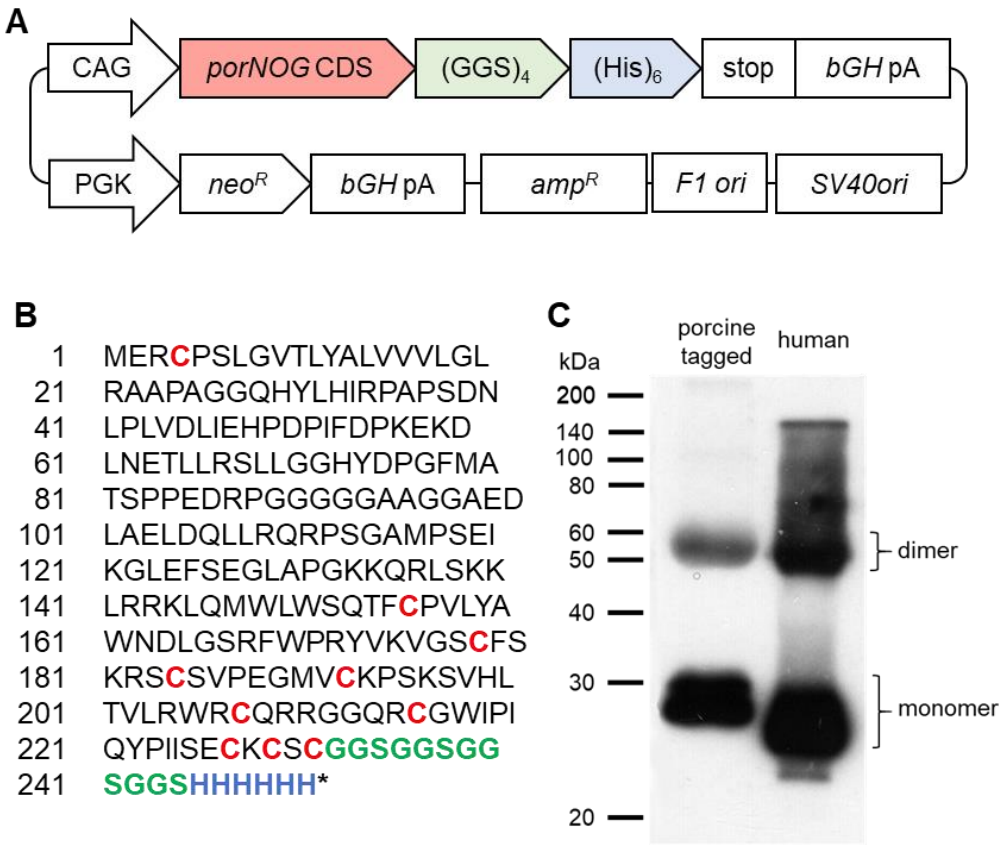

Figure 20 Design of an expression vector to produce porcine Noggin conditioned medium. The protein coding sequence of the porcine Noggin gene (Gene ID 574073) was cloned into an expression vector containing the *SV40ori* for strong expression in HEK293T cells. A His6-tag and a $(Gly\text{-}Gly\text{-}Ser)_4$-spacer were inserted upstream of the stop codon for affinity purification (Ni-NTA) of the protein from cell culture medium. Successfully transfected cells express the *neo resistance* gene and were selected with G418 (A). The amino acid sequence of the recombinant Noggin is shown. Ten Cys-residues stabilise the tertiary structure via disulfide bonds. The GGS repeats were inserted as spacer to avoid steric interference of the His-tag with the Cys-residues at the C-terminus (B). Porcine Noggin was detected by Western Blot in conditioned medium produced by HEK293T cells. Human recombinant Noggin was used as control (C). The spacer and tag increase the amino acid sequence of the porcine recombinant Noggin by 18 aa. The size of porcine recombinant Noggin is 27.3 kDa; the size of the control is 25.7 kDa. Western Blot indicates dimer formation, most likely due to incomplete reduction of disulfide bonds.

Cells were selected with G418 for stable integration after transfection as described for the hWnt3a expression vector. Conditioned medium was produced as described earlier.

The secretion of porcine noggin was verified by Western Blot using human recombinant noggin as control (Figure 20 C). The lowest bands represent the monomer with 25 kDa (glycosylated human protein without tag) and the tagged porcine protein of 27 kDa. A second band appeared over the porcine monomer possibly due to presence of uncleaved signal peptide (19 aa) or different post translational modification (glycosylation). Both the porcine and human recombinant protein gave bands around 50 kDa which indicate noggin dimer that did not dissociated because disulfide bonds were incompletely reduced prior to SDS-PAGE.

The concentration of porcine noggin was determined by indirect ELISA using a polyclonal mouse anti-human noggin primary antibody and an HRP-linked anti-mouse IgG secondary antibody. recombinant human noggin was used to create a standard curve and serial dilutions of conditioned medium were tested (Figure 21). The concentration was 7.8 µg/mL, which is 78 times the concentration needed for culture medium (100 ng/mL).

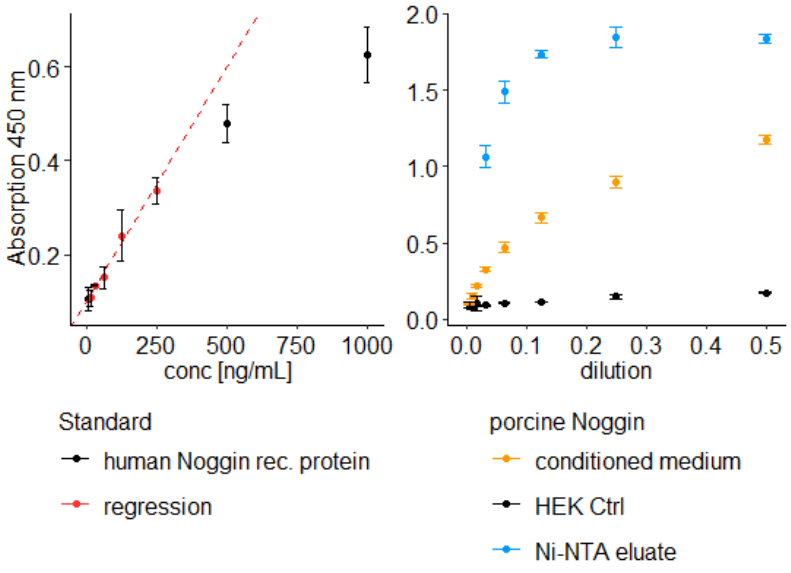

Figure 21 ELISA of porcine recombinant Noggin in conditioned medium. The concentration of porcine recombinant noggin was determined by indirect ELISA. Absorption was measured at 450 nm. Human recombinant noggin was used as standard (Left). Conditioned medium (CM) harvested from HEK293T culture was tested before and after Ni-NTA purification (Right). Medium harvested from untransfected HEK293T cells was used as negative Ctrl. The concentration of noggin in CM was calculated as 7.8 µg/mL using linear regression (red). The concentration of purified Noggin was approximately 10-25 times higher than the concentration in CM.

Affinity purification with Ni-NTA beads further increased the concentration 10-25-fold in the eluate but was not used for enteroid culture because the concentration in unprocessed conditioned medium was sufficient to achieve a final concentration of 100 ng/mL in enteroid growth medium. Later, I show that human recombinant noggin and porcine noggin conditioned medium equally support enteroid growth (Figure 22).

3.3. Optimisation of the porcine enteroid media formulation

The composition of supplements described in the literature is optimised for the development of mouse and human enteroids but the medium composition for porcine enteroid culture is not fully defined. Therefore, optimising the medium formulation for porcine enteroids was essential to extend the longevity of the culture.

Seven supplements that interfere with signalling pathways of the epithelial cell are used for human and mouse enteroid cultures (Figure 22 A). Conditioned media of Wnt and R-spondin[115] and the small molecule glycogen synthase kinase (GSK) 3 inhibitor CHIR[116] stimulate the canonical Wnt pathway. Human recombinant epidermal growth factor (EGF) activates mitogen-activated protein kinase (MAPK) pathway and contributes to the proliferation signal from Wnt signalling. The small molecule inhibitors Galunisertib[117] (LY2157299) and SB202190[118] interfere with Transforming Growth Factor-Beta (TGFβ) and p38 MAPK signalling, respectively. Noggin inhibits bone morphogenic proteins and supports maintenance of undifferentiated cells[119]. In summary, these supplements favour proliferation, stem cell self-renewal, control differentiation and apoptosis. The removal of Wnt, R-spondin and noggin from growth medium induces differentiation of human enteroids which highlights their essential role for IESC self-renewal[120].

I aimed to identify the supplements indispensable for porcine colon enteroid growth and adjust their concentration in the culture medium to improve the longevity of the culture. First, I identified the supplements essential for enteroid growth by removal of medium components. Since 3D and 2D enteroid-derived monolayers contain the major intestinal cell types I used monolayer cultures for the experiment as they facilitate the quantification of growth and decline of the culture using computer-assisted counting. Second, I compared the growth of single enteroids in 3D at increasing concentrations of each component.

To this end, I cultivated 2D monolayers derived from wildtype colon enteroids in media deprived of one or two (Wnt and R-spondin) supplements. The dissociated enteroids were seeded at low density (2x10^3 single cells per well of 48well plate) to measure cell proliferation. Cells were stained with DAPI eight days after seeding and nuclei were counted digitally on fluorescent images. As controls, cells were grown in basic medium without supplements and fully supplemented growth medium with either human recombinant noggin or porcine noggin conditioned medium (Figure 22 B).

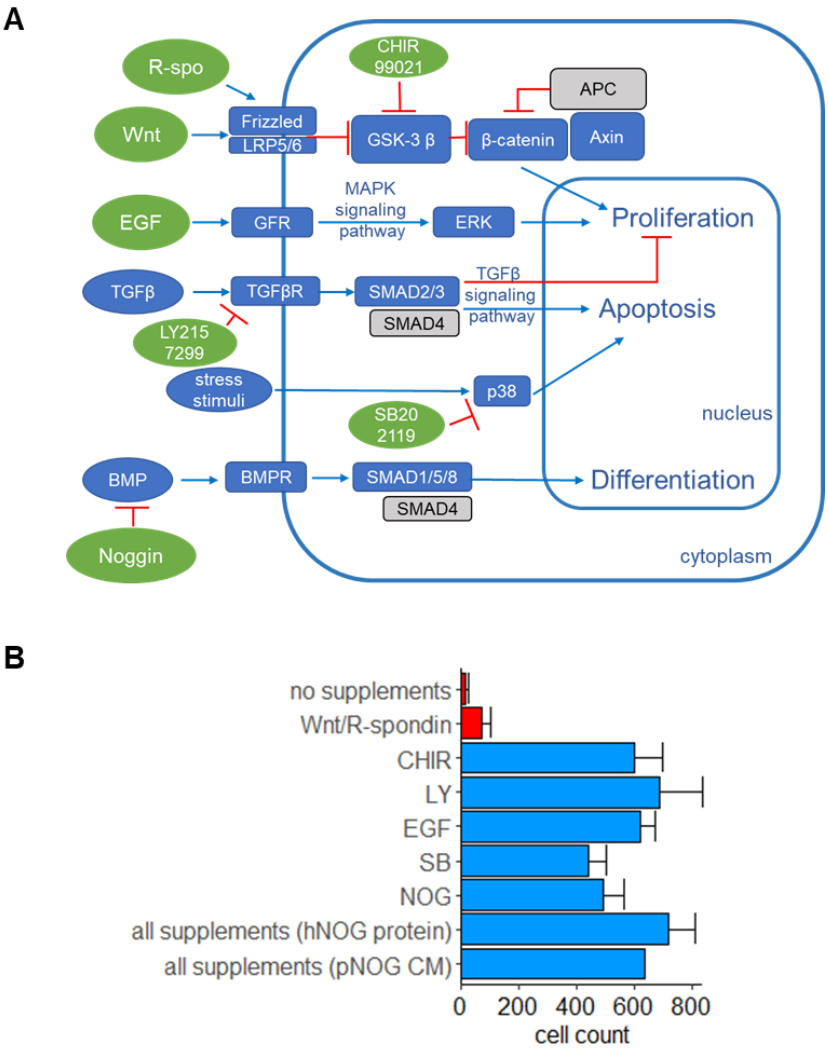

Figure 22 Identification of essential supplements for colon enteroids by supplement deprivation. Enteroids depend on the balance of signals that control proliferation and differentiation. According to the literature several supplements are needed to cultivate human and mouse colon enteroids. The proposed effects of each supplement (green) and two TSGs (gray) on cellular pathways (blue) are depicted (A). Colon enteroids from a *WT* pig were seed as 2D culture on a 48 well plate at a concentration of 2x10^3 cells/well. The cells were cultivated for one passage in supplement deprived medium. Single supplements (CHIR, LY, EGF, SB, Noggin) or the combination of Wnt and R-spondin were removed from complete growth medium. After 8 days, cells were stained with DAPI and fluorescent images were taken. The nuclei were counted and compared to cultures grown in basic medium (no supplements) or complete growth medium (all supplements) which contained either human noggin recombinant protein or porcine noggin conditioned medium. Error bars indicated the standard deviation from the mean within triplicates (B). The combination of Wnt and R-spondin is essential for enteroid growth, whereas the deprivation of other supplements was not detrimental for short-term cultivation.

The removal of Wnt and R-spondin inhibited the growth of the culture comparable to basic medium indicating that Wnt signalling is the major driver for enteroid proliferation. Deprivation of other supplements was not detrimental for proliferation. Consequently, the shortage of Wnt protein in the medium which results in reduced Wnt signalling in IESCs might be the reason for the rapid decline of the culture seen in previous experiments.

Pigs were established at the Chair of Livestock Biotechnology that carry a premature STOP codon at position 1311 in one allele of *APC*^{75}. *APC* is a tumour suppressor and negative regulator of Wnt signalling. Animals carrying the mutant *APC*^{1311} allele develop aberrant neoplasms in the colonic mucosa (polyps). I assumed that *APC*$^{1311/wt}$ enteroids isolated from polyps have a growth advantage as they carry only one functional gene variant. Surprisingly, the culture of colon enteroids from *APC*$^{1311/wt}$ pigs was limited to three passages like *APC-WT* isolates.

In order to understand if Wnt signalling is required for growth of *APC*$^{1311/wt}$ colon enteroids, I performed TOPFlash Assay using different Wnt concentrations and assessed enteroid proliferation by counting single cells of dissociated enteroids. Colon enteroids, derived from polyps of a *APC*$^{1311/wt}$ pig, were dissociated (passage 2) and 1x10^{6} single cells were electroporated with TOPFlash plasmids. The transfected cells were resuspended in Matrigel and seeded in 50 µL drops in 9 wells of a 24well plate. The culture was incubated with 25% or 50% mWnt3a conditioned medium which accounts for 30 or 60 ng/mL of Wnt protein. A concentration of 160 ng/mL was tested by adding recombinant murine Wnt3a to 50% conditioned medium. The concentrations were tested in triplicate and TOPFlash assay was performed 48 h after electropermeabilisation. Proliferation was measured by counting single cells of dissociated enteroids with Neubauer chambers seven days after transfection. Both, proliferation and Wnt signalling increased from 25% to 50% mWnt3a conditioned medium. Supplementing conditioned medium with recombinant mWnt3a protein did not improve Wnt signalling nor the proliferation of colon enteroids (Figure 23). Of note, previous experiments have shown that medium that is supplemented with murine Wnt3a recombinant protein instead of Wnt conditioned medium does not support enteroid formation.

The data show that the loss of one functional *APC* allele is not sufficient for Wnt-independent enteroid growth. Furthermore, recombinant mWnt3a protein cannot improve growth of porcine enteroids.

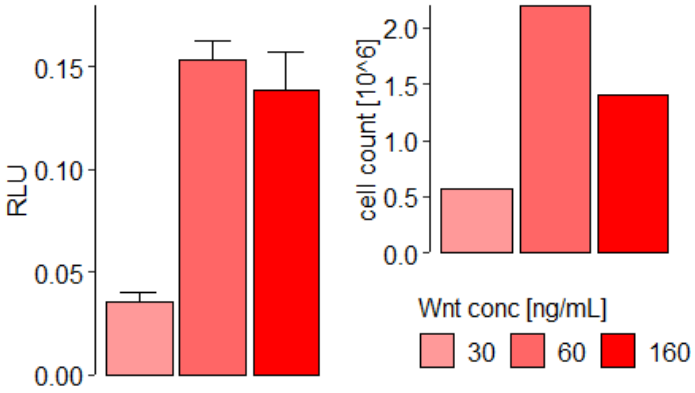

Figure 23 Wnt supplementation of enteroid culture. Colon enteroids were generated from a *APC*$^{1311/wt}$ pig and transfected with TOPFlash plasmids. The culture was cultivated in medium supplemented with 25% (30 ng/mL) and 50% (60 ng/mL) Wnt conditioned medium or 160 ng/mL Wnt by addition of recombinant protein. TOPFlash assay was performed 48 h after transfection and single cells were counted after 7 days. The number of cells and Wnt signalling reached a maximum at 60 ng/mL and was not increased by addition of Wnt recombinant protein. Error bars indicate deviation from the mean of three technical replicates.

Consistent with this observation, purified Wnt protein is reported to be ineffective for organoid cultivation because it rapidly loses activity in culture medium[112], I tested if increasing the concentration of other supplements could improve the growth of colon enteroids. Promising candidates are R-spondin, that enhances signalling of Wnt, and EGF that activates proliferation via MAPK pathway in IESCs.

It has been proposed that dissociation of enteroids into single cells adversely affects the longevity of the culture[121]. Hence, an alternative to single cell dissociation for measuring enteroids proliferation had to be found. The proliferation of enteroids is often assessed by counting of enteroids under the microscope. However, this approach is error-prone because it does not account for the difference in enteroid size which is characteristic of 3D cultures. I developed a computer-assisted approach based on the machine learning algorithm 'Cellpose'[122] to measure the size and number of single enteroids in Matrigel on 2D bright-field images.

Wildtype colon enteroids (passage 2) were dissociated into clusters of 3-10 cells, seeded at a concentration of 3000 cells/25 µL Matrigel and incubated with 1-, 2-, 4-, and 8-fold the recommended concentrations of supplements (according to human enteroid culture). Bright-field images were taken from the centre of the Matrigel drop

after seven days and the number and area of enteroids were compared to reference medium (1x the recommended concentrations of supplements). Clusters smaller than 300 μm^2 were excluded from the analysis as these are dead single cell agglomerates that do not show an inner cavity characteristic of viable enteroids. Enteroid proliferation for each condition was evaluated by the number of enteroids (Figure 24 A a), the area distribution of single enteroids (boxplots), and the total area (transparent bars) covered by enteroids (total area = sum of individual enteroid size, Figure 24 A b). A representative example for the digital process is shown for enteroids grown at two different concentrations of human EGF (Figure 24 B).

The two-fold increase of hR-spondin depleted enteroids evident in the extensive accumulation of dead cells in the lumen of enteroids. Increasing concentrations of SB202119, a p38 MAPK inhibitor, were also harmful to the cells. Interestingly, some colonies survived in these dying cultures and grew to considerable size (4-, and 8-fold SB202119) but they did not expanded after passaging. The enteroid forming efficiency was increased by doubling the concentration of EGF to 100 ng/mL and the size of enteroids was significantly enlarged. This effect was not observed for higher concentrations. Increasing the concentration of LY2157299, a TGFβ inhibitor, and noggin conditioned medium had no effect on enteroid formation efficiency nor the size of enteroids.

Taking the last two experiments into consideration, Wnt signalling and enteroid growth cannot be ameliorated by adding recombinant murine Wnt protein or increasing the concentration of R-spondin. Instead, the increased mortality of enteroids due to hR-spondin suggests that overstimulation of Wnt signalling might be harmful. IWR1-endo is a Wnt pathway inhibitor that was shown to maintain pluripotency in porcine blastocyst-derived cell culture at concentrations between 1.5 and 2.5 μM[123]. Thus, I supplemented complete growth medium with IWR1-endo and analysed the number and size of enteroids (Supplementary Figure 5). The size of enteroids was significantly reduced for all IWR1-endo concentrations tested (1.25 -10 uM) and none of the IWR-treated cultures could be expanded.

Based on these observations, the original human enteroid medium could not be improved to expand the longevity of porcine enteroids. However, porcine noggin conditioned medium can substitute recombinant purified noggin and 100 ng/mL

human EGF recombinant protein improves size and number of porcine enteroids compared to the original protocol.

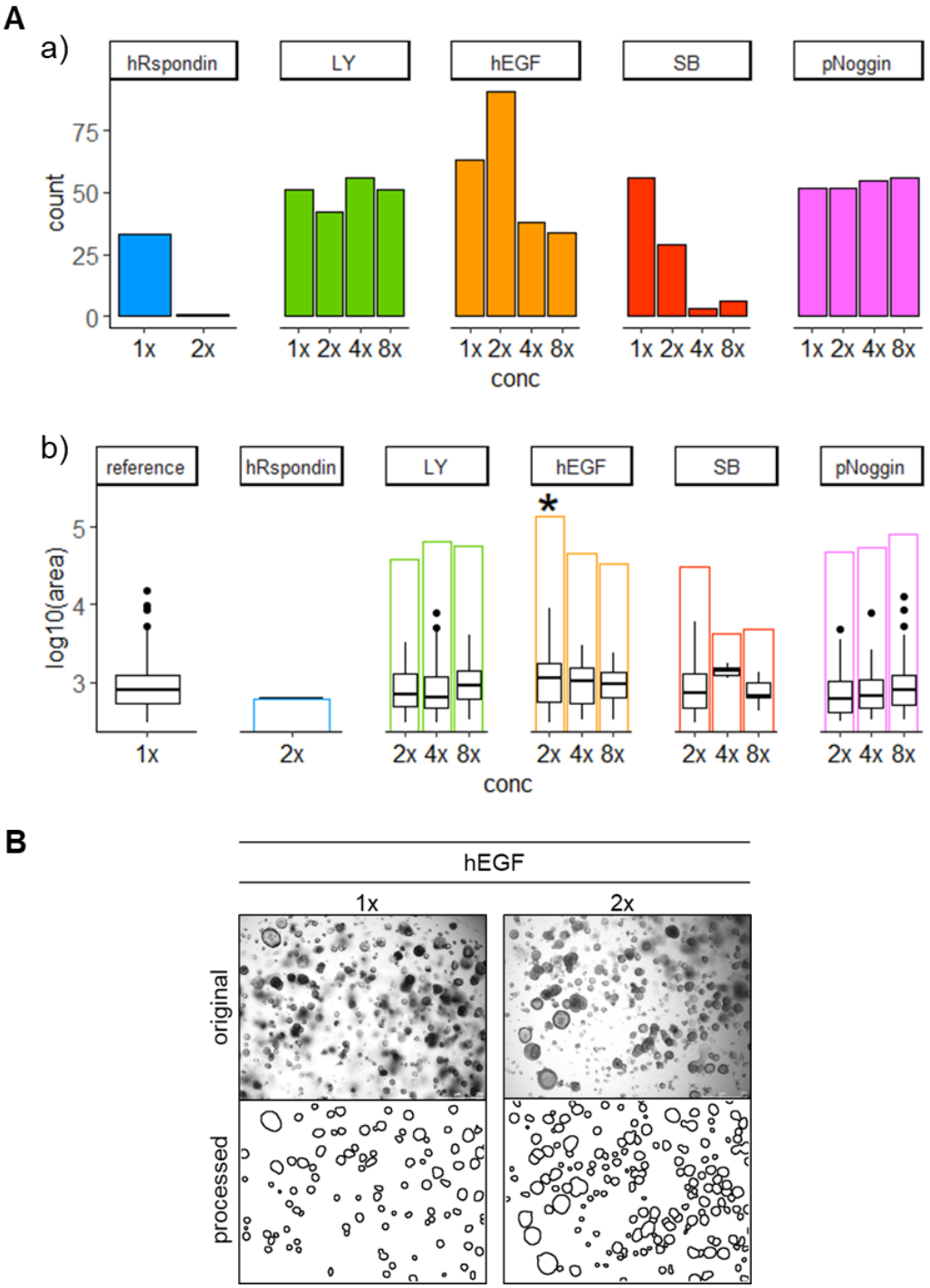

Figure 24 Effect of increased supplement concentrations on enteroid growth. Colon enteroids were derived from a *WT* pig and cultivated at increasing concentrations of supplements starting at the concentration recommended for human colon enteroids (1x) up to 8x the standard concentration. Bright field images were taken and processed with a machine learning algorithm to analyse single enteroids. Using open-source software (Cellpose, Fiji, R), single enteroids were counted and their size was estimated by the area they covered on 2D images (A). I compared the enteroid formation efficiency (A, a) by counting single colonies, the area distribution of individual enteroids (boxplots), and the total area (transparent bars) covered by the enteroids (A, b). A representative example for the digital process is shown for two concentrations of human EGF (B). T-test with Welch approximation was used to identify differences in enteroid size between the reference (1x) and increased supplement concentrations. Significant differences of the mean enteroid size are indicated (*) for a p-value < 0.05.

In 2018, Fujii et al. presented an organoid cultivation medium with improved culture efficiency for human enteroids[83]. The authors state that the addition of the growth factors IGF-1 and FGF-2 to the medium and the removal of nicotinamide, N2 supplements, and SB202119 improve long-term cultivation and cellular diversity.

In order to test if this also applies to porcine cultures, I cultivated colon and duodenum enteroids from a wildtype pig in the original and improved medium for three passages. The cultures were passaged every seven days and samples were taken to measure the expression of intestinal cell markers (described in Figure 14 A) by qPCR.

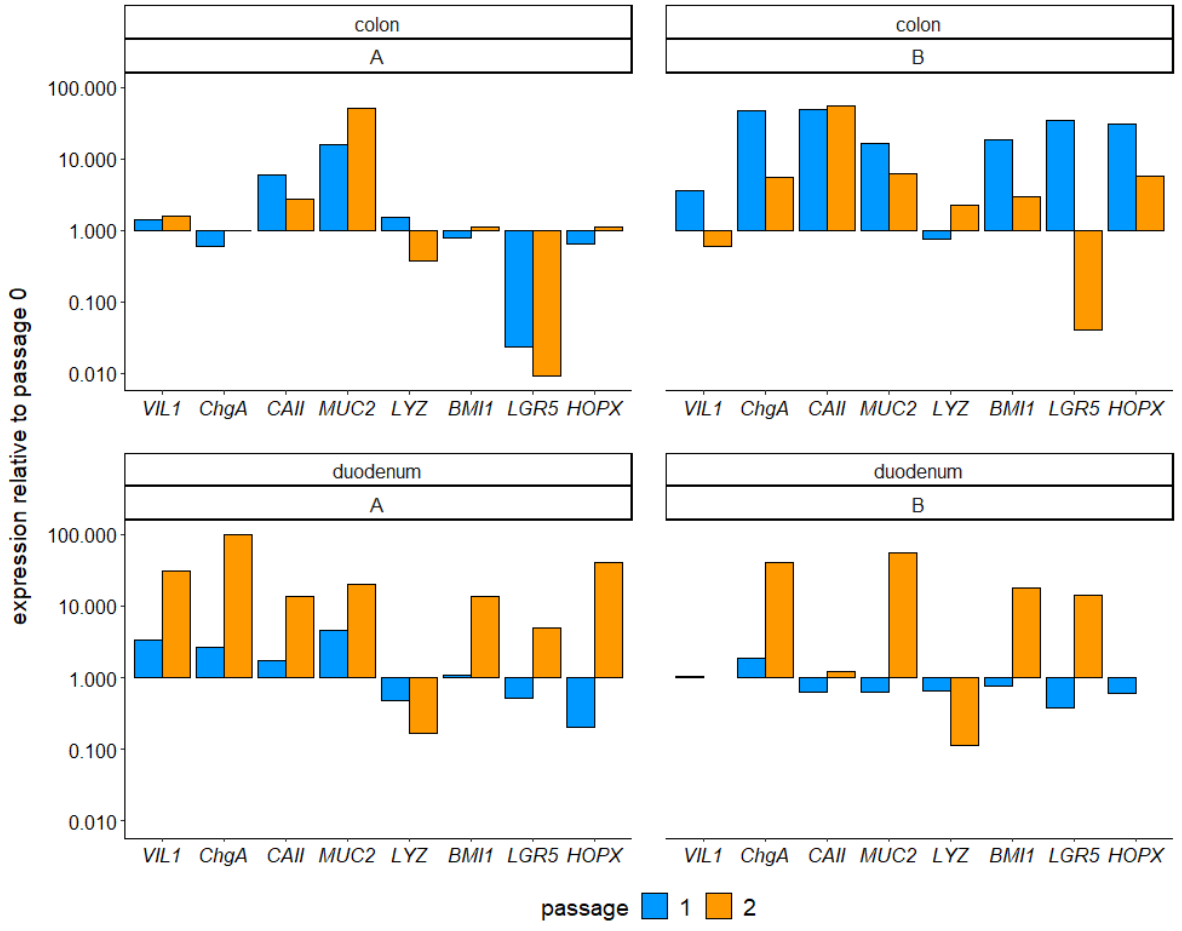

Figure 25 Influence of media on cellular diversity of colon and duodenum enteroids. Two media are described in literature for human and murine intestinal organoid culture that contain different supplements. The medium described by Clevers and Sato was based on insights from developmental biology of the intestine (medium A) and improved for enriched cell diversity (medium B) later. The small and large intestine is composed of various cell types along the crypt and villus. Intestinal crypts isolated from colon and duodenum of a *WT* pig were cultivated for two passages in either medium, A or B. In each group the expression of eight markers was compared to the respective crypt culture (passage 0). The media show opposing effects on colon and duodenum enteroids regarding the stability of expression intestinal cell markers.

None of the media allowed enteroids to expand after the third passage. For this reason, expression analysis was limited to passage 1 and 2. Expression is plotted as

fold-change compared to crypts (passage 0) cultivated for seven days in the respective medium (Figure 25). Medium A is the original enteroid medium; medium B is the improved variant.

In general, the expression pattern of enteroids changed considerably within both cultures after passaging. The expression profile of the crypt culture was best preserved in colon enteroids grown in medium A and duodenum enteroids grown in medium B after the first passage. Expression changes of one to two magnitudes were detected at the end of the cultures, especially for goblet cells (*MUC2*). In contrast, the expression indicative for differentiated cells markedly increased in colon enteroids grown in medium B and duodenum enteroids in medium A. Expression of *LGR5* was dramatically reduced in colon enteroids which was not observed for duodenum enteroids. Besides, the expression of reserve stem cells (*HOPX*, *BMI1*) was mostly stable or increased at the end of passage 2.

Intending to model the *in vivo* conditions of the porcine colon with enteroids, I decided to continue the experiments in the original medium which ensured the most stable expression of intestinal markers similar to the initial crypt culture.

3.4. *In vitro* characterisation of polyposis phenotypes

APC$^{1311/wt}$ pigs develop polyps within the first year of age similar to precancerous lesions observed in FAP patients. Two phenotypes can be distinguished by the severity of polyposis in these pigs (Figure 26 A). Endoscopy of the colon was recorded for 37 animals and the number of polyps in the distal colon (approximately 60 cm) was counted by eye. A phenotype of less than 80 polyps was classified as mild (MP) and a polyp load between 100 and 300 polyps as severe polyposis (SP, Figure 26 B). The protocols established in this work have enabled the cultivation of intestinal cells from this model for the first time. I asked if enteroids generated from normal mucosa specimen of either phenotype show different growth characteristics that could explain the severity of polyposis.

Crypts were isolated from normal mucosa of pig siblings with either MP and SP and enteroids were cultivated until the fifth passage. Using the digital image processing algorithm, their number and size (individual enteroid area and total area per well) was analysed (Figure 26 C). The viability was examined with live/dead staining using FITC-diacetate, which is hydrolysed by living cells to release green fluorescent FITC,

and propidium iodide, that accumulates in dead cells and exhibit red fluorescence (Figure 26 D). Both cultures developed equally in number and size until the end of the second passage. Starting at passage 3, cells were seeded at five times higher density ($5x10^4$/50 µL Matrigel) to compensate for the reduction in viability and proliferation.

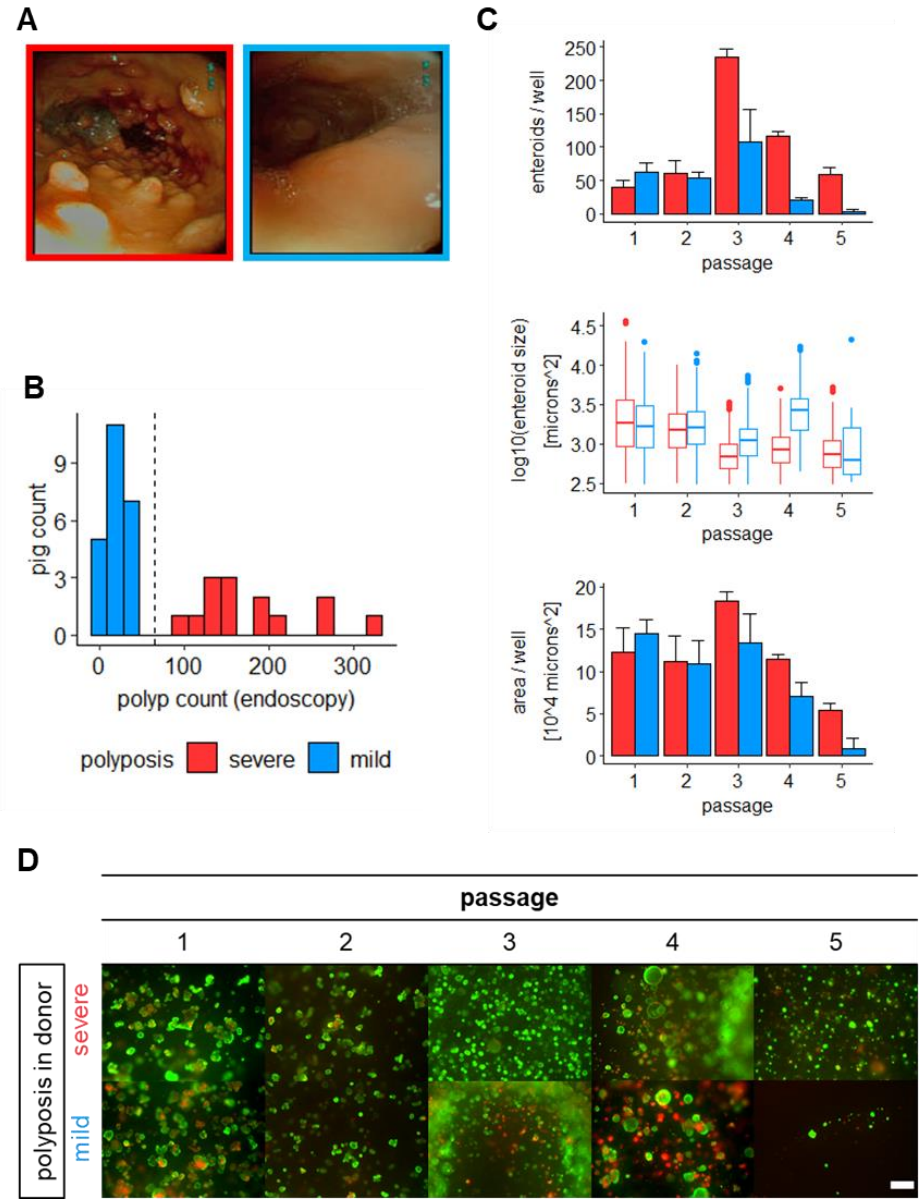

Figure 26 Phenotypic characterisation of the porcine FAP model. Pigs were generated carrying a truncation mutation in one allele of the porcine *APC* gene (*APC*^{1311}) orthologous to the human early stop mutation *APC*^{1307}. The animals can be classified by their degree of polyposis measured by endoscopy (A). Polyps were counted on videos of endoscopy (B). Animals with mild polyposis present with a polyp load of <100. Between 100 and 300 polyps per video were counted for the severe phenotype. Enteroids were generated from normal mucosa of siblings with different phenotypes and their growth characteristics (C) analysed. In addition, live/dead staining was performed for each passage (D). Enteroids were cultivated for five passages with six technical replicates and bright field images were taken at the end of each passage before splitting. The images were used for growth evaluation with the following parameters: amount of single enteroids per well, area distribution of single enteroids, total area covered by the enteroids per well. Enteroids generated from the animal with severe polyposis were increased in number and total culture size. Enteroids from this phenotype were viable until passage 5, whereas the cells of the sibling with mild polyposis could not be further expanded. Error bars indicate standard deviation from the mean of technical replicates. Scale bar 400 µm.

Enteroids derived from normal mucosa of the SP donor showed smaller enteroids due to the high density of developing clusters in Matrigel. These enteroids surpassed cultures from MP mucosa in number and total area from passage 3-5. The live/dead staining of passages 3 and 4 suggest that enteroids generated from the SP donor are more viable than cultures derived from the animal with MP.

In conclusion, a minor growth advantage was detectable for enteroids from SP mucosa compared to MP tissue. However, the observed effect is not strong enough to explain the phenotypic differences visible in the animal. Moreover, the precancerous lesions observed in the FAP model do not develop into malignant disease until the age of 2-3 years. In general, cancer cells undergo genetic and epigenetic alterations that selectively promote an invasive phenotype *in vivo*[124].

3.5. Optimisation of DNA delivery into enteroids

The aim of my work was to improve the current FAP model by inducing invasive disease in young animals. The oldest *APC*$^{1311/WT}$ pig was 48 months old and did not show invasive CRC. I assumed that cancer progression could be accelerated if epithelial cells were transformed *in vitro* and transplanted back into the donor animal. For this purpose, I established the delivery of plasmid DNA into enteroids to precisely edit porcine TSGs involved in CRC progression. In this section, I present the optimisation of porcine enteroid transfection and a multiplex CRISPR/Cas construct for the simultaneous inactivation of five TSGs relevant for enteroid transformation and CRC modelling.

The delivery of foreign DNA into mammalian cells is key to modifying any *in vitro* culture for experimentation. Different means of DNA transfer exist and can be achieved by viral (transduction) or non-viral (transfection) methods of 2D and 3D cultures[125]. Among the viruses used for transduction lentiviruses are of advantage as they enable the delivery of transgenes into primary cells that are usually difficult to transfect. Furthermore, they have a packaging capacity of up to 7 kb and drive long- or short-term transgene expression by integrating into the genome or as non-integrating variant[126].

Transduction of enteroids was performed by centrifugation of dissociated enteroids with lentivirus, a process termed spinoculation. The non-integrating recombinant lentivirus was produced by Dr. Marcel Rommel at the Paul-Ehrlich-Institute to

express *Cre* recombinase under the *spleen focus forming virus* (SFFV) *promoter* (Lenti-Cre, Supplementary Figure 6). In order to visualize transduction, enteroids were generated from a pig line that carries a dual fluorochrome cassette driven by the CAG promoter at the *ROSA26* locus (*TGROSA*)[127]. Cells switch expression after Cre-mediated recombination from membrane-targeted tandem dimer Tomato (red) to membrane-targeted green fluorescent protein (GFP, Figure 27 A).

Enteroids were harvested from crypt culture (passage 0) of a *TGROSA* pig and dissociated into clusters of 3-10 cells. Lenti-Cre was added to the clusters at a virus-to-cell ratio (MOI, multiplicity of infection) of 1:1, 10:1 and 50:1. Transduction enhancer solution, TransDux Virus Transduction Reagent (BioCat), was added to the suspension and cells were spinoculated at 600xg, 32°C for 1h in culture medium without serum. After infection, the cells were washed and cultivated in Matrigel.

Lenti-Cre-mediated recombination of the TGROSA cassette was observed by fluorescent microscopy but efficiency and survival after spinoculation was low (Figure 27 B) independent of the MOI.

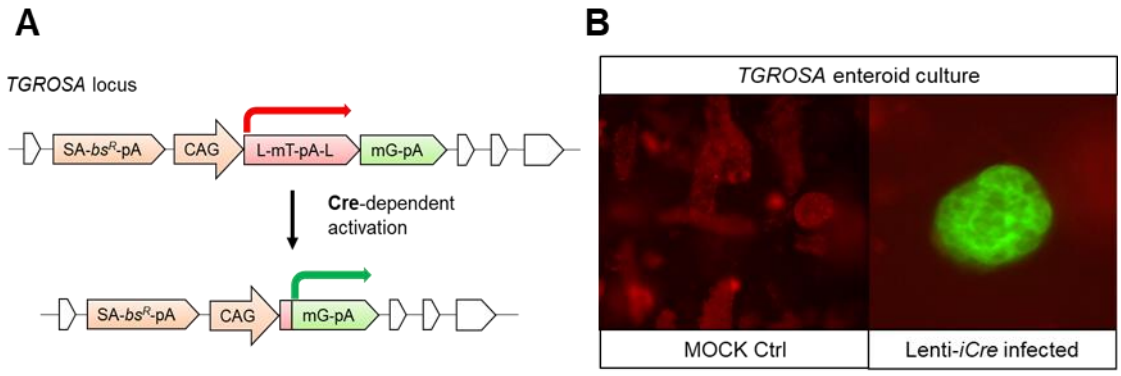

Figure 27 Lentiviral transduction of colon enteroids. Colon enteroids were generated from *TGROSA* reporter pigs and infected with a non-integrating lentivirus which carries a *Cre* expression cassette. Successful transduction was observed by the Cre-dependent switch from mt-Tomato to mt-GFP fluorescence (A). Representative fluorescent images are shown for lentivirus and mock treated cultures (B).

Non-viral transfection methods like lipofection and electropermeabilisation depend on physicochemical properties of cells and DNA. The transport into the cell is either based on the fusion of lipid-DNA complexes with the membrane or the formation of membrane pores by electrical pulses. Lipofection shows high transfection efficiency in fast cycling cell lines and although several parameters must be optimised for electropermeabilisation - such as the voltage, the number, and the length of pulses – non-viral transfection has significant advantages. First, the identity and amount of

DNA can be combined flexibly for transfection and, secondly, transfection can be performed under S1 conditions.

Lipofection and electropermeabilisation were tested with a GFP expressing construct (Supplementary Figure 7) for enteroids generated from a pig that carried a silent dominant negative mutation in both alleles of the *TP53* gene (*TP53*$^{LSL\text{-}R167H/\ LSL\text{-}R167H}$). Since the full length mRNA of *TP53* is not expressed in this line, the enteroids show a growth advantage and could be expanded until passage 5 to obtain enough single cells to test various settings of electropermeabilisation and lipofection simultaneously. Lipofectamine 2000 was tested with single cell suspension of enteroids according to the manufacturer's instructions but no green fluorescence was observed (data not shown). Adding spinoculation to the protocol did not improve lipofection.

I optimised electropermeabilisation by applying pulses different in voltage, number, and length on enteroid-derived single cells resuspended in in-house sodium phosphate transfection buffer. After transfection, cells were cultivated in Matrigel. Two days later, the culture was imaged by fluorescent microscopy and single cells were analysed by flow cytometry with exclusion of dead cells (Figure 28, gating strategy is shown in Supplementary Figure 8).

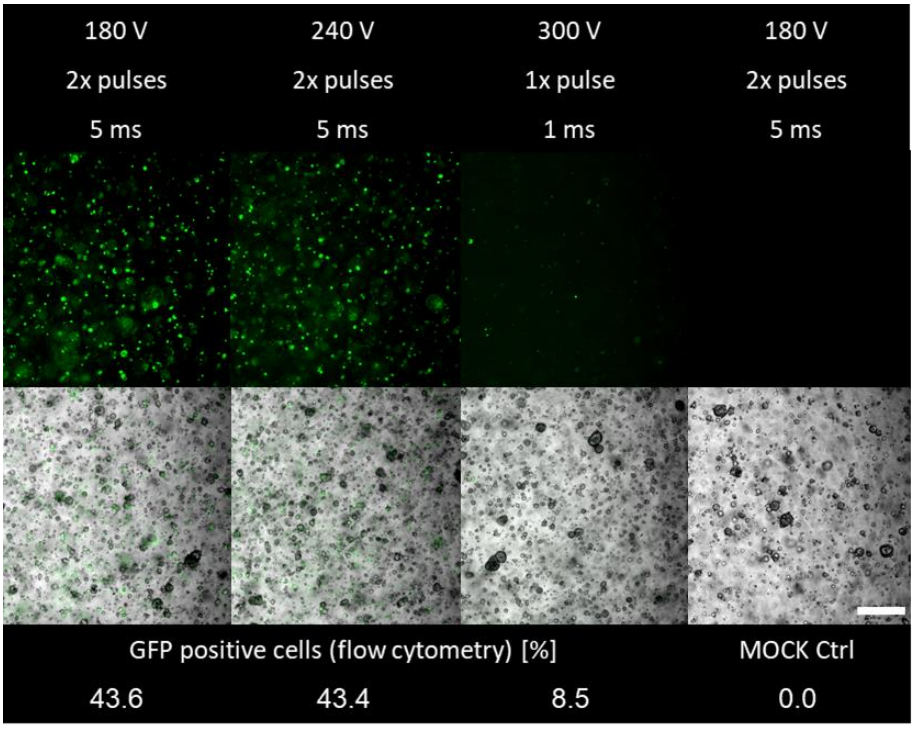

Figure 28 Optimisation of electropermeabilisation of colon enteroids. Colon enteroids were generated from *TP53*$^{R167H/R167H}$ pigs and electroporated with a plasmid coding for *eGFP* (Supplementary Figure 7). The voltage, number of pulses, and pulse length was varied to find the optimal combination. The ratio of green fluorescent GFP+ cells was quantified by flow cytometry. Representative fluorescent images and the bright field overlays are shown for three combinations. Scale bar is 400 µm.

The essential parameter for electropermeabilisation was the pulse length of 5 ms. No difference of the transfection efficiency and the viability was detectable by flow cytometry between 180V and 240V. Under these conditiones, the maximal proportion of green-fluorescent cells was 43% and viability was higher than 90% (Figure 28). Therefore, the optimal parameters were defined as 180V and 5 ms per pulse with a pulse interval of 100 µsec.

Since electropermeabilisation achieved unprecedented transfection efficiencies, all future modifications of enteroids were conducted with this protocol.

3.6. Genome editing of porcine enteroids

I aimed to simultaneous inactivate multiple TSGs relevant for colorectal cancer progression to accelerate tumour formation in the FAP pig. To this end, I used the CRISPR/Cas system to introduce double strand breaks in early exons shared between all known splice variants of the genes. The regions of interest were uploaded in CRISPOR (http://crispor.tefor.net/), an online tool for crRNA design, to predict efficient target sites for the S. pyogenes Cas9 endonuclease. The sequences for the corresponding target sites, called crRNAs, were separately subcloned into a CRISPR/Cas9 vector. This vector carries the *U6 promoter* that expresses the *guide RNA* which is the crRNA sequence linked to the trans-activating crRNA (tracrRNA) that is required for complex formation of Cas9 and guide RNA. In addition, the vector encodes *Cas9* driven by the *CAG promoter* (Supplementary Figure 9). The efficiency of each guide RNA was tested *in vitro* by transfection of the CRISPR/Cas vector into primary kidney-derived cells (pKDCs) which are well established for guide RNA testing at the Chair of Livestock Biotechnology. Using puromycin selection for two days, successfully transfected cells were expanded for sequencing analysis. The target region was amplified by PCR from cell lysate and sequenced. Uploading the sequencing readout to the online InDel prediction tool ‘ICE Analysis’ (Synthego) the percentage of insertions, deletions (InDels), and frame shift mutations was predicted for each guide RNA.

Four crRNAs targeting *SMAD4*, *p16INK4a*, *PTEN* and *TP53* were already tested by M.Sc. Daniela Kalla and Dr. Carolin Perleberg. I tested crRNAs targeting exon 3 of the *APC* gene in pKDCs. According to sequencing analysis, the gene was inactivated with an efficiency of 54% in puromycin-selected pKDCs.

The selection of primary enteroids with a five-fold knockout of CRC relevant TSGs would be difficult if separate CRISPR/Cas vectors were used. Instead, transfecting a single construct that enabled the transcription of all five crRNAs would increase cell viability and selection. For this purpose, a multiplex cloning strategy was developed to clone all five crRNAs into one CRISPR vector of 10 kb (pentaplex). The guide RNAs are transcribed by the *U6 promoter* as one transcript and spliced into single guide RNAs by the cellular tRNA splicing machinery (Figure 29 A).

Enteroids were generated from polyps sampled during colon biopsy of two pigs. $APC^{1311/WT}$ enteroids were generated from pig #1636 (4 months old). In addition to the mutant *APC-1311* allele, pig #1658 (5 months old) carried a silent oncogenic *KRAS-G12D* allele, which will be discussed in the next chapter, where activation of *KRAS-G12D* is shown upon recombination by Cre.

The growth of $APC^{1311/WT}$ and $APC^{1311/WT}$ $KRAS^{LSL-G12D}$ enteroids was monitored throughout the experiment by counting single cells after passaging. Enteroids were transfected with the pentaplex at day 10 (end of passage 1). The culture was expanded until the end of passage 5 (day 34). The number of untransfected cells cultivated as control, decreased between passage 3 and 5 and only transfected cells could be expanded (Figure 29 B). Obviously, the pentaplex-induced transformation created a growth advantage that could be used to select for successfully transfected cells.

The target sites were amplified by PCR and sequenced to estimate the proportion of gene editing in enteroids (Figure 29 C). According to ICE Analysis of the sequencing results, all loci were edited with high efficiency (> 80%) and inactivation by frame shift mutations was expected in 50-90% of amplified alleles (Figure 29 D). The sequencing analysis is shown for line #1658 but were also conducted for line #1636 (Supplementary Figure 11).

The criteria for the CRISPR/Cas target site in a TSG were proximity to the start codon and presence in all transcript isoforms (Figure 29 E). Thereby, frame shift mutations should affect all transcripts and inactivate the TSG. In conclusion, the pentaplex allowed simultaneous editing of all five TSGs with high efficiency.

CRISPR/Cas editing did not disrupt transcription of TSGs because the mRNA transcripts were detected by RT-PCR (Supplementary Figure 12). In order to verify

the knockout of the edited genes by Western Blot, several anti-mouse and anti-human antibodies were tested for porcine tumour suppressor proteins. The lysate of pKDCs was used as unmodified wildtype control for Western Blots because the amount of wildtype enteroids was limited. Knockout of *p53* and *SMAD4* was verified by Western Blot in enteroid lines #1636 and #1658 (Figure 29 F). However, I was not able to detect porcine APC, p16 and PTEN with the antibodies used in this work (Supplementary Figure 14).

Transformed cells accumulate loss of function mutations in TSGs and gain of function mutations in oncogenes, such as *KRAS-G12D*[128]. In the next section, I will show that the silent oncogene present in enteroid line #1658 was activated by Cre recombinase.

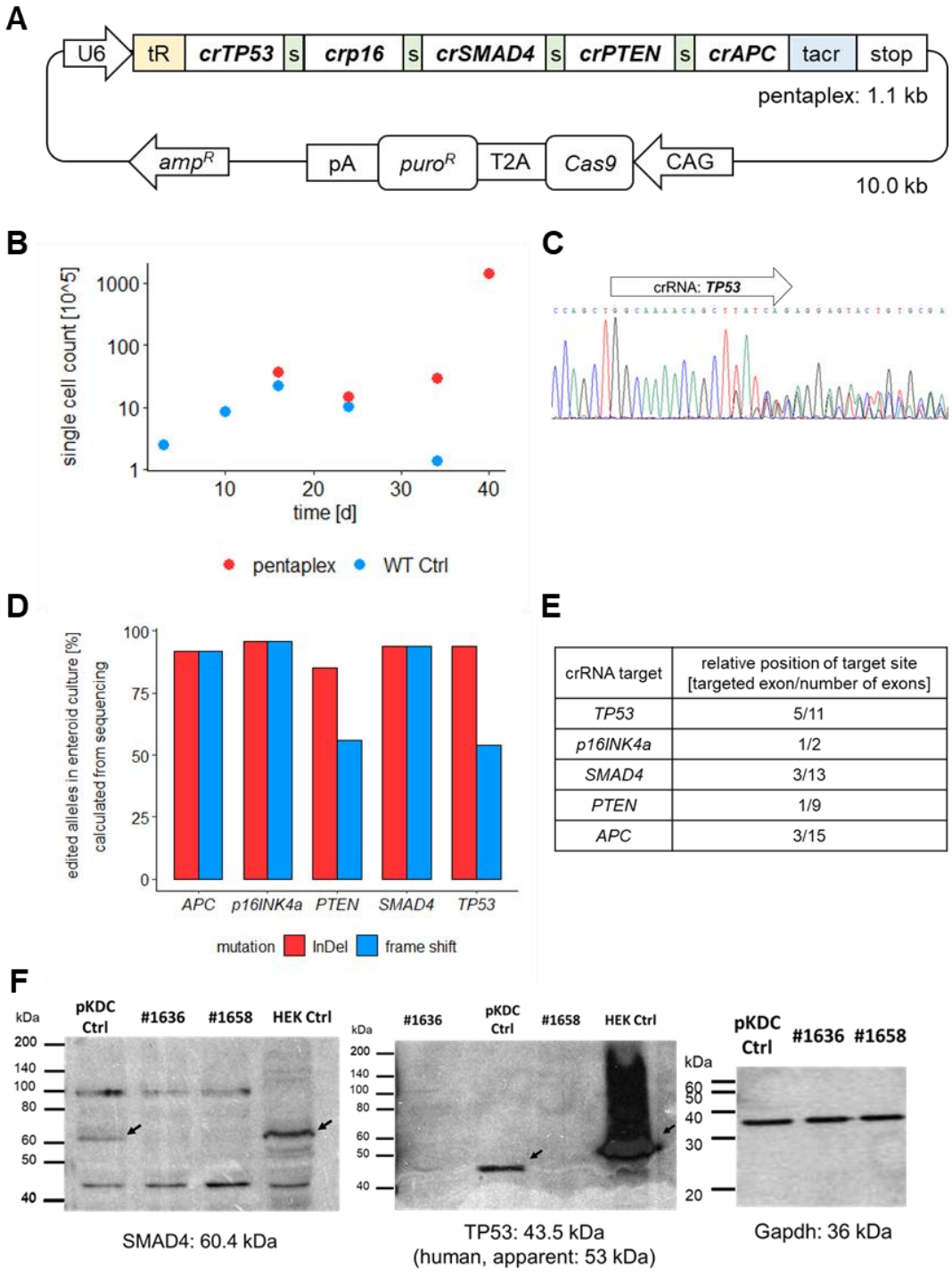

Figure 29 TSG editing in enteroids by the CRISPR/Cas pentaplex. Colon enteroids were generated from polyps of an *APC*$^{1311/WT}$ (#1636) and an *APC*$^{1311/WT}$ *KRAS*$^{LSL-G12D}$ pig (#1658) and transfected with the CRISPR/Cas9 pentaplex (A) that targets five TSGs (*TP53, p16INK4a, SMAD4, PTEN, APC*). Transcription of the pentaplex is driven by the U6 promoter. Within the pentaplex the crRNA sequences are separated by spacers ('s') that are composed of two elements. The first element is the pre-tRNA sequence ('tR') that is used for endogenous processing into single gRNAs. The second element is the tracrRNA sequence ('tacr') which is a linker between crRNA and Cas9 protein. Enteroids were analysed at passage 5 (day 34) when untransfected cells were dead (B). Successful gene editing was verified by PCR and sequencing analysis. An example is shown for *TP53* (C). The sequencing results were used to predict the proportion of edited alleles in the culture. The proportion of mutations (insertions, deletions and frame shift) are shown (D). The probability of a gene knockout increases if the frame shift occurs early in the reading frame. The relative position of the targeted exon within the gene is listed (E). The target sites were chosen for proximity to the start codon, targeting efficiency and presence in all reported transcripts. The knockout of the tumour suppressors Smad4 and p53 was proven by Western blots for lines #1636 and #1658; HEK293 lysate served as human positive Ctrl and pKDCs as untransformed porcine Ctrl (F).

3.7. Activation of the *KRAS-G12D* oncogene by *Cre* recombinase and verification of tumour suppressor knockouts by Western Blot

Oncogenes are hyperactive mutants of proto-oncogenes that promote cell growth. Under physiological conditions proliferative signals and cell cycle progression is controlled by TSGs. The loss of this balance due to constitutively active oncogene signalling and TSG inactivation is a hallmark of cancer[102]. Thus, the combination of *KRAS-G12D* oncogene activation and TSG inactivation should augment malignancy of transformed enteroids after transplantation back into the donor animal (autologous transplantation).

Enteroids were generated from polyps sampled during colon biopsy of an $APC^{1311/WT}$ $KRAS^{LSL\text{-}G12D/WT}$ pig (#1658). The latent oncogene *KRAS-G12D* can be activated by Cre-mediated excision of the *lox-STOP-lox* (LSL) cassette (Figure 30 A).

Oncogene activation and gene editing in enteroid line #1658 were achieved by co-transfecting an equimolar mix of the pentaplex and pPGK-Cre vector (Supplementary Figure 10) in enteroids. Recombination of the $KRAS^{LSL\text{-}G12D}$ allele was detected by PCR amplification across the LSL cassette in #1658 enteroids (Figure 30 A, blue arrows). The silent $KRAS^{LSL\text{-}G12D}$ allele generates a 1.5 kb PCR fragment. The recombined fragment is 201 bp long and appears directly above the *wt-KRAS* fragment of 167 bp. Transcription of *wt-KRAS* and *KRAS-G12D* RNA was confirmed by sequence analysis of the RT-PCR product. The sequencing results shows a double peak marked by two arrows in Figure 30 B, which indicates a guanine-to-adenine transition in the mutant transcript that is responsible for the glycine-to-aspartic acid substitution. Expression of the mutated constitutively active Ras protein was tested by Ras Activation Assay. In order to obtain enough protein from $KRAS^{LSL\text{-}G12D/WT}$ cells as control, enteroids from a $KRAS^{LSL\text{-}G12D/WT}$ pig were transformed by CRISPR/Cas9 editing of *p16INK4a* or *TP53* but not transfected with *pPGK-Cre*. For the assay, enteroid-derived 2D cultures were cultivated without serum. Ras-GTP protein was elevated in *KRAS-G12D* activated cells (#1658) compared to the control (Figure 30 C).

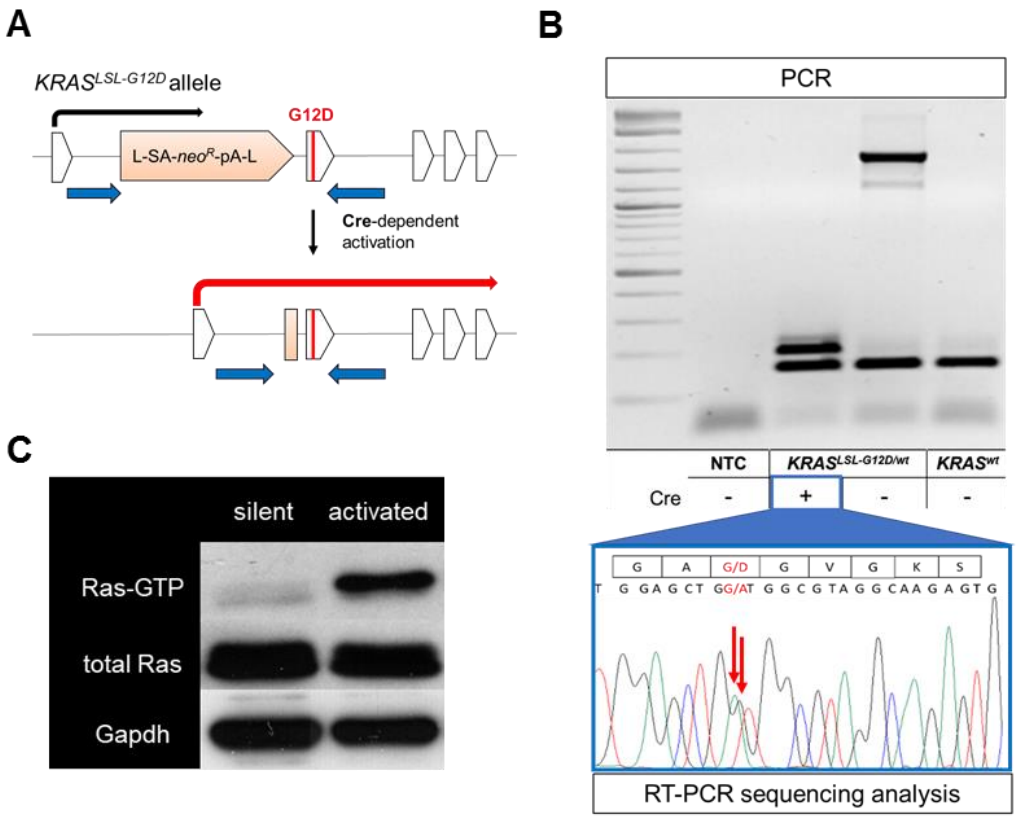

Figure 30 Molecular analysis of transformed *APC*$^{1311/WT}$ *KRAS*$^{LSL-G12D/WT}$ enteroids. Colon enteroids were generated from an *APC*$^{1311/WT}$ *KRAS*$^{LSL-G12D/WT}$ pig (#1658) and transformed by editing of TSGs and activation of the *KRAS-G12D* oncogene. Cre-dependent activation and the position of sequencing primers is depicted (A). Oncogene activation was achieved by electroporation of a *pPGK-Cre* plasmid. The removal of the *lox-STOP-lox* cassette was verified by PCR and RT-PCR followed by sequencing confirmed the transcription of *wt-KRAS* and *KRAS-G12D* (B). Ras-pulldown Assay confirmed that activated Ras protein (Ras-GTP) was elevated in #1658 enteroids (in absence of serum and Wnt ligands) compared to enteroids with silent *KRAS*$^{LSL-G12D}$ (C).

In the next section, I examine the properties of these genome engineered porcine enteroids. I will further refer to pentaplex edited enteroids as *TGΔ*^{5} and pentaplex edited, *KRAS-G12D* activated cells as *TGΔ*^{5}*KRAS*^{G12D}.

3.8. Transformed enteroids display hallmarks of cancer

Hanahan and Weinberg described eight characteristics of cancer cells that are universal among all human cancers[102], which are:

- sustaining proliferative signalling
- evading growth suppressors
- enabling replicative immortality
- resisting cell death
- deregulating cellular energetics
- activating invasion and metastasis
- inducing angiogenesis

- avoiding immune destruction

I asked if transformed enteroids acquire these hallmarks. To answer this question, I analysed CRISPR/Cas-edited enteroids for their composition, growth, and behaviour *in vitro* and *in vivo*.

3.8.1. Combined TSG inactivation avoids senescence of enteroids

As shown earlier, the transformation of primary enteroids was achieved by CRISPR/Cas editing of TSGs within 2 weeks. In order to identify the knockouts essential for this rapid transformation, I transfected *TGROSA KRAS*^{LSLG12D} enteroids with combinations of CRISPR/Cas vectors and p*PGK-Cre*. The advantage of this genotype is that both loci are activated by Cre-mediated excision of the LSL-cassettes, thereby, cells with activated *KRAS-G12D* can be monitored by fluorescent microscopy within the culture to evaluate the growth advantage contributed by the oncogene.

Enteroids (passage 1) were dissociated into single cells, transfected with combinations of single guide RNA-CRISPR/Cas vectors and cultivated as Matrigel-free 2D cultures. Guide RNAs were tested alone or in combination with the TP53-guide RNA vector and/or pPGK-Cre. Untransfected cells and cells only transfected with *pPGK-Cre* were also cultivated. No antibiotic treatment was used for selection. Brightfield and fluorescent images were taken three weeks after transfection (Figure 31).

Initially, all cultures grew after transfection but declined towards the end of the second week (passage 2) except those that were transfected with the *p16INK4a*-guide RNA vector. The three combinations *p16INK4a TP53*, *p16INK4a KRAS*^{G12D} and *p16INK4a TP53 KRAS*^{G12D} grew confluent and a considerable proportion of green-fluorescent cells indicated growth advantage of the activated oncogene. KRAS-G12D activation was verified by Ras Activation Assay and editing of *p16INK4a* and *TP53* was confirmed by sequencing analysis (Supplementary Figure 15).

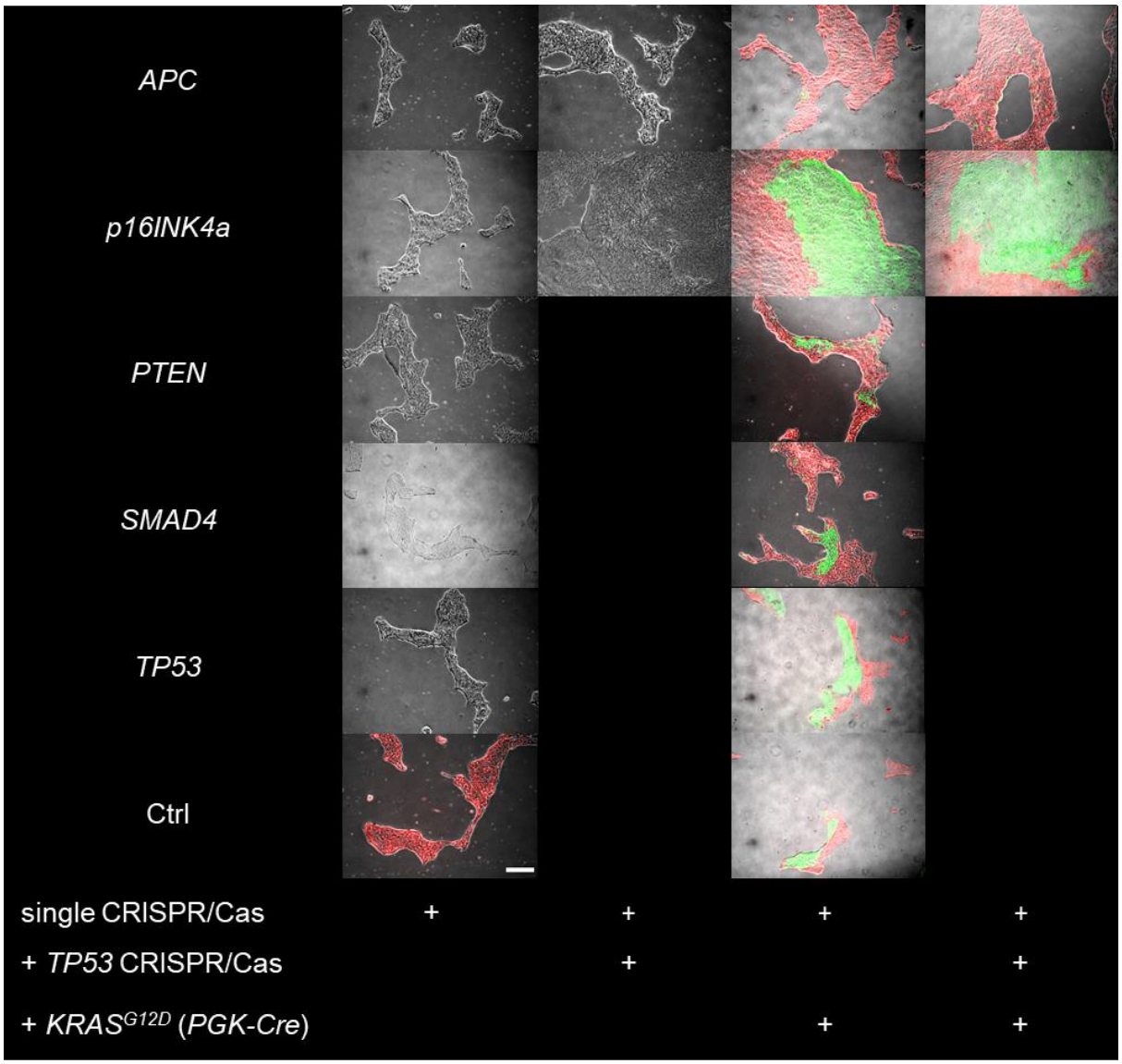

Figure 31 Identification of mutations required for transformation of *TGROSA KRAS*$^{LSL\text{-}G12D/WT}$ colon enteroids. Colon enteroids were generated from a *TGROSA KRAS*$^{LSL\text{-}G12D/WT}$ pig and transfected with plasmids for expression of *Cre* or CRISPR/Cas9 complexes targeting TSGs. Single guide RNA vectors and combinations with *TP53*-guide RNA vector and/or *pPGK-Cre* were transfected to analyse the effect of combined inactivation of TSGs and KRAS-G12D oncogene activation. Single cells were cultivated as 2D cultures after transfection. Representative bright field and fluorescent images were taken 23 days after transfection. For *PGK-Cre* transfections, bright field and fluorescent images were merged. Untransfected cells (Ctrl) and cells only transfected with the *pPGK-Cre* were cultivated as control. Scale bar is 400 µm.

Activation of the *KRAS*^{G12D} allele without editing of TSGs did not promote proliferation. Transfections without *p16INK4a*-guide RNA vector were monitored by microscopy for three additional weeks but no proliferation was observed. Taken together, editing of *p16INK4a* is essential for transformation and proliferation is enhanced by edited *TP53* and *KRAS-G12D* expression.

3.8.2. Transformed genotypes show supplement addiction

The growth of the three transformed lines generated in the last experiment (*p16INK4a*^{mut} *TP53*^{mut}, *p16INK4a*^{mut} *KRAS*^{G12D} and triple mutant *p16INK4a*^{mut}

TP53^{mut} *KRAS*^{G12D}) was tested in a supplement deprivation experiment. The transformed cells were seeded at low density (1000 cells/well) as 2D culture on uncoated 48well plates and cultivated in medium deprived of one or two supplements for one week, as described in section 3.3. Cells were stained with DAPI eight days after seeding and counted digitally. Basic medium (without supplements) and complete growth medium were used as references (Figure 32). The triple mutant showed the least sensitivity to supplement deprivation. The *p16INK4a*^{mut} *KRAS*^{G12D} double mutant only tolerated noggin deprivation but required all other supplements to grow.

The *p16INK4a*^{mut} *TP53*^{mut} double mutant showed a growth advantage compared to *p16INK4a*^{mut} *KRAS*^{G12D} but performed worse than the triple mutant.

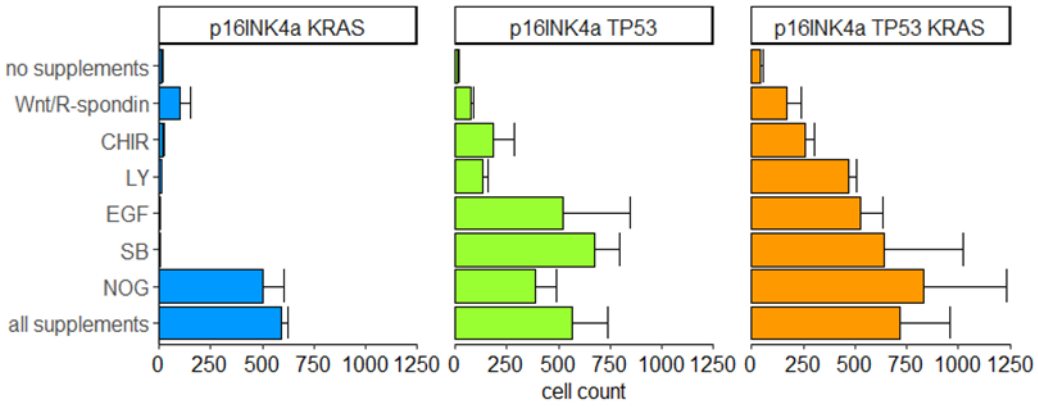

Figure 32 Supplement addiction of transformed enteroids. Colon enteroids from a *TGROSA KRAS*$^{LSL-G12D}$ pig were transformed by certain combinations of *KRAS-G12D* activation and CRISPR/Cas9 mediated editing of the TSGs *p16INK4a* and *TP53*. Cultures were expanded until passage 4 when the culture of WT cells was dead to select for transformed cells. Transformed cells were seed as 2D culture on a 48 well plate at a concentration of 2x10^3 cells/well. The cells were cultivated in supplement deprived medium. Single supplements (CHIR, LY, EGF, SB, Noggin) or the combination of Wnt and R-spondin were removed from culture medium. After 8 days the cells were stained with DAPI and fluorescent images were taken. The nuclei were counted and compared to cultures grown in basic medium (no supplements) or complete growth medium (all supplements). Error bars indicate the standard deviation from the mean of technical triplicates. The triple mutant (right) culture was most robust to supplement deprivation, whereas the *p16INK4a KRAS*^{G12D} mutant (left) culture was addicted to most of the supplements.

Compared to wildtype cultures, that grew in absence of most small molecule supplements (Figure 22 B), the growth of the *p16INK4a KRAS*^{G12D} mutant strongly depended on the Wnt pathway (Wnt, R-spondin, CHIR99021), TGFβ signalling (LY2157299), the EGF-dependent MAPK pathway, and the p38 MAPK signalling (SB202119). This addiction to supplements confirms that – although inactivation of *p16INK4a* is required to overcome senescence – it is the inactivation of *TP53* that allows growth if proliferative stimuli are limited. Comparing the *p16INK4a*^{mut} *TP53*^{mut}

mutant and the triple mutant, activated *KRAS-G12D* inhibited pro-apoptotic and anti-proliferative TGFβ signalling similar to LY2157299 in the culture medium.

Survival in supplement deprived medium was also tested for transformed polyp-derived enteroids (lines #1636, #1658) that carry frame shift mutations in *APC*, *p16INK4a*, *PTEN*, *SMAD4* and *PTEN*. These cultures survived as Matrigel-free 2D monolayers in medium without Wnt, R-spondin and EGF, however, small molecule inhibitors were required to expand the cultures. Since the enteroid lines #1636 and #1658 were generated from colon biopsies of FAP pigs they will be used for autologous re-transplantation. Before transplantation, the degree of differentiation, Wnt signalling, invasiveness, and tumour formation *in ovo* were tested with these cultures.

3.8.3. Differentiation and the regulation of Wnt signalling are lost in transformed enteroids

The degree of differentiation of transformed 2D cultures was tested for enteroid lines #1636 and #1658 by qPCR and 2D staining (Figure 33). The expression of differentiated intestinal cell types was dramatically reduced compared to wildtype crypt cultures except for reserve stem cells (*HOPX*). Expression of *HOPX* nearly doubled compared to wildtype enteroids and HOP-positive cells were stained in 2D cultures. No ChgA-positive cells were detected although *ChgA* expression was halved in qPCR. No absorptive or secretory cells were detected by staining.

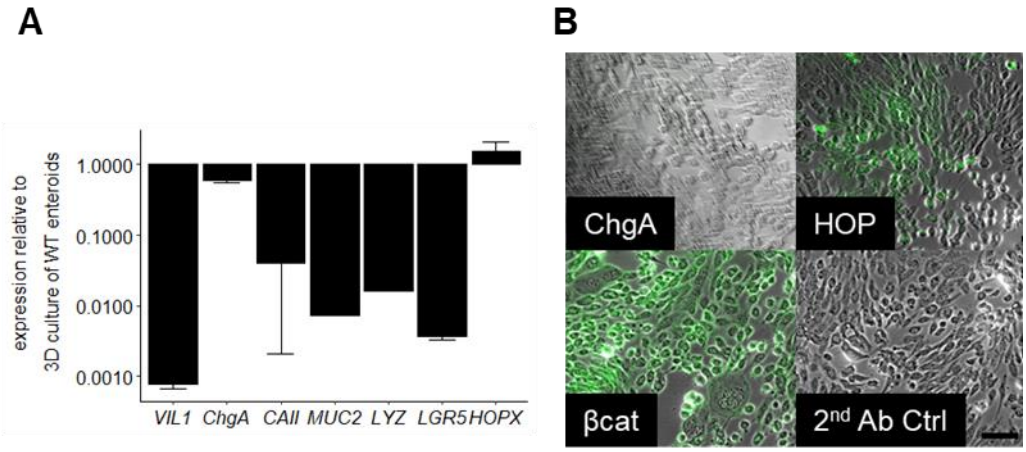

Figure 33 Expression of cell lineage markers in transformed enteroids compared to *WT* culture. Colon enteroids were generated from *APC*$^{1311/WT}$ (#1636) and *APC*$^{1311/WT}$ *KRAS*$^{LSL\text{-}G12D/WT}$ (#1658) pigs and transformed (passage 7-10) by *KRAS*^{G12D} activation and CRISPR/Cas mediated editing of five TSGs (*APC, TP53, p16INK4a, SMAD4, PTEN*). The expression fold change of intestinal cell lineage markers was compared to untransformed *WT* colon enteroids (passage 0) by qPCR. The expression of differentiated cells and fast cycling *LGR5*+ cells was barely detectable. *HOPX* expression is comparable to the *WT* (A). Expression of HOP was also detected by staining of 2D cultures. Other intestinal cell types were not detectable by immunofluorescent staining. Beta-catenin (βcat) staining performed as positive control and 2nd antibody staining (2nd Ab Ctrl) are shown (B). Scale bar is 100 µm.

TGΔ^{5}*KRAS*^{G12D} line (#1658) was expanded without Wnt and R-spondin for more than 20 passages. In order to test if Wnt signalling is still active in these cultures, TOPFlash assay was performed with increasing concentrations of mWnt3a conditioned medium (Figure 34). The response was compared to *APC*^{WT} *p16INK4a*^{mut} *KRAS*^{G12D} double mutant as transformed control and untransfected enteroids from an *APC*$^{1311/WT}$ *KRAS*$^{LSL\text{-}G12D}$ pig as untransformed control.

In absence of Wnt no Wnt pathway activation was detected in transformed cultures. The control lines responded to Wnt in a concentration dependent manner. The pentaplex transfected line showed no Wnt pathway activation in absence of conditioned medium but a high response unrelated to the concentration. The response of pentaplex edited enteroids at medium concentration (25%) was equal to the double mutant and unmodified cells at high concentration (50%).

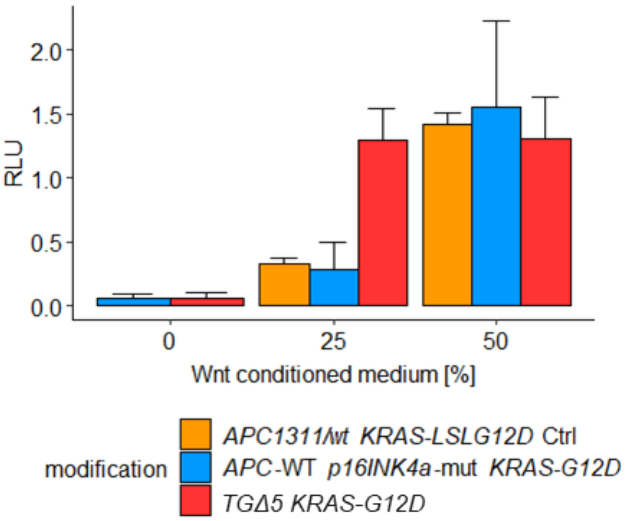

Figure 34 Wnt response assay indicates dysregulation of the Wnt pathway in *APC* edited enteroids. Colon enteroids were generated from three pigs. *APC*$^{1311/WT}$ *KRAS*$^{LSL\text{-}G12D/WT}$ enteroids from pig #1658 were transformed by *KRAS*^{G12D} activation and the CRISPR/Cas pentaplex (*TGΔ5 KRAS-G12D*). *WT-APC KRAS*$^{LSL\text{-}G12D/WT}$ enteroids were transformed by *KRAS*^{G12D} activation and editing of *p16INK4a*. Unmodified *APC*$^{1311/WT}$ *KRAS*$^{LSL\text{-}G12D/WT}$ enteroids were used as untransformed control. The cells were transfected with TOPFlash plasmids and exposed to different concentrations of Wnt conditioned medium for 48h. The relative expression of Wnt-dependent Firefly and constitutive Renilla activity (RLU) was assayed as described earlier. Error bars indicate the standard deviation from of mean of technical triplicates. The transformed line generated by editing of all five TSGs is more sensitive to Wnt at a concentration of 25% than the line where only *p16INK4a* was edited.

In conclusion, *TGΔ*^{5}*KRAS*^{G12D} enteroids were responsive to Wnt but gained sensitivity presumably due to inactivation of *APC*. Constant hyperactivation of Wnt signalling could also explain the absence of differentiated intestinal cell types that are usually enriched by deprivation of Wnt and R-spondin in human enteroid cultures[120].

3.8.4. Transformed enteroids show an invasive phenotype

Invasion of the extracellular matrix and dissemination via blood and lymph vessels involve a degree of motility that cancer cells must acquire in malignant disease. Epithelial cells change to this mesenchymal-like phenotype in carcinoma progression where they undergo a process called epithelial-to-mesenchymal transition[129].

Invasion of *TGΔ^{5}KRAS^{G12D}* enteroids was visible in Matrigel as multicellular protrusions that spontaneously evaded from the 3D clusters into the matrix (Supplementary Figure 16). Transwell Invasion Assay was performed to compare invasiveness of transformed and wildtype enteroids.

Wells of a 24well plate were equipped with inserts that allow diffusion of medium components between the insert and the well via membrane pores of 8 µm. The membrane was either coated with 12.5% of Matrigel (in basic medium) or left uncoated to test invasion or migration, respectively. Wildtype enteroids and the transformed 2D culture of *TGΔ^{5}KRAS^{G12D}* cells (#1658, passage 13) were dissociated into single cells, seeded on the membrane at high density (3.3x 10^{6}/cm^{2}) and overlaid with medium deprived of Wnt, R-spondin and EGF (WRE). The bottom was filled with complete growth medium to generate a gradient of WRE.

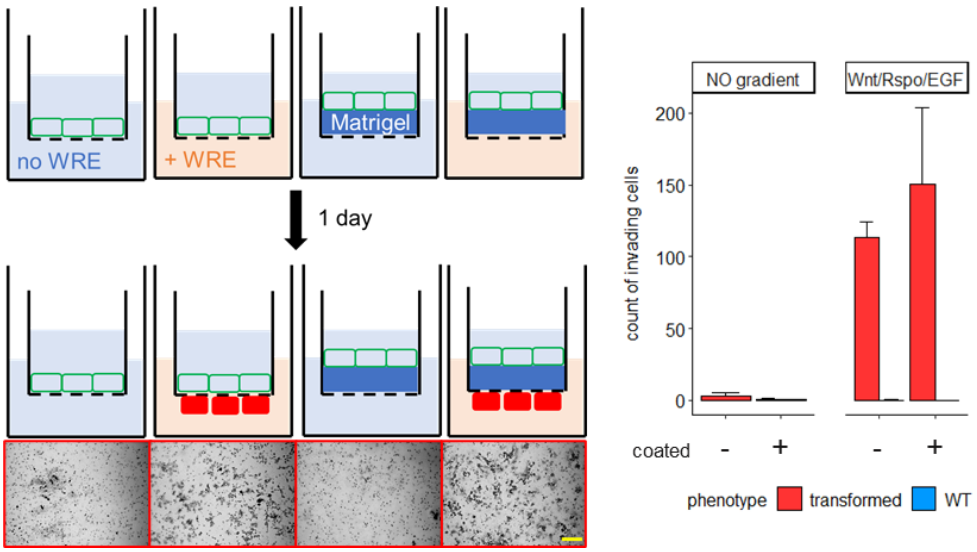

Figure 35 Transwell Invasion Assay with colon enteroids. Colon enteroids were generated from an *APC$^{1311/WT}$ KRAS$^{LSL-G12D/WT}$* pig (#1658) and transformed by *KRAS^{G12D}* activation and CRISPR/Cas mediated inactivation of five TSGs (*APC, TP53, p16INK4a, SMAD4, PTEN*). Enteroids were dissociated into single cells and seeded on 8 µm transwell membranes. The culture was incubated for 19 h to measure the migration of cells through the membrane towards a gradient of Wnt/R-spondin/EGF. Cell migration was tested in uncoated transwells. Cell invasion was tested in transwells that were coated with 12.5% Matrigel. The experimental setup and representative images of cells that were stained with Crystal violet at the bottom of the transwell after invasion are shown (left, scale bar 200 µm) Stained cells were counted at four membrane regions for each condition under the microscope (the condition: *WT* enteroids - no coating - no gradient was not tested). Error bars indicate standard deviation from the mean of four counts. Migration was only detected by transformed cells if the gradient was applied.

The cultures were incubated for 19h. Cells that invaded the Matrigel and migrated through the membrane were stained with crystal violet (in methanol) at the bottom of the membrane and counted under the microscope (Figure 35). Migration and invasion were only detected for transformed cells if a gradient of WRE was applied. Wildtype cells showed no sign of migration and invasion.

In order to induce an invasive phenotype in enteroids for autologous transplantation, I analysed the effect of the culture environment on the expression of epithelial and mesenchymal markers. Furthermore, I asked if EMT is reversible by changing the cultivation environment between 2D and 3D.

For this purpose, I sequentially cultivated transformed enteroids in 2D, 3D and 2D culture again and observed the growth behaviour of transformed lines #1636 and #1658 (passage >10; Figure 36 A). The cells were analysed by qPCR for the expression of markers which are routinely used to assess epithelial-to-mesenchymal transition (EMT) and will be further summarized as 'EMT markers'[130]:

- epithelial markers: E-cadherin (*CDH*), tight junction protein 1 (*TJP*)
- mesenchymal markers: fibronectin (*FN*), vimentin (*VIM*)

Wildtype enteroids grown in 3D culture were used as reference for qPCR analysis (Figure 36 B).

Both lines accumulated floating cells in the medium that shed from confluent monolayers. Live/dead staining revealed that half of these cells were alive indicated by the enzymatic hydrolysis of FITC-diacetate (green) and repulsion of propidium iodide (red) by the intact cytoplasmatic membrane. Shed cells were embedded in Matrigel to observe growth and survival as they could represent a viable enteroid subpopulation that adapted to suspension. However, these cells did not grow after embedding in Matrigel and died within two weeks. As expected, dissociated cells from adherent 2D cultures formed enteroids in Matrigel. Next, intact enteroids were harvested and seeded without dissociation on uncoated 6wells. Two different growth characteristics were observed: The $TG\Delta^{5}$ enteroids of line #1636 opened and formed a dense 2D monolayer overnight. $TG\Delta^{5}KRAS^{G12D}$ enteroids from line #1658 expanded in suspension and only few colonies grew as monolayers.

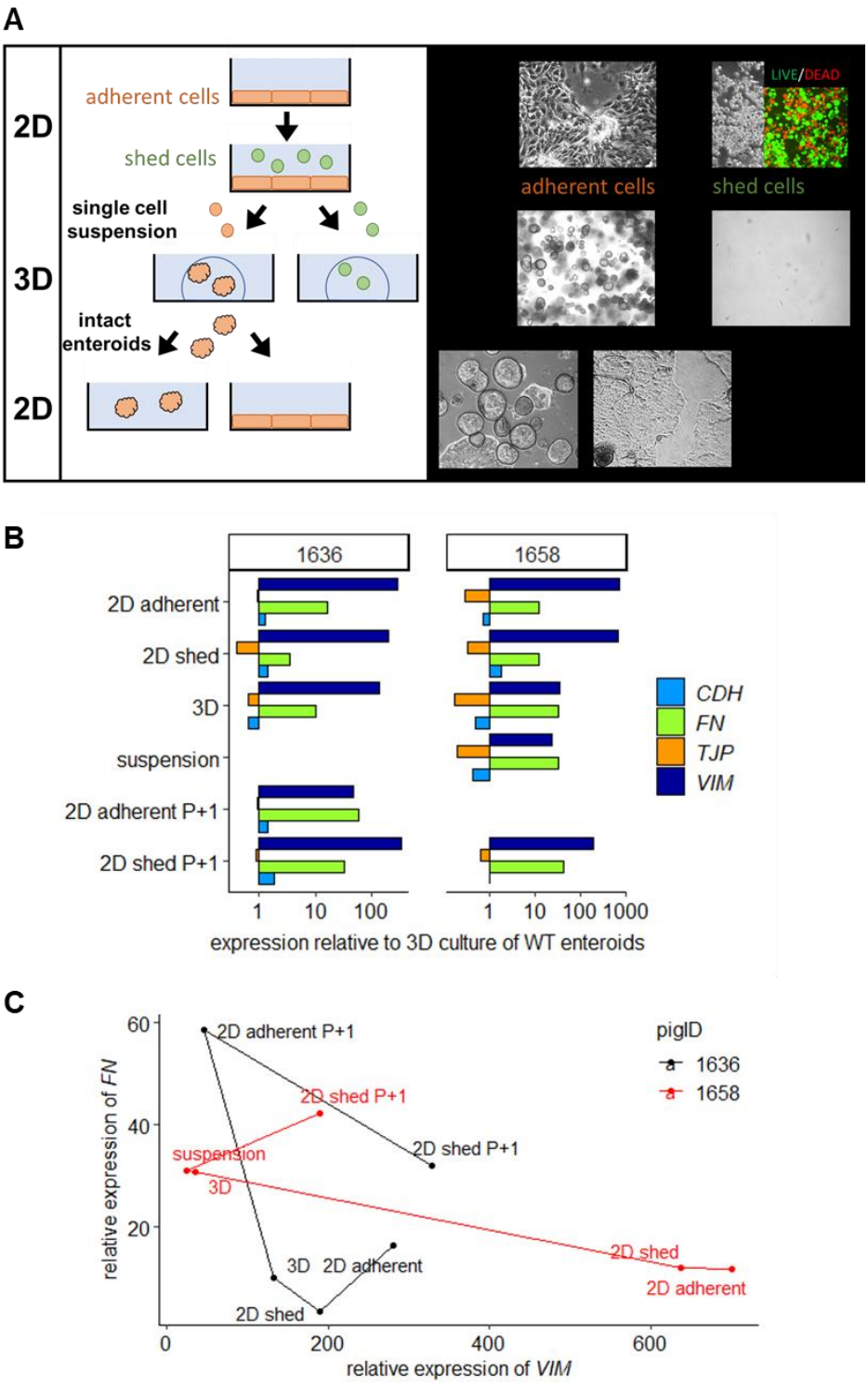

Figure 36 Characteristics of epithelial and mesenchymal markers in transformed enteroids grown in different culture environments. Colon enteroids were generated from *APC*$^{1311/WT}$ (#1636) and *APC*$^{1311/WT}$ *KRAS*$^{LSL\text{-}G12D/WT}$ (#1658) pigs and transformed (passage 10-13) by *KRAS*^{G12D} activation and CRISPR/Cas mediated editing of five TSGs (*APC, TP53, p16INK4a, SMAD4, PTEN*). Cells were sequentially cultivated in 2D, 3D, suspension and finally 2D again. The different culture environments are schematically depicted and representative bright filed and fluorescent images are shown. Live/dead staining was performed on shed cells that accumulated in 2D culture (A). The expression fold change of epithelial markers (E-cadherin, *CDH* and fibronectin, *FN*) and mesenchymal markers (tight junction protein 1, *TJP* and vimentin, *VIM*) was compared to *WT* colon enteroids (3D culture, passage 0). Two isolates were analysed (pig# 1636, 1658) from each environment. Adherent cells and cells that shed from 2D culture were collected (B). Mesenchymal to epithelial transition between 2D and 3D culture was examined by plotting the relative expression of *FN* and *VIM* separately (C). The line between data points represents the course of cultivation as it connects observations made from sequentially collected samples.

Expression analysis revealed strong upregulation of *FN* and *VIM* in both lines. Expression of *TJP1* was similar (#1636) or downregulated (#1658) compared to wildtype enteroids. *CDH* expression was upregulated in most 2D cultures but reduced in 3D enteroids.

Since the expression of *FN* and *VIM* were considerably elevated compared to the initial wildtype culture, I focused on these markers to describe EMT. Therefore, I plotted the expression fold change of *FN* against *VIM* to depict the transition from an epithelial to mesenchymal phenotype (Figure 36 C). The line connecting the data points represents the course of cultivation.

TGΔ^{5}KRAS^{G12D} line #1658 showed a dominant mesenchymal phenotype indicated by high *VIM* expression in the initial 2D monolayer that decreased after cultivation in Matrigel. Cultivation in 3D was associated with elevated *FN* expression. Cultivating intact enteroids in suspension without Matrigel did not change the expression of these two markers.

In contrast to *TGΔ^{5}KRAS^{G12D}* line #1658, the changes in *VIM* and *FN* expression from the initial 2D culture to 3D enteroids were more discreet for *TGΔ^{5}* line #1636. Furthermore, the expression pattern of the initial 2D culture was not replicated in the final culture. Instead, expression of *FN* markedly increased and *VIM* was downregulated compared to the 3D culture.

To conclude, 3D enteroids can be expanded as Matrigel-free monolayers after transformation, Cultivating enteroids for several passages as 2D monolayers creates a mesenchymal phenotype indicated by elevated *FN* and *VIM* expression. Furthermore, expression of these mesenchymal markers changes in response to the cultivation environment.

Taken together, transformed 3D epithelial cultures acquired the ability to expand in 2D culture and changed the expression of EMT markers in response to the environment.

The experiment indicates that dissociation of enteroids into single cells followed by the cultivation as Matrigel-free monolayer induces a mesenchymal phenotype. This phenotype could support dissemination of transformed enteroids after autologous transplantation and could promote invasiveness *in vivo*.

3.8.5. Transformed status tested via chorioallantoic membrane (CAM) assay

The genome engineered enteroids exhibit crucial hallmarks of cancer cells that should result in tumour growth *in vivo*. The growth of the transformed *TGΔ*^{5} enteroids #1636 and *TGΔ*^{5}*KRAS*^{G12D} #1658 was tested on chicken embryos in collaboration with Prof. Benjamin Schusser at the Chair or Reproduction (WZW, TUM). The use of chicken embryos for the study of mammalian tumours dates back to the work of Rous and Murphy in 1911[131]. Experimentation with chicken embryos requires no ethical approval and can be easily performed at low costs.

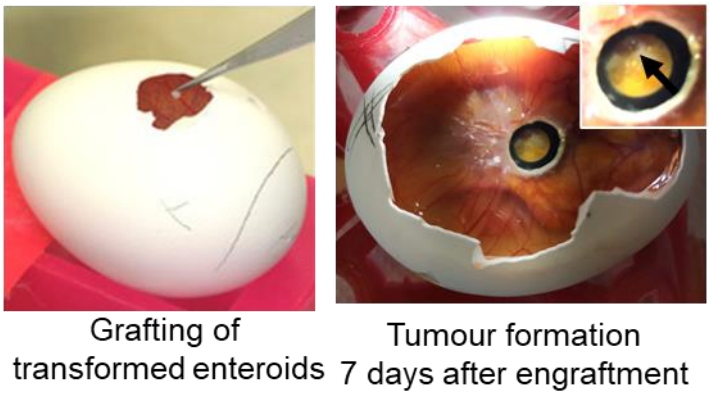

Figure 37 CAM Assay with transformed colon enteroids. Colon enteroids were generated from *APC*$^{1311/WT}$ (#1636) and *APC*$^{1311/WT}$ *KRAS*$^{LSL\text{-}G12D/WT}$ (#1658) pigs and transformed (passage 19-23) by *KRAS*^{G12D} activation and CRISPR/Cas mediated editing of five TSGs (*APC, TP53, p16INK4a, SMAD4, PTEN*). Single cells were obtained from 2D culture and 1x10^{6} cells were resuspended in 100 µL of Matrigel. Chorioallantoic membrane (CAM) assay was performed by the Group of Prof. Dr. Schusser at the Chair of Reproduction (WZW, TUM). Successful engraftment was detected within 7 days by dark tumours growing on the membrane.

The shell was opened to access the CAM which is highly vascularized to permit gas and waste exchange for the growing embryo. Seven days after laying, a plastic ring was placed on top of the CAM and 3x10^{6} single cells of each cell line in basic medium with 10% Matrigel were implanted. Engraftment was imaged after seven days. Two eggs were implanted with either cell line. Implanted eggs of *TGΔ*^{5} enteroids #1636 died during incubation most likely due to the procedure since no neoplastic tissue had formed. Tumour formation from *TGΔ*^{5}*KRAS*^{G12D} enteroids #1658 was observed in one egg (Figure 37). Histological analysis of the tumour mass remains to be done. The assay proves that porcine epithelial cells that were transformed *in vitro* can form tumours in an immunologically naïve environment, like the chicken embryo. However, transplants in the adult organism are at risk to be eliminated by a fully developed innate and trained adaptive immune system.

3.9. Modification of enteroids to evade recognition by the immune system

The lifelong risk of transplant rejection after allotransplantation demonstrates the effectiveness of the immune system to recognize and destroy foreign epitopes. Therefore, autologous transplantation was to be performed by injecting transformed enteroids under the colonic mucosa of the same donor to reduce the cytotoxic response of the porcine immune system. However, transformation of the original enteroid culture might generate novel antigens (neoantigens), that can lead to elimination of transformed cells by cytotoxic T cells and macrophages. Hence, I used two strategies proven to inhibit the human $CD8^+$ cytotoxic T cell response against porcine cells[132,133].

The first strategy addresses the recognition of neoantigens by cytotoxic T cells (Figure 38 A). Neoantigens are novel peptides that arise from mutated proteins that are presented as antigens by the SLA-1 complex (*Swine Leukocyte Antigen class I*, orthologous to human HLA-1). Binding of the T cell receptor to the antigen activates the cytotoxic T cell response that kills cancer cells by inducing apoptosis or perforation of the membrane. The functional SLA-1 complex requires stabilisation by β2-microglobulin (β2M) which is non-covalently linked to the α-chain and encoded by *B2M*. Knockout of *B2M* should prevent the assembly of the transmembrane α-chain and prevent antigen presentation by SLA-1[132,134].

The second strategy undermines the CD28 costimulation required for T cell activation (Figure 38 B). Macrophages and dendritic cells present antigens to naïve lymphocytes to stimulate the immune response. In addition, naïve T cells require binding of CD28 with its ligands, CD80 and CD86, on antigen presenting cells for complete activation. LEA29Y is a human CTLA4 derivative fused to the constant domain of the human IgG1 antibody (Fcγ) with high affinity to both CD80 and CD86 and thus a potent inhibitor of CD28 costimulation. LEA29Y, also known as Belatacept, is indicated to prevent rejection after kidney transplantation. Consequently, stable expression and secretion of LEA29Y in transformed cells should protect cancer cells from T cell mediated rejection[133].

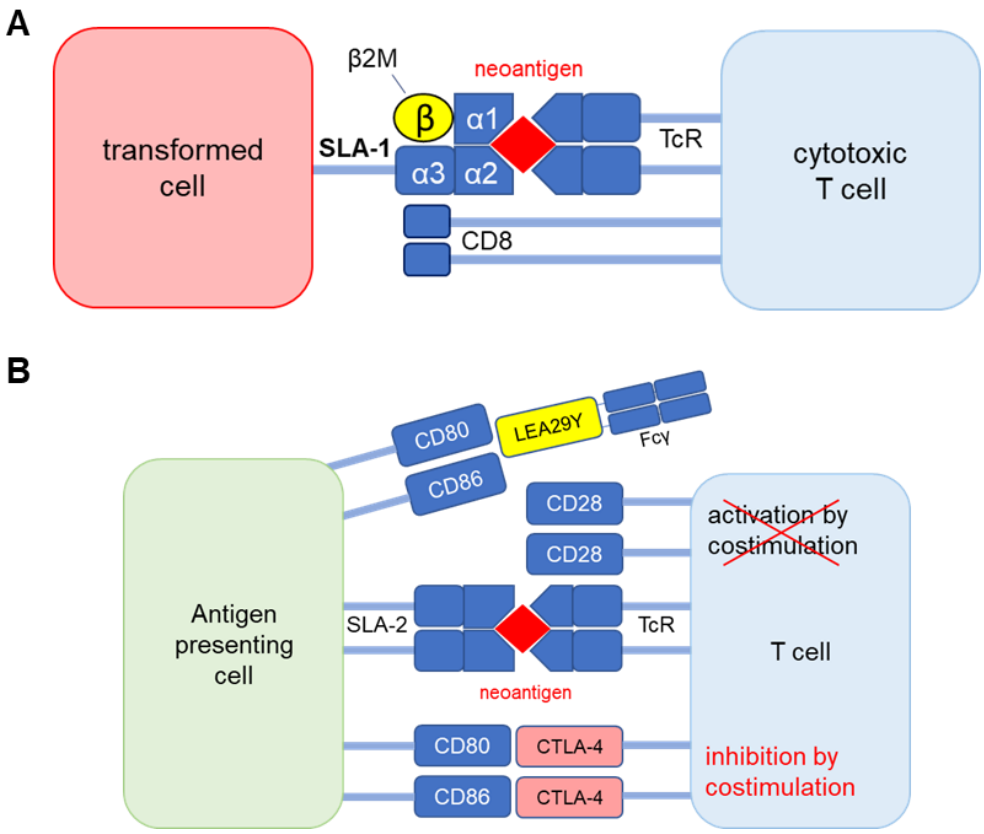

Figure 38 Strategies to reduce the immune response against transformed cells after transplantation. Two strategies were adopted to reduce the immune response against transplanted transformed enteroids. Neoantigens are novel peptides that arise due to mutations in proteins and are presented by the SLA-1 complex (orthologous to human MHC class I complex) to immune cells. Tumour cells have evolved strategies to downregulate antigen presenting complexes to evade the cytotoxic immune response. Therefore, I aimed to downregulate the SLA-1 complex by knockout of its stabilising factor beta-2-microglobulin (*B2M*). Consequently, the SLA-1 restricted cytotoxic T-cell activity should be reduced (A). Neoantigens are also presented on the SLA-2 complex (orthologous to human MHC class II complex) by antigen presenting cells. The activation of T cells requires costimulation of CD28 with CD80 and CD86, whereas binding to CTLA-4 has the opposite effect. LEA29Y is an artificial fusion protein (Belatacept) of a high affinity variant of CTLA-4 and the IgG1 Fc fragment and is indicated for immunosuppressive combination therapy (B). Stable knockin of an LEA29Y expression vector into transformed enteroids should reduce the adaptive immune response.

The knockout of β2M and stable integration of a recombinant *CAG-LEA29Y* expression cassette in transformed enteroids was achieved via two consecutive transfections.

First, polyp-derived enteroids from an $APC^{1311/WT}$ $KRAS^{LSL\text{-}G12D}$ pig (#1658) were co-transfected with three plasmids. One plasmid encoded for *Cas9* endonuclease and the crRNA directed against *B2M* (cr*B2M*). A second plasmid carried the crRNAs of the pentaplex but lacked *Cas9*. The third plasmid, *pPGK-Cre*, was used for oncogene activation. An equimolar ratio of all three plasmids was transfected and the culture was expanded until transformed cells outgrew. Oncogene activation and inactivation of all five tumour suppressors and *B2M* was detected by PCR, sequence analysis and Ras activation assay (Supplementary Figure 13, Supplementary Figure 11, Figure 30 C). Enteroids were dissociated into single cells and stained with an anti-

β2M antibody for analysis by flow cytometry (Figure 39 A). Transformed *B2M*^{WT} cells (*TGΔ*^{5} line #1636) were used as control.

Flow cytometry confirmed that the knockout of B2M was achieved in enteroid line #1658.

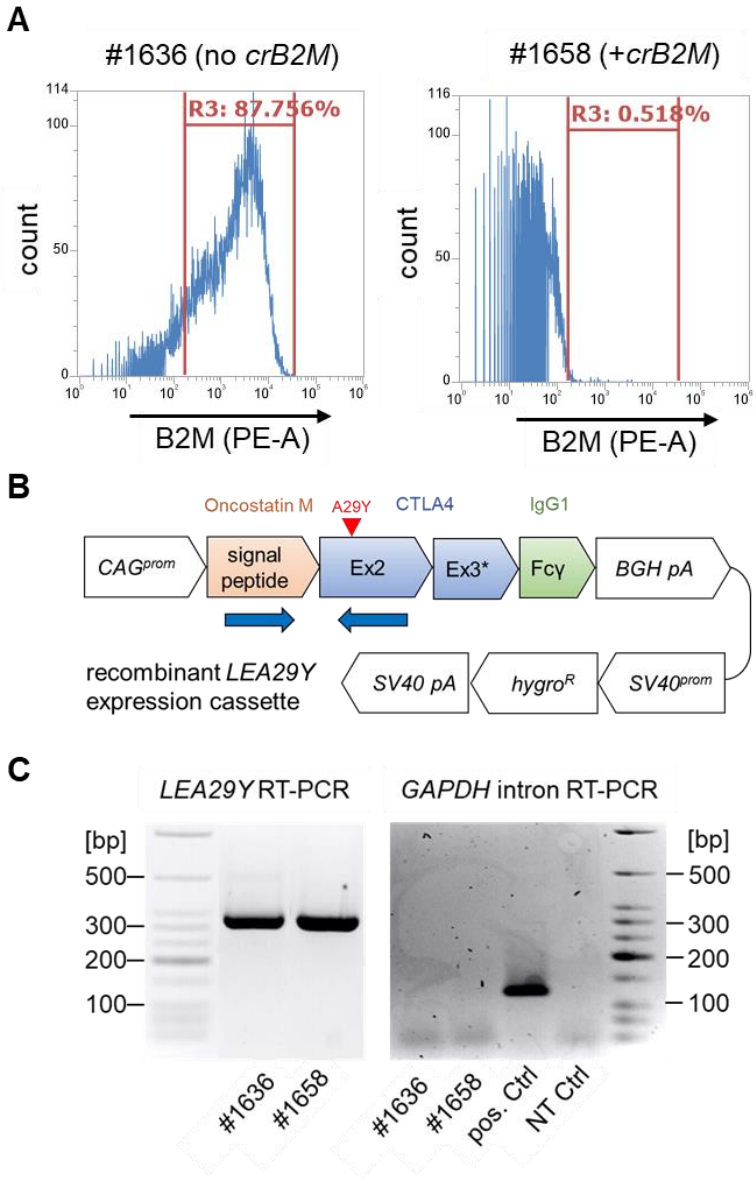

Figure 39 Transformed enteroids were modified to reduce immune response after transplantation. Colon enteroids (#1658) were transformed in combination with a CRISPR/Cas plasmid targeting the porcine *B2M.* Knockout of the SLA-1 associated protein was verified by surface staining with an anti-B2M PE-conjugated antibody and flow cytometry. No β2-microglobulin was detectable in these enteroids compared to transformed enteroids (*TGΔ5* line #1636) not transfected with the *crB2M*-CRISPR/Cas vector (A). Transformed cells with *B2M-KO TGΔ5 KRAS-G12D* (#1658) and *B2M-WT TGΔ5* (#1636) were transfected with a linearized vector expressing LEA29Y (B, Supplementary Figure 17) and selected with hygromycin for 8 days. The culture was expanded for 11 days and RNA was isolated for expression analysis. LEA29Y expression was confirmed by RT-PCR in both lines. The absence of genomic DNA in the RNA isolate was verified by PCR using primers that bind in the first intron of *GAPDH* (C).

Secondly, transformed enteroids were transfected with a the *LEA29Y* expression construct (Figure 39 B) and selected for random integration of the cassette with the

antibiotic hygromycin B. Performing a hygromycin B killing experiment with transformed enteroids not transfected with the *LEA29Y construct*, the minimal concentration of hygromycin B for selection was determined as 200 µg/mL in medium without Wnt, R-spondin, and EGF. At this concentration transformed cells died within 7 days. Transfection was performed in transformed $B2M^{KO}TG\Delta^{5}KRAS^{G12D}$ (#1658) and $B2M^{WT}TG\Delta^{5}$ (#1636) cells to analyse the effect of $B2M^{KO}$ after autologous re-transplantation. The *LEA29Y-hygro*^{R} expression construct (Supplementary Figure 17) was linearised using restriction enzymes and 1.4 µg were used for transfection of 5x 10^5 cells. The cells were selected for 8 days with 200 µg/mL hygromycin B. Selected untransfected controls of each line were cultivated for two additional weeks and the absence of proliferating cells verified that selection was complete.

Primers that bind in the signal peptide of human *Oncostatin M* and the second exon of human *CTLA4* (blue arrows in Figure 39 B) were used to confirm the transcription of the *LEA29Y* coding sequence by RT-PCR. The expected fragment of 330 bp was amplified in both lines (Figure 39 C). Since the *LEA29Y* expression cassette did not contain introns genomic DNA contamination would give a false positive signal in RT-PCR. In order to test if the amount of genomic DNA in the RNA eluate was negligible, a PCR was run to amplify the first intron of *GAPDH* in the sample. The PCR was negative indicating that *LEA29Y* expression was verified by qPCR. Additionally, I tried to detect the presence of LEA29Y protein in the cell lysate. However, the anti-human IgG antibody, used for Western Blot, showed unspecific binding and LEA29Y protein could not be detected (Supplementary Figure 18).

Finally, the modified enteroids were dissociated into single cells for injection into the respective donor animal. Transplantation was performed by injection under the skin to easily assess tumour growth. The two isolates (#1636, #1658) with the following genetic modifications were injected at four positions at a concentration of 0.5-4x10^6 cells/300 µL (PBS):

- line #1636: APC^{mut} $p16INK4a^{mut}$ $PTEN^{mut}$ $SMAD4^{KO}$ $TP53^{KO}$ $B2M^{WT}$ $KRAS^{WT}$ *LEA29Y*
- line #1658: APC^{mut} $p16INK4a^{mut}$ $PTEN^{mut}$ $SMAD4^{KO}$ $TP53^{KO}$ $B2M^{KO}$ $KRAS^{G12D}$ *LEA29Y*

Line #1658 was used for autologous re-transplantation into the 12 months old pig but pig #1636 had died at the age of 13 months before cells could be transplanted. Therefore, line #1636 was injected into *TP53*$^{LSL\text{-}R167H/\ LSL\text{-}R167H}$ *KRAS*$^{LSL\text{-}G12D}$ pig #1947 (allotransplantation) which was four months old. One injection was performed behind each ear and hindquarter. The injection sites were examined for 4 months in pig #1658 (autologous transplantation) and for more than 7 months in pig #1947 (monitoring of allotransplantation is ongoing). No tumour has been visible and no palpable mass has been found. The animals were not biopsied to avoid any risk to future orthotopic transplantation.

3.10. Generation of *TNF*$^{\Delta ARE}$ pigs to induce inflammation in the porcine colon

Patients with inflammatory bowel disease (IBD) suffer from recurrent inflammation of the gut. The risk between colitis and colorectal cancer is well-established and incidence of cancer increases ten years after diagnosis[135]. Given the strong correlation of prolonged inflammation of the colon and colorectal cancer, I assumed that the breeding of pigs predisposed to colitis with FAP pigs might result in enhanced colorectal cancer progression. The TNF$^{\Delta ARE}$ mouse which carries a deletion in the tumour necrosis factor (*TNF*) regulatory elements is a model for IBD[80]. It is characterized by elevated TNFα levels which causes inflammation of the intestine. I aimed to replicate the *TNF*$^{\Delta ARE}$ genotype in pigs, to generate pigs with a predisposition to colitis.

The porcine *TNF* locus was annotated to identify regulatory elements in the 3' UTR for precise excision using the CRISPR/Cas system (Figure 40 A). Three regulatory sites were localised in the porcine 3' UTR by sequence comparison with the orthologs of human and mouse. The sites contain binding motifs for RNA degrading factors, which ensure TNF homeostasis after inflammation. The AU rich element (ARE) is encoded by repeating and overlapping ATTTA motifs. In contrast to ARE, the constitutive decay elements, CDE 1 and CDE 2 allow mRNA degradation in presence of strong inflammation signals, like LPS[136].

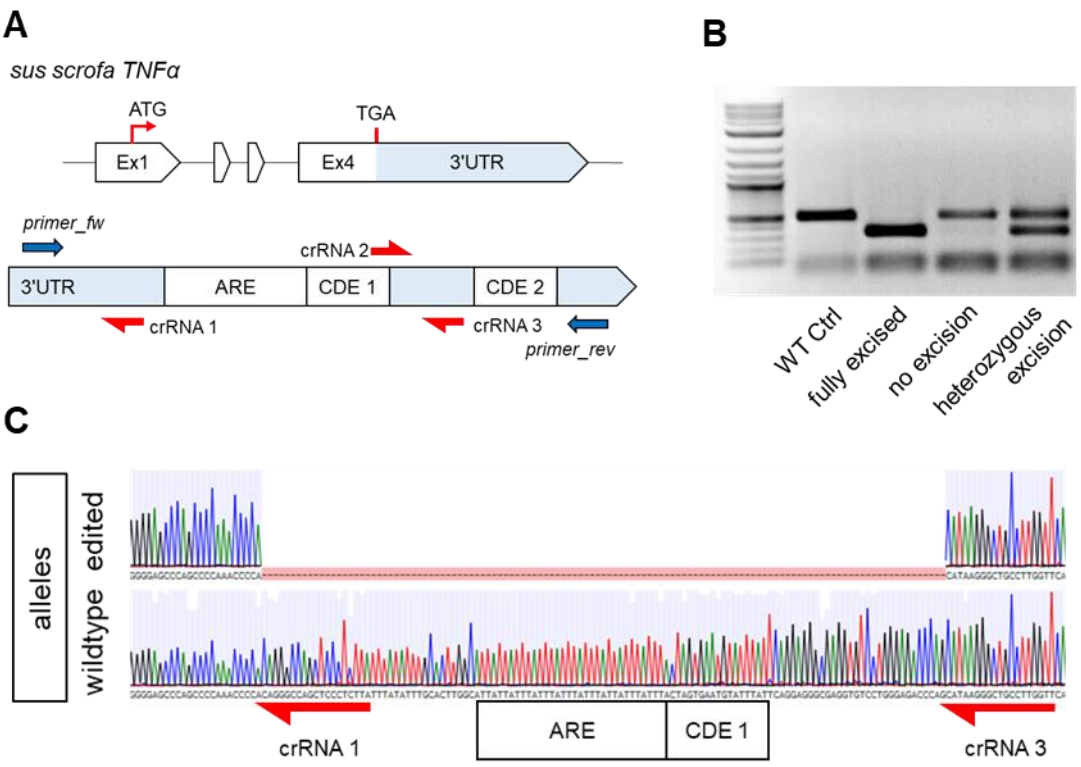

D

picked (P2)	expanded (P3)	**heterozygous**	homozygous	expanded (P6-7)	**confirmed by sequencing**
120	63	22	9	5	4
100%	53%	35%	14%	4.2%	3.3%

Figure 40 *TNFα* editing in porcine primary fibroblasts. Porcine primary fibroblasts were transfected with CRISPR/Cas plasmids for precise excision of the regulatory elements in the 3' UTR of the *TNFα* locus. Three editing constructs were used to excise two of the three elements annotated in this work: the AU-rich element (ARE) and the first of two constitutive decay elements (CDE). ARE and CDEs reduce the half-life of the transcript to control TNFα levels (A). The precise monoallelic excision was confirmed by PCR (B) and subsequent sequencing (C) of both alleles. Single cell clones heterozygous for the excision of ARE and CDE1 were expanded and cryoconserved for somatic cell nuclear transfer. In another approach fertilised oocytes were microinjected with a duplex expressing crRNA1 and crRNA2. This experiment was performed by Dr. Bernhard Klinger at the Chair of Livestock Biotechnology and correctly edited piglets were born. These animals are currently investigated for dysregulation of TNFα and an inflammatory pathophenotype by Thomas Klinger at the Chair of Livestock Biotechnology.

I assumed that the phenotype induced by deletion of all elements would be potentially harmful to non-gnotobiotic animals. I tested guide RNAs (see Table 10) to excise ARE and CDE 1 (red arrows) in wildtype pKDCs as described earlier. The efficiencies were 86% (crRNA1) and 84% (crRNA3) and 64% (crRNA2). Successful excision was detected for one and both *TNF* alleles by PCR in single cell clones (Figure 40 B). A fragment of 274 bp is amplified from the excised allele and the wildtype sequence is 368 bp long. Single cell clones were screened for a heterozygous genotype to maintain *TNF* regulation by one allele for a moderate pro-

inflammatory phenotype. These cells could be used for somatic cell nuclear transfer to generate *TNF*$^{\Delta ARE\ \Delta CDE1}$ pigs. Sequence analysis showed that single cell colonies were obtained with only one truncated allele and a wildtype second allele after selection with 1.5 µg/mL of puromycin (Figure 40 C). In total 3% of all cultivated single cell clones were heterozygous for the excision as detected by PCR. Sequence analysis of the PCR products verified the precise excision of ARE and CDE1 in one allele and InDel mutations of up to 2 bp in the second allele (Figure 40 D).

Direct genome editing in the porcine embryo is an alternative to somatic cell nuclear transfer. For this purpose, two *U6 promoter-guide RNA* cassettes were combined on one CRISPR/Cas9 vector which reduces the proportion of cells edited by only one guide RNA. Despite the lower editing efficiency of crRNA2 compared to crRNA3, crRNA1 was combined with crRNA2 to shorten the length of the deleted fragment.

TNF edited pigs were generated by microinjection of porcine zygotes with this CRISPR/Cas vector by Dr. Bernhard Klinger at the Chair of Livestock Biotechnology. Phenotypic analysis on the F1 generation is ongoing.

4. Discussion

The major aim of this work was to establish protocols for the isolation, cultivation and genetic manipulation of intestinal crypts as 3D cultures from porcine biopsies based on protocols available for human and murine enteroids. These enteroids cultures represent the only suitable system to expand intestinal stem cells for analysis and further experimentation. In this work, electropermeabilisation was used as transfection method to deliver vectors for genome engineering of enteroids. TSGs were inactivated and activation of a silent endogenous *KRAS*^{G12D} oncogene was achieved. The genome-engineered intestinal cultures exhibited hallmarks of cancer cells and were subjected to autologous or allogeneic transplantation to study tumour formation in the porcine recipient.

In 2017, Callesen et al. described an oncogenic minipig model that carries a Flp recombinase-inducible transgenic cassette comprised of *KRAS*^{G12D}, *cMyc* and *SV40LT*. Flp recombinase was controlled by the murine Villin (*VIL*) promoter and activated upon tamoxifen administration[88]. This model relies on the intestinal specificity of the *VIL* promoter to activate two potent oncogenes and inhibit the tumour suppressor proteins p53 and Rb via expression of the SV40 large T antigen. They provided proof of principle that one of three tamoxifen-treated minipigs develop neuroendocrine carcinoma of the duodenum with proximal lymph node infiltration. Although this model might require local administration of tamoxifen to induce colorectal tumours, it is the only report of an intestinal cancer model that shows an invasive phenotype in pigs. However, no further studies with this model have been published.

The *APC*$^{1311/WT}$ pig developed at the Chair of Livestock Biotechnology is the only endogenous CRC model that develops colorectal polyps due to an endogenous *APC* truncation mutation but does not show invasion or metastasis.

4.1. Generation and transformation of porcine enteroids

Eleven years of research on the *APC*$^{1311/WT}$ pig at the Chair of Livestock Biotechnology have shown that these pigs do not develop invasive disease from benign polyps as fast as rodent CRC models. The progression to malignant disease in the pig might require additional genetic alterations that accumulate over time (approximately ten years) as described for human patients who carry the *APC*^{1309*}

mutation which is causative for familial adenomatous polyposis. Therefore, a strategy was developed to introduce oncogenic mutations into colonic mucosa of *APC*$^{1311/WT}$ pigs *in vitro* to accelerate colorectal cancer progression upon transplantation (Figure 41).

First, pigs underwent colonoscopy to harvest polyps for primary culture of intestinal crypts within 1-2h after biopsy. Crypts formed 3D structures that yielded sufficient enteroids for transfection within 2-3 weeks depending on the amount of starting material. Senescence was overcome by inactivation of *p16INK4a* and *TP53* and niche factor independence was acquired after inactivation of *APC* and *KRAS-G12D* oncogene activation. The transfected cultures were expanded for 2-3 weeks until wildtype enteroids were depleted. The remaining transformed culture could be expanded indefinitely and carried frame shift mutations in all TSGs targeted by the CRISPR/Cas9 pentaplex. Cre-mediated recombination of the silent oncogene cassette resulted in expression of constitutively active Ras protein. Taken together, transformed intestinal cultures can be obtained for autologous transplantation 5-6 weeks after crypt isolation from pigs. Selecting CRISPR/Cas9 transfected enteroids with puromycin could reduce the generation of transformed cultures from five to three weeks as reported for the generation of genetically edited human enteroids[137].

These cells exhibited further hallmarks of cancer cells, such as the ability to migrate through extracellular matrix and the formation of tumours *in ovo*.

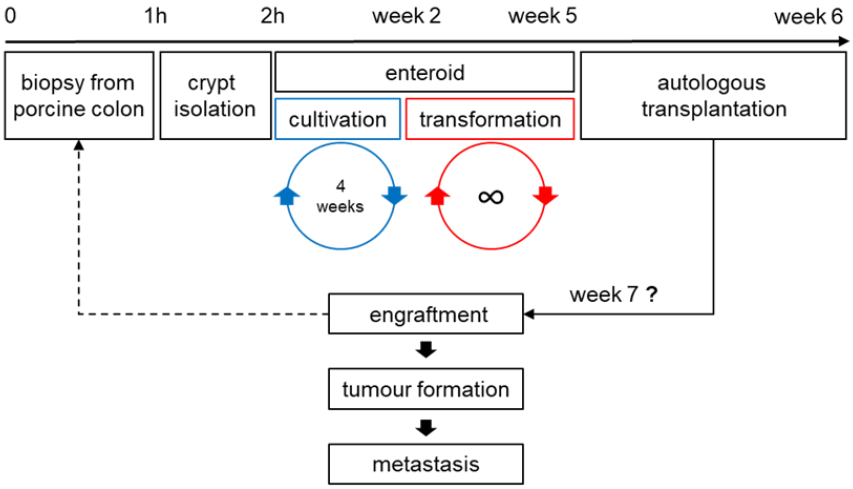

Figure 41: Schematic representation of the strategy for colorectal cancer acceleration with primary enteroids. Colonic crypts were isolated from porcine biopsies and cultivated within 2 hours. Porcine enteroids form within 3-7 days and were cultivated for 3-5 passages (3-5 weeks). Enteroids were harvested after 2 weeks of cultivation and transformed by tumour suppressor gene knockout and oncogene activation. Transformed enteroids outgrow within 3 weeks (passage 5). Afterwards the culture was expanded as 2D culture and used for autologous transplantation. Cells should engraft within 1 week as observed in CAM assay. Tumour formation and metastasis require further adaptation of the engrafted cells to in vivo conditions. Additional modifications can be introduced by repeated biopsy (dashed line).

The cell growth of transformed enteroids that was observed in the CAM assay after one week suggests that the cells rapidly adapted to the new environment which should favour engraftment after injection in pigs. However, tumour growth of transformed intestinal cells under the porcine skin has not been observed. Compared to injection under the skin, orthotopic injection of transformed enteroids under the colonic mucosa might improve engraftment as it is their native environment. In addition, injection sites should be analysed by immunohistochemistry to identify the composition of immune cells that could deplete the transplant.

Similarly, a colonoscopy-based approach was taken by Roper et al. [100] to induce tumours in the colon of mice that usually develop polyps in the small but not the large intestine. They present a colonoscopy-based CRC mice model by orthotopic transplantation of intact CRISPR/Cas9-edited organoids. The immune deficient NOD scid gamma (NSG) strain was used as recipient for organoids whose *APC* alleles were edited by CRSIPR/Cas9. Tumorigenesis was observed and engraftment rates were higher in NSG recipients compared to syngeneic immunocompetent strains that form mature T cells, B cells, and natural killer cells. Benign polyps that did not form tumours six weeks after successful colonoscopy-guided mucosal injection were only observed in immunocompetent syngeneic strains. Regarding these polyps, the injection site was diffusely infiltrated with lymphocytes and the structure of crypts was not adenomatous. As pigs have an functional immune system which may result in rejection, we extended the genetic modification from CRC-associated mutations to immunologically relevant mutations including a *B2M* knockout and integration of a *LEA29Y* expression cassette. By corrupting the immune recognition of injected transformed cells, we expect to minimize the immune response against neoantigens that might arise after transformation and, consequently, improve engraftment of the intestinal cancer-like cells after injection.

Roper and colleagues report that injection of organoids with an *APC* knockout led to the formation of primary tumours in the colon of NSG recipients but knockout of *TP53* and $KRAS^{G12D}$ expression were required to invade the muscularis propria (layers of smooth muscle for peristalsis) and metastasize to the liver in 33% of mice three months after engraftment. Likewise, porcine enteroids acquired broad niche factor independence by inactivation of *APC* and *TP53* and expression of $KRAS^{G12D}$. In addition, invasiveness was observed in Matrigel and by transwell invasion assay,

although, the combination of TSG knockouts that contribute to this phenotype remains to be identified.

Alternatively, the researchers discuss the use of lentiviral vectors to trigger tumour formation in mice to avoid the need of enteroid cultivation and transformation. Using viral vectors that deliver Cre for activation of conditional oncogenic mutations or target TSGs with siRNAs or CRISPR/Cas9 components, the murine colonic epithelium was engineered *in vivo*. However, upscaling the injection volumes or infectious titres of lentivirus and the need for S2 facilities hamper the application for large animals. Allometric scaling [138] can be used to estimate the injection dose required for the pig. The calculation is based on the normalization of dose to body surface area as recommended by the FDA to calculate the human equivalent to a pharmacological dose determined in animal studies. Of note, the body surface area and metabolic rate of humans and pigs (represented by the exponent value of 0.33) are almost identical [138], which allows the formula for humans to be applied for pigs. According to the protocol by Roper et al., a standard mouse of 20 g requires $6x10^5$ TU (viral transducing units), or $3x10^7$ TU/kg, of CRISPR/Cas9 lentivirus per colonoscopy-based injection to form colonic tumours. The allometric factor to calculate the equivalent dose for a pig is

$$\left(\frac{0.02}{60}\right)^{0.33} \approx 0.152.$$

Consequently, the equivalent injection dose is

$$3 \cdot 10^7 \ \mathrm{TU/kg} \cdot 0.152 \ \approx 0.5 \cdot 10^7 \ TU/kg.$$

Therefore, the equivalent injection dose for a pig of 100 kg is $5x10^8$ TU, which is almost 1000 times the dose required for the mouse and not achievable for a single dose.

Due to the lack of *in vivo* transduction methods for pigs and time-consuming procedures to generate genetically modified animals, novel approaches must be taken to accelerate CRC progression in the *APC*$^{1311/WT}$ pig model. The local re-transplantation of polyp-derived organoids carrying oncogenic mutations represents the most feasible approach to induce tumour progression specifically in the colon or rectum. In future experiments, autologous orthotopic re-transplantation of transformed porcine enteroids should be performed and the injection site should be

closely monitored by colonoscopy to understand the immediate reaction of the tissue and to estimate the degree of transplant rejection.

After successful engraftment of genetically modified cells, tumour tissue should be isolated from the injection site (dashed arrow in Figure 41) to determine the combination of mutations that are necessary for cancer cell dissemination *in vivo*.

4.2. Medium composition for porcine enteroids

The use of Wnt conditioned medium was essential to generate porcine enteroids from intestinal crypts. Purified recombinant Wnt protein was not able to substitute conditioned medium possibly due to the low solubility in growth medium and did not ameliorate the growth of enteroids. Although the concentrations of Wnt in conditioned medium could not be elevated, wildtype enteroids were cultivated for a maximum of five passages resulting in a cultivation period of 4-5 weeks. Noteworthy, transformed enteroid that had a growth advantage in the suboptimal culture medium could be successfully selected to obtain uniformly edited, niche-factor independent mutants for transplantation. Compared to cultivation times of porcine enteroids reported as 3-6 months in literature [87,90], further efforts are needed to exploit the full potential of the culture.

IntestiCult, a commercial medium for human and mouse organoids, is widely used for porcine cultures [90] [88,93,94]. However, it is expensive and modification of the medium is limited, which are substantial disadvantages compared with conditioned media. These are more laborious to produce and to standardize but also more flexible regarding supplement addition or deprivation. Furthermore, the supplementation with separate conditioned media for Wnt, R-spondin and noggin would be used to control differentiation of the culture. Barnett and colleagues reported that porcine enteroids that were grown in WRN-conditioned medium produced by L-WRN cells (cell line that secrets Wnt, R-spondin, and noggin) were mainly comprised of undifferentiated cell types and showed increased gene expression of *SOX9* and *LGR5* compared to colon[*139*]*.* These findings support the hypothesis that the medium used in this work insufficiently stimulates stem cell self-renewal and promotes differentiation of enteroids.

Mihara and colleagues designed an expression vector for production of Wnt conditioned medium that avoids sera [140] which might stimulate stem cell self-renewal

and differentiation differently due to batch-to-batch variation. In order to stabilize Wnt in absence of serum, the glycoprotein afamin is co-expressed and secreted by the cell line. Whether afamin-Wnt3a serum-free conditioned medium increases the *LGR5*-positive stem cell population and improves the longevity of porcine enteroids remains to be tested.

4.3. The use of in silico segmentation for porcine enteroid studies

The detection of cell clusters in three-dimensional culture is a difficult task due to badly defined boundaries. However, measuring the number and size of organoids on 2D images is often used to assess viability and proliferation. Common parameters are the formation efficiency, growth area on 2D images[141] or budding rate[142] of organoids. These data are mostly collected manually containing small datasets that do not provide the reader with a representative picture of the culture. Alternatively, colorimetric assays, like the MTT assay, which relies on the metabolic reduction of yellow tetrazolium salt (MTT) to purple formazan, are used[91]. In such endpoint assays, the culture is lost either due to the toxic accumulation of the product or the need to lyse the cells to measure intracellular ATP concentration which is translated into a luminescent signal[143]. Nevertheless, only the combination of number, size, and density provides researchers with sufficient information to evaluate the proliferation and viability of 3D clusters. In addition, analysing changes during growth and passaging of organoids is essential to identify trends that progress slowly, like the continuous decline of a culture, or document sudden changes, like the abrupt growth arrest of porcine enteroids observed in this work. In lieu of error-prone manual counting, researchers can train software with representative 2D images from confocal and bright field microscopes, a principle called ‘machine learning’. Recently, a segmentation tool was developed that outperformed existing open-access programs for automated analysis of multi-layered tissues even processing time-lapse movies[144]. A major bottleneck of these programs is the long processing time of 20-106 min/image which is required for accurate segmentation. Furthermore, as these programs were developed for multi-layered tissues, organoids are usually divided into smaller units, a problem called ‘oversegmentation’.

Inspired by the use of the cell segmentation tool ‘Cellpose’ by Wolny and colleagues, who wrote an algorithm to segment plant tissues into single cells[145], I implemented the versatile Cellpose application in the image analysis freeware Fiji/ImageJ. The

program was used to segment more than 1000 porcine enteroids on 2D bright field images to test if the mucosa of severe and mild polyposis *APC*$^{1311/+}$ pigs show different growth characteristics. The descriptive statistics is comprised of three plots and describes the culture's growth characteristics in detail by summarizing the number, size, and density of enteroids in Matrigel. It will be a valuable tool to measure enteroid proliferation and viability in intervention studies with toxins[146], drugs[147], and dietary metabolites[91], for example.

4.4. The use of electropermeabilisation to transfect of porcine enteroids

Compared to Sharbati et al., who used nucleofection (a commercial mammalian electropermeabilisation system) to deliver miRNAs[86], we first report electropermeabilisation as an efficient, versatile DNA-transfection method for porcine enteroids that are usually transduced with lentiviral vectors[86,148]. Our protocol is based on the work of Fujii et al. who used separate pulses for enteroid pore formation and DNA transfer[137]. We found that the two poring pulses were sufficient to achieve high transfection efficiencies of more than 40% in our in house-made transfection buffer and that the pulse length was crucial. The buffer composition was adapted from a US patent (Patent No.: US 8,039,259 B2). In comparison with the electropermeabilisation settings that we optimized for porcine kidney-derived primary cells and cell lines, that are easily transfected by lipofection, HEK293T and CHO cells e.g., the pulse length for porcine enteroids is five times higher, which indicates that the membrane of enteroids is stiffer and consequently more resistant to lipofection.

4.5. Introduction of multiple oncogenic mutations in enteroids with a modified CRISPR/Cas9 multiplexing strategy

Frame shift mutations were introduced in five tumour suppressor genes with high efficiencies using a CRISPR/Cas9 multiplexing strategy, which was inspired by a protocol from Xie et al.[99]. The authors described an array of multiple guideRNAs interspaced by a tRNA precursor sequence that uses the cellular tRNA-processing system, namely RNase P and RNase Z, to cleave the immature RNA sequence, thereby, releasing single guideRNAs from one polycistronic RNA. The system offers many advantages over conventional CRISPR/Cas9 systems. First, multiplexing of guideRNAs on a single vector reduces the size of the construct from 420 bp to 170 bp per guideRNA, which is a major concern for cloning of viral vectors due to limited

packaging capacity. Since lentiviral transduction was mostly described in the literature to transfect intestinal enteroid cultures, it was considered the most promising transfection method for porcine enteroids before efficient electropermeabilisation was established. Secondly, the expression of all guideRNAs is guaranteed by transfection of a single vector, which increases the proportion of completely edited genomes. Thirdly, it eliminates the need to express Csy4, an additional endoribonuclease that has been described previously to cleave a polycistronic RNA into single guideRNAs[149]. Forthly, there is no need to alter guideRNA sequences to place a guanine at their 5' end which is required for transcription by the U6 promoter but could affect CRISPR/Cas9 editing efficiency.

In the original protocol, Golden Gate cloning was used to assemble up to eight guideRNAs into one CRISPR/Cas9 multiplex to target genes coding for mitogen-activated protein kinases in rice by excising fragments up to 760 bp. The researchers observed enhanced targeting efficiency compared to CRISPR/Cas9 constructs with single guideRNAs which was explained by the presence of enhancer elements in the tRNA precursor sequences. The tRNA precursor sequence used in this work is identical to the porcine and human gene encoding *tRNA-Gln* (GenBank: X58792.1) and is highly conserved among animals. Since the cloning protocol showed a high degree of unspecific PCR products, the strategy was modified by performing shorter overlap extension PCRs to improve the amplification of duplexes for the cost of additional cloning steps (see section 2.2.4). The protocol has been successfully applied by collaborating laboratories, like the Chair of Viral Replication in Cellular Chromatin of Prof. Sabrina Schreiner, which used a multiplex to visualize viral replication in human cell lines (not published).

In lieu of efficient guideRNA multiplexing, Matano and colleagues[68] had to use multiple cycles of CRISPR/Cas9-mediated editing, cell culture cloning, and selective niche factor-deprived media to introduce defined genetic mutations in human enteroids from normal colonic epithelium. The study addresses many aspects of this work as it targets the five signalling pathways recurrently altered in colorectal cancer – Wnt, MAP kinase, PI3K/Akt, TGFβ and p53 signalling pathways. They electropermeabilized enteroids with single guideRNA CRISPR/Cas9 vectors and donor templates encoding oncogenic mutations to be stably transfected via homology directed repair. Using niche factor deprivation and growth factor inhibitors, the group

successively selected human enteroids for knockout of *APC*, *SMAD4*, *TP53* and oncogenic mutations in endogenous *KRAS* (*KRAS*^{G12V}) and *PI3KCA* (*PI3KCA*^{E545K}). However, these engineered enteroids maintained genetic stability and a well-differentiated epithelium as measured by immunohistochemistry. Comparing the expression profile and copy number variations of engineered enteroids with patients' adenoma and CRC data revealed that these enteroids resembled adenomas and lacked expression of CRC-associated genes, such as *EREG* (epiregulin, member of the EGF family of proteins) and *ETV4* (ETS variant transcription factor 4). Consequently, the growth of engineered human enteroids was restricted to two months after xenotransplantation into the kidney of NSG mice and the transplant was not invasive. In contrast, human enteroids derived from CRC samples constantly grew and invaded the adjacent tissue in vivo over this period. The study indicates that driver mutations that are commonly found in human CRC confer niche independence but are not sufficient to induce an advanced, malignant CRC phenotype when introduced as defined genetic mutations.

We additionally inactivated *p16INK4a*, which rapidly transformed porcine enteroids, and *PTEN* which is a repressor of the PI3K/Akt pathway, thereby effecting the PI3K/Akt pathway similarly as the E545K oncogenic mutation of *PI3KCA*. Likewise, the increase in niche factor independence was evident by niche deprivation of cultures with increased tumour load and culminated in the survival of transformed enteroids in basic medium without FCS or supplements. In contrast to the cited study, we observed invasion of porcine engineered enteroids through Matrigel and showed that enteroids were attracted by Wnt, R-spondin, and EGF, although these stimuli were dispensable for growth. Interestingly, the authors identified chromosomal instability (CIN) in one enteroid line after knockout of *SMAD4* and *TP53*. After introduction of the *KRAS*^{G12V} mutation, this line formed metastasis in NSG mice. In default of gene expression microarrays for pigs, other assays, like the sister chromatid exchange assay, the bleomycin assay, and the comet assay exist to assess CIN and are well-established in agrigenomics [150]. Selection of chromosome instable colonic adenomas or transformed enteroids could improve malignant progression in the FAP model after transplantation and would fulfil another feature of CMS2 tumours (Table 1) – in addition to early oncogenic mutations in *APC* and *TP53*.

In summary, we could replicate the growth advantage described for human enteroids after knockout of TSGs and oncogene activation in CRISPR/Cas9-engineered porcine intestinal cultures. Compared to previous studies, the generation of porcine enteroids with numerous transforming mutations was greatly accelerated with an improved CRISPR/Cas9 multiplexing approach and an *in vitro* culture system that favoured outgrowth of transformed cells.

In summary, I optimized the culture of porcine enteroids from small and large intestine including the genetic manipulation using electroporation and CRISPR/Cas9 multiplexing. I further conducted preliminary work on the characterisation of these cultures on cellular and molecular level by testing markers for the identification of intestinal cell types and for gene expression analysis. By establishing cell segmentation for 3D cultures, I provided a useful tool to quantify enteroid growth during cultivation. These are useful techniques not only for the transformation of porcine enteroids but for various studies at the effects of metabolites[91,92,141,142,146,147,151], enteric viruses[94,152–155] and microbes[93].

4.6. Sets of mutations that leads to invasive CRC progression in vivo

If autologous transplantation of these transformed enteroids leads to progression of CRC remains to be tested. A study conducted in 2017 by Fumagalli and colleagues[156] analysed the impact of CRC-associated mutations on metastasis of CRISPR/Cas9-engineered enteroids that were generated from healthy human colon. Four months after orthotopic transplantation under the caecal wall of NSG mice, enteroids with oncogenic mutations of *APC*, *KRAS*^{G12D}, and *TP53* (triple enteroids) formed primary tumours in all tested animals. Using different sets of oncogenic mutations, *APC*^{KO} and *KRAS*^{G12D} were attributed to extensive tumour proliferation *in vivo* and further knockout of SMAD4 (quadruple enteroids) formed poorly differentiated adenocarcinomas that invaded the surrounding stroma. In addition, migration of enteroids was measured by repeated intravital fluorescent imaging and was significantly higher in quadruple than in triple *SMAD4*^{WT} enteroids, which highlights the need of *SMAD4* knockout to induce invasive disease in the FAP model. Compared to the results of Matano et al. who used heterotopic transplantation of similarly engineered enteroids[68] invasiveness might be favoured in an orthotopic transplantation model. Moreover, only quadruple enteroids metastasized from the primary tumour to liver and lung in 44% of transplanted mice. Noteworthy, triple

enteroids that were injected into the mesenteric vein to circumvent the need to disseminate into the blood stream failed to colonize the liver.

Taken together, the orthotopic autologous transplantation of porcine enteroids with knockouts in *APC*, *PTEN*, *SMAD4*, *TP53* and activated *KRAS*^{G12D} represents the most promising approach to accelerate the progression from adenoma to carcinoma in the FAP pig model. Further analysis is needed to test whether chromosomal instable enteroids can be generated using this strategy to increase the malignancy after transplantation. However, low *LGR5* expression in human CRC – as observed in wildtype and transformed porcine enteroids – is associated with better prognosis indicated by recurrence-free survival after curative therapy[157]. Low *LGR5* expression might reduce the aggressiveness of the graft and the survival *in vitro* since reduced *LGR5* levels have been reported in enteroids grown in WRN conditioned medium from pig, cat and horse compared to isolated crypts[87].

We intended to preserve *LGR5* expression after transformation by transfecting wildtype colonic enteroids with an *LGR5*-dependent Cas9 multiplex vector. For this purpose, 500 bp of the proximal *LGR5 promoter* sequence were amplified by PCR from the porcine genome to drive Cas9 expression by *LGR5 core promoter* elements which were predicted with the software 'Genomatix'. However, preliminary experiments with an *LGR5*^{prom}*-GFP* construct revealed that the promoter element lacked specificity as the fluorescent cassette was equally expressed in primary kidney-derived cells and colonic enteroids (data not shown). In literature, experiments that require *LGR5 promoter* activity use knockin of traceable markers into the endogenous *LGR5* instead of a transgenic *LGR5 promoter* cassette[14,106,157,158], which indicates that the repressor elements, that might confer intestinal stem cell specificity, are unknown.

Besides defined genetic modifications, cancer malignancy has been associated with the ability of epithelial cells to acquire a migratory phenotype, usually attributed to mesenchymal cells[159]. We detected upregulation of fibronectin and vimentin expression – genes that are routinely used to assess epidermal to mesenchymal transition (EMT). The mesenchymal expression profile was induced by complete dissociation of transformed enteroids independent of the presence of Matrigel. Therefore, we propose to completely dissociate transformed enteroids prior to autologous transplantation to favour dissemination into the injection site.

Activation of the oncogenic *KRAS*^{G12D} mutation induced EMT in murine small intestinal tumour organoids with *APC*$^{\Delta 716}$ *TGFβR*^{KO} genotype which metastasized to the liver after allotransplanation into the spleen of NSG mice[160]. Of note, these invasive tumour cells still expressed E-cadherin, an epithelial cell marker, indicating that invasive cancer cells retain epithelial and mesenchymal characteristics. Identification of the EMT-initiating mutation in porcine enteroids remains to be investigated.

To conclude, we introduced a set of defined oncogenic mutations that has been associated with an aggressive, malignant phenotype of mouse and human intestinal cancer cells in porcine enteroids derived from normal mucosa and polyps. *In vitro* analysis including qPCR expression analysis and transwell invasion assay indicates that transformed enteroids acquired the ability to invade the extracellular matrix after EMT. Besides, transformed enteroids showed no sign of differentiation as measured by qPCR and fluorescent immunostaining. Similarly, murine adenocarcinomas, that were generated by Cre-mediated heterozygous inactivation of *APC* and *KRAS*^{G12D} activation, showed undifferentiated epithelium as indicated by the lack of goblet cells and uniform expression of the stem cell markers β-catenin, Mcm6, and Msi1 in the dysplastic tissue[161]. Haigis and colleagues conclude that activated Ras signalling and β-catenin accumulation synergistically suppress differentiation. We observed WRE-independent growth in transformed enteroids and verified constitutively active Ras protein by Western Blot and increased β-catenin signalling by Wnt sensitivity assay.

Close monitoring of tumours that grow on the chorioallantois (CAM assay) will clarify if these enteroids induce angiogenesis – another hallmark of cancer cells. Bright field images should be taken around the site of implantation to image and measure the density of blood vessels under a stereomicroscope. In addition, immunoperoxidase staining could be performed to visualize infiltration of the chorioallantois by transformed enteroids. For this purpose, α-Gal epitopes, which are expressed on porcine but not on chicken cells, are bound by biotin-conjugated isolectin B4. Streptavidin-conjugated horseradish peroxidase is used to stain infiltrating porcine intestinal cells with 3,3'-diaminobenzidine[162].

4.7. Strategies to alter the innate immune system of pigs to favour CRC progression

Due to the introduction of frame shift mutations in several TSGs, our engineered enteroids are expected to express neoantigens that are recognized by the immune system leading to the destruction of the autograft. Two strategies were developed to reduce the recognition of transformed porcine enteroids after autologous transplantation.

First, the response of cytotoxic $CD8^+$ T cells against autografts was inhibited by depleting the light β-chain of the SLA-1 complex. Using a modified CRISPR/Cas9 system that consisted of the guideRNA pentaplex on one vector and the anti-*B2M* guideRNA with Cas9 endonuclease on the second vector, transformed intestinal cells with a complete knockout of the SLA-1 component, β2-microglobulin, were realised. Using the same crRNA against *B2M*, surface SLA-1 was depleted in pigs carrying knockouts in *B2M* and three xenoreactive antigen genes[132]. In a rat myocardial infarction model human umbilical mesenchymal stem cells were injected after CRISPR/Cas9 targeting of *B2M* which significantly reduced infiltration of rat $CD8^+$ T cells compared to unmodified xenografts[163]. The activation of porcine $CD8^+$ T cells by transformed autologous enteroids and the protective effects conferred by a knockout of B2M remains to be verified. For this purpose, porcine $CD8^+$ T cells should be isolated from the blood and purified by magnetic-activated cell sorting for co-cultivation with irradiated transformed autologous enteroids. Lymphocyte activation can be assessed by measuring proliferation using ^{3}H-thymidine and a scintillator counter as described by Fischer et al.[132]

Secondly, we intended to locally repress the activation of professional antigen presenting cells, like macrophages and dendritic cells, by stable integration of a *CAG-LEA29Y* expression cassette into transformed enteroids. The protective effect of a transgenic LEA29Y expression cassette has been verified in different in vivo models. It repressed lymphocyte infiltration of porcine islet cells after transplantation into NSG mice[164], preserved skin transplants in pig-to-mice xenografts[165], and prolonged rejection of porcine cornea xenotransplants by reducing macrophage infiltration in primates[166]. These studies used tissue specific expression of LEA29Y. Bähr and colleagues were the first to generate a pig with ubiquitous expression of *CAG-LEA29Y*. Expression of LEA29Y was verified in cell lysates by

immunohistochemistry and indirect ELISA using anti-human IgG-antibodies from mouse (monoclonal) and rabbit (polyclonal)[133]. In Western Blot, we observed poor specificity of the antibody which will complicate detection of LEA29Y. For this reason, the biological function of LEA29Y, which is secreted into the supernatant and inhibits T cell activation, should be used for detection as described for *B2M*.

Thirdly, inspired by the tumorigenic phenotype observed in $TNF^{\Delta ARE}$ mice[48,49] we aimed to induce chronic inflammation in the intestine of $APC^{1311/WT}$ pigs. Using CRISPR/Cas9, two homologous sequences (*ARE* and *CDE1*) that are involved in posttranscriptional regulation of porcine TNFα levels were successfully excised *in vitro* and piglets were born that carried the mutation in one allele. Breeding with $APC^{1311/WT}$ pigs will show whether the proinflammatory phenotype promotes colorectal cancer progression. Besides murine studies, a study in DSS-induced IBD in rat supports the assumption that mucosal inflammation and APC inactivation supports colorectal adenocarcinoma[167]. Treating the rats with pentoxifylline decreased TNFα and IL-6 levels and reduced colorectal adenomas in number, size, and incidence. Whole-exome sequencing of tumour specimen of 31 IBD patients indicate that colorectal tumours develop differently from sporadic colorectal tumours[168]. The researchers found significantly lower mutation rates for *APC* and *KRAS* in IBD patients compared to sporadic colorectal tumours. Moreover, the recurrent mutations in the IBD group suggest that non-canonical Wnt signalling plays a role for IBD-associated colorectal cancer formation. Mechanistically, the colitis-stimulated turnover of epithelial cells and increased reactive oxygen species may contribute to the formation of adenomas in colitis-associated cancer which show high rates of oncogenic *TP53* mutations. In progressed disease *APC* mutations occur[169].

5. Conclusion and Outlook

In this work, I described the culture of 3D intestinal epithelial cells from pig to study tumour progression in a porcine model for human colorectal adenocarcinoma. For this purpose, I adapted existing protocols for murine and human enteroid cultivation and developed a porcine-specific noggin-secreting cell line. Porcine enteroids were cultivated for up to five weeks in which five frame shift mutations in CRC-associated TSGs were introduced using a CRISPR/Cas9 pentaplex and oncogenic KRAS-G12D mutation was activated. Further research has to be conducted to verify the knockout of all TSGs by Western Blot and to identify the LGR5-positive stem cell population in enteroids. Although results from tumour assays performed *in vitro* are promising, colonoscopy-based autologous transplantation of transformed enteroids under the mucosa of pigs remains to be performed to test whether it accelerates the progression to invasive colorectal adenocarcinoma *in vivo*. In order to reduce destruction of transformed enteroids by the immune system, the cells were engineered to avoid presentation of neoantigens and to secret a potent T cell suppressor.

In addition to the versatile CRISPR/Cas9 multiplexing cloning protocol, *in silico* segmentation and electroporation were established as useful tools to analyse and genetically modify enteroids for future experimentation.

Finally, breeding of pigs predisposed to colitis and the FAP-pig will introduce a new porcine model for colitis-associated colorectal cancer.

6. Supplements

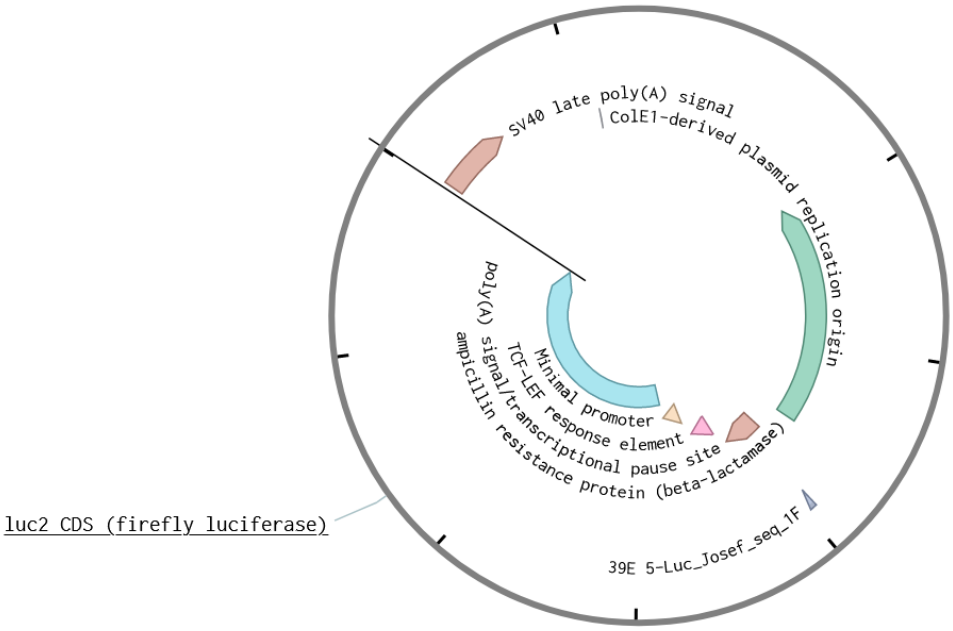

Supplementary Figure 1: TOPFlash plasmid for expression of Wnt-responsive Firefly Luciferase (pGL4-TCF/LEF-Luc2)

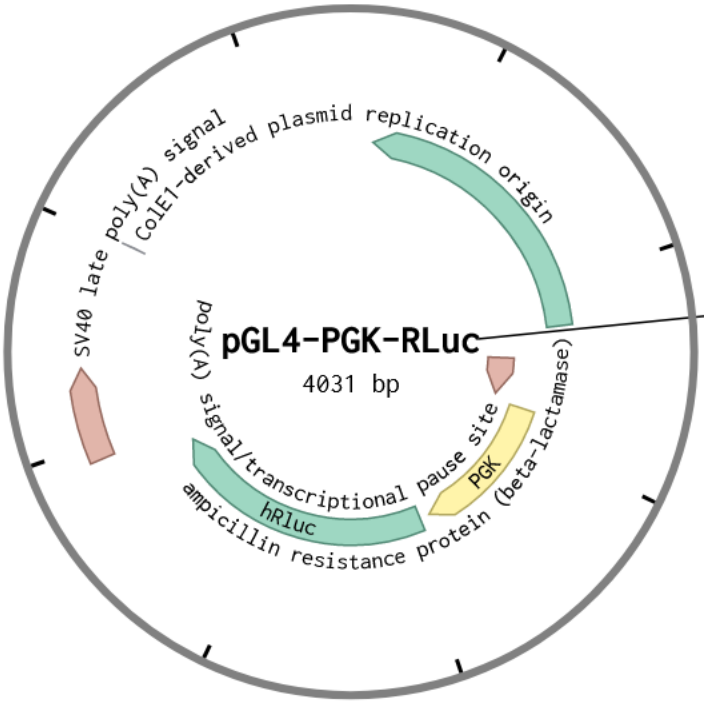

Supplementary Figure 2: TOPFlash plasmid for constitutive expression of Renilla Luciferase (pGL4-PGK-Renilla)

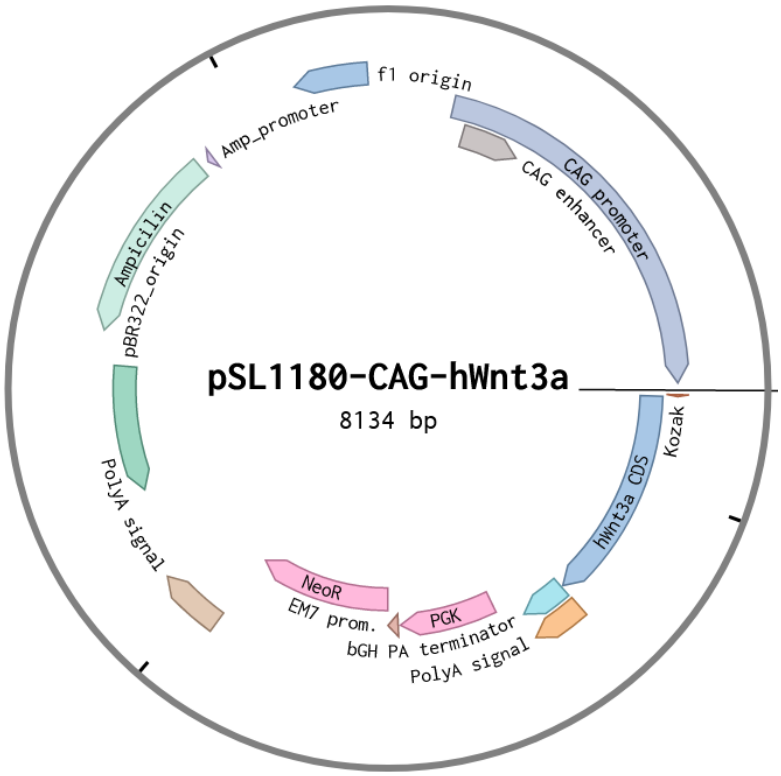

Supplementary Figure 3: Expression vector for human Wnt3a

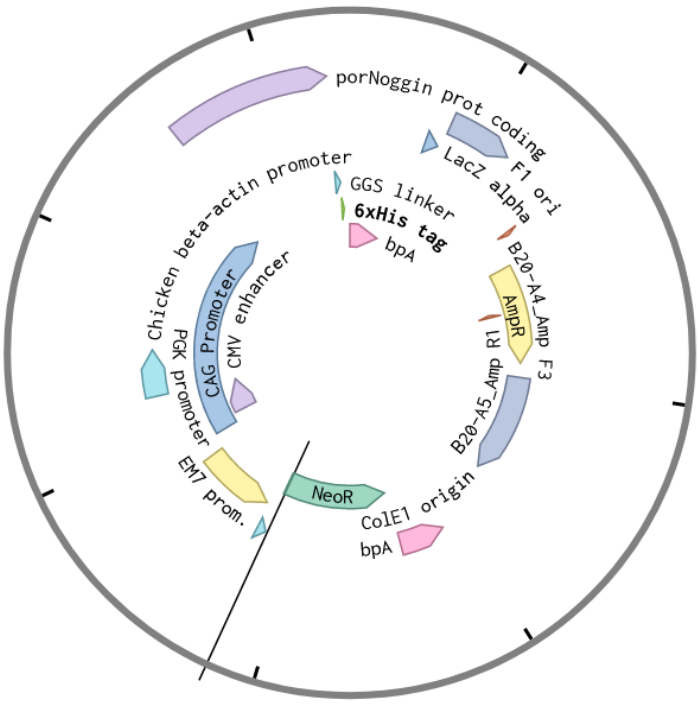

Supplementary Figure 4: porcine Noggin expression vector

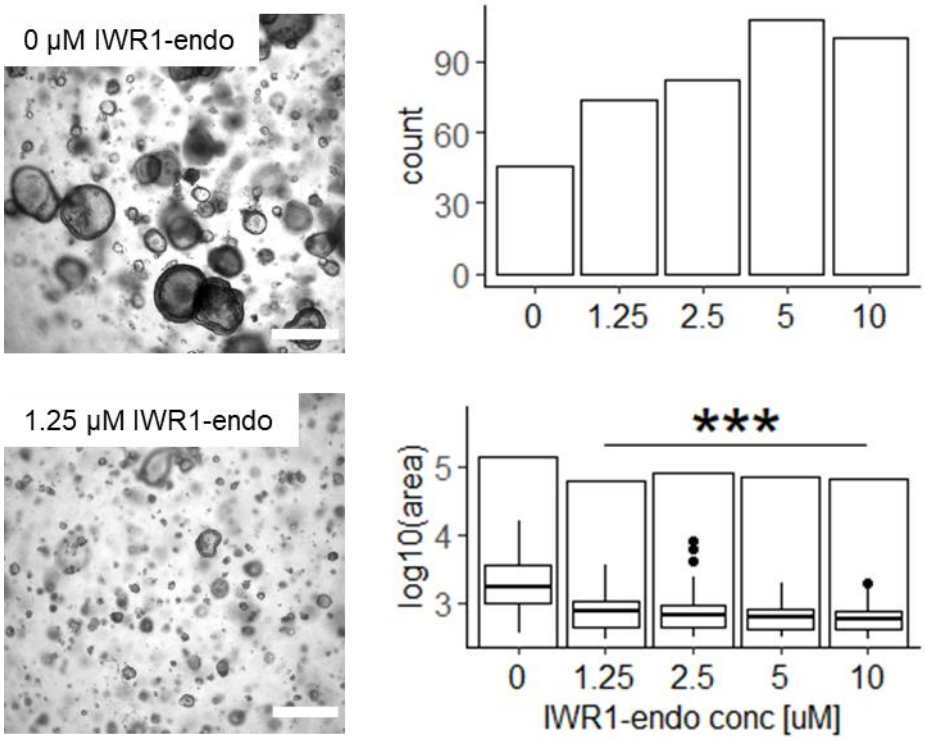

Supplementary Figure 5: IWR1-endo (Wnt inhibitor) supplementation and *APC*$^{1311/WT}$ enteroid growth analysis. *APC*$^{1311/WT}$ enteroids were cultivated in complete growth medium supplemented with different concentrations of IWR1-endo, an inhibitor of canonical Wnt signalling. Bright field images were taken (examples shown for 0 µM and 1.25 µM IWR1-endo) and the number and size of enteroids were analysed digitally. IWR1-endo decreased enteroid size significantly ($p < 0.001$, ***). Scale bar is 400 µm.

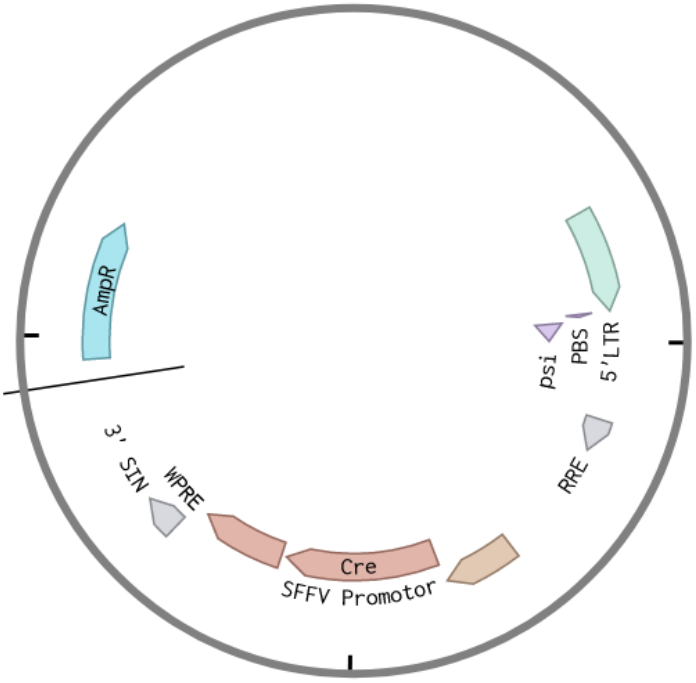

Supplementary Figure 6: non integrating Lenti-*iCre* vector

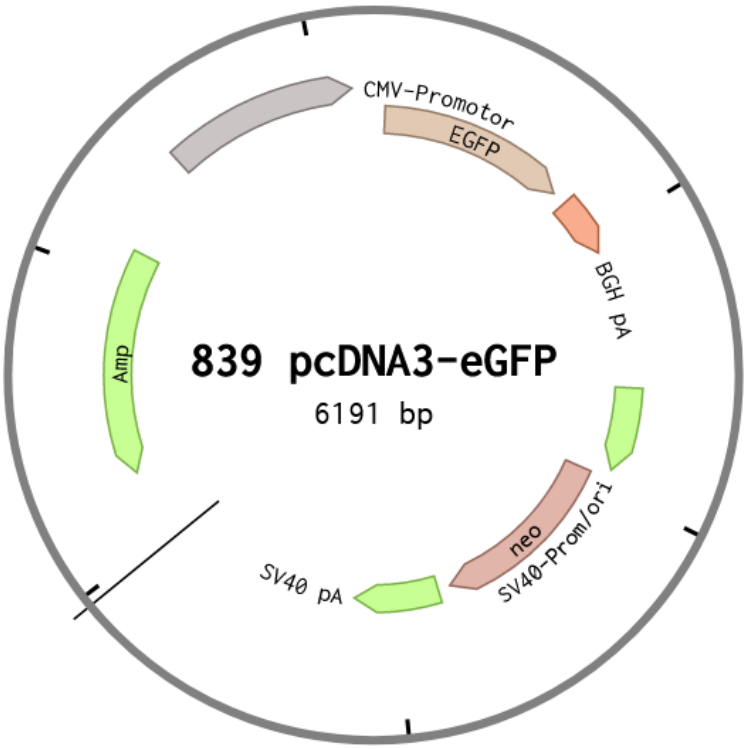

Supplementary Figure 7: Fluorescence plasmid for transfection control (pcDNA-CMV-*eGFP*)

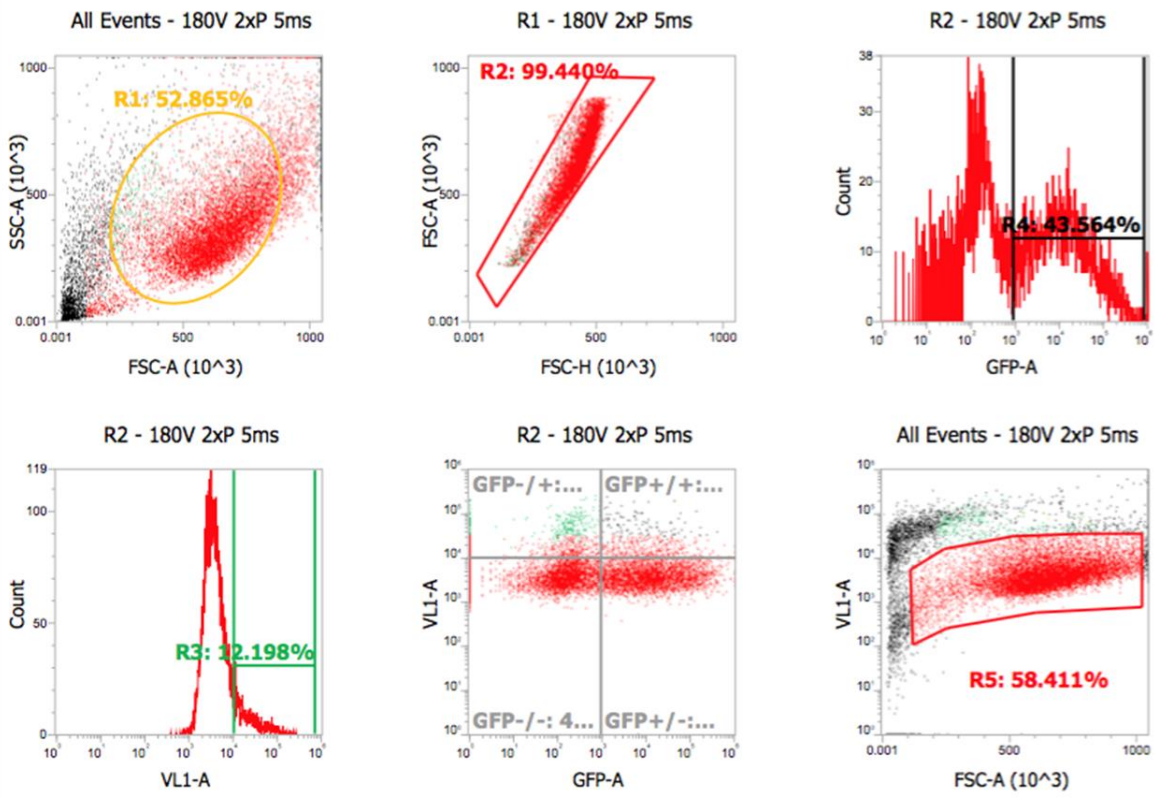

Supplementary Figure 8: Gating strategy for GFP expressing enteroids

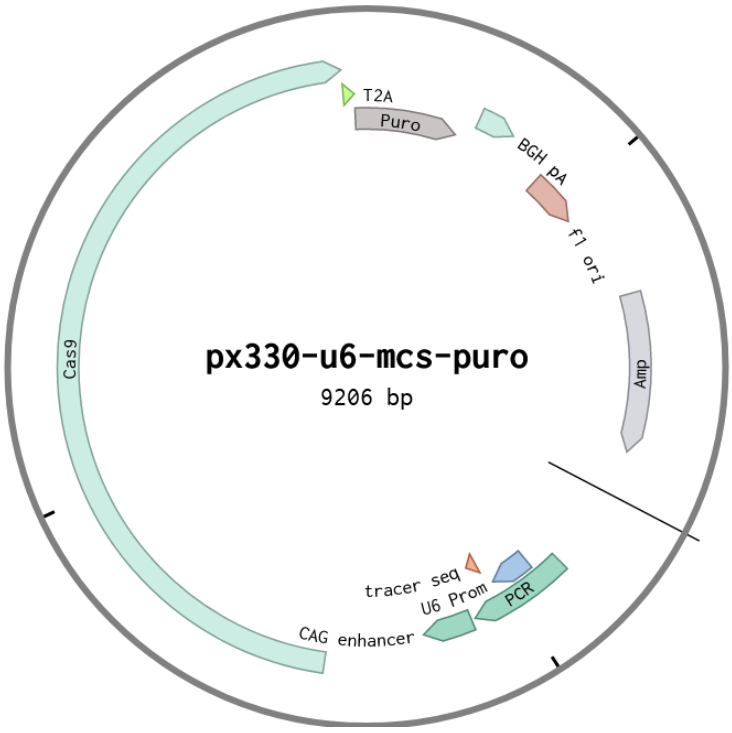

Supplementary Figure 9: CRISPR/Cas9 single guide RNA cloning vector

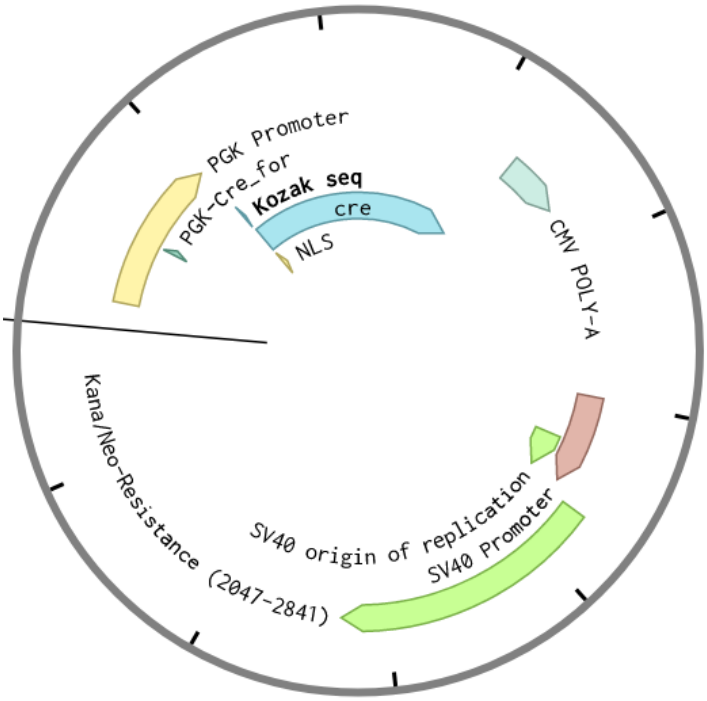

Supplementary Figure 10: *pPGK-Cre* expression vector for activation of *KRAS*$^{LSL\text{-}G12D}$ allele in enteroids

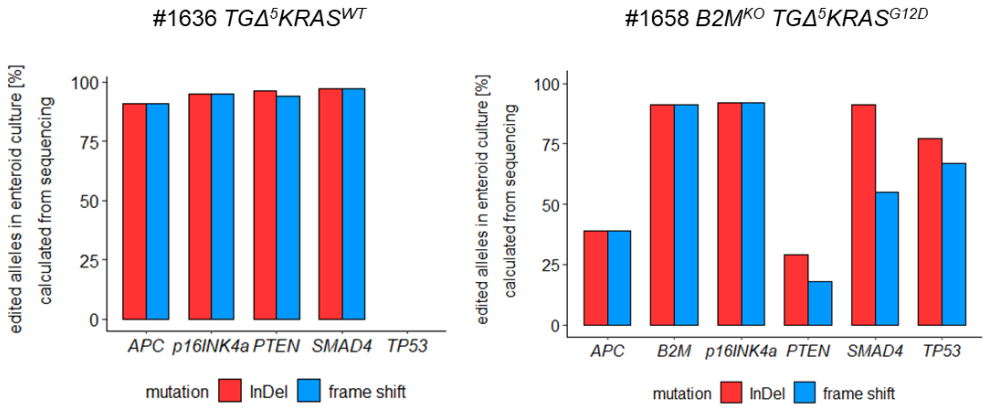

Supplementary Figure 11: InDel analysis of transformed enteroids for transplantation. The proportion of InDel and frame shift mutations were analysed in *TGΔ5* enteroids lines #1636 (no *crB2M; KRAS-WT*) and #1658 (+cr*B2M; KRAS-G12D*). Amplification and sequencing of *TP53* was repeated several times for line #1636 but the quality was insufficient for InDel analysis. Except of *TP53* of line #1636, moderate or high rates of inactivation were predicted for most alleles.

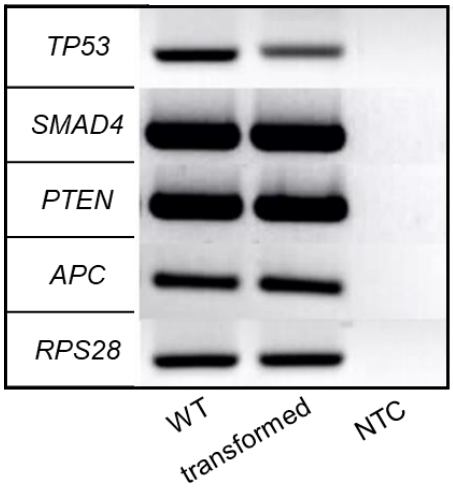

Supplementary Figure 12: Detection of mRNA transcripts of TSGs after editing with the CRISPR/Cas9 pentaplex by RT-PCR. Colon enteroids from polyps of *APC*$^{1311/WT}$ *KRAS*$^{LSL-G12D}$ pig #1658 were transfected with the CRISPR/Cas pentaplex to edit five TSGs. The latent KRAS-G12D allele was activated by transfection with pPGK-Cre. The mRNA transcripts of all edited TSGs were detected by RT-PCR except of p16INK4a which eluded amplification by RT-PCR. This indicates that gene editing did not disrupt transcription of TSGs.

Editing of TSGs was detected by sequencing but transcription of each genes remained active.

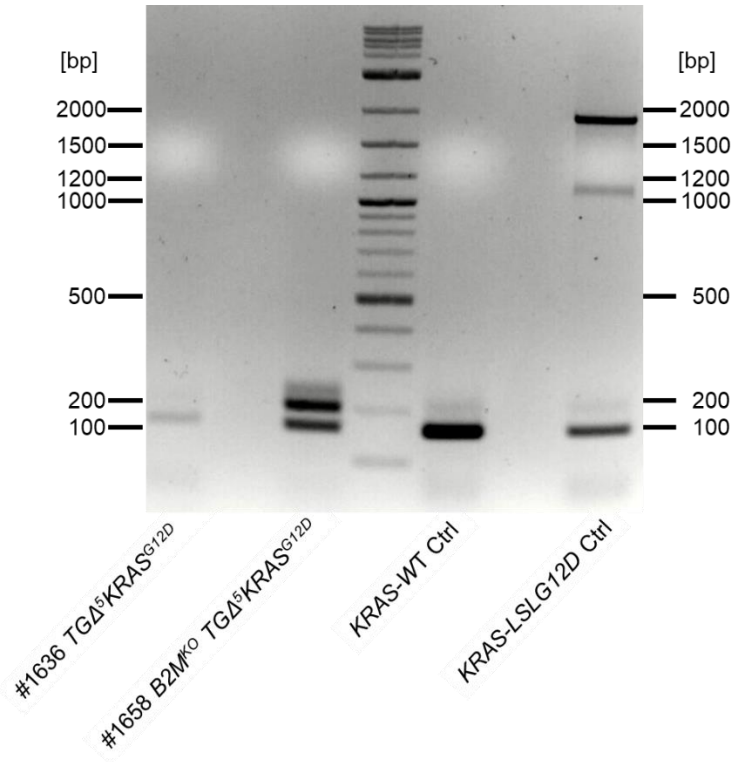

Supplementary Figure 13: PCR for detection of activated *KRAS-G12D* allele after Cre-mediated excision of the LSL cassette. Recombination of KRAS-LSLG12D by transfection with pPGK-Cre was detected in #1658 enteroids by the appearance of the recombined fragment of 201 bp. Line #1636 only showed the *KRAS-WT* band like the *WT* Ctrl. Line #1636 could be derived from an *APC-1311/WT KRAS-WT* animal by mistake.

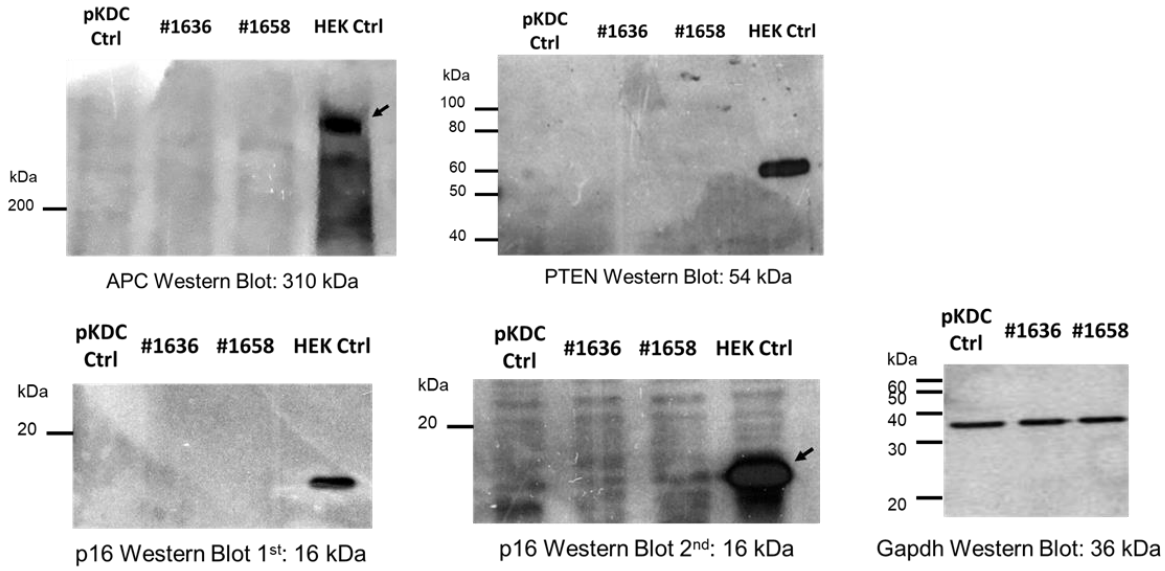

Supplementary Figure 14: Knockout of TSGs detected by Western Blot. *TGΔ5* enteroids lines #1636 (*KRAS-WT*) and #1658 (*KRAS-G12D*) were lysed and mouse anti-human antibodies were tested to detect porcine tumour suppressor proteins. Detection was performed with mouse IgGkappa-binding protein linked to horseradish peroxidase. Only the antibodies directed against SMAD4 and TP53 were cross-reactive for porcine cell lysate (see Figure 30 D). The tested anti-human antibodies against APC, PTEN and p16INK4a showed no band for the porcine protein or many bands due to low specificity.

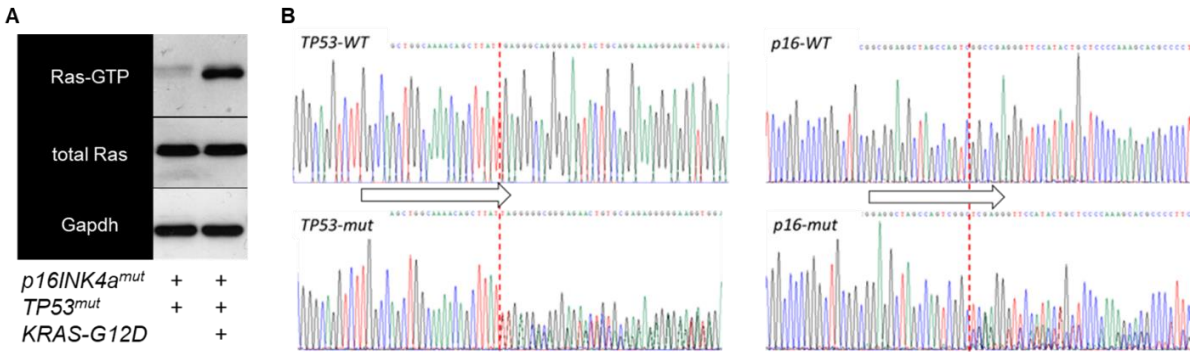

Supplementary Figure 15: Ras Activation Assay and sequence analysis for *TGROSA KRAS-LSLG12D* enteroids transfected with single CRISPR/Cas vectors and *pPGK-Cre*. *TGROSA KRAS-LSLG12D* enteroids were transfected with combinations of CRISPR/Cas vectors carrying crRNAs for either *p16INK4a* or *TP53*. By co-transfection with pPGK-Cre silent *KRAS-G12D* was activated as shown by Ras Activation Assay (Western Blot). Total Ras was detected after saturation with a stabilised GTP-derivate and Gapdh was detected as positive Ctrl (A). Sequence analysis of the cell pool shows that both genes were edited within the target region indicated by the red dotted line. Using Synthego's online InDel prediction tool, frame shift is predicted > 80% of *p16INK4a* and *TP53* alleles in the cell pool compared to the *WT* Ctrl (B).

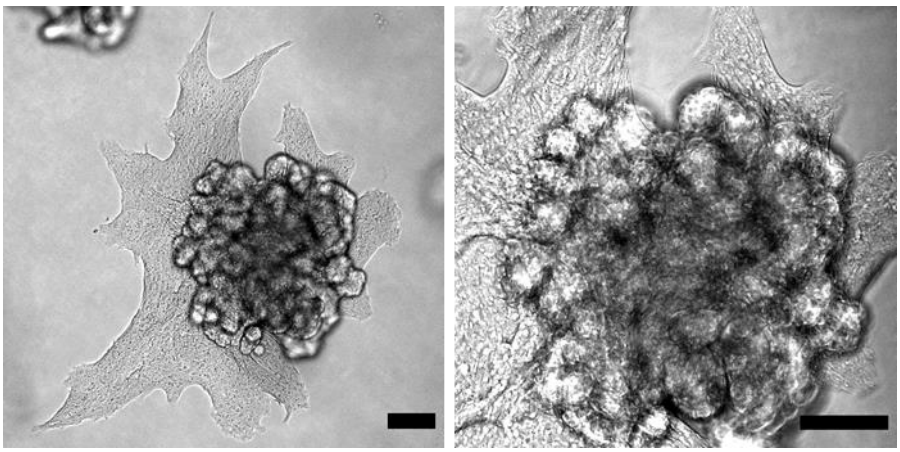

Supplementary Figure 16: Invasion of transformed enteroids in Matrigel. Bright filed image of the *TGΔ5 KRAS-G12D* enteroid line #1658 that invades the Matrigel surrounding the central cluster. Scale bar is 100 µm.

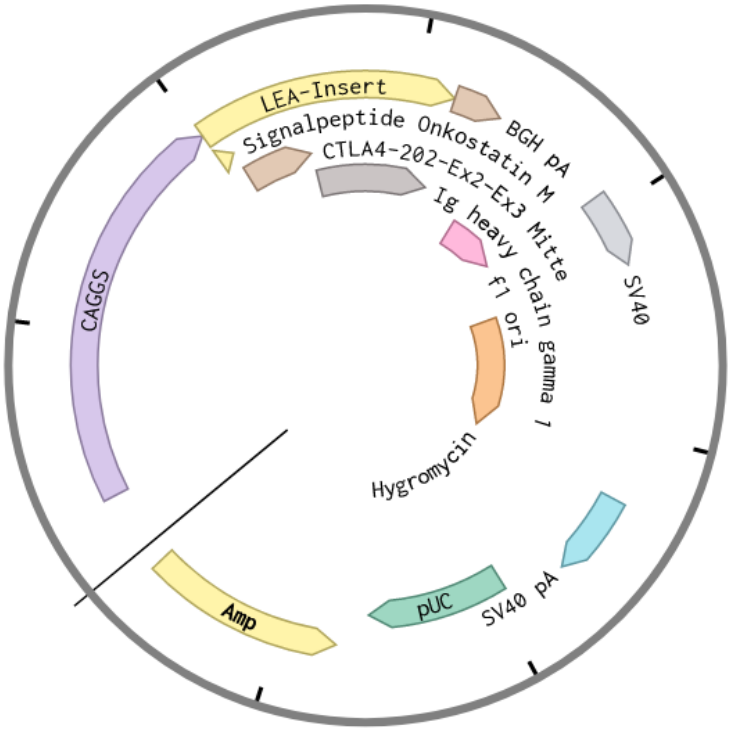

Supplementary Figure 17: LEA29Y expression vector

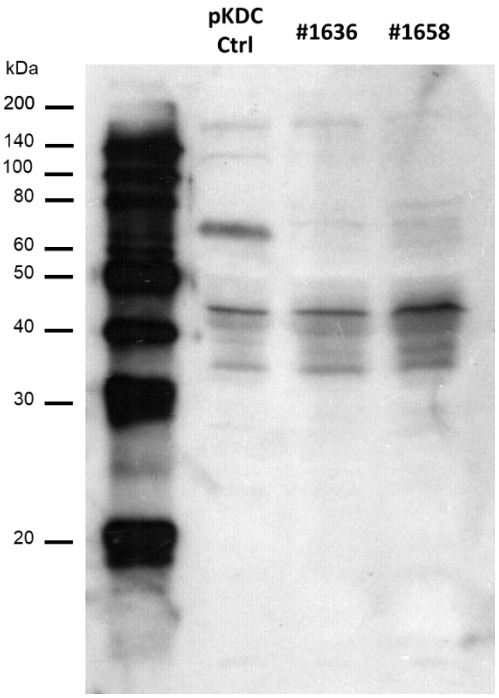

Supplementary Figure 18: LEA Western Blot. *TGΔ5 KRAS-G12D* enteroids lines #1636 and #1658 transfected with the LEA29Y expression construct were lysed to detect LEA29Y protein by Western Blot. Anti-human IgG1-HRP antibody was that should bind the IgG1-Fcγ domain of the recombinant protein. LEA29Y has a molecular weight of 42 kDa but could not be detected due to unspecific binding of the antibody.

Supplementary Table 1: RT-PCR/qPCR primers

target gene	primer	sequence	amplicon [bp]	reference
FN1, fibronectin	porFN-1 RT-PCR_F	GGCACAAGATTCGGGAGG	104	Shi, Liu et al. 2013[170]
	porFN-1 RT-PCR_R	ATGGGAAACCGTGTAGGG		
VIM, vimentin	porVIM RT-PCR_F	CGAGAGCACTTTGCAGTCTTT	199	
	porVIM RT-PCR_R	GAGGTCAGGCTTGGAAACATC		
CDH1, E-cadherin	porCDH1 RT-PCR_F	GCAATCCTGGCTTTGGCG	156	
	porCDH-1 RT-PCR_R	CGGTGCCCACTTTGAATCG		
TJP1, tight junction protein	porTJP-1 RT-PCR_F	ATCTCGGAAAAGTGCCAGGAA	202	
	porTJP-1 RT-PCR_R	AAGGTCATCACTTGTAGCGCC		
CA2, carbonic anhydrase 2	porCAII RT-PCR_F1	ATTGTCAACAACGGCCACTC	150	
	porCAII RT-PCR_R1	AGTATGCTCAGAACCTTGCCC		
ChgA, chromogranin	porChgA RT-PCR_F1	GAATAAGGGGGACACCGAGG	174	
	porChgA RT-PCR_R1	GCGAGGTCTTGGAGCTCTTT		
HOPX, HOP homeobox	porHOPX RT-PCR_F1	TCAACAAGGTCAACCGGCAT	151	
	porHOPX RT-PCR_R1	ACAGATCTGCACTCTGAGGGA		
LGR5, L-rich repeat containing GPR5	porLgr5 RT-PCR_F2	CAGAAATCCCTGTCCAGGCT	187	
	porLgr5 RT-PCR_R2	TCTAGGCTGTGGAGCCCATC		
VIL1, villin	porVIL1 RT-PCR_F3	GTCCATCTTCAAGGGACGCA	195	
	porVIL1 RT-PCR_R3	CAGCAGGACTGGGTCTTGAG		
MUC2, mucin	Muc2_Fw	GCCGACAACAAGAAGAACGT	120	Thomas Winogrodzki
	Muc2_Rev	GTGGGAGGATGGTTGGAAGA		
RPS28, ribosomal protein S28	RPS28_1F	GTTACCAAGGTTCTGGGCAG	197	
	RPS28_1R	CAGATATCCAGGACCCAGCC		
LYZ, lysozyme	Lyz1_Fw_qPCR	TGGCGAACTGGGTGTGTTT	165	Thomas Winogrodzki
	Lyz1_Rev_qPCR	TGCAGGATATGTGACAGGCA		
BMI1, polycomb ring finger (BMI1)	porBMI-1 RT-PCR_F	GACGCTGCCAATGGCTCTAA	193	
	porBMI-1 RT-PCR_R	CTGCTGGGCACCGTAAATATC		
APC, adenomatous polyposis coli	porAPC RT-PCR_F	GACATTGCGTGAAGTTGGCA	194	
	porAPC RT-PCR_R	TCTGGCTCCGGTAAGTGAGA		
TP53, tumour protein 53	TP53_9F	TCCTGCAGTACTCCCCTGCC	236	
	TP53_1R	ATTCCCTTCCACCCGGATGA		
SMAD4, SMAD family member 4	porSMAD4 RT-PCR_F	AGCCATTGAGAGAGCAAGGT	215	
	porSMAD4 RT-PCR_R	GACGATGACACTGACGCAAA		
PTEN, phosphatase and tensin homolog	porPTEN RT-PCR_F	AGGCACAAGAGGCCCTAGAT	216	
	porPTEN RT-PCR_R	GGCAGACCACAAACTGAGGA		
LEA29Y transgene	Lea seq F2	GGTCCTTGCACTCCTGTTTCC	330	
	LEAexpr2R	ATGAGCTCCACCTTGCAGAT		

7. Abbreviations

amplicon	amplified PCR product
A-overhang	terminal adenosine added to 3' ends of PCR products by Taq polymerases
APC	Adenomatous polyposis coli tumour suppressor gene
aq	solution prepared in water
B2M	β2-microglobulin
backbone	rudimentary bacterial plasmid used as basis for the insertion of DNA fragments
BMI1	BMI1 proto-oncogene
CAG	artificial mammalian promoter comprised of cytomegalovirus early enhancer element; the promoter region, the first exon, and the first intron of chicken beta-Actin gene, and the splice acceptor of the rabbit beta-Globin gene
CDKN2A/p16INK4A	cyclin dependent kinase inhibitor 2A
ChgA	chromogranin A
CHO	Chinese Hamster Ovary
CIMP	CpG island methylator phenotype
CIN	chromosomal instability, chromosomal instability
cMyc	cellular MYC proto-oncogene
CRISPR/Cas9	Clustered Regularly-Interspaced Short Palindromic Repeats and Cas9 endonuclease
crRNA	CRISPR RNA species that is homologous to the region within the genome to be edited using the CRISPR/Cas9 system
ddH2O	double-destilled, sterilised water
DH10B	electrocompetent Escherichia coli strain
dNTP	deoxynucleoside triphosphate (adenine/ cytosine/ guanine/ thymine triphosphate)
dsOligo	hybridised single stranded oligonucleotides with overhangs for molecular cloning of the crRNA
DSS	dextran sulfate sodium
E. coli	Escherichia coli
ELISA	Enzyme-linked Immunosorbent Assay
EMT	epidermal to mesenchymal transition
enteroid	organoid generated from adult stem cells that were isolated from the intestine

EREG	epiregulin, member of the EGF family of proteins
ETV4	ETS variant transcription factor 4
FAP	familial adenomatous polyposis
FDA	U.S. Food and Drug Administration
Flp recombinase	flippase recombinase, derived from Saccharomyces cerevisiae
G418	geneticin, antibiotic used for selection of successfully transfected vectors in mammalian cell culture, aminoglycoside 3'-phosphotransferase (neo gene) confers resistance to G418
guideRNA	artificial RNA for gene editing with the CRISPR/Cas system; a fusion product of crRNA and tracrRNA
HEK	Human Embryonic Kidney
HEK293T	Human Embryonic Kidney expressing a mutant version of the large T antigen from Simian Virus 40
HOPX	HOP homeobox
HRP	horse-radish peroxidase
IBD	inflammatory bowel disease
IESC	intestinal epithelial stem cell
IgG	immunoglobulin G class antibody
Ki67	marker of proliferation Ki67
LEA29Y	belatacept, a high-affinity variant of CTLA4-Ig with potent immunosuppressive properties
LGR5	leucine rich repeat containing G protein coupled receptor 5
L-WRN	cell line that secrets Wnt, R-spondin, and noggin
L-WRN cells	cell line that secrets Wnt, R-spondin, and noggin
Lyz	lysozyme
M	molecular concentration unit, 1 M ≈ 6.02x 1023 molecules/L
MAP kinase	mitogen-activated protein kinase
Mcm6	minichromosome maintenance complex component 6
MMR	Mismatch Repair
ms	milliseconds
MSI	microsatellite instability
Msi1	musashi RNA binding protein 1
MSS	microsatellite stability
MTT	tetrazolium salt, used for MTT viability assay

NSG	NOD.Cg-Prkdcscid Il2rgtm1Wjl/SzJ mice strain
PFA	paraformaldehyde
PI3K	phosphatidylinositol 3-kinase/ protein kinase B
PI3KCA	phosphatidylinositol-4,5-bisphosphate 3-kinase, catalytic subunit alpha
pKDCs	primary porcine kidney-derived cells
PTEN	phosphatase and tensin homolog
qPCR	quantitative real-time PCR of reversely transcribed RNA (cDNA)
RNase	Ribonuclease, enzyme that catalyses the hydrolysis of phosphodiester bonds in ribonucleic acids
RPS28	gene coding for ribosomal protein S28
RT-PCR	reverse transcriptase PCR, polymers, reverse transcriptase PCR, end point polymerase chain reaction that uses a DNA as template that has been transcribed from RNA
SCNT	somatic cell nuclear transfer
Screening PCR	Polymerase chain reaction used to verify the insertion of a transgene or mutation in mammalian genomes
siRNA	non-protein-coding small interfering RNA
SLA-1	porcine homologue of human MHC class I antigen 1
SMAD4	Mothers against decapentaplegic homolog 4
SOX9	SRY-box transcription factor 9
ssDNA	single stranded deoxyribonucleic acid
SV40LT	large T antigen from Simian Virus 40
T4	DNA Ligase that originates from the T4 bacteriophage
TCF/LEF	T cell factor/lymphoid enhancer factor family
TGFβ	transforming growth factor β
TGFβR	transforming growth factor β receptor
TNFα	tumour necrosis factor α
TP53	tumour suppressor protein 53
tracrRNA	trans-activating CRISPR RNA
tRNA	transfer RNA
tRNA-Gln	translation RNA coding for glutamine
TU	viral transduction units

U	units of active enzyme, measured by an enzyme-specific activity assay by the provider
VIL1	villin
xg	unit of gravitation force applied on a sample during centrifugation
α-Gal	Galactose-alpha-1,3-galactose, strong xenoreactive antigen for humans
ΔΔCt method	formula to calculate the relative fold change in gene expression between two conditions using a constitutively expressed gene not affected by the conditions as reference; also known as 2-ΔΔCt method

8. List of tables

9. List of figures

10. Acknowledgements

Ich bedanke mich bei Frau Prof. Dr. Angelika Schnieke für die Gelegenheit meine Promotion am Lehrstuhl durchzuführen und für die Betreuung von Dr. habil. Tatiana Flisikowska. Ebenso danken möchte ich Dr. habil. Krzysztof Flisikowski für die Probennahme.

Ein großer Dank geht auch an Sulith Christan für die tatkräftige Unterstützung im Laboralltag. Auf ihre Erfahrung und Unterstützung konnte ich mich jederzeit verlassen. Das Arbeiten wäre eine Mühsal gewesen ohne die vielen helfenden Hände der wissenschaftlichen Assistenten. Im Besonderen möchte ich daher Alexander Carrapeiro, Nina Simm und meiner langjährigen Laborpartnerin Johanna Tebbing danken. Für ihren Pragmatismus und ihr Engagement danke ich Barbara Bauer, die die Reihe derer schließt, die das grandioses Klima unter den Kollegen hegen und pflegen.

Alle Kollegen und Doktoranden wissen, dass der Zusammenhalt untereinander und die gegenseitige Hilfsbereitschaft unerlässlich für das Gelingen dieser Arbeit waren. Ich möchte daher allen meinen KollegenInnen und FreundenInnen meinen Dank aussprechen.

Andrea Fischer, die mich durch die Anfangsphase meiner Promotion begleitet hat, wünsche ich einen guten Abschluss ihrer Promotion und alles Glück für ihre junge Familie. Dr. Bernhard Klinger, der mir noch als Promotionsstudent die kritische Sicht auf eine akademische Karriere bewusst machte, wünsche ich die berufliche und persönliche Erfüllung, nach der wir uns alle sehnen. Melanie Nusselt verstand es mir neue Perspektiven zu eröffnen, wenn die Situation verfahren und eine Lösung unerreichbar schien. Dank ihr werde ich nie vergessen, dass ein erfolgreicher Forscher immer auch über seinen Tellerrand hinausschauen muss. Und schließlich danke ich Daniela Kalla, die mir eine liebe Freundin geworden ist. Melanie und Daniela wünsche ich das Selbstvertrauen und Glück selbst in stürmischem Wasser den sicheren Hafen zu finden.

Eine Doktorarbeit ist immer auch eine persönliche Prüfung. Glücklicherweise standen mir hierbei meine langjährigen Freunde und Vertraute Katharina und Samuel Hofmann zur Seite. Ohne euren Zuspruch und Gastfreundschaft hätte ich diese

Lebensphase nicht so gut gemeistert. Umso mehr freue ich mich auf die gemeinsame Arbeit an der Medizinischen Hochschule Hannover.

Abschließend gilt mein Dank meinen größten Gönnern, meinen verständnisvollsten Kritikern, und meinen unangefochtenen Vorbildern, meine Eltern, Emilia und Arnold Grodziecki, die mir all das ermöglicht haben, wovon sie immer geträumt hatten. Diesen Weg hätte ich nie ohne euch gehen können.

References

1. Cancer today. Available at https://gco.iarc.fr/today/online-analysis-map?v=2018&mode=population&mode_population=continents&population=900&populations=900&key=asr&sex=0&cancer=39&type=0&statistic=5&prevalence=0&population_group=0&ages_group%5B%5D=0&ages_group%5B%5D=17&nb_items=10&group_cancer=1&include_nmsc=1&include_nmsc_other=1&projection=natural-earth&color_palette=default&map_scale=quantile&map_nb_colors=5&continent=0&rotate=%255B10%252C0%255D (2020).
2. Siegel, R. L., Jemal, A. & Ward, E. M. Increase in incidence of colorectal cancer among young men and women in the United States. *Cancer epidemiology, biomarkers & prevention : a publication of the American Association for Cancer Research, cosponsored by the American Society of Preventive Oncology* **18,** 1695–1698; 10.1158/1055-9965.EPI-09-0186 (2009).
3. Rawla, P., Sunkara, T. & Barsouk, A. Epidemiology of colorectal cancer: incidence, mortality, survival, and risk factors. *Przeglad gastroenterologiczny* **14,** 89–103; 10.5114/pg.2018.81072 (2019).
4. Dekker, E., Tanis, P. J., Vleugels, J. L. A., Kasi, P. M. & Wallace, M. B. Colorectal cancer. *Lancet (London, England)* **394,** 1467–1480; 10.1016/S0140-6736(19)32319-0 (2019).
5. Darmkrebs_BlaueRatgeber_DeutscheKrebshilfe.
6. Mucci, L. A. *et al.* Familial Risk and Heritability of Cancer Among Twins in Nordic Countries. *JAMA* **315,** 68–76; 10.1001/jama.2015.17703 (2016).
7. DE-SOUZA, A. S. C. & COSTA-CASAGRANDE, T. A. ANIMAL MODELS FOR COLORECTAL CANCER. *Arquivos Brasileiros de Cirurgia Digestiva : ABCD* **31,** e1369; 10.1590/0102-672020180001e1369 (2018).
8. Ballinger, A. B. & Anggiansah, C. Colorectal cancer. *BMJ (Clinical research ed.)* **335,** 715–718; 10.1136/bmj.39321.527384.BE (2007).
9. Ben Ho Park & Bert Vogelstein. The APC Gene. In *Holland-Frei Cancer Medicine. 6th edition,* edited by B. H. Park & B. Vogelstein (BC Decker2003).
10. Palma, F. D. E. de *et al.* The Molecular Hallmarks of the Serrated Pathway in Colorectal Cancer. *Cancers* **11**; 10.3390/cancers11071017 (2019).
11. Fearon, E. R. & Vogelstein, B. A genetic model for colorectal tumorigenesis. *Cell* **61,** 759–767; 10.1016/0092-8674(90)90186-I (1990).
12. Rowan, A. J. *et al.* APC mutations in sporadic colorectal tumors: A mutational "hotspot" and interdependence of the "two hits". *Proc Natl Acad Sci USA* **97,** 3352–3357; 10.1073/pnas.97.7.3352 (2000).
13. Fearnhead, N. S., Britton, M. P. & Bodmer, W. F. The ABC of APC. *Human molecular genetics* **10,** 721–733; 10.1093/hmg/10.7.721 (2001).
14. Shimokawa, M. *et al.* Visualization and targeting of LGR5+ human colon cancer stem cells. *Nature* **545,** 187–192; 10.1038/nature22081 (2017).
15. Jordan, P. (ed.). *Targeted Therapy of Colorectal Cancer Subtypes* (Springer International Publishing, Cham, 2018).

16. Burn, J. *et al.* Long-term effect of aspirin on cancer risk in carriers of hereditary colorectal cancer: an analysis from the CAPP2 randomised controlled trial. *Lancet (London, England)* **378,** 2081–2087; 10.1016/S0140-6736(11)61049-0 (2011).

17. Spranger, S., Bao, R. & Gajewski, T. F. Melanoma-intrinsic β-catenin signalling prevents anti-tumour immunity. *Nature* **523,** 231–235; 10.1038/nature14404 (2015).

18. APC APC regulator of WNT signaling pathway [Homo sapiens (human)] - Gene - NCBI. Available at https://www.ncbi.nlm.nih.gov/gene/324 (2020).

19. Ben Ho Park & Bert Vogelstein. The APC Gene. In *Holland-Frei Cancer Medicine. 6th edition,* edited by B. H. Park & B. Vogelstein (BC Decker2003).

20. Newton, K. F. *et al.* Genotype-phenotype correlation in colorectal polyposis. *Clinical genetics* **81,** 521–531; 10.1111/j.1399-0004.2011.01740.x (2012).

21. Seth, C. & Ruiz I Altaba, A. Metastases and Colon Cancer Tumor Growth Display Divergent Responses to Modulation of Canonical WNT Signaling. *PloS one* **11,** e0150697; 10.1371/journal.pone.0150697 (2016).

22. Allen, W. L. *et al.* Transcriptional subtyping and CD8 immunohistochemistry identifies poor prognosis stage II/III colorectal cancer patients who benefit from adjuvant chemotherapy. *JCO precision oncology* **2018**; 10.1200/PO.17.00241 (2018).

23. Thanki, K. *et al.* Consensus Molecular Subtypes of Colorectal Cancer and their Clinical Implications. *International biological and biomedical journal* **3,** 105–111 (2017).

24. Smeby, J. *et al.* CMS-dependent prognostic impact of KRAS and BRAFV600E mutations in primary colorectal cancer. *Annals of oncology : official journal of the European Society for Medical Oncology* **29,** 1227–1234; 10.1093/annonc/mdy085 (2018).

25. WARBURG, O. On the origin of cancer cells. *Science (New York, N.Y.)* **123,** 309–314; 10.1126/science.123.3191.309 (1956).

26. Ying, H. *et al.* Oncogenic Kras maintains pancreatic tumors through regulation of anabolic glucose metabolism. *Cell* **149,** 656–670; 10.1016/j.cell.2012.01.058 (2012).

27. Guinney, J. *et al.* The consensus molecular subtypes of colorectal cancer. *Nature medicine* **21,** 1350–1356; 10.1038/nm.3967 (2015).

28. Karapetis, C. S. *et al.* K-ras mutations and benefit from cetuximab in advanced colorectal cancer. *The New England journal of medicine* **359,** 1757–1765; 10.1056/NEJMoa0804385 (2008).

29. Flight, M. H. A sweet blow for cancer cells. *Nature reviews. Drug discovery* **10,** 734; 10.1038/nrd3566 (2011).

30. Li, Q. *et al.* Butyrate Suppresses the Proliferation of Colorectal Cancer Cells via Targeting Pyruvate Kinase M2 and Metabolic Reprogramming. *Molecular & cellular proteomics : MCP* **17,** 1531–1545; 10.1074/mcp.RA118.000752 (2018).

31. Li, S. *et al.* Viable pigs with a conditionally-activated oncogenic KRAS mutation. *Transgenic research* **24,** 509–517; 10.1007/s11248-015-9866-8 (2015).

32. Homo sapiens tumor protein p53 (TP53), RefSeqGene (LRG_321) on chromos - Nucleotide - NCBI. Available at https://www.ncbi.nlm.nih.gov/nuccore/NG_017013.2?from=5001&to=24149&report=genbank (2020).

33. D.P. Lane. p53, guardian of the genome. *Nature,* 15–16 (1992).

34. DAVID MALKIN, FREDERICK P. Li, LouISE C. STRONG, JOSEPH F. FRAUMENI, JR., CAMILLE E. NELSON, DAVID H. KIM, JAYNE KASSEL, MAGDALENA A. GRYKA, FARIDEH Z. BISCHOFF, MICHAEL A. TAINSKY, STEPHEN H. FRIEND*. Germ Line p53 Mutations in a Familial Syndrome of Breast Cancer, Sarcomas, and Other Neoplasms, 1233–1238 (1990).

35. Yamamoto, S. & Iwakuma, T. Regulators of Oncogenic Mutant TP53 Gain of Function. *Cancers* **11**; 10.3390/cancers11010004 (2018).

36. Beauséjour, C. M. *et al.* Reversal of human cellular senescence: roles of the p53 and p16 pathways. *The EMBO journal* **22,** 4212–4222; 10.1093/emboj/cdg417 (2003).

37. Rayess, H., Wang, M. B. & Srivatsan, E. S. Cellular senescence and tumor suppressor gene p16. *International journal of cancer* **130,** 1715–1725; 10.1002/ijc.27316 (2012).

38. Schwitalle, Y. *et al.* Immune response against frameshift-induced neopeptides in HNPCC patients and healthy HNPCC mutation carriers. *Gastroenterology* **134,** 988–997; 10.1053/j.gastro.2008.01.015 (2008).

39. Phillips, S. M. *et al.* Tumour-infiltrating lymphocytes in colorectal cancer with microsatellite instability are activated and cytotoxic. *The British journal of surgery* **91,** 469–475; 10.1002/bjs.4472 (2004).

40. Le, D. T. *et al.* PD-1 Blockade in Tumors with Mismatch-Repair Deficiency. *The New England journal of medicine* **372,** 2509–2520; 10.1056/NEJMoa1500596 (2015).

41. Rotte, A. Combination of CTLA-4 and PD-1 blockers for treatment of cancer. *Journal of experimental & clinical cancer research : CR* **38,** 255; 10.1186/s13046-019-1259-z (2019).

42. Li, H. *et al.* The tumor microenvironment: An irreplaceable element of tumor budding and epithelial-mesenchymal transition-mediated cancer metastasis. *Cell adhesion & migration* **10,** 434–446; 10.1080/19336918.2015.1129481 (2016).

43. Labayle, D. *et al.* Sulindac causes regression of rectal polyps in familial adenomatous polyposis. *Gastroenterology* **101,** 635–639; 10.1016/0016-5085(91)90519-Q (1991).

44. Jess, T., Frisch, M. & Simonsen, J. Trends in overall and cause-specific mortality among patients with inflammatory bowel disease from 1982 to 2010. *Clinical gastroenterology and hepatology : the official clinical practice journal of the American Gastroenterological Association* **11,** 43–48; 10.1016/j.cgh.2012.09.026 (2013).

45. Ananthakrishnan, A. N. Epidemiology and risk factors for IBD. *Nature reviews. Gastroenterology & hepatology* **12,** 205–217; 10.1038/nrgastro.2015.34 (2015).

46. Khor, B., Gardet, A. & Xavier, R. J. Genetics and pathogenesis of inflammatory bowel disease. *Nature* **474,** 307–317; 10.1038/nature10209 (2011).

47. Ben-Neriah, Y. & Karin, M. Inflammation meets cancer, with NF-κB as the matchmaker. *Nature immunology* **12,** 715–723; 10.1038/ni.2060 (2011).

48. Shaked, H. *et al.* Chronic epithelial NF-κB activation accelerates APC loss and intestinal tumor initiation through iNOS up-regulation. *Proceedings of the National Academy of Sciences of the United States of America* **109,** 14007–14012; 10.1073/pnas.1211509109 (2012).

49. Schwitalla, S. *et al.* Intestinal tumorigenesis initiated by dedifferentiation and acquisition of stem-cell-like properties. *Cell* **152,** 25–38; 10.1016/j.cell.2012.12.012 (2013).

50. Milestones in Cancer Research and Discovery. Available at https://www.cancer.gov/research/progress/250-years-milestones (2020).

51. Moser, A. R., Pitot, H. C. & Dove, W. F. A dominant mutation that predisposes to multiple intestinal neoplasia in the mouse. *Science (New York, N.Y.)* **247,** 322–324; 10.1126/science.2296722 (1990).

52. Di Nicolantonio, F. & Bardelli, A. Mouse models of Kras-mutant colorectal cancer: valuable GEMMs for drug testing? *Clinical cancer research : an official journal of the American Association for Cancer Research* **19,** 2794–2796; 10.1158/1078-0432.CCR-13-0339 (2013).

53. Ren, J., Sui, H., Fang, F., Li, Q. & Li, B. The application of ApcMin/+ mouse model in colorectal tumor researches. *Journal of cancer research and clinical oncology* **145,** 1111–1122; 10.1007/s00432-019-02883-6 (2019).

54. Hinoi, T. *et al.* Mouse model of colonic adenoma-carcinoma progression based on somatic Apc inactivation. *Cancer research* **67,** 9721–9730; 10.1158/0008-5472.CAN-07-2735 (2007).

55. Kalla, D., Kind, A. & Schnieke, A. Genetically Engineered Pigs to Study Cancer. *International journal of molecular sciences* **21**; 10.3390/ijms21020488 (2020).

56. Fumagalli, A. *et al.* A surgical orthotopic organoid transplantation approach in mice to visualize and study colorectal cancer progression. *Nat Protoc* **13,** 235–247; 10.1038/nprot.2017.137 (2018).

57. Johnson J I, et al. Relationships between drug activity in NCI preclinical in vitro and in vivo models and early clinical trials.

58. Iorio, F. *et al.* A Landscape of Pharmacogenomic Interactions in Cancer. *Cell* **166,** 740–754; 10.1016/j.cell.2016.06.017 (2016).

59. Mouradov, D. *et al.* Colorectal cancer cell lines are representative models of the main molecular subtypes of primary cancer. *Cancer research* **74,** 3238–3247; 10.1158/0008-5472.CAN-14-0013 (2014).

60. Julien, S. *et al.* Characterization of a large panel of patient-derived tumor xenografts representing the clinical heterogeneity of human colorectal cancer. *Clinical cancer research : an official journal of the American Association for Cancer Research* **18,** 5314–5328; 10.1158/1078-0432.CCR-12-0372 (2012).

61. Hidalgo, M. *et al.* A pilot clinical study of treatment guided by personalized tumorgrafts in patients with advanced cancer. *Molecular cancer therapeutics* **10,** 1311–1316; 10.1158/1535-7163.MCT-11-0233 (2011).

62. Ben-David, U. *et al.* Patient-derived xenografts undergo mouse-specific tumor evolution. *Nature genetics* **49,** 1567–1575; 10.1038/ng.3967 (2017).

63. Michael Hay, David W Thomas, John L Craighead, Celia Economides & Jesse Rosenthal. Clinical development success rates for investigational drugs. *Nature biotechnology,* 40–51 (2014).

64. Sato, T. *et al.* Long-term expansion of epithelial organoids from human colon, adenoma, adenocarcinoma, and Barrett's epithelium. *Gastroenterology* **141,** 1762–1772; 10.1053/j.gastro.2011.07.050 (2011).

65. Weeber, F., Ooft, S. N., Dijkstra, K. K. & Voest, E. E. Tumor Organoids as a Pre-clinical Cancer Model for Drug Discovery. *Cell Chemical Biology* **24,** 1092–1100; 10.1016/j.chembiol.2017.06.012 (2017).

66. Beshiri, M. L. *et al.* A PDX/Organoid Biobank of Advanced Prostate Cancers Captures Genomic and Phenotypic Heterogeneity for Disease Modeling and Therapeutic Screening. *Clinical cancer research : an official journal of the American Association for Cancer Research* **24,** 4332–4345; 10.1158/1078-0432.CCR-18-0409 (2018).

67. O'Rourke, K. P. *et al.* Transplantation of engineered organoids enables rapid generation of metastatic mouse models of colorectal cancer. *Nature biotechnology* **35,** 577–582; 10.1038/nbt.3837 (2017).

68. Matano, M. *et al.* Modeling colorectal cancer using CRISPR-Cas9-mediated engineering of human intestinal organoids. *Nature medicine* **21,** 256–262; 10.1038/nm.3802 (2015).

69. Annapoorni Rangarajan, R. A. Comparative biology ofmouse versus human cells: modelling human cancer in mice. *Nature Reviews Cancer,* 952–959 (2003).

70. Martignoni, M., Groothuis, G. M. M. & Kanter, R. de. Species differences between mouse, rat, dog, monkey and human CYP-mediated drug metabolism, inhibition and induction. *Expert opinion on drug metabolism & toxicology* **2,** 875–894; 10.1517/17425255.2.6.875 (2006).

71. Tzachi Hagai *et al.* Gene expression variability across cells and species shapes innate immunity.

72. Hoffe, B. & Holahan, M. R. The Use of Pigs as a Translational Model for Studying Neurodegenerative Diseases. *Frontiers in physiology* **10,** 838; 10.3389/fphys.2019.00838 (2019).

73. Schook, L. B. *et al.* Unraveling the swine genome: implications for human health. *Annual review of animal biosciences* **3,** 219–244; 10.1146/annurev-animal-022114-110815 (2015).

74. Roth, W. J. *et al.* Assessment of juvenile pigs to serve as human pediatric surrogates for preclinical formulation pharmacokinetic testing. *The AAPS journal* **15,** 763–774; 10.1208/s12248-013-9482-6 (2013).

75. Flisikowska, T. *et al.* A porcine model of familial adenomatous polyposis. *Gastroenterology* **143,** 1173-1175.e7; 10.1053/j.gastro.2012.07.110 (2012).

76. Sikorska, A. *et al.* Elevated expression of p53 in early colon polyps in a pig model of human familial adenomatous polyposis. *Journal of applied genetics* **59,** 485–491; 10.1007/s13353-018-0461-6 (2018).

77. Perkowska, A. *et al.* The expression of TAP1 candidate gene, but not its polymorphism and methylation, is associated with colonic polyp formation in a porcine model of human familial adenomatous polyposis. *Animal biotechnology* **31,** 306–313; 10.1080/10495398.2019.1590377 (2020).

78. Fleming, N. I. *et al.* SMAD2, SMAD3 and SMAD4 mutations in colorectal cancer. *Cancer research* **73,** 725–735; 10.1158/0008-5472.CAN-12-2706 (2013).

79. Oyanagi, H. *et al.* SMAD4 alteration associates with invasive-front pathological markers and poor prognosis in colorectal cancer. *Histopathology* **74,** 873–882; 10.1111/his.13805 (2019).

80. Kontoyiannis, D., Pasparakis, M., Pizarro, T. T., Cominelli, F. & Kollias, G. Impaired On/Off Regulation of TNF Biosynthesis in Mice Lacking TNF AU-Rich Elements. *Immunity* **10,** 387–398; 10.1016/S1074-7613(00)80038-2 (1999).

81. Wang, J. *et al.* Characteristic and functional analysis of a newly established porcine small intestinal epithelial cell line. *PloS one* **9,** e110916; 10.1371/journal.pone.0110916 (2014).

82. Rossi, G., Manfrin, A. & Lutolf, M. P. Progress and potential in organoid research. *Nat Rev Genet* **19,** 671–687; 10.1038/s41576-018-0051-9 (2018).

83. Fujii, M. *et al.* Human Intestinal Organoids Maintain Self-Renewal Capacity and Cellular Diversity in Niche-Inspired Culture Condition. *Cell Stem Cell* **23,** 787-793.e6; 10.1016/j.stem.2018.11.016 (2018).

84. Miura, S. & Suzuki, A. Generation of Mouse and Human Organoid-Forming Intestinal Progenitor Cells by Direct Lineage Reprogramming. *Cell Stem Cell* **21,** 456-471.e5; 10.1016/j.stem.2017.08.020 (2017).

85. Spence, J. R. *et al.* Directed differentiation of human pluripotent stem cells into intestinal tissue in vitro. *Nature* **470,** 105–109; 10.1038/nature09691 (2011).

86. Sharbati, J., Hanisch, C., Pieper, R., Einspanier, R. & Sharbati, S. Small molecule and RNAi induced phenotype transition of expanded and primary colonic epithelial cells. *Scientific reports* **5,** 12681; 10.1038/srep12681 (2015).

87. Powell, R. H. & Behnke, M. S. WRN conditioned media is sufficient for in vitro propagation of intestinal organoids from large farm and small companion animals. *Biology open* **6,** 698–705; 10.1242/bio.021717 (2017).

88. Callesen, M. M. *et al.* A genetically inducible porcine model of intestinal cancer. *Molecular oncology* **11,** 1616–1629; 10.1002/1878-0261.12136 (2017).

89. van der Hee, B. *et al.* Optimized procedures for generating an enhanced, near physiological 2D culture system from porcine intestinal organoids. *Stem cell research* **28,** 165–171; 10.1016/j.scr.2018.02.013 (2018).

90. Derricott, H. *et al.* Developing a 3D intestinal epithelium model for livestock species. *Cell and tissue research* **375,** 409–424; 10.1007/s00441-018-2924-9 (2019).

91. Zhu, M., Qin, Y.-C., Gao, C.-Q., Yan, H.-C. & Wang, X.-Q. l-Glutamate drives porcine intestinal epithelial renewal by increasing stem cell activity via upregulation of the EGFR-ERK-mTORC1 pathway. *Food & function*; 10.1039/c9fo03065d (2020).

92. Zhu, M. *et al.* Extracellular Glutamate-Induced mTORC1 Activation via the IR/IRS/PI3K/Akt Pathway Enhances the Expansion of Porcine Intestinal Stem Cells. *Journal of agricultural and food chemistry* **67,** 9510–9521; 10.1021/acs.jafc.9b03626 (2019).

93. Resende, T. P., Medida, R. L., Vannucci, F. A., Saqui-Salces, M. & Gebhart, C. Evaluation of swine enteroids as in vitro models for Lawsonia intracellularis infection1,2. *Journal of animal science* **98**; 10.1093/jas/skaa011 (2020).

94. Guo, Y., Candelero-Rueda, R. A., Saif, L. J. & Vlasova, A. N. Infection of porcine small intestinal enteroids with human and pig rotavirus A strains reveals contrasting roles for histo-blood group antigens and terminal sialic acids. *PLoS pathogens* **17,** e1009237; 10.1371/journal.ppat.1009237 (2021).

95. Cramer, J. M., Thompson, T., Geskin, A., LaFramboise, W. & Lagasse, E. Distinct human stem cell populations in small and large intestine. *PloS one* **10,** e0118792; 10.1371/journal.pone.0118792 (2015).

96. Jinek, M. *et al.* RNA-programmed genome editing in human cells. *eLife Sciences Publications, Ltd* (2013).

97. Bhaya, D., Davison, M. & Barrangou, R. CRISPR-Cas systems in bacteria and archaea: versatile small RNAs for adaptive defense and regulation. *Annual review of genetics* **45,** 273–297; 10.1146/annurev-genet-110410-132430 (2011).

98. Zaboikin, M., Zaboikina, T., Freter, C. & Srinivasakumar, N. Non-Homologous End Joining and Homology Directed DNA Repair Frequency of Double-Stranded Breaks Introduced by Genome Editing Reagents. *PloS one* **12,** e0169931; 10.1371/journal.pone.0169931 (2017).

99. Xie, K., Minkenberg, B. & Yang, Y. Boosting CRISPR/Cas9 multiplex editing capability with the endogenous tRNA-processing system. *Proceedings of the National Academy of Sciences of the United States of America* **112,** 3570–3575; 10.1073/pnas.1420294112 (2015).

100. Roper, J. *et al.* Colonoscopy-based colorectal cancer modeling in mice with CRISPR-Cas9 genome editing and organoid transplantation. *Nat Protoc* **13,** 217–234; 10.1038/nprot.2017.136 (2018).

101. Perleberg, C., Kind, A. & Schnieke, A. Genetically engineered pigs as models for human disease. *Disease models & mechanisms* **11**; 10.1242/dmm.030783 (2018).

102. Hanahan, D. & Weinberg, R. A. Hallmarks of cancer: the next generation. *Cell* **144,** 646–674; 10.1016/j.cell.2011.02.013 (2011).

103. Artegiani, B. & Clevers, H. Use and application of 3D-organoid technology. *Human molecular genetics* **27,** R99-R107; 10.1093/hmg/ddy187 (2018).

104. Choi, K.-H. *et al.* Pluripotent pig embryonic stem cell lines originating from in vitro-fertilized and parthenogenetic embryos. *Stem cell research* **49,** 102093; 10.1016/j.scr.2020.102093 (2020).

105. Bowcutt, R. *et al.* Heterogeneity across the murine small and large intestine. *World journal of gastroenterology* **20,** 15216–15232; 10.3748/wjg.v20.i41.15216 (2014).

106. Sato, T. *et al.* Single Lgr5 stem cells build crypt-villus structures in vitro without a mesenchymal niche. *Nature* **459,** 262–265; 10.1038/nature07935 (2009).

107. van Landeghem, L. *et al.* Activation of two distinct Sox9-EGFP-expressing intestinal stem cell populations during crypt regeneration after irradiation. *American journal of physiology. Gastrointestinal and liver physiology* **302,** G1111-32; 10.1152/ajpgi.00519.2011 (2012).

108. Sato, T. *et al.* Paneth cells constitute the niche for Lgr5 stem cells in intestinal crypts. *Nature* **469,** 415–418; 10.1038/nature09637 (2011).

109. Wang, C. *et al.* Human Milk Oligosaccharides Protect against Necrotizing Enterocolitis by Inhibiting Intestinal Damage via Increasing the Proliferation of Crypt Cells. *Molecular nutrition & food research* **63,** e1900262; 10.1002/mnfr.201900262 (2019).

110. Negoro, R. *et al.* Efficient Generation of Small Intestinal Epithelial-like Cells from Human iPSCs for Drug Absorption and Metabolism Studies. *Stem cell reports* **11,** 1539–1550; 10.1016/j.stemcr.2018.10.019 (2018).

111. Mariotto, A., Pavlova, O., Park, H.-S., Huber, M. & Hohl, D. HOPX: The Unusual Homeodomain-Containing Protein. *The Journal of investigative dermatology* **136,** 905–911; 10.1016/j.jid.2016.01.032 (2016).

112. Tüysüz, N. *et al.* Lipid-mediated Wnt protein stabilization enables serum-free culture of human organ stem cells. *Nature communications* **8,** 14578; 10.1038/ncomms14578 (2017).

113. Lu, Y. Post-translational modifications and secretion of Wnt proteins. *BJSTR* **9**; 10.26717/BJSTR.2018.09.001824 (2018).

114. Pipas, J. M. Common and unique features of T antigens encoded by the polyomavirus group. *Journal of virology* **66,** 3979–3985; 10.1128/JVI.66.7.3979-3985.1992 (1992).

115. Nam, J.-S., Turcotte, T. J., Smith, P. F., Choi, S. & Yoon, J. K. Mouse cristin/R-spondin family proteins are novel ligands for the Frizzled 8 and LRP6 receptors and activate beta-catenin-dependent gene expression. *The Journal of biological chemistry* **281,** 13247–13257; 10.1074/jbc.M508324200 (2006).

116. Ying, Q.-L. *et al.* The ground state of embryonic stem cell self-renewal. *Nature* **453,** 519–523; 10.1038/nature06968 (2008).

117. Liu, Z. *et al.* VEGF and inhibitors of TGFbeta type-I receptor kinase synergistically promote blood-vessel formation by inducing alpha5-integrin expression. *Journal of cell science* **122,** 3294–3302; 10.1242/jcs.048942 (2009).

118. Jiang, Y. *et al.* Characterization of the structure and function of a new mitogen-activated protein kinase (p38beta). *The Journal of biological chemistry* **271,** 17920–17926; 10.1074/jbc.271.30.17920 (1996).

119. Urbischek, M. *et al.* Organoid culture media formulated with growth factors of defined cellular activity. *Scientific reports* **9,** 6193; 10.1038/s41598-019-42604-0 (2019).

120. Zhao, X. *et al.* Human Intestinal Organoids Recapitulate Enteric Infections of Enterovirus and Coronavirus. *Stem cell reports* **16,** 493–504; 10.1016/j.stemcr.2021.02.009 (2021).

121. Broutier, L. *et al.* Culture and establishment of self-renewing human and mouse adult liver and pancreas 3D organoids and their genetic manipulation. *Nat Protoc* **11,** 1724–1743; 10.1038/nprot.2016.097 (2016).

122. Stringer, C., Wang, T., Michaelos, M. & Pachitariu, M. Cellpose: a generalist algorithm for cellular segmentation. *bioRxiv,* 2020.02.02.931238; 10.1101/2020.02.02.931238 (2020).

123. Choi, K.-H. *et al.* Chemically Defined Media Can Maintain Pig Pluripotency Network In Vitro. *Stem cell reports* **13,** 221–234; 10.1016/j.stemcr.2019.05.028 (2019).

124. Valastyan, S. & Weinberg, R. A. Tumor metastasis: molecular insights and evolving paradigms. *Cell* **147,** 275–292; 10.1016/j.cell.2011.09.024 (2011).

125. Kim, T. K. & Eberwine, J. H. Mammalian cell transfection: the present and the future. *Analytical and bioanalytical chemistry* **397,** 3173–3178; 10.1007/s00216-010-3821-6 (2010).

126. Banasik, M. B. & McCray, P. B. Integrase-defective lentiviral vectors: progress and applications. *Gene therapy* **17,** 150–157; 10.1038/gt.2009.135 (2010).

127. Li, S. *et al.* Dual fluorescent reporter pig for Cre recombination: transgene placement at the ROSA26 locus. *PloS one* **9,** e102455; 10.1371/journal.pone.0102455 (2014).

128. Cordon-Cardo, C. & Sheinfeld, J. Molecular and immunopathology studies of oncogenes and tumor-suppressor genes in bladder cancer. *World journal of urology* **15,** 112–119; 10.1007/BF02201982 (1997).

129. Sun, J. *et al.* TRIM29 facilitates the epithelial-to-mesenchymal transition and the progression of colorectal cancer via the activation of the Wnt/β-catenin signaling pathway. *Journal of experimental & clinical cancer research : CR* **38,** 104; 10.1186/s13046-019-1098-y (2019).

130. Nfonsam, L. E., Jandova, J., Jecius, H. C., Omesiete, P. N. & Nfonsam, V. N. SFRP4 expression correlates with epithelial mesenchymal transition-linked genes and poor overall survival in colon cancer patients. *World journal of gastrointestinal oncology* **11,** 589–598; 10.4251/wjgo.v11.i8.589 (2019).

131. Murphy, J. B. & Rous, P. THE BEHAVIOR OF CHICKEN SARCOMA IMPLANTED IN THE DEVELOPING EMBRYO. *The Journal of experimental medicine* **15,** 119–132; 10.1084/jem.15.2.119 (1912).

132. Fischer, K. *et al.* Viable pigs after simultaneous inactivation of porcine MHC class I and three xenoreactive antigen genes GGTA1, CMAH and B4GALNT2. *Xenotransplantation* **27,** e12560; 10.1111/xen.12560 (2020).

133. Bähr, A. *et al.* Ubiquitous LEA29Y Expression Blocks T Cell Co-Stimulation but Permits Sexual Reproduction in Genetically Modified Pigs. *PloS one* **11,** e0155676; 10.1371/journal.pone.0155676 (2016).

134. Sake, H. J. *et al.* Possible detrimental effects of beta-2-microglobulin knockout in pigs. *Xenotransplantation* **26,** e12525; 10.1111/xen.12525 (2019).

135. Lakatos, P.-L. & Lakatos, L. Risk for colorectal cancer in ulcerative colitis: changes, causes and management strategies. *World journal of gastroenterology* **14,** 3937–3947; 10.3748/wjg.14.3937 (2008).

136. Stoecklin, G., Lu, M., Rattenbacher, B. & Moroni, C. A constitutive decay element promotes tumor necrosis factor alpha mRNA degradation via an AU-rich element-independent pathway. *Molecular and cellular biology* **23,** 3506–3515; 10.1128/mcb.23.10.3506-3515.2003 (2003).

137. Fujii, M., Matano, M., Nanki, K. & Sato, T. Efficient genetic engineering of human intestinal organoids using electroporation. *Nat Protoc* **10,** 1474–1485; 10.1038/nprot.2015.088 (2015).

138. Nair, A. B. & Jacob, S. A simple practice guide for dose conversion between animals and human. *Journal of Basic and Clinical Pharmacy* **7,** 27–31; 10.4103/0976-0105.177703 (2016).

139. Barnett, A. M. *et al.* Porcine colonoids and enteroids keep the memory of their origin during regeneration. *American journal of physiology. Cell physiology* **320,** C794-C805; 10.1152/ajpcell.00420.2020 (2021).

140. Mihara, E. *et al.* Active and water-soluble form of lipidated Wnt protein is maintained by a serum glycoprotein afamin/α-albumin. *eLife* **5**; 10.7554/eLife.11621 (2016).

141. Zhou, J.-Y. *et al.* Methionine and Its Hydroxyl Analogues Improve Stem Cell Activity To Eliminate Deoxynivalenol-Induced Intestinal Injury by Reactivating Wnt/β-Catenin Signaling. *Journal of agricultural and food chemistry* **67,** 11464–11473; 10.1021/acs.jafc.9b04442 (2019).

142. Wang, Z. *et al.* Dietary vitamin A affects growth performance, intestinal development, and functions in weaned piglets by affecting intestinal stem cells. *Journal of animal science* **98**; 10.1093/jas/skaa020 (2020).

143. Phan, N. *et al.* A simple high-throughput approach identifies actionable drug sensitivities in patient-derived tumor organoids. *Communications Biology* **2,** 78; 10.1038/s42003-019-0305-x (2019).

144. Hailstone, M. *et al.* CytoCensus, mapping cell identity and division in tissues and organs using machine learning. *eLife* **9**; 10.7554/eLife.51085 (2020).

145. Wolny, A. *et al.* Accurate and versatile 3D segmentation of plant tissues at cellular resolution. *eLife* **9**; 10.7554/eLife.57613 (2020).

146. Li, X.-G. *et al.* Acute exposure to deoxynivalenol inhibits porcine enteroid activity via suppression of the Wnt/β-catenin pathway. *Toxicology Letters* **305,** 19–31; 10.1016/j.toxlet.2019.01.008 (2019).

147. Zhou, J.-Y. *et al.* Hydrolyzed wheat gluten alleviates deoxynivalenol-induced intestinal injury by promoting intestinal stem cell proliferation and differentiation via upregulation of Wnt/β-catenin signaling in mice. *Food and chemical toxicology : an international journal published for the British Industrial Biological Research Association* **131,** 110579; 10.1016/j.fct.2019.110579 (2019).

148. Khalil, H. A. *et al.* A novel culture system for adult porcine intestinal crypts. *Cell and tissue research* **365,** 123–134; 10.1007/s00441-016-2367-0 (2016).

149. Nissim, L., Perli, S. D., Fridkin, A., Perez-Pinera, P. & Lu, T. K. Multiplexed and programmable regulation of gene networks with an integrated RNA and CRISPR/Cas toolkit in human cells. *Molecular Cell* **54,** 698–710; 10.1016/j.molcel.2014.04.022 (2014).

150. Wójcik, E. & Sokół, A. Assessment of chromosome stability in boars. *PloS one* **15,** e0231928; 10.1371/journal.pone.0231928 (2020).

151. Ferrandis Vila, M. *et al.* Dietary fiber sources and non-starch polysaccharide-degrading enzymes modify mucin expression and the immune profile of the swine ileum. *PloS one* **13,** e0207196; 10.1371/journal.pone.0207196 (2018).

152. Luo, H. *et al.* Utility Evaluation of Porcine Enteroids as PDCoV Infection Model in vitro. *Frontiers in microbiology* **11,** 821; 10.3389/fmicb.2020.00821 (2020).

153. Zhou, J.-Y. *et al.* Heat-stable enterotoxin inhibits intestinal stem cell expansion to disrupt the intestinal integrity by downregulating the Wnt/β-catenin pathway. *Stem cells (Dayton, Ohio)* **39,** 482–496; 10.1002/stem.3324 (2021).

154. Li, L. *et al.* Porcine Intestinal Enteroids: a New Model for Studying Enteric Coronavirus Porcine Epidemic Diarrhea Virus Infection and the Host Innate Response. *Journal of virology* **93**; 10.1128/JVI.01682-18 (2019).

155. Li, Y. *et al.* Next-Generation Porcine Intestinal Organoids: an Apical-Out Organoid Model for Swine Enteric Virus Infection and Immune Response Investigations. *Journal of virology* **94**; 10.1128/JVI.01006-20 (2020).

156. Fumagalli, A. *et al.* Genetic dissection of colorectal cancer progression by orthotopic transplantation of engineered cancer organoids. *Proceedings of the National Academy of Sciences of the United States of America* **114,** E2357-E2364; 10.1073/pnas.1701219114 (2017).

157. Merlos-Suárez, A. *et al.* The intestinal stem cell signature identifies colorectal cancer stem cells and predicts disease relapse. *Cell Stem Cell* **8,** 511–524; 10.1016/j.stem.2011.02.020 (2011).

158. Barker, N. *et al.* Identification of stem cells in small intestine and colon by marker gene Lgr5. *Nature* **449,** 1003–1007; 10.1038/nature06196 (2007).

159. Polyak, K. & Weinberg, R. A. Transitions between epithelial and mesenchymal states: acquisition of malignant and stem cell traits. *Nature reviews. Cancer* **9,** 265–273; 10.1038/nrc2620 (2009).

160. Sakai, E. *et al.* Combined Mutation of Apc, Kras, and Tgfbr2 Effectively Drives Metastasis of Intestinal Cancer. *Cancer research* **78,** 1334–1346; 10.1158/0008-5472.CAN-17-3303 (2018).

161. Haigis, K. M. *et al.* Differential effects of oncogenic K-Ras and N-Ras on proliferation, differentiation and tumor progression in the colon. *Nature genetics* **40,** 600–608; 10.1038/ng.115 (2008).

162. Park, S., Kim, W.-H., Choi, S.-Y. & Kim, Y.-J. Removal of alpha-Gal epitopes from porcine aortic valve and pericardium using recombinant human alpha galactosidase A. *Journal of Korean medical science* **24,** 1126–1131; 10.3346/jkms.2009.24.6.1126 (2009).

163. Shao, L. *et al.* Knockout of beta-2 microglobulin enhances cardiac repair by modulating exosome imprinting and inhibiting stem cell-induced immune rejection. *Cellular and molecular life sciences : CMLS* **77,** 937–952; 10.1007/s00018-019-03220-3 (2020).

164. Klymiuk, N. *et al.* Xenografted islet cell clusters from INSLEA29Y transgenic pigs rescue diabetes and prevent immune rejection in humanized mice. *Diabetes* **61,** 1527–1532; 10.2337/db11-1325 (2012).

165. Wang, Y. *et al.* Transgenic expression of human cytoxic T-lymphocyte associated antigen4-immunoglobulin (hCTLA4Ig) by porcine skin for xenogeneic skin grafting. *Transgenic Res* **24,** 199–211; 10.1007/s11248-014-9833-9 (2015).

166. Vabres, B. *et al.* hCTLA4-Ig transgene expression in keratocytes modulates rejection of corneal xenografts in a pig to non-human primate anterior lamellar keratoplasty model. *Xenotransplantation* **21,** 431–443; 10.1111/xen.12107 (2014).

167. Shirakami, Y. *et al.* Inhibitory effects of pentoxifylline on inflammation-related tumorigenesis in rat colon. *Oncotarget* **9,** 33972–33981; 10.18632/oncotarget.26119 (2018).

168. Robles, A. I. *et al.* Whole-Exome Sequencing Analyses of Inflammatory Bowel Disease-Associated Colorectal Cancers. *Gastroenterology* **150,** 931–943; 10.1053/j.gastro.2015.12.036 (2016).

169. Rogler, G. Chronic ulcerative colitis and colorectal cancer. *Cancer letters* **345,** 235–241; 10.1016/j.canlet.2013.07.032 (2014).

170. Shi, J.-W. *et al.* The enforced expression of c-Myc in pig fibroblasts triggers mesenchymal-epithelial transition (MET) via F-actin reorganization and RhoA/Rock pathway inactivation. *Cell cycle (Georgetown, Tex.)* **12,** 1119–1127; 10.4161/cc.24164 (2013).